Chapter 3

Results and Discussions

3.1. Introduction

The analytical and the FE formulation derived in the previous chapter is utilized here to determine the static and dynamic responses of traditional laminated composites, sandwich plates and smart composite plate structures. The section starts with the static analysis of traditional laminated composites and sandwich plates under the action of mechanical load followed by the static analysis of smart composite plates subjected to time-independent electrical and mechanical loads. Then the dynamic analysis of the laminated composites and soft-core sandwich plate structures are presented in which the natural frequencies and the higher modes of vibration of the plates are obtained by exploiting various material and geometrical features of the plates, followed by the transient responses of laminated composite plates subjected to time-dependent mechanical loads. Various forms of blast loadings are also considered in the dynamic analysis to determine the dynamic behavior of composites. The formulation is then extended to determine the forced vibration responses of smart composite plates under the action of various time-dependent electromechanical loads. Then the active vibration control (AVC) of smart composite plates is presented by creating a control strategy with a feedback controller. The analytical and the FE formulations are programmed in MATLAB and implemented to examine the static and dynamic responses. The solutions obtained are first validated with the elasticity solutions based on the availability and responses obtained various mathematical models.

3.2. Static Analysis of traditional laminated composites and sandwich plates

In this section, the static responses of laminated composite plates are presented under the action of uniformly distributed load (UDL) and doubly sinusoidal load (SSL) in the spatial domain. The non-dimensional parameters and the material properties used for obtaining the results are presented in sections 2.9 and 2.10 in the previous chapter and also separately mentioned under all the tables and figures in this chapter.

3.2.1. Three-layered laminated composite plate (0/90/0) subjected to uniformly distributed pressure

A square laminated composite plate with three layers and diaphragm support at all the edges is considered in this example. The non-dimensional transverse displacements for various span-thickness ratios ranging from 4 to 100 are presented in Table 3.1. The Navier's solution for a sinusoidally distributed load is a one-term solution. For other kinds of loads like the uniformly distributed variation, Navier's solution is a series solution and needs to be evaluated for a sufficient number of terms until the convergence is achieved. The convergence of the analytical solution is first shown in Figure 3.1a for a thick plate (S = 4). Similarly, the FE convergence of the solution with the same span-thickness ratio is shown in Figure 3.1b. The convergence is accepted when the results are exactly the same up to three decimal places. The analytical results have converged when the first five odd mode numbers m, n are considered, *i.e*., $m = n$ =1, 3, 5...11 whereas the FE results have converged at a mesh size of 8x8, *i.e*, 64 number of elements. The present results are compared with the elasticity results of Pagano (1970) and the solutions obtained by exploiting different plate theories like the zigzag theory with secant function (ZZTSF) (Sahoo and Singh, 2014), polynomial zigzag theory (Singh *et al*., 2011), and ESL based

FSDT and HSDT (Sheikh and Chakrabarti, 2003, and Reddy, 1984). The present results are observed to be in close agreement with elasticity solutions (Pagano, 1970).

Table 3.1. Non-dimensional deflection ($\bar{U}_3$) of a three-layered (0/90/0) plate subjected to uniformly distributed load (material property: MM1; non-dimensional parameter: ND1)

References	l/h = 100	l/h = 50	l/h = 20	l/h = 10	l/h = 4
Present Analytical	0.6714	0.6873	0.7963	1.1587	3.0256
Present FEM	0.6714	0.6872	0.7962	1.1586	3.0621
Pagano (1970)[1]	0.6712	-	-	1.1533	3.0416
Sahoo and Singh (2014)	0.6706	0.6843	0.7785	1.0981	2.9096
Singh *et al*. (2011)	0.6706	0.6843	0.7785	1.0981	2.9096
Sheikh and Chakrabarti (2003)[2]	0.6708	0.6841	0.7763	1.091	2.9093
Sheikh and Chakrabarti (2003)[3]	0.6707	0.6813	0.7588	1.0235	2.6608
Reddy (1984)[2]	0.6705	0.6838	0.776	1.09	2.9091
Reddy (1984)[3]	0.6697	0.6807	0.7573	1.0219	2.6596

[1]Elasticity Solution; [2]HSDT; [3]FSDT

3.2.2. Three-layered square and rectangular laminated composite plate (0/90/0) subjected to doubly sinusoidal load

The three-layered laminated composite plate is considered again with the same material and geometrical properties. In this example, the mechanical load is doubly sinusoidal in the x_1 and x_2-direction. The convergence of the FE solutions of deflection and stresses are shown in Figure 3.2 for a thick plate (S = 10). It is observed in the figure that the results of transverse deflection ($\bar{w}$) have converged at a mesh size of 8x8, *i.e*, 64 number of elements whereas the stresses have converged at a mesh size of 20x20, *i.e*, 400 elements for getting the same results up to three decimal places. The normalized transverse deflection and all the stresses are collected in Table 3.2 for various span-thickness ratios, ranging from thick to thin.

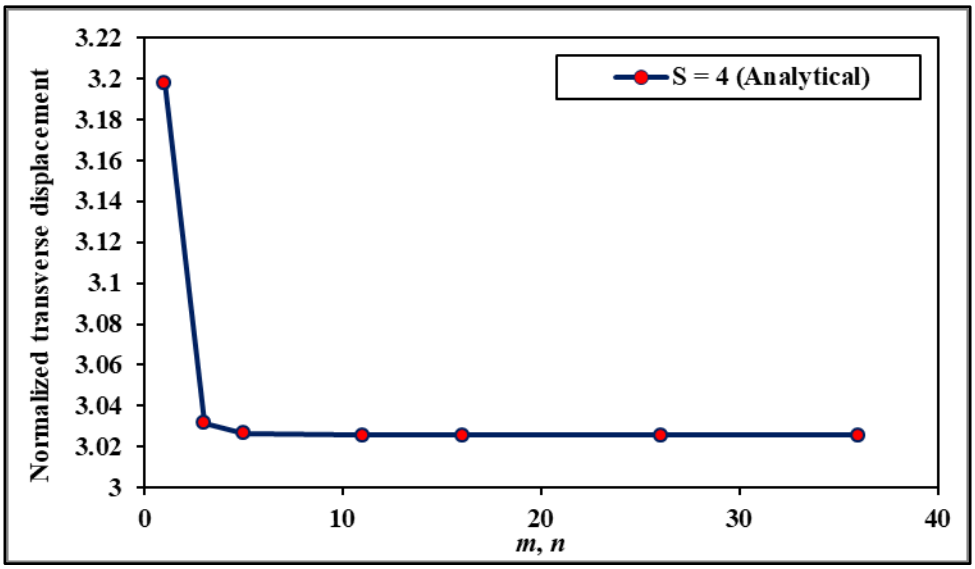

(a)

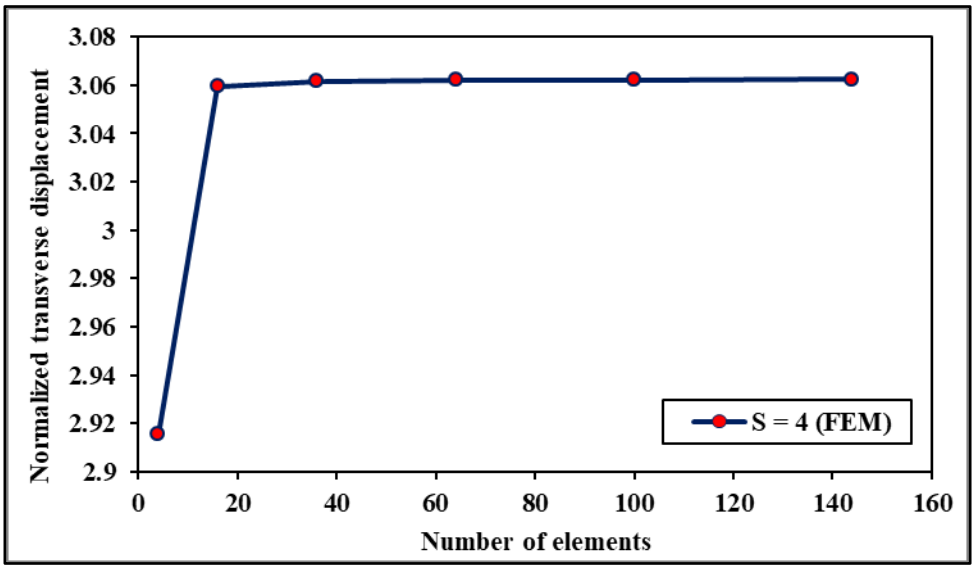

(b)

Figure 3.1. (a) Convergence of the analytical solution. (b) Convergence of the FE solutions (material property: MM1; non-dimensional parameter: ND1)

As the stresses have converged at a mesh size of 20x20, therefore, the results of deflections are also provided at a mesh size of 20x20 in the table. Unless specified, the responses obtained for all the examples under this section and in the subsequent sections are obtained at a mesh size of 20x20.The present results are compared with the elasticity solutions (Pagano, 1970) and results reported in the literature with various plate theories. The table shows an excellent correlation of the present results with the elasticity solutions (Pagano, 1970) with a maximum discrepancy of 1.864 % (analytical) and 1.958 % (FE) in the response of transverse displacement. The results of stresses have maximum discrepancies of 0.814 %, 1.528 %, and 2.113 % (analytical), and 0.535 %, 1.632 % and 2.113 % (FE) in the responses of in-plane normal ($\bar{\sigma}_{11}, \bar{\sigma}_{22}$) and in-plane shear stress ($\bar{\tau}_{12}$), respectively for the thick plate (S =10). While the in-plane normal and shear stresses are fairly estimated with the stress-strain constitutive relationships (CR) of the material, the transverse shear stresses are not very accurately predicted using the CR. Therefore, the transverse shear stresses are also obtained by using the 3D equilibrium equations (EE) of elasticity. The application of EE is observed to significantly increase the accuracy of the results of transverse shear stresses collected in the table. The maximum discrepancies in the response of $\bar{\tau}_{12}$ and $\bar{\tau}_{23}$ for S = 10 are reduced from 3.529 % to 0.196 % and 34.87 % to 1.057 % by using the EE, respectively. Figure 3.3 illustrates the through-thickness variations of the in-plane displacement (U_1) for various span-thickness ratios. It is observed in the figure that the U_1 has a linear variation without any slope discontinuity or changes in slope $\left(\frac{\partial U_1}{\partial x_3}\right)$ at the interfaces for thin plate (S =100). As the plate becomes thick, the changes in slopes are prominent at the interfaces. The variation of the in-plane normal stresses ($\bar{\sigma}_{11}$,$\bar{\sigma}_{22}$) across the thickness of the plate are presented in Figures 3.4a and 3.4b, respectively. The value of

the in-plane stress '$\bar{\sigma}_{11}$' is maximum at the top and bottom surface of the laminated plate whereas the maximum value of $\bar{\sigma}_{22}$ is at the interface of the plate. The in-plane stresses are discontinuous at any k^{th} interface due to dissimilar transformed reduced stiffness coefficients '$\bar{Q}_{ij}$' of the k^{th} and $(k+1)^{\text{th}}$ layer. Figure 3.5 shows the through-thickness variations of the in-plane shear stress. It is maximum at the top and bottom surface of the laminate plate and is also found to be continuous, unlike the in-plane normal stresses. The transformed reduced stiffness coefficient '$\bar{Q}_{66}$' relating the in-plane shear stress and in-plane shear strain is the same for both the layers. As a result, the stresses do not have any discontinuities at the interfaces. However, slope discontinuities at the interface are observed in the figure for thick plate (S = 10). Figure 3.6a and 3.6b shows the through-thickness variation of the transverse shear stresses $(\bar{\tau}_{13}, \bar{\tau}_{23})$ obtained using CR and EE. It is observed in Figure 3.6a that the CR overestimates the value of $\bar{\tau}_{13}$ at the midplane in comparison to the results obtained using EE which is found to be more accurate in Table 3.2. At the top and bottom layers, the variations of $\bar{\tau}_{13}$ from both approaches do not have much difference. However, a significant difference is noticed in the variation of $\bar{\tau}_{23}$ in Figure 3.6b. The probable reason for this is the choice of the shear strain function that produces more consistent results of $\bar{\tau}_{13}$ in comparison to $\bar{\tau}_{23}$. Therefore, it is concluded that the results of transverse shear stresses obtained using EE are more efficient than the results obtained using CR.

Table 3.2. Non-dimensional deflection and stresses of three-layered (0/90/0) laminated composite plate subjected to doubly sinusoidal mechanical load (material property: MM1; non-dimensional parameter: ND1)

l/*h*	References	$(\bar{U}_3)$ $\left(\frac{l}{2},\frac{b}{2}\right)$	$\bar{\sigma}_{11}$ $\left(\frac{l}{2},\frac{b}{2},\frac{h}{2}\right)$ (CR)	$\bar{\sigma}_{22}$ $\left(\frac{l}{2},\frac{b}{2},\frac{h}{6}\right)$ (CR)	$\bar{\tau}_{12}$ $\left(0,0,\frac{h}{2}\right)$ (CR)	$\bar{\tau}_{13}$ $\left(0,\frac{b}{2},0\right)$ (CR)	$\bar{\tau}_{13}$ $\left(0,\frac{b}{2},0\right)$ (EE)	$\bar{\tau}_{23}$ $\left(\frac{l}{2},0,0\right)$ (CR)	$\bar{\tau}_{23}$ $\left(\frac{l}{2},0,0\right)$ (EE)
100	Present FEM	0.4347	0.5415	0.1820	0.0215	0.4023	-	0.0588	-
	% error	[0]	[0.464]	[0.552]	[0.938]	[1.925]	-	[29.156]	
	Present Analytical	0.4347	0.5393	0.1809	0.0214	0.4022	0.3945	0.0559	0.0830
	% error	[0]	[0.056]	[0.055]	[0.469]	[1.9]	[0.051]	[32.651]	[0]
	3D Elasticity (1970)	0.4347	0.5390	0.1810	0.0213	0.3947	0.3947	0.0830	0.0830
	Sahoo and Singh (2014)	0.4341	0.5462	0.1830	0.0216	0.3428	-	0.0733	-
	Karama *et al*. (2009)	0.435	0.5380	0.1800	0.0213	0.2890	-	0.0780	-
	Sheikh and Chakrabarti (2003)	0.435	0.5496	0.1828	0.0215	0.2401	-	0.0749	-
	Kant and Swaminathan (2002)	0.4343	0.5392	0.1807	0.0214	-	-	-	-
50	Present FEM	0.4452	0.5432	0.1858	0.0217	0.4011	-	0.0597	-
	% error	-	[0.406]	[0.432]	[0.463]	[2.061]	-	[28.928]	-
	Present Analytical	0.4452	0.541	0.1847	0.0216	0.4011	0.3932	0.0567	0.0844
	% error	-	[0]	[0.162]	[0]	[2.061]	[0.051]	[32.5]	[0.476]
	3D Elasticity (1970)	-	0.5410	0.1850	0.0216	0.3930	0.3930	0.0840	0.0840
	Sahoo and Singh (2014)	0.4432	0.5477	0.1862	0.0218	0.3318	-	0.0742	-
	Karama *et al*. (2009)	0.444	0.5400	0.1830	0.0216	0.2890	-	0.0790	-
	Kant and Swaminathan (2002)	0.4432	0.5406	0.1838	0.0231	-	-	-	-

20	Present FEM	0.5169	0.5550	0.2118	0.0235	0.3923	-	0.0658	-
	% error	-	[0.543]	[0.857]	[0.427]	[1.896]	-	[30]	-
	Present Analytical	0.5168	0.5531	0.2108	0.0234	0.3935	0.3844	0.0625	0.0942
	% error	-	[-0.199]	[-0.381]	[0]	[-2.208]	[0.156]	[33.511]	[-0.213]
	3D Elasticity (1970)	-	0.5520	0.2100	0.0234	0.3850	0.3850	0.0940	0.0940
	Sahoo and Singh (2014)	0.5056	0.5579	0.2077	0.0234	0.3352	-	0.0809	-
	Karama *et al*. (2009)	0.508	0.5480	0.2050	0.0231	0.2850	-	0.0860	-
	Kant and Swaminathan (2002)	0.5053	0.5504	0.2049	0.0231	-	-	-	-
10	Present FEM	0.755	0.5931	0.2927	0.029	0.3649	-	0.0848	-
	% error	[1.958]	[0.525]	[1.632]	[2.113]	[2.213]	-	[31.056]	-
	Present Analytical	0.7543	0.5948	0.2924	0.0290	0.3696	0.3563	0.0801	0.1243
	% error	[1.864]	[0.814]	[1.528]	[2.113]	[3.529]	[0.196]	[34.878]	[1.057]
	3D Elasticity (1970)	0.7405	0.5900	0.2880	0.0284	0.3570	-	0.1230	-
	Sahoo and Singh (2014)	0.7173	0.5924	0.2748	0.0299	0.3140	-	0.1010	-
	Karama *et al*. (2009)	0.723	0.5760	0.2720	0.0281	0.2720	-	0.1080	-
	Sheikh and Chakrabarti (2003)	0.714	0.5806	0.2722	0.0279	0.2437	-	0.1015	-
	Kant and Swaminathan (2002)	0.7151	0.5836	0.2705	0.0279	-	-	-	-

CR: Constitutive Relations; EE: Equilibrium Equations

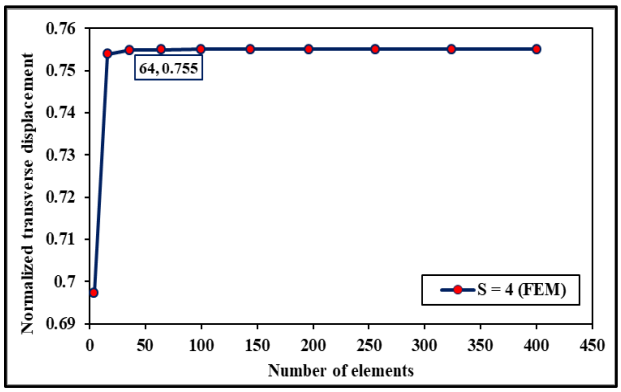

$(\bar{U}_3)$

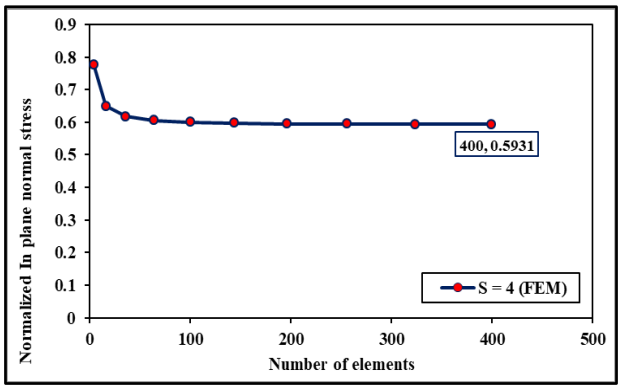

$(\bar{\sigma}_{11})$

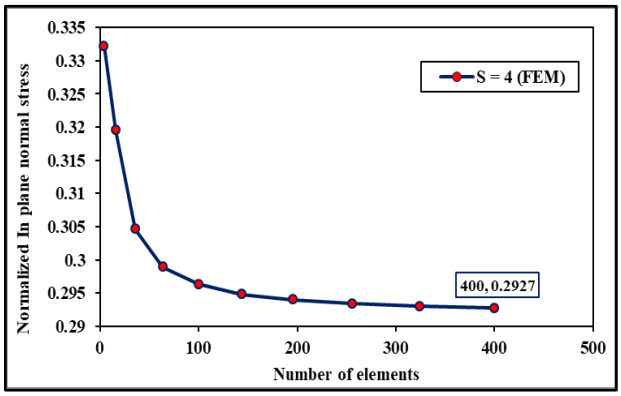

$(\bar{\sigma}_{22})$

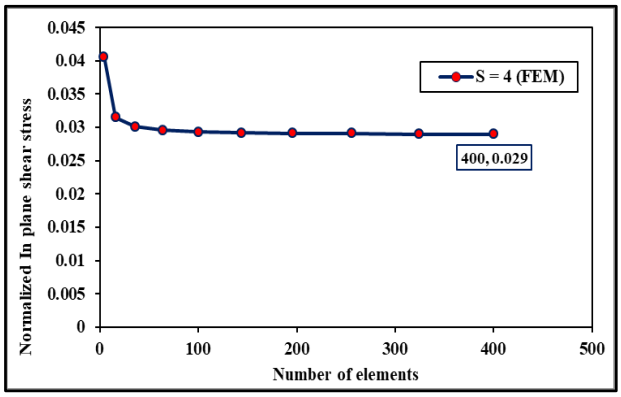

$(\bar{\tau}_{12})$

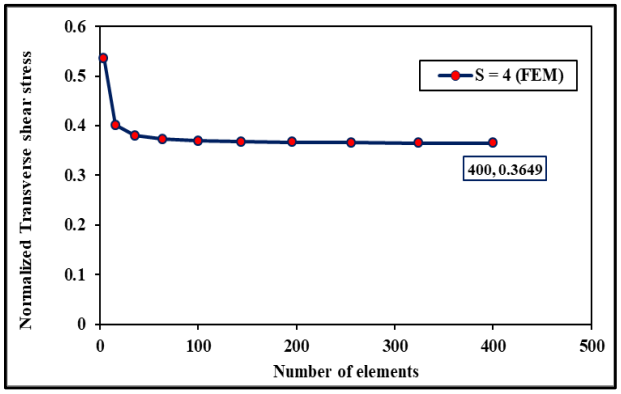

$(\bar{\tau}_{13})$

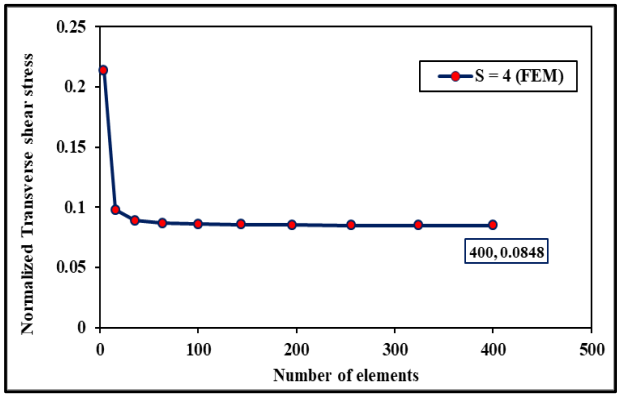

$(\bar{\tau}_{23})$

Figure 3.2. Convergence of the FE results for a 0/90/0 plate subjected to SSL (material property: MM1; non-dimensional parameter: ND1)

As a further example, the static responses of the same plate having a rectangular geometry (b =3l) instead of the square geometry are presented in Table 3.3. The results are compared with the responses obtained by Pagano (1970), Sahoo and Singh (2014), Kulkarni and Kapuria (2007), Sheikh and Chakrabarti (2003) and Chalak *et al*. (2012a). The table shows an excellent correlation of the present results with the results of the aforementioned references.

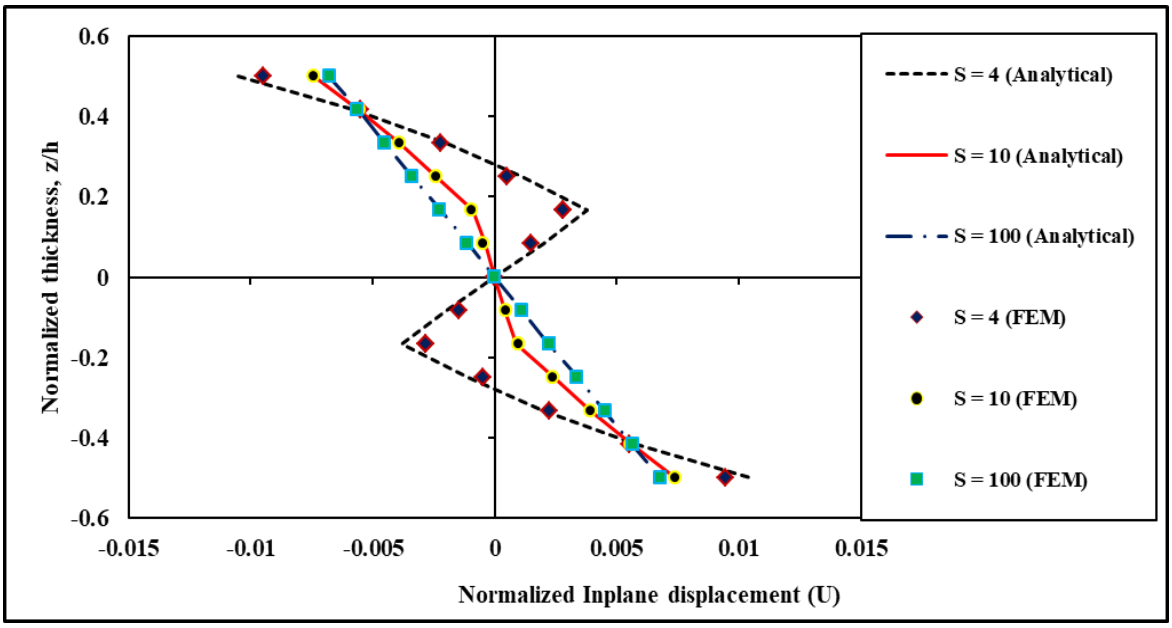

Figure 3.3: Through-thickness variations of normalized in plane displacement (U_1) for a 0/90/0 plate subjected to SSL (material property: MM1; non-dimensional parameter: ND1)

3.2.3. Four-layered laminated composite plate (0/90/90/0) subjected to doubly sinusoidal load

Now, a diaphragm-supported four-layered laminated composite plate subjected to sinusoidal load is considered to derive the static response. The results of transverse displacement and in-plane normal and shear stresses are collected in Table 3.4 while the transverse shear stresses are presented in Table 3.5.

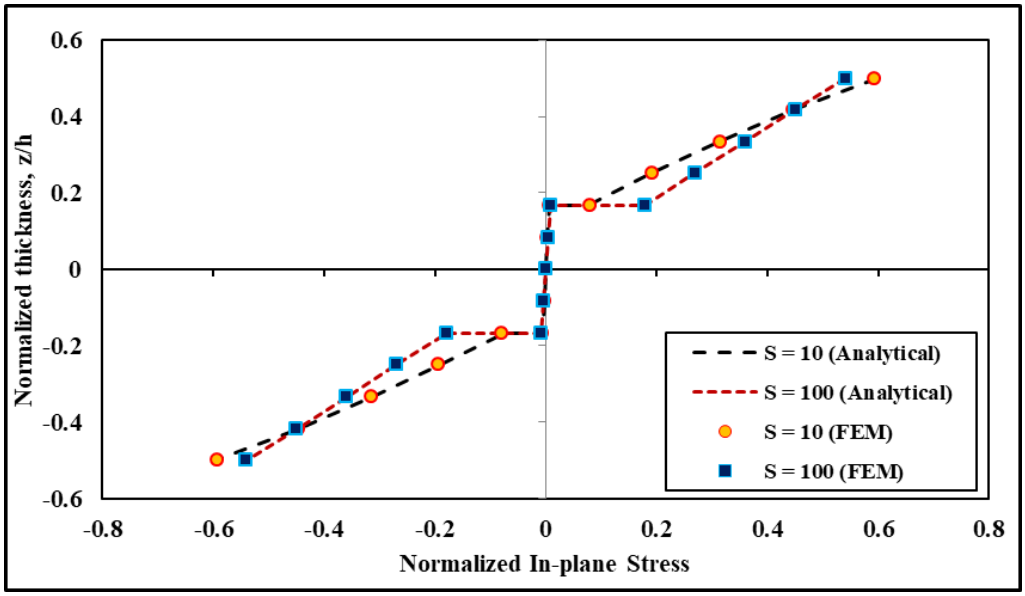

(a)

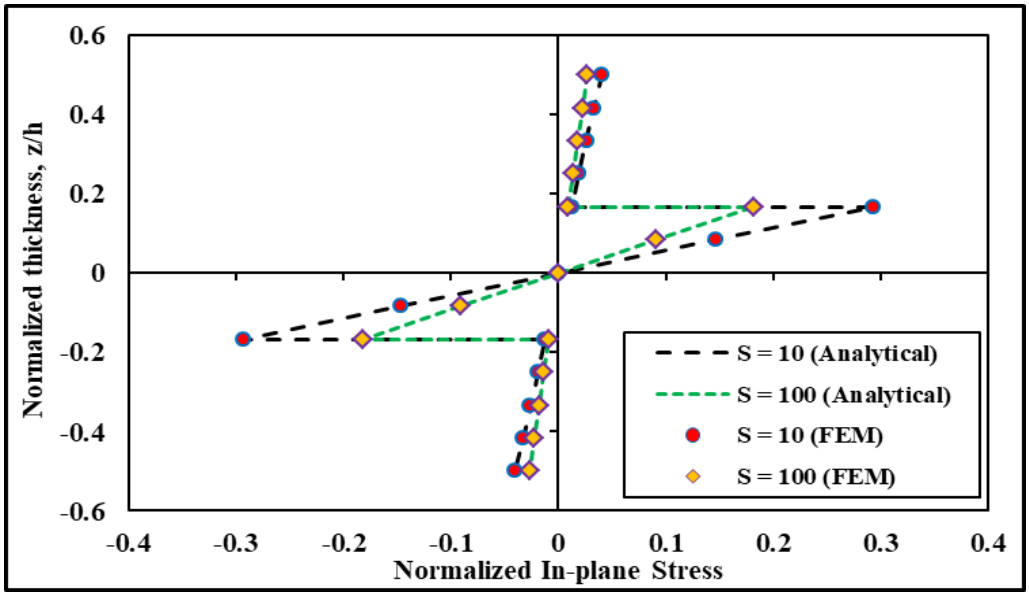

(b)

Figure 3.4: (a) Through-thickness variations of normalized in plane normal stress $(\bar{\sigma}_{11})$ for a 0/90/0 plate subjected to SSL. (b) Through-thickness variations of normalized in plane normal stress $(\bar{\sigma}_{22})$ for a 0/90/0 plate subjected to SSL
(material property: MM1; non-dimensional parameter: ND1)

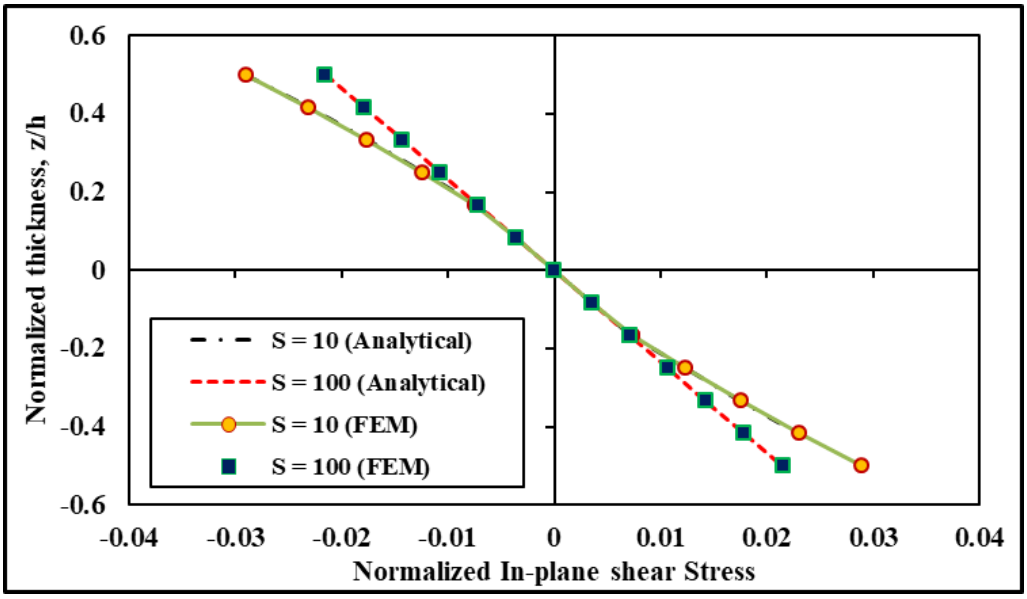

Figure 3.5: Through-thickness variations of normalized in plane shear stress $(\bar{\tau}_{12})$ for a 0/90/0 plate subjected to SSL (material property: MM1; non-dimensional parameter: ND1)

The present responses are compared with elasticity solutions of Pagano and Hatfield (1972) and results obtained by exploiting various 2 D models in the literature. The maximum error in the values of transverse displacement is calculated to be 2.45 % and 0.94 % (analytical) and 1.63 % and 0.88 % (FEM) for thick plates, (S = 4 and 10), respectively. The normalized stresses '$\bar{\sigma}_{11}$' and '$\bar{\sigma}_{22}$' are also found to be in good agreement with the 3 D solutions (Pagano and Hatfield, 1972). The present results are found to be slightly overestimated for very thick plate (S = 4) with discrepancies of 2.30% and 5.65% (analytical), and 4.83 % and 7.33 % (FEM) for $\bar{\sigma}_{11}$ and $\bar{\sigma}_{22}$, respectively.

As expected, the values of transverse shear stress '$\bar{\tau}_{13}$' obtained using the 3 D equilibrium equations have a marginal error of 3.69% and 0.29% for S = 4 and 10, respectively. The maximum error in $\bar{\tau}_{23}$ for S = 4 and 10 is calculated to be 8.24 % and 1.83%, respectively.

The present results of transverse shear stresses are more efficient than the results reported by the references in the table.

3.2.4. Three-layered sandwich plate (0/C/0) subjected to sinusoidal load (SSL)

After deriving the static responses of laminated composite plates, the static responses of sandwich plates are now investigated. Sandwich plates have thin face sheets made up of strong materials and thick core layers made up of weak materials in comparison to the materials of the face sheets. Such a configuration facilitates weight reduction. In this example, two face sheets are considered at the top and bottom of the sandwich plate with a thickness of 0.1h and the middle layer is the core layer with a thickness of 0.8h. Sinusoidal varying mechanical pressure is considered to act on the top of the plate in both x_1 and x_2-direction. The convergence of all the stresses and displacements obtained using FEM is shown in Figure 3.7. An excellent convergence can be found in the results of both deflection and stresses. The results of non-dimensional deflection and in-plane stresses are presented in Table 3.6. The results are compared with the 3D elasticity solutions (Pagano, 1970) and results reported by various references in the literature. The results in the table are observed to be in excellent agreement with the elasticity solutions. The maximum discrepancy in the present results of transverse deflection ($\bar{U}_3$) is noted to be 0.452% (analytical) and 0.6 % (FEM) for a very thick plate (S = 4) whereas the maximum error reported by Pandit *et al*. (2008) and Singh *et al*. (2011) are 0.777% and 3.415%, respectively. The present model predicts $\bar{\sigma}_{11}$ with an error of 0.18% (analytical) and 1.22 % (FEM) for a very thick plate with a span-thickness ratio, S = 4. The transverse shear stresses obtained using the constitutive and equilibrium equations for different span-thickness ratios are presented in Table 3.7.

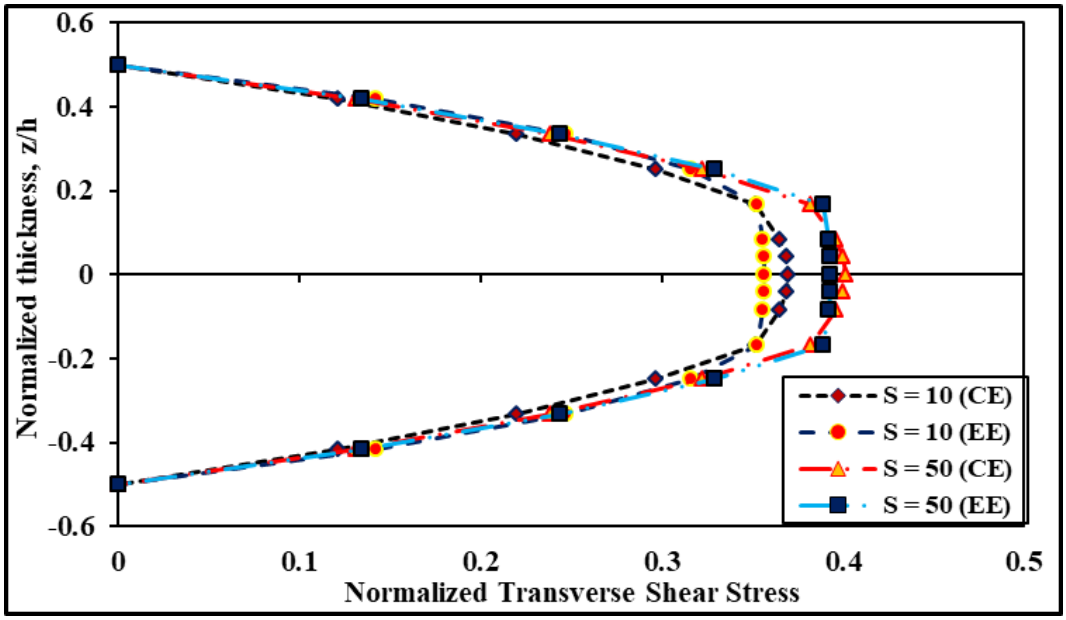

(a)

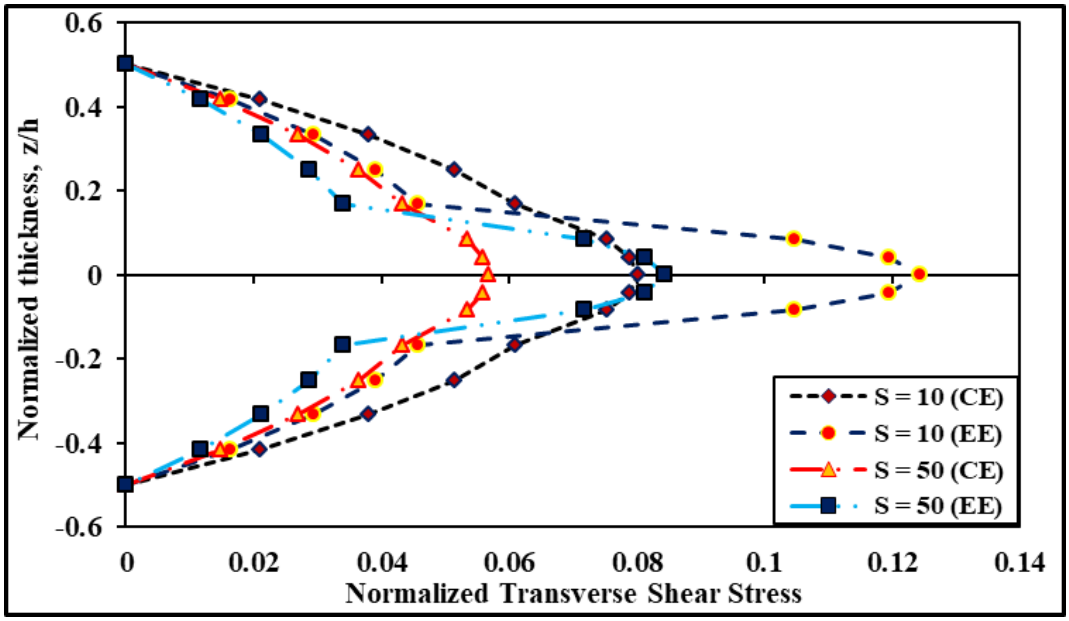

(b)

Figure 3.6. (a) Through-thickness variations of normalized transverse shear stress $(\bar{\tau}_{13})$ for a 0/90/0 plate subjected to SSL. (b) Through-thickness variations of normalized transverse shear stress $(\bar{\tau}_{23})$ for a 0/90/0 plate subjected to SSL (material property: MM1; non-dimensional parameter: ND1) (CE: Constitutive Equations; EE: Equilibrium Equations)

Table 3.3. Non-dimensional deflection and stresses of simply supported rectangular (b = 3a) laminated composite plate (0/90/0) subjected to SSL
(material property: MM1; non-dimensional parameter: ND1)

a/h	References	$\bar{U}_3\left(\frac{l}{2},\frac{b}{2}\right)$	% error	$\bar{\sigma}_{11}\left(\frac{l}{2},\frac{b}{2},\frac{h}{2}\right)$	% error	$\bar{\sigma}_{22}\left(\frac{l}{2},\frac{b}{2},\frac{h}{6}\right)$	% error	$\bar{\tau}_{12}\left(0,0,\frac{h}{2}\right)$	% error
100	Present FEM	0.5078	0.95	0.6271	0.49	0.0255	0.79	0.0084	1.20
	Present Analytical	0.5078	0.95	0.6245	0.08	0.0253	0.00	0.0083	0.00
	Pagano (1970)	0.503	-	0.6240	-	0.0253	-	0.0083	-
	Sahoo and Singh (2014)	0.507	0.80	0.6162	1.25	0.0256	1.19	0.0084	1.20
	Kulkarni and Kapuria (2007)	0.5078	0.95	0.6255	0.24	0.0253	0.00	0.0083	0.00
	Sheikh and Chakrabarti (2003)	0.5097	1.33	0.6457	3.48	0.0253	0.00	0.0084	1.20
	Chalak *et al*. (2012a)	0.5052	0.44	0.6276	0.58	0.0253	0.00	0.0083	0.00
50	Present FEM	0.5207	0.04	0.6303	0.43	0.0260	0.00	0.0085	0.00
	Present Analytical	0.5207	0.04	0.6278	0.03	0.0258	0.77	0.0084	1.18
	Pagano (1970)	0.5205	-	0.6276	-	0.0260	-	0.0085	-
	Sahoo and Singh (2014)	0.5182	0.44	0.6189	1.39	0.0261	0.38	0.0085	0.00
	Chalak *et al*. (2012a)	0.5181	0.46	0.631	0.54	0.0258	0.77	0.0085	0.00
20	Present FEM	0.6101	0.02	0.6529	0.44	0.0297	0.66	0.0093	0.00
	Present Analytical	0.6101	0.02	0.6508	0.12	0.0295	1.34	0.0093	0.00
	Pagano (1970)	0.6100	-	0.6500	-	0.0299	-	0.0093	-
	Sahoo and Singh (2014)	0.5958	2.33	0.6548	0.74	0.032	7.02	0.0092	1.08
	Sheikh and Chakrabarti (2003)	0.5965	2.21	0.6634	2.06	0.0274	8.36	0.0092	1.08
	Chalak *et al*. (2012a)	0.6074	0.43	0.6537	0.57	0.0291	2.68	0.0093	0.00
10	Present FEM	0.9210	0.21	0.7286	0.49	0.0423	2.75	0.0122	0.81
	Present Analytical	0.9203	0.14	0.7307	0.79	0.0420	3.45	0.0122	0.81
	Pagano (1970)	0.9190	-	0.7250	-	0.0435	-	0.0123	-
	Sahoo and Singh (2014)	0.8690	5.44	0.7216	0.47	0.0455	4.6	0.0118	4.07
	Kulkarni and Kapuria (2007)	0.8636	6.03	0.6939	4.29	0.0399	8.28	0.0115	6.50
	Sheikh and Chakrabarti (2003)	0.8649	5.89	0.7164	1.19	0.0383	11.95	0.0117	4.88
	Chalak *et al*. (2012a)	0.9181	0.1	0.7297	0.65	0.0405	6.9	0.0122	0.81

Table 3.4 Non-dimensional deflection and in-plane stresses of four-layered (0/90/90/0) plate subjected to SSL (material property: MM1; non-dimensional parameter: ND1)

a/h	References	$\bar{U}_3\left(\frac{l}{2},\frac{b}{2}\right)$	% error	$\bar{\sigma}_{11}\left(\frac{l}{2},\frac{b}{2},\frac{h}{2}\right)$	% error	$\bar{\sigma}_{22}\left(\frac{l}{2},\frac{b}{2},\frac{h}{4}\right)$	% error	$\bar{\tau}_{12}\left(0,0,\frac{h}{2}\right)$	% error
4	Present FEM	1.9222	1.63	0.6852	4.83	0.7116	7.33	0.0429	8.72
	Present Analytical	1.9060	2.45	0.7366	2.30	0.7005	5.65	0.0434	7.66
	Pagano and Hatfield (1972)	1.9540	-	0.7200	-	0.6630	-	0.0470	-
	Sahoo and Singh (2014)	1.9016	2.68	0.7149	0.71	0.6391	3.60	0.0467	0.64
	Grover *et al.* (2013b)	1.8935	3.09	0.6650	7.64	0.6322	4.64	0.0441	6.17
	Reddy (1984)	1.8937	3.08	0.6650	7.64	0.6320	4.67	0.0440	6.38
	Akhras *et al.* (1994)	1.8939	3.07	0.6806	5.47	0.6463	2.52	0.0450	4.25
	Ferreira (2005)	1.9075	2.38	0.6420	10.83	0.6228	6.06	0.0441	6.17
	Roque *et al.* (2005)	1.8842	3.57	0.7560	5.00	0.6777	2.22	0.0430	8.51
10	Present FEM	0.7364	0.88	0.5598	0.14	0.4103	2.32	0.0274	2.14
	Present Analytical	0.7360	0.94	0.561	0.36	0.4082	1.79	0.0274	2.14
	Pagano and Hatfield (1972)	0.7430	-	0.5590	-	0.4010	-	0.0280	-
	Sahoo and Singh (2014)	0.721	2.96	0.5682	1.65	0.3962	1.19	0.0276	1.43
	Grover *et al.* (2013b)	0.7147	3.81	0.5456	2.39	0.3888	3.04	0.0268	4.28
	Reddy (1984)	0.7147	3.81	0.5460	2.33	0.3890	2.99	0.0270	3.57
	Akhras *et al.* (1994)	0.7149	3.78	0.5589	0.02	0.3974	0.89	0.0273	2.50
	Ferreira (2005)	0.7309	1.63	0.5496	1.68	0.3956	1.34	0.0273	2.50
	Roque *et al.* (2005)	0.735	1.07	0.5637	0.84	0.4055	1.12	0.0272	2.86

Table 3.5 Non-dimensional transverse shear stresses of four-layered (0/90/90/0) plate subjected to SSL (material property: MM1; non-dimensional parameter: ND1)

a/h	References	$\bar{\tau}_{13}\left(0,\frac{b}{2},0\right)$ (CR)	% error	$\bar{\tau}_{13}\left(0,\frac{b}{2},0\right)$ (EE)	% error	$\bar{\tau}_{23}\left(\frac{a}{2},0,0\right)$ (CR)	% error	$\bar{\tau}_{23}\left(\frac{a}{2},0,0\right)$ (EE)	% error
4	Present FEM	0.2232	1.92	-	-	0.2328	20	-	-
	Present Analytical	0.2298	4.93	0.2109	3.69	0.2281	21.61	0.3150	8.24
	Pagano and Hatfield (1972)	0.2190	-	0.2190	-	0.2910	-	0.2910	-
	Sahoo and Singh (2014)	0.2366	8.04	-	-	0.2913	0.10	-	-
	Grover *et al.* (2013b)	0.2063	5.79	-	-	0.2389	17.90	-	-
	Reddy (1984)	0.2060	5.93	-	-	0.2390	17.86	-	-
	Akhras *et al.* (1994)	0.2109	3.69	-	-	0.2444	16.01	-	-
	Ferreira (2005)	0.2166	1.09	-	-	-	-	-	-
	Roque *et al.* (2005)	0.1885	13.92	-	-	-	-	-	-
10	Present FEM	0.3115	3.48	-	-	0.1473	24.84	-	-
	Present Analytical	0.3138	4.25	0.3001	0.29	0.1453	25.86	0.1996	1.83
	Pagano and Hatfield (1972)	0.3010	-	0.3010	-	0.1960	-	0.1960	-
	Sahoo and Singh (2014)	0.3385	12.45	-	-	0.1963	0.15	-	-
	Grover *et al.* (2013b)	0.2639	12.32	-	-	0.1531	21.88	-	-
	Reddy (1984)	0.2640	12.29	-	-	0.1530	21.93	-	-
	Akhras *et al.* (1994)	0.2697	10.39	-	-	0.1568	20.00	-	-
	Ferreira (2005)	0.2888	4.05	-	-	-	-	-	-
	Roque *et al.* (2005)	0.2908	3.38	-	-	-	-	-	-

It is observed in the table that for a very thick configuration (S = 4), the maximum error in $\bar{\tau}_{13}$ is 6.06 % (analytical) and 6.1 % (FEM) when evaluated using constitutive relationships and 0.042% (analytical) when obtained using the equilibrium equations. Excellent accuracy is also observed in the results of $\bar{\tau}_{23}$ in which the maximum discrepancy is noted to be 1.30% (analytical) for a very thick system (S = 4). The post-processing approach used for predicting the transverse shear stresses is able to predict some of the transverse shear stresses with zero error for some span-thickness ratios.

3.2.5. Three-layered soft-core sandwich plate (0/C/0) subjected to uniform pressure

Here, we consider the same structural configuration of the sandwich plate like that of the previous example. The material properties of the core layer '$[Q]_{core}$' is given by the following constitutive matrix.

$$[Q]_{core} = \begin{bmatrix} 0.999781 & 0.231192 & 0 & 0 & 0 \\ 0.231192 & 0.524886 & 0 & 0 & 0 \\ 0 & 0 & 0.262931 & 0 & 0 \\ 0 & 0 & 0 & 0.26681 & 0 \\ 0 & 0 & 0 & 0 & 0.1559914 \end{bmatrix}$$

The material properties of the face-sheets are obtained by multiplying the properties of the core with a constant 'R', *i.e,* $[Q]_{face-sheets} = R[Q]_{core}$. The mechanical pressure is assumed to act in the form of uniformly distributed variation in both x_1 and x_2-direction. The static responses for this example are presented in Table 3.8 and also compared with the exact elasticity solutions of Srinivas and Rao (1970) and results obtained from various 2 D models in the literature. A fine correlation of the present results with the elasticity results and the results of other references can be observed in the table.

Table 3.6. Non-dimensional deflection and in-plane stresses of sandwich plate (0/C/0) subjected to SSL (material property: MM1 (face-sheets), MM2 (core); non-dimensional parameter: ND1)

a/h	References	$\bar{U}_3\left(\frac{l}{2},\frac{b}{2}\right)$	% error	$\bar{\sigma}_{11}\left(\frac{l}{2},\frac{b}{2},\frac{h}{2}\right)$	% error	$\bar{\sigma}_{22}\left(\frac{l}{2},\frac{b}{2},\frac{h}{2}\right)$	% error	$\bar{\tau}_{12}\left(0,0,\frac{h}{2}\right)$	% error
4	Present FEM	7.6422	0.60	1.5369	1.22	0.2527	2.62	0.1481	3.06
	Present Analytical	7.6305	0.45	1.5589	0.18	0.2528	2.58	0.1485	3.34
	Pagano (1970)*	7.5962	-	1.5560	-	0.2595	-	0.1437	-
	Sahoo and Singh (2014)	7.6351	0.51	1.5503	0.37	0.2549	1.77	0.1469	2.23
	Chalak *et al.* (2012a)	7.5822	0.18	1.5306	1.63	0.2581	0.54	0.1445	0.56
	Pandit *et al.* (2008)	7.6552	0.78	1.5218	2.19	0.2506	3.43	0.1468	2.16
	Singh *et al.* (2011)	7.8556	3.41	1.5488	0.46	-		0.1671	16.28
10	Present FEM	2.2017	0.05	1.1577	0.40	0.1096	0.72	0.0716	1.27
	Present Analytical	2.2012	0.03	1.1553	0.20	0.1092	1.09	0.0714	0.99
	Pagano (1970)*	2.2004	-	1.1530	-	0.1104	-	0.0707	-
	Sahoo and Singh (2014)	2.1999	0.02	1.1680	1.30	0.1105	0.10	0.0712	0.71
	Chalak *et al.* (2012a)	2.1775	1.04	1.1528	0.02	0.1143	3.53	0.0705	0.28
	Pandit *et al.* (2008)	2.002	9.02	1.1483	0.41	0.1086	1.63	0.0709	0.28
	Singh *et al.* (2011)	2.2389	1.75	1.1594	0.56	-	-	0.0707	0.00
20	Present FEM	1.2264	0.00	1.1144	0.15	0.0700	0.00	0.0514	0.58
	Present Analytical	1.2263	0.08	1.1104	0.51	0.0697	0.42	0.0512	0.19
	Pagano (1970)*	1.2264	-	1.1161	-	0.0700	-	0.0511	-
	Sahoo and Singh (2014)	1.2257	0.06	1.1244	0.74	0.0706	0.86	0.0515	0.78
	Chalak *et al.* (2012a)	1.2121	1.17	1.1103	0.52	0.0742	6.00	0.0508	0.58
	Pandit *et al.* (2008)	1.2252	0.10	1.1055	0.95	0.0694	0.86	0.0509	0.39
	Singh *et al.* (2011)	1.2424	1.31	1.1100	0.55	-	-	0.0536	4.89
50	Present FEM	0.9348	0.00	1.1035	0.40	0.0571	0.35	0.0448	0.44
	Present Analytical	0.9348	0.00	1.0991	0.01	0.0569	0.00	0.0446	0.00
	Pagano (1970)*	0.9348	-	1.0990	-	0.0569	-	0.0446	-
	Sahoo and Singh (2014)	0.9338	0.11	1.1134	1.31	0.0576	1.23	0.0451	1.12
	Chalak *et al.* (2012a)	0.9234	1.22	1.0997	0.06	0.0611	7.38	0.0443	0.67
	Pandit *et al.* (2008)	0.9341	0.08	1.0948	0.38	0.0566	0.53	0.0445	0.22
	Singh *et al.* (2011)	0.9458	1.18	1.1050	0.55	-	-	0.0465	4.26
100	Present FEM	0.8924	0.07	1.102	0.36	0.0552	0.00	0.0439	1.38
	Present Analytical	0.8924	0.07	1.0975	0.04	0.0550	0.36	0.0437	0.92
	Pagano (1970)*	0.8917	-	1.0980	-	0.0552	-	0.0433	-
	Sahoo and Singh (2014)	0.8921	0.05	1.1119	1.27	0.0557	0.91	0.0442	2.08
	Chalak *et al.* (2012a)	0.8814	1.16	1.0982	0.02	0.0592	7.25	0.0433	0.00
	Pandit *et al.* (2008)	0.8917	0.00	1.1093	1.03	0.0547	0.91	0.0434	0.23
	Singh *et al.* (2011)	0.9017	1.12	1.1020	0.36	-	-	0.0453	4.62

*Elasticity Solutions

Table 3.7. Non-dimensional transverse shear stresses of sandwich plate (0/C/0) subjected to SSL (material property: MM1 (face-sheets), MM2 (core); non-dimensional parameter: ND1)

a/h	References	$\bar{\tau}_{13}\left(0,\frac{b}{2},0\right)$ (CR)	% error	$\bar{\tau}_{13}\left(0,\frac{b}{2},0\right)$ (EE)	% error	$\bar{\tau}_{23}\left(\frac{a}{2},0,0\right)$ (CR)	% error	$\bar{\tau}_{23}\left(\frac{a}{2},0,0\right)$ (EE)	% error
	Present FEM	0.2536	6.10	-	-	0.1162	8.39	-	-
	Present Analytical	0.2535	6.06	0.2389	0.04	0.1170	9.10	0.1058	1.30
	Pagano (1970)*	0.2390	-	0.2390	-	0.1072	-	0.1072	-
4	Sahoo and Singh (2014)	0.2225	6.90	-	-	0.0913	14.83	-	-
	Chalak *et al.* (2012a)	0.2436	1.92	-	-	0.1147	6.99	-	-
	Pandit *et al.* (2008)	0.2520	5.43	-	-	0.1156	7.83	-	-
	Singh *et al*. (2011)	0.2611	9.24	-	-	-	-	-	-
	Present FEM	0.3184	6.13	-	-	0.0573	8.72	-	-
	Present Analytical	0.3177	5.9	0.3000	0	0.0576	9.29	0.0523	0.75
	Pagano (1970)*	0.3000	-	0.3000	-	0.0527	-	0.0527	-
10	Sahoo and Singh (2014)	0.2821	5.96	-	-	0.0454	13.85	-	-
	Chalak *et al.* (2012a)	0.3058	1.93	-	-	0.0575	9.10	-	-
	Pandit *et al.* (2008)	0.3158	5.26	-	-	0.0570	8.15	-	-
	Singh *et al*. (2011)	0.3287	9.56	-	-	-	-	-	-
	Present FEM	0.337	6.17	-	-	0.0393	8.86	-	-
	Present Analytical	0.3362	5.92	0.3174	0	0.0396	9.69	0.0360	0.27
	Pagano (1970)*	0.3174	-	0.3174	-	0.0361	-	0.0361	-
20	Sahoo and Singh (2014)	0.2986	5.92	-	-	0.0315	12.74	-	-
	Chalak *et al.* (2012a)	0.3272	3.08	-	-	0.0399	10.52	-	-
	Pandit *et al.* (2008)	0.3342	5.29	-	-	0.0392	8.58	-	-
	Singh *et al*. (2011)	0.3429	8.03	-	-	-		-	-
	Present FEM	0.3431	6.22	-	-	0.0334	9.15	-	-
	Present Analytical	0.3422	5.94	0.3231	0.03	0.0336	9.80	0.0305	0.32
	Pagano (1970)*	0.3230	-	0.3230	-	0.0306	-	0.0306	-
50	Sahoo and Singh (2014)	0.3040	5.88	-	-	0.0270	11.76	-	-
	Chalak *et al.* (2012a)	0.3300	2.16	-	-	0.0341	11.43	-	-
	Pandit *et al.* (2008)	0.3403	5.35	-	-	0.0333	8.82	-	-
	Singh *et al*. (2011)	0.3617	11.98	-	-	-		-	-
	Present FEM	0.344	13.15	-	-	0.0325	9.42	-	-
	Present Analytical	0.3431	12.86	0.3240	6.57	0.0327	10.10	0.0297	0
	Pagano (1970)*	0.3040	-	0.3040	-	0.0297	-	0.0297	-
100	Sahoo and Singh (2014)	0.3048	0.26	-	-	0.0263	11.44	-	-
	Chalak *et al.* (2012a)	0.3426	12.69	-	-	0.0332	11.78	-	-
	Pandit *et al.* (2008)	0.3412	12.23	-	-	0.0324	9.09	-	-
	Singh *et al*. (2011)	0.4079	34.17	-	-	-		-	-

CR: Constitutive relation; EE: Equilibrium equation; * Elasticity Solutions

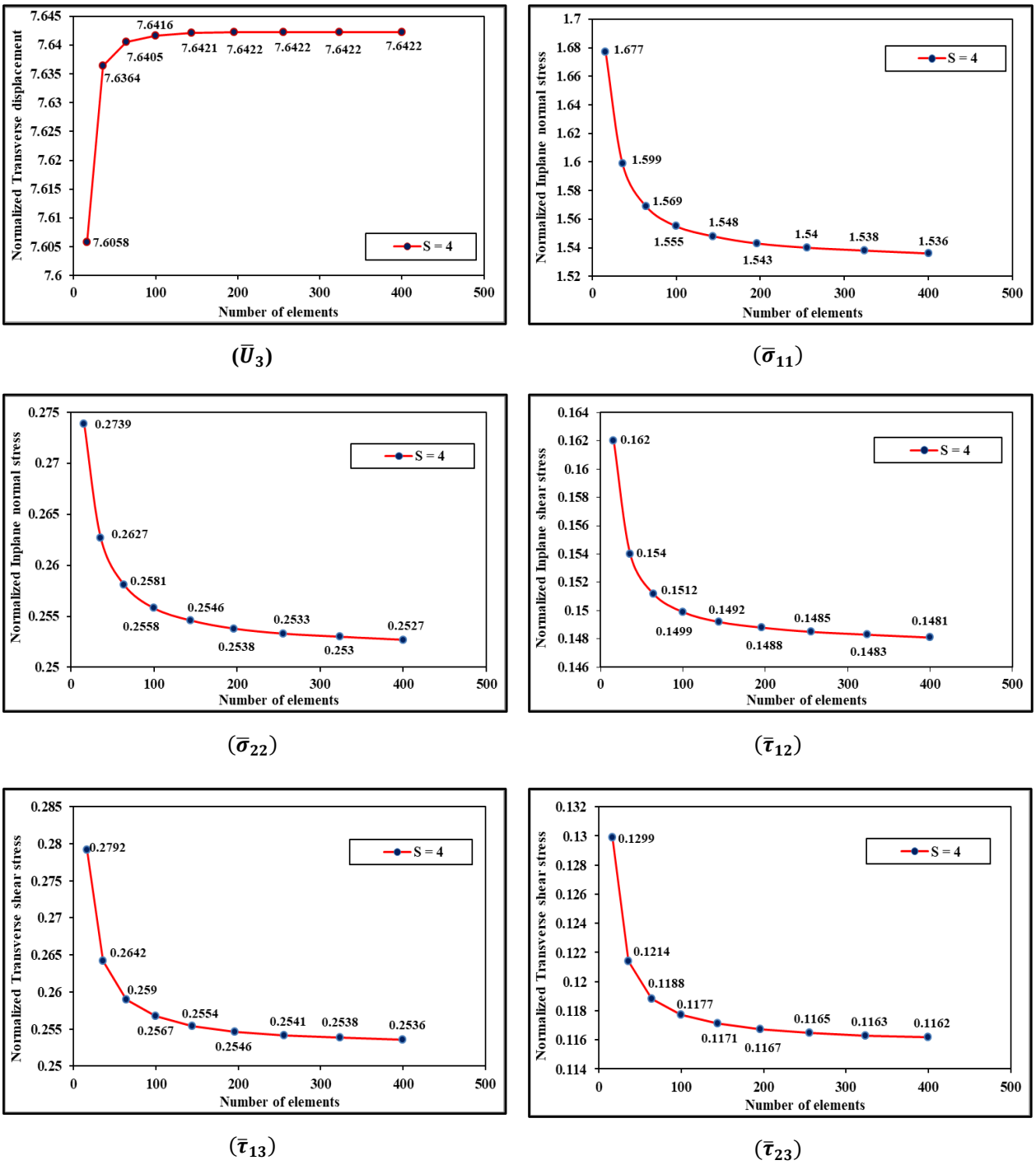

Figure 3.7: Convergence of the normalized FE results of 0/C/0 sandwich plate subjected to SSL (material property: MM1 (face-sheets), MM2 (core); non-dimensional parameter: ND1)

3.2.6. Five-layered square and rectangular symmetric sandwich plate (0/90/C/90/0) subjected to SSL

In this example, two thin face sheets (0/90) are symmetrically placed at the top and bottom of the core layer (C). The thickness of the core layer remains the same like that of the previous sandwich plate, *i.e*, 0.8h and the thickness of each face sheet has now reduced to 0.05h. Therefore, the total number of layers has now increased from three to five. The static responses of the five-layered symmetric sandwich plate for both square and rectangular shapes are collected in Table 3.9. For comparison, the elasticity results of Pagano (1970) and the results of Pandit *et al*. (2010a) obtained using a polynomial ZZ theory are also collected in the table. An excellent agreement of the present responses of the transverse displacement ($\bar{U}_3$) can be observed in the table with an error of 0.212 % (analytical) and 0.124 % (FEM) for *b*/*l* = 2 and *l*/*h* = 10. Also, the discrepancies noted for other span-thickness ratios and aspect ratios are less than 1% in both analytical and FE solutions. The in-plane stresses are very close to the exact solutions (Pagano, 1970) with an error of 0.377% (analytical) and 0.586 % (FEM) in $\bar{\sigma}_{11}$ for a square and thick (*S* = 10) plate configuration, and 7.723 % (analytical) and 8.118 % (FEM) in $\bar{\sigma}_{22}$ for a square and thin (*S* = 100) plate configuration. The maximum error reported in the results of Pandit *et al*. (2010a) is 0.383% in $\bar{\sigma}_{11}$ and 7.129 % in $\bar{\sigma}_{22}$ for a square and thin (*S* = 100) plate configuration. The performance of the present model is again observed to be excellent while deriving the transverse shear stresses using the 3 D equilibrium equations of elasticity. The maximum error associated with the results of transverse shear stresses is observed to be 0.447% using the equilibrium equations whereas the maximum error noted using the constitutive relationships is 8.388%.

3.2.7. Five-layered anti-symmetric sandwich plate (0/90/C/0/90) subjected to SSL

In this example, the face sheets (0/90) are placed at the top and bottom of the core layer in an anti-symmetric fashion so that the effects of the coupling between the force and moment resultants to the mid-plane strains and curvatures on the static responses can be examined. The surface tractions are sinusoidal in both x_1 and x_2-direction. The static responses of the sandwich plate are presented in Table 3.10 along with the results of Pagano (1970) and Khandelwal *et al*. (2013a). The results of Pagano (1970) are exact elasticity solutions while the results of Khandelwal *et al*. (2013a) are FE solutions obtained by exploiting a higher-order ZZ theory. The present responses are observed to be more close to the elasticity solutions (Pagano, 1970) than the results of Khandelwal *et al*. (2013a). The responses of the anti-symmetric sandwich plate are not significantly different from those of the symmetric sandwich plate considered in the previous example as the thickness of the face sheets is very small.

3.3. Static analysis of smart composite plates

In this section, the coupled electromechanical static responses of smart composite plates with piezoelectric actuators and sensors are presented using TZZT. PVDF and PFRC are considered as the piezoelectric materials acting as distributed actuators and sensors. Electromechanical loads are assumed to act on the top surface of the smart composite plate and can have a uniform and a doubly sinusoidal variation in the spatial domain.

3.3.1. Static analysis of five-layered smart composite plate with PVDF actuator and sensor (PVDF/0/90/0/PVDF) subjected to electromechanical load

Smart composite plates are integrated with smart materials to form smart composites and the structures have self-controlling and self-monitoring capabilities. Piezoelectric materials are one of the smart materials which are widely used with the traditional

composites to control the static and dynamic responses of the smart laminated composite plates. In this example, we wish to accurately model the static coupled electromechanical responses of a smart composite plate with a PVDF actuator and a sensor placed at the top and bottom of the laminated composite plate. The PVDF layers, under the piezoelectric coefficients e_{31} and e_{32} will generate electrical forces when electrical voltages (V) are applied. These forces are responsible for the actuation in the static responses of the smart laminated composite plates. The material and geometrical properties of the PVDF actuator/sensor and the laminated plate are obtained from Tzou and Tseng (1990) and Pagano (1970), respectively. The electrical (V) and mechanical loads (q_{mn}) are assumed to be sinusoidal in both x_1 and x_2-direction. The non-dimensional transverse deflection ($\overline{U}_3$) and the in-plane stress ($\bar{\sigma}_{11}$) for span-thickness ratios, S = 10 and 100 are presented in Table 3.11. The results corresponding to only mechanical load (q_{mn} =10 N/m^2; V = 0) and electromechanical load (q_{mn} =10 N/m^2; V = 100) are presented in the same table so that the actuation in the responses due to the electrical loads can be realized. The responses are also compared with the elasticity solutions reported by Ray *et al*. (1993) and numerically obtained results based on a higher-order ZZ theory by Khandelwal *et al*. (2013c) with FEM. It is observed in the table that the present results are in close agreement with the exact solutions (Ray *et al*., 1993) and the results reported by Khandelwal *et al*. (2013c). The actuation in the responses can be observed in the table due to the presence of the piezoelectric layers when the electromechanical load (q_{mn} =10 N/m^2; V = 100) is applied as the transverse displacement increases by 2.893 times the static deflection when purely mechanical load (q_{mn} =10 N/m^2; V = 0) is applied on the top surface of the plate.

Table 3.8. Non-dimensional deflection and stresses of sandwich plate (0/C/0) subjected to uniform pressure (S = 10)) (non-dimensional parameter: ND9)

R	References	$(\bar{U}_3)$	$(\bar{\sigma}_{11}^1)$	$(\bar{\sigma}_{11}^2)$	$(\bar{\sigma}_{11}^3)$	$(\bar{\sigma}_{22}^1)$	$(\bar{\sigma}_{22}^2)$	$(\bar{\sigma}_{22}^3)$	$(\bar{\tau}_{13}^1)$
	Present FEM	259.2693	60.5143	46.7165	9.3433	38.6522	30.2347	6.0469	4.5113
	Present Analytical	259.2695	60.3308	46.5819	9.3164	38.5462	30.1574	6.0315	4.4546
	Srinivas and Rao (1970)	258.9700	60.3530	46.6230	9.3400	38.4910	30.0970	6.1610	4.3640
	Sahoo and Singh (2014)	258.7963	59.9393	47.4492	9.4898	38.4414	30.5516	6.1100	3.7000
5	Grover *et al*. (2013a)	256.9900	60.4560	46.9898	9.3980	38.5026	30.2357	6.0472	-
	Pandya and Kant (1988)	256.1300	62.3800	46.9100	9.3820	38.9300	30.3300	6.0650	3.0890
	Xiang *et al*. (2009)	253.9890	60.1230	47.0970	9.4190	38.2490	30.1870	6.0370	-
	Ferreira (2005)	257.5230	59.9675	46.2906	9.2581	38.3209	29.9740	5.9948	4.0463
	Roque *et al*. (2005)	259.1200	60.3400	46.5700	9.3100	38.5500	30.1500	6.0290	4.5400
	Present FEM	159.5935	65.4819	48.9298	4.8930	43.8068	33.6255	3.3626	4.2346
	Present Analytical	159.5937	65.2830	48.7900	4.8790	43.6857	33.5410	3.3541	4.1791
	Srinivas and Rao (1970)	159.3800	65.3320	48.8570	4.9030	43.5660	33.4130	3.5000	4.0950
	Sahoo and Singh (2014)	159.2702	63.9471	50.7720	5.0722	42.4400	33.7975	3.3797	3.5810
10	Grover *et al*. (2013a)	154.5100	65.4849	49.9066	4.9907	43.2900	33.5994	3.3600	-
	Pandya and Kant (1988)	152.3300	64.6500	51.3100	5.1310	42.8300	33.9700	3.3970	3.1470
	Xiang *et al*. (2009)	153.1390	65.0500	50.2060	5.0200	43.0150	33.6530	3.3650	-
	Ferreira (2005)	158.3799	64.8462	48.4434	4.8443	43.3989	33.3062	3.3306	3.9237
	Roque *et al*. (2005)	159.5000	65.2800	48.2800	4.8800	43.6800	33.5200	3.3500	4.2900
	Present FEM	121.9009	66.9234	48.3547	3.2236	46.7060	35.2054	2.3470	4.0964
	Present Analytical	121.9010	66.7210	48.2169	3.2145	46.5763	35.1171	2.3411	4.0420
	Srinivas and Rao (1970)	121.7200	66.7870	48.2990	3.2320	46.4240	34.9550	2.4940	3.9638
	Sahoo and Singh (2014)	122.2913	61.4680	49.0106	3.2674	44.5400	35.6105	2.3740	3.4933
15	Grover *et al*. (2013a)	114.5050	67.0400	50.2160	3.3477	45.6768	35.1074	2.3405	-
	Pandya and Kant (1988)	110.4300	66.6200	51.9700	3.4650	44.9200	35.4100	2.3610	3.0350
	Xiang *et al*. (2009)	113.9640	66.5440	50.6790	3.3780	45.4310	35.2780	2.3510	-
	Ferreira (2005)	120.9883	66.2911	47.8992	3.1933	46.2924	34.8898	2.3260	3.8311
	Roque *et al*. (2005)	121.8800	66.7300	48.2000	3.2100	46.5900	35.1100	2.3400	4.1668

It is also observed in the table that the structural responses under the action of only mechanical load and electromechanical load do not have much differences for very thin plate (S = 100). The probable reason behind this is that a thin plate when subjected to mechanical load experiences higher deflection and generates a larger amount of stresses in comparison to the thick plates due to lower flexural rigidity. The deflection and stresses are counteracted by the electrical loads by the application of the voltages. As the voltage 'V' applied in both the cases of thick and thin plates is constant, therefore a greater part of the electrical load is required to counteract the deflection and stresses for the thin plates, resulting in smaller net deflection and stresses.

Next, the transverse deflection ($\bar{U}_3$) for various span-thickness ratios and electromechanical loads are presented in Figure 3.8 and compared with the exact solutions of Ray *et al*. (1993). The responses are observed to be in excellent agreement with the exact solutions. The through-thickness variations of the in-plane displacement ($\bar{U}_1$) are presented in Figure 3.9a for various electromechanical loads. It is observed that by changing the polarity of the electrical loads, the PVDF layers cause a reversal effect on the in plane displacement ($\bar{U}_1$). Now, we wish to evaluate the total amount of electrical load required to completely eradicate the transverse displacement from the plate by applying electrical loads. This will also ensure the static deflection controlling capacity of the piezoelectric patch. Therefore, the static deflection control of a thick same smart composite plate (S =10) is shown in Figure 3.9b by eradicating the mechanical deflection with counteracting electrical loads. It is observed in the figure that an electrical voltage (V) of 25.5 V suppresses the mechanical deflection of the smart composite plate.

Table 3.9. Non-dimensional deflection and stresses of five layered symmetric sandwich (0/90/C/90/0) plate subjected to SSL (material property: MM1 (face-sheets), MM2 (core); non-dimensional parameter: ND1)

b/a	a/h	References	$\bar{U}_3\left(\frac{l}{2},\frac{b}{2}\right)$	$\bar{\sigma}_{11}\left(\frac{l}{2},\frac{b}{2},\frac{h}{2}\right)$	$\bar{\sigma}_{22}\left(\frac{l}{2},\frac{b}{2},\frac{h}{2}\right)$	$\bar{\tau}_{13}\left(0,\frac{b}{2},0\right)$ (CR)	$\bar{\tau}_{13}\left(0,\frac{b}{2},0\right)$ (EE)	$\bar{\tau}_{23}\left(\frac{a}{2},0,0\right)$ (CR)	$\bar{\tau}_{23}\left(\frac{a}{2},0,0\right)$ (EE)	$\bar{\tau}_{12}\left(0,0,\frac{h}{2}\right)$
1	100	Present FEM	0.8867	1.1018	0.0546	0.1997	-	0.1824	-	0.0436
		% error	[0.000]	[0.400]	[8.118]	[7.945]	-	[8.120]	-	[0.460]
		Present Analytical	0.8866	1.0975	0.0544	0.2002	0.185	0.1816	0.1687	0.0434
		% error	[0.011]	[0.009]	[7.723]	[8.216]	[0]	[7.647]	[0]	[0]
		Pagano (1970)	0.8867	1.0974	0.0505	0.185	0.185	0.1687	0.1687	0.0434
		Pandit *et al.* (2010a)	0.886	1.0932	0.0541	0.1981	-	0.181	-	0.0432
		% error	[0.079]	[0.383]	[7.129]	[7.081]	-	[7.291]	-	[0.461]
	10	Present FEM	1.7227	1.135	0.0612	0.1984	-	0.1832	-	0.0473
		% error	[0.075]	[0.586]	[3.164]	[7.884]	-	[8.146]	-	[0.424]
		Present Analytical	1.7219	1.146	0.0608	0.1991	0.1839	0.1823	0.1692	0.0473
		% error	[0.122]	[0.377]	[3.797]	[8.265]	[0]	[7.615]	[0.118]	[0.425]
		Pagano (1970)	1.724	1.1417	0.0632	0.1839	0.1839	0.1694	0.1694	0.0471
		Pandit *et al.* (2010a)	1.7209	1.138	0.0606	0.1968	-	0.1817	-	0.0471
		% error	[0.18]	[0.324]	[4.114]	[7.015]	-	[7.261]	-	[0]
2	100	Present FEM	1.6126	1.9903	0.0398	0.3398	-	0.0536	-	0.0397
		% error	[0.006]	[0.403]	[0.251]	[8.010]	-	[7.847]	-	[0.252]
		Present Analytical	1.6126	1.9824	0.0397	0.3409	0.3146	0.0534	0.0497	0.0396
		% error	[0.006]	[0.005]	[0]	[8.36]	[0]	[7.445]	[0]	[0]
		Pagano (1970)	1.6127	1.9823	0.0397	0.3146	0.3146	0.0497	0.0497	0.0396
		Pandit *et al.* (2010a)	1.6118	1.9751	0.0395	0.3376	-	0.0531	-	0.0394
		% error	[0.056]	[0.363]	[0.504]	[7.311]	-	[6.841]	-	[0.505]
	10	Present FEM	2.9675	1.9951	0.0497	0.331	-	0.0721	-	0.0496
		% error	[0.124]	[0.607]	[4.606]	[8.028]	-	[7.451]	-	[0.404]
		Present Analytical	2.9649	2.0126	0.0497	0.3321	0.3064	0.0718	0.0668	0.0496
		% error	[0.212]	[0.264]	[4.607]	[8.388]	[0]	[7.004]	[0.447]	[0.405]
		Pagano (1970)	2.9712	2.0073	0.0521	0.3064	0.3064	0.0671	0.0671	0.0494
		Pandit *et al.* (2010a)	2.9652	2.0001	0.0494	0.3284	-	0.0716	-	0.0493
		% error	[0.202]	[0.359]	[5.182]	[7.18]	-	[6.706]	-	[0.202]

Table 3.10. Non-dimensional deflection and stresses of five-layered anti-symmetric sandwich plate (0/90/C/0/90) under SSL
(material properties: MM1 (face-sheets), MM2 (core); non-dimensional parameter: ND1)

a/h	References	$\bar{U}_3\left(\frac{l}{2},\frac{b}{2}\right)$	$\bar{\sigma}_{11}\left(\frac{l}{2},\frac{b}{2},\frac{h}{2}\right)$	$\bar{\tau}_{13}\left(0,\frac{b}{2},0\right)$ (CR)	$\bar{\tau}_{13}\left(0,\frac{b}{2},0\right)$ (EE)	$\bar{\tau}_{23}\left(\frac{a}{2},0,0\right)$ (CR)	$\bar{\tau}_{23}\left(\frac{a}{2},0,0\right)$ (EE)
10	Present FEM	1.7252	1.095	0.1913	-	0.1913	-
	% error	[0.115]	[0.472]	[8.079]	-	[8.079]	-
	Present Analytical	1.7249	1.1039	0.191	0.1769	0.191	0.1769
	% error	[0.133]	[-0.336]	[-7.91]	[0.056]	[-7.91]	[0.056]
	Pagano (1970)	1.7272	1.1002	0.177	0.177	0.177	0.177
	Khandelwal *et al*. (2013a)	1.7177	1.127	0.1909	0.1741	0.1883	0.1714
	% error	[0.55]	[-2.436]	[-7.853]	[1.638]	[-6.384]	[3.164]
100	Present FEM	0.8888	1.0542	0.1916	-	0.1916	-
	% error	[0.00]	[1.326]	[8.065]	-	[8.065]	-
	Present Analytical	0.8888	1.05	0.1913	0.1773	0.1913	0.1773
	% error	[0.00]	[-0.923]	[-7.896]	[0]	[-7.896]	[0]
	Pagano (1970)	0.8888	1.0404	0.1773	0.1773	0.1773	0.1773
	Khandelwal *et al*. (2013a)	0.8782	1.082	0.1878	0.1751	0.1812	0.1734
	% error	[1.193]	[-3.998]	[-5.922]	[1.241]	[-2.2]	[2.2]

Table 3.11. Normalized static transverse deflection and inplane normal stress of PVDF/0/90/0/PVDF plate structure subjected to sinusoidal electromechanical load
(material property: MM3 (substrate), MP1 (piezoelectric layer); non-dimensional parameter: ND1)

References	q_{mn} =10 N/m^2; V = 0			q_{mn} =10 N/m^2; V = 100		
	$\bar{U}_3$	$\bar{\sigma}_{11}$ (top)	$\bar{\sigma}_{11}$ (bottom)	$\bar{w}$	$\bar{\sigma}_{11}$ (top)	$\bar{\sigma}_{22}$ (bottom)
l/h = 10						
Present FEM	0.7698	0.6029	-0.6029	-2.2126	-2.9557	1.5744
Present Analytical	0.7691	0.6045	-0.6045	-2.2252	-2.8738	1.4981
Ray *et al*. (1993)	0.774	0.589	-0.589	-2.35	-3.12	1.48
Khandelwal *et al*. (2013c)[1]	0.754	0.593	-0.593	-2.21	-2.971	1.587
l/h = 100						
Present FEM	0.4464	0.5511	-0.5511	0.4242	0.5168	-0.5306
Present Analytical	0.4464	0.5489	-0.5489	0.4242	0.5147	-0.5285
Ray *et al*. (1993)	0.471	0.538	-0.538	0.447	0.518	-0.504
Khandelwal *et al*. (2013c)[1]	0.434	0.542	-0.542	0.412	0.521	-0.507

[1] Polynomial ZZ theory

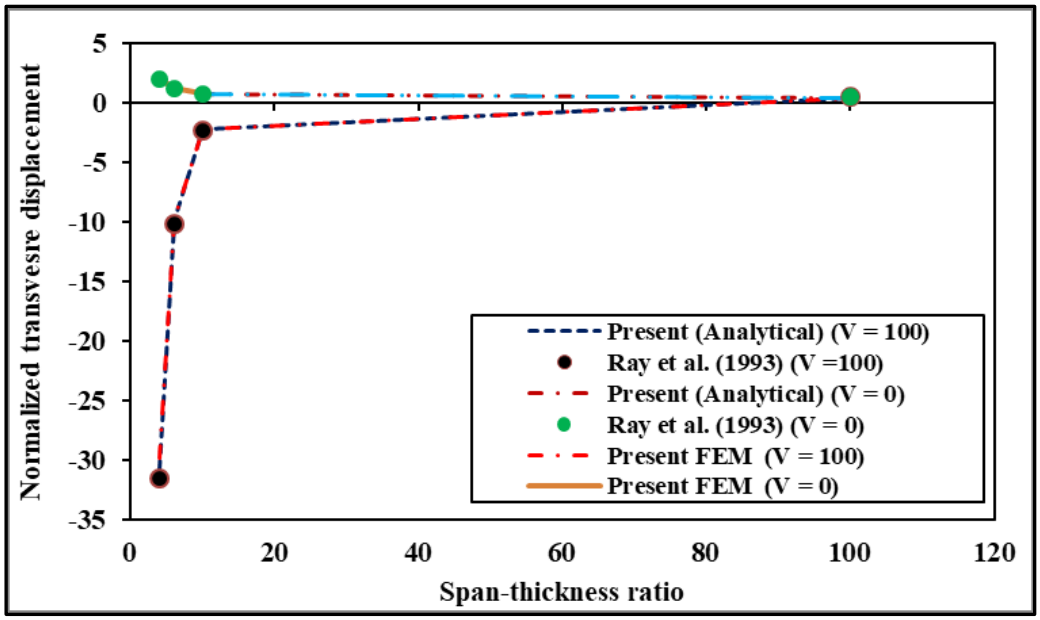

Figure 3.8. Non-dimensional transverse displacement of a five-layered smart laminated plate (PVDF/0/90/0/PVDF) subjected to sinusoidal electromechanical load (material property: MM3 (substrate), MP1 (piezoelectric layer); non-dimensional parameter: ND1)

3.3.2. Static analysis of four-layered smart composite plate with PFRC actuator (PFRC/0/90/0) subjected to electromechanical load of sinusoidal variation

We now consider a relatively new piezoelectric material namely, the piezoelectric fiber-reinforced composite (PFRC) as the actuator of the smart composite plate. The effective coefficients of the PFRC layer are derived by Mallik and Ray (2003) in which they have found out that the piezoelectric coefficient 'e_{31}' that couples the in-plane stress '$\bar{\sigma}_{11}$' and the constant electric field 'E_3' in the thickness direction is comparatively higher than the conventional piezoelectric materials. The piezoelectric constant 'e_{31}' is responsible for the actuation in the normal stress '$\bar{\sigma}_{11}$' when an electric field is applied in the thickness direction of the PFRC layer. Since the piezoelectric coefficient 'e_{31}' is higher in PFRC, therefore, such materials can be used as an efficient distributed actuator for the smart composite plates.

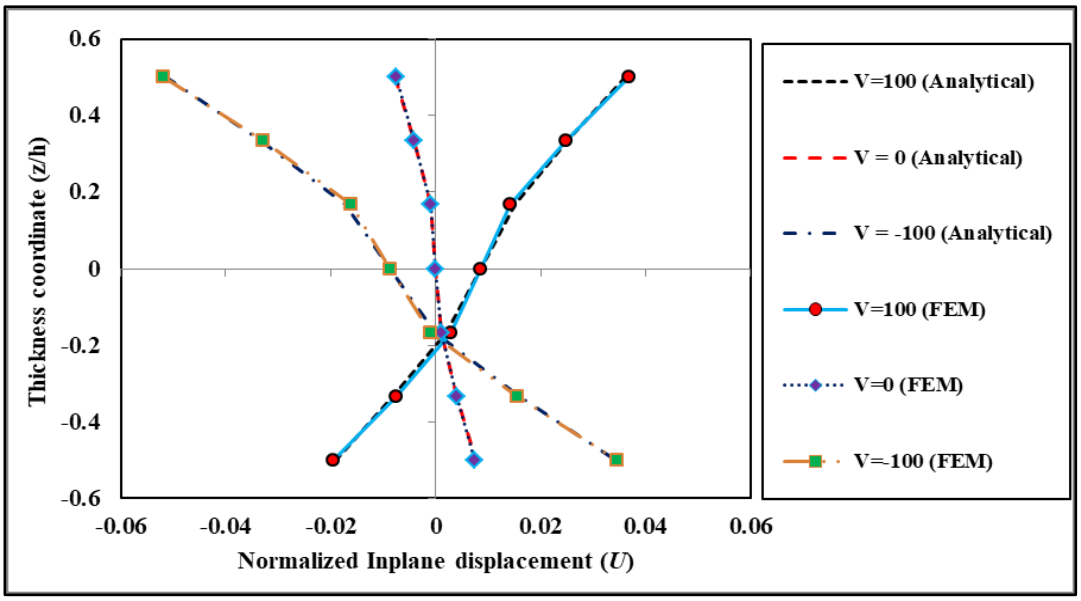

(a)

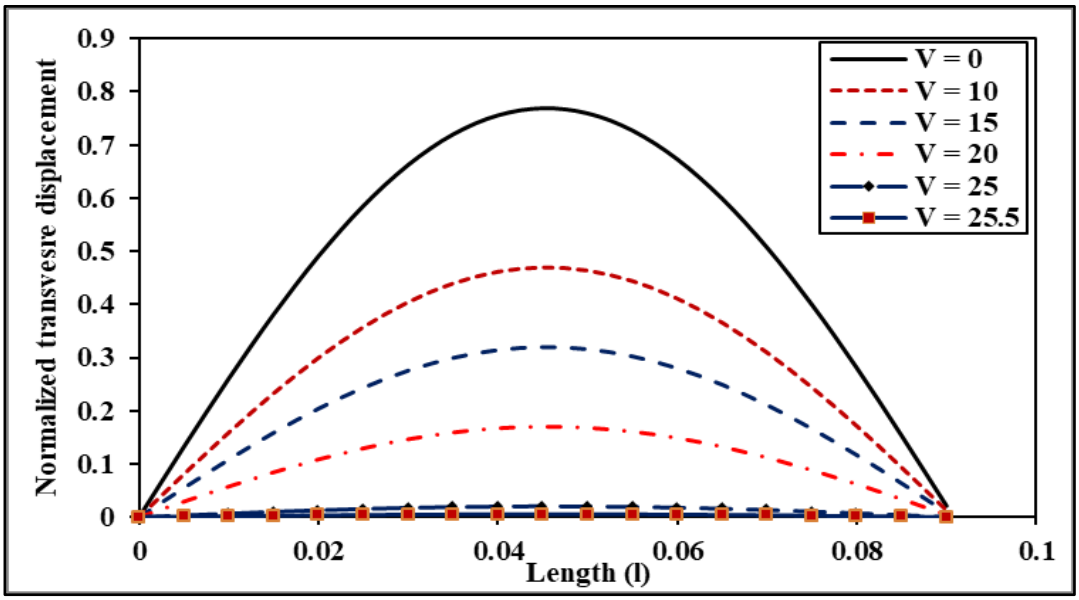

(b)

Figure 3.9(a). Through thickness variation of normalized in-plane displacement ($\bar{U}$) of a smart composite plate (PVDF/0/90/0/PVDF) for various electrical loadings. (b). Static deflection control of a PVDF/0/90/0/PVDF plate (material property: MM3 (substrate), MP1 (piezoelectric layer); non-dimensional parameter: ND1)

In this example, the actuation in the static responses of smart composite plates is examined subjected to pure mechanical loads and electromechanical loads. A three-layered traditional laminated composite plate with a ply thickness of 1 *mm* each is considered. The PFRC layer is placed at the top of the plate surface and the electromechanical loads are assumed to be sinusoidal in both x_1 and x_2-direction. The material properties of the laminated composite plate and the PFRC layer are obtained from Mallik and Ray (2004). The static responses in the form of in-plane displacements and transverse displacements for various span-thickness ratios are collected in Table 3.12. For comparison, the exact elasticity solutions obtained by Mallik and Ray (2004) and solutions obtained with ESL-based theories by Shiyekar and Kant (2011), Ray and Mallik (2004) and Rouzegar and Abad (2015) are also provided in the table. It is observed in the table that the present responses are very close to the elasticity solutions (Mallik and Ray, 2004). The transverse displacement responses are in excellent agreement with the elasticity solutions (Mallik and Ray, 2004) with a maximum discrepancy of 1.91 % (analytical) and 1.94 % (FEM) for a thin smart system. For the thick smart systems subjected to electromechanical loads, the present model shows remarkable performance as the maximum discrepancy noted in the results are 0.03 % (analytical) and 1.48 % (FEM). The discrepancies in the results of Ray and Mallik (2004), Shiyekar and Kant (2011) and Rouzegar and Abad (2015) are found to be 7.85 %, 2.89 % and 3.35 %, respectively. The mathematical model adopted by Ray and Mallik (2004) is the FSDT whereas Shiyekar and Kant (2011) and Rouzegar and Abad (2015) have adopted ESL-based HSDTs with different order of through-thickness variations of in-plane and transverse displacement. The HSDT in Shiyekar and Kant (2011) has a cubic expansion of all the displacement components (U_1, U_2 and U_3) in the thickness direction. Therefore, the effect of the transverse normal strain (ε_{33}) is considered in their

work. The problem considered in this example does not show significant thickness stretching of normal in the results of transverse displacement, thus the effects of transverse normal strains are negligible. It is shown by Kant and Swaminathan (2002) that in problems where the thickness stretching effects are insensitive, the mathematical models discarding the effects of transverse normal strain produces more efficient responses than those which incorporate the effects of the transverse normal strain even at low span-thickness ratio. Therefore, the present responses are more efficient than those produced by Shiyekar and Kant (2011). Rouzegar and Abad (2015) used the ESL based-four-variable HSDT of Shimpi (2002) in which the non-linear nature of the transverse shear strains are accommodated using a polynomial shear strain function, *i.e*, $f(z) = x_3\left(\frac{1}{4} - \frac{5}{3}\frac{{x_3}^2}{h^2}\right)$. The present shear strain function is a non-polynomial function of the form, $f(z) = x_3 \sec\left(\frac{rx_3}{h}\right)$. It can be shown that the present shear strain function is richer than the shear strain function used in Rouzegar and Abad (2015). The expansion of the present shear-strain function can be written in the following manner with the help of the Maclaurin series.

$$x_3 \sec(rx_3/h) = x_3\left(1 + \left(\frac{rx_3}{h}\right)^2\frac{1}{2} + \left(\frac{rx_3}{h}\right)^4\frac{5}{24} + \left(\frac{rx_3}{h}\right)^6\frac{61}{720}\ldots\ldots\ldots\infty\right) \quad 3.1$$

Shimpi (2002), Rouzegar and Abad (2015)

$$x_3\left(\frac{1}{4} - \frac{5}{3}\frac{{x_3}^2}{h^2}\right) = \frac{x_3}{4} - \frac{5{x_3}^3}{3h^2} \quad 3.2$$

It is observed from the expansions that the present shear strain function has implicitly accommodated the higher-order bending modes given by the odd powered terms of x_3. However, the shear strain function used in Rouzegar and Abad (2015) has only two higher-order terms. This can be the probable reason for obtaining more efficient responses with the present model in comparison to the HSDTs used in Rouzegar and Abad (2015) and

Shiyekar and Kant (2011). Also, the inter-laminar continuity conditions of transverse shear stresses are not satisfied at the interfaces in these works which can be another reason for more accurate responses obtained from the present model. From the actuation point of view, we observe in Table 3.12 that the responses of transverse displacement ($\bar{U}_3$) when subjected to electromechanical load $\left(q_{mn} = 40\frac{N}{m^2}; V = 100\right)$ have increased to 189.28 times the static deflection of a thick smart plate (S = 10) when subjected to purely mechanical load $\left(q_{mn} = 40\frac{N}{m^2}; V = 0\right)$. Even the in-plane response at the top surface of the thick plate subjected to electromechanical load have significant actuation of 428.95 times the in-plane response of the same plate subjected to purely mechanical load. The in-plane normal stresses for various span-thickness ratios and electromechanical loads are presented in Table 3.13. As expected, the value of $\bar{\sigma}_{11}$ for a thick activated smart composite plate (S =10, V = 100, $q_{mn} = 40\frac{N}{m^2}$) has increased to 425.48 times the value of $\bar{\sigma}_{11}$ at the top surface of the inactivated thick smart composite plate (S =10, V = 0, $q_{mn} = 40\frac{N}{m^2}$). It is also visible in the table that the increase in the magnitudes of $\bar{\sigma}_{11}$ is more than $\bar{\sigma}_{22}$. The probable reason for this is the placement of the piezoelectric fibers in the global x_1-direction in the PFRC layer. Also, the piezoelectric coefficient 'e_{31}' that couples the normal stress $\bar{\sigma}_{11}$ and the electric field 'E_3' is significantly higher than the coefficient 'e_{32}' which is zero in this case. The values of $\bar{\sigma}_{22}$ is much more at the interfaces of the smart composite plate due to the placement of graphite fibers at an angle of 90^0 to the global x_1-axis. Present results of in-plane normal stress '$\bar{\sigma}_{11}$' and '$\bar{\sigma}_{22}$' deviate by 9.82 % and 0.34 % (analytical), and 5.75 % and 3.03 % (FEM) at the top surface of the plate for a span-thickness ratio of 10. The higher deviations in the values of $\bar{\sigma}_{11}$ may be attributed to the selection of the present shear strain function which produces more consistent responses of $\bar{\sigma}_{22}$. It is also reflected in the

works produced by Grover *et al*. (2013a) and Aydogdu (2009) that the various shear strain functions have a different level of accuracy while predicting the stresses. For moderately thick and thin smart composite systems, the discrepancies are found to reduce and the overall performance of the present model is quite appreciable. In-plane shear stress and the transverse shear stresses are tabulated in Table 3.14. The in plane shear stress ($\bar{\tau}_{12}$) and the transverse shear stresses $(\bar{\tau}_{13,}\bar{\tau}_{23})$ have deviations of 5.86 %, 1.67 % and 3.5 % from the exact elasticity solutions (Mallik and Ray, 2004) for S =10, respectively. The through-thickness variation of the in-plane displacement 'U_1' for S = 100 and various magnitudes of electromechanical loads are shown in Figure 3.10. The maximum value of U_1 is at the top surface of the smart composite when electromechanical loads are applied. The presence of the PFRC layer and the application of electric voltages at the top surface of the actuator are responsible for the higher magnitudes of U_1 at the top surface and not at the bottom surface. Also, it is visible in the figure that the mid-plane experiences some amount of stretching when the PFRC layer gets activated on the application of the electric voltages due to the bending-extensional coupling stiffness. Figure 3.11 shows the across variations of the in-plane normal stresses. It is observed in Figure 3.11a and 3.11b that the maximum value of $\bar{\sigma}_{11}$ is at the extreme surfaces of the smart composite plates whereas the maximum value of $\bar{\sigma}_{22}$ is at the interfaces of the plate, a behavior that is similar to the traditional laminated composite plates. However, we observe in Figure 3.12a that when the combined mechanical and electrical loadings are applied, the across variations of $\bar{\tau}_{13}$ are significantly different from those of the traditional laminated plates. The maximum value of $\bar{\tau}_{13}$ is attained at the top-most interface between the PFRC layer and the laminated plate. Interestingly, such a variation is not visible when only mechanical loadings are applied and

the resulting variations are quite similar to the variations of $\bar{\tau}_{13}$ in traditional laminated plates. For comparison, we have also presented the results obtained from both equilibrium equations (EE) and constitutive relations (CR). The variations obtained from EE are similar to the exact variations of $\bar{\tau}_{13}$ reported by Mallik and Ray (2004). Though the variations obtained using CR and EE are agreeing well during the case of purely mechanical loads (V=0) however, a significant disagreement in the results of CR and EE is observed in the figure when electromechanical loads are applied. The shear-strain functions available in the literature used in non-polynomial HSDTs for expressing the displacement components (U_1 and U_2) have an anti-symmetric through-thickness variation about the mid-plane, and the derivatives with respect to thickness coordinates are symmetric. The derivatives of shear-strain functions are required while calculating the transverse shear strains. Therefore, it is quite evident that the variations of the transverse shear stresses calculated using CR which takes into account the strain-displacement relations and materials properties would also generate a symmetrical profile of $\bar{\tau}_{13}$ about the mid-plane. In reality, such variations of $\bar{\tau}_{13}$ do exist in the case of traditional laminated composite plates subjected to purely mechanical loads (ref: Figure 3.6a and Figure 12a (V=0)). In those cases, the variations obtained using CR and EE agree well with each other. When the PFRC layer gets activated on the application of electric voltages ($V\neq0$), the symmetric variation of $\bar{\tau}_{13}$ does not exist anymore as observed in Figure 3.12a. However, the variations obtained using CR is still symmetric due to the inherent symmetrical profile of the derivatives of the shear-strain functions and a total mismatch in the variations of $\bar{\tau}_{13}$ occur. This may be the probable reason for erroneous estimations of $\bar{\tau}_{13}$ using CR. Figure 3.12b shows the through-thickness variations of $\bar{\tau}_{23}$ for various magnitudes of electromechanical loads. Though the

variations of $\bar{\tau}_{23}$ in smart composites subjected to electromechanical loads are nearly similar to the variations in the traditional multilayered composites, yet the magnitudes of $\bar{\tau}_{23}$ obtained using CR and EE have some differences at different points in the thickness coordinate. Such differences are also observed in Figure 3.6b in which the through-thickness variations of $\bar{\tau}_{23}$ for the traditional composite plates are shown. It was observed earlier in Tables 3.2, 3.5 and 3.7 that the present shear-strain function produces more efficient responses of $\bar{\tau}_{13}$ in comparison to $\bar{\tau}_{23}$ for the traditional laminated composites when CR is used. Similarly, the estimations of $\bar{\tau}_{23}$ using CR are found to have larger discrepancies for the case of smart composites. However, the responses of $\bar{\tau}_{13}$ and $\bar{\tau}_{23}$ obtained using EE are found to very efficient.

3.3.3. Static analysis of four-layered smart composite plate with PFRC actuator (PFRC/0/90/0) subjected to electromechanical load of uniform variation

In this example, the variation of the electromechanical load in the spatial domain is assumed to be uniformly distributed (UD) and the static responses of the same PFRC/0/90/0 plate are obtained in the form of transverse displacement. The Navier solution for a sinusoidal distributed electromechanical load is a one-term solution. However, for other types of loading conditions, the Navier solution is a series solution and is required to be evaluated for an adequate number of terms until convergence is achieved. Therefore, the convergence is first shown in Figure 3.13 for a thick plate (S = 10). The responses are presented in Table 3.15 and compared with the FE-based FSDT and HSDT results of Ray and Mallik (2004) and Rouzegar and Abbasi (2018), respectively.

Table 3.12. Non dimensional in-plane and transverse displacement of smart composite plate (PFRC/0/90/0) with PFRC actuator at the top of the plate subjected to mechanical and electrical loading
(material property: MM4 (substrate), MP2 (piezoelectric layer); non-dimensional parameter: ND1)

References	S=10			S=20			S=100		
	V=0	V=100	V=-100	V=0	V=100	V=-100	V=0	V=100	V=-100
$\bar{U}_1\left(0,\frac{b}{2},\frac{h}{2}\right)$									
Present FEM	0.0065	-2.9478	2.9608	0.0062	-0.7030	0.7155	0.0061	-0.0219	0.0341
% error	[1.51]	[6.15]	[6.13]	[1.58]	[2.75]	[2.73]	[1.61]	[1.79]	[1.44]
Present Analytical	0.00660	-2.83110	2.8443	0.0062	-0.6952	0.7077	0.0061	-0.0218	0.03410
% error	[0]	[9.86]	[9.82]	[1.58]	[3.83]	[3.79]	[1.61]	[2.24]	[1.44]
Shiyekar and Kant (2011)	0.00632	-3.11842	3.13105	0.00617	-0.71474	0.72709	0.00613	-0.0219	0.03416
% error	[4.24]	[0.71]	[0.73]	[2.06]	[1.12]	[1.15]	[1.12]	[1.79]	[1.27]
Ray and Mallik (2004)	0.00580	-2.8204	2.8319	0.006	-0.6929	0.7049	0.0061	-0.0217	0.0339
% error	[12.12]	[10.20]	[10.21]	[4.76]	[4.15]	[4.17]	[1.61]	[2.69]	[2.02]
Rouzegar and Abad (2015)	0.00671	-2.85984	2.87327	0.0063	-0.70527	0.71797	0.0062	-0.02216	0.03463
% error	[-1.66]	[8.95]	[8.90]	[-0.79]	[2.43]	[2.39]	[-0.48]	[0.62]	[-0.08]
Mallik and Ray (2004)	0.00660	-3.1410	3.1542	0.0063	-0.7229	0.7356	0.0062	-0.0223	0.0346
$\bar{U}_3\left(\frac{l}{2},\frac{b}{2}\right)$									
Present FEM	-0.7044	130.9244	-132.331	-0.4809	29.8288	-30.7906	-0.4034	0.7720	-1.5788
% error	[0.78]	[1.48]	[1.46]	[1.17]	[1.67]	[1.65]	[1.34]	[1.94]	[1.63]
Present Analytical	-0.7024	132.9469	-134.3517	-0.4806	29.9174	-30.8787	-0.4034	0.7722	-1.5789
% error	[1.07]	[0.03]	[0.03]	[1.23]	[1.38]	[1.37]	[1.34]	[1.91]	[1.62]
Shiyekar and Kant (2011)	-0.66806	129.0550	-130.391	-0.47112	29.7724	-30.7146	-0.40432	0.77533	-1.58397
% error	[5.90]	[2.89]	[2.91]	[3.18]	[1.86]	[1.90]	[1.12]	[1.52]	[1.31]

Ray and Mallik (2004)	-0.65110	122.46000	-124.7	-0.4571	28.287	-29.201	-0.4022	0.7632	-1.5776
% error	[8.29]	[7.85]	[7.14]	[6.06]	[6.75]	[6.73]	[1.63]	[3.06]	[1.70]
Rouzegar and Abad (2015)	-0.57405	128.43902	-129.5871	-0.4483	30.0524	-30.9491	-0.40794	0.78957	-1.60545
% error	[19.14]	[3.35]	[3.50]	[7.86]	[0.93]	[1.15]	[0.23]	[-0.28]	[-0.02]
Mallik and Ray (2004)	-0.71	132.9	-134.3	-0.4866	30.337	-31.31	-0.4089	0.7873	-1.605

Table 3.13. Non dimensional in-plane stresses of smart composite plate (PFRC/0/90/0) with PFRC actuator at the top of the plate subjected to mechanical and electrical loading
(material property: MM4 (substrate), MP2 (piezoelectric layer); non-dimensional parameter: ND1)

References	S = 10			S = 20			S = 100		
	V = 0	V = 100	V = -100	V = 0	V = 100	V = -100	V = 0	V = 100	V = -100
$\bar{\sigma}_{11}\left(\frac{l}{2},\frac{b}{2},\frac{h}{2}\right)$									
Present FEM	-0.5232	234.4360	-235.4824	-0.4973	55.9214	-56.9161	-0.4882	1.7372	-2.7137
% error	[0.92]	[5.75]	[5.73]	[1.23]	[2.35]	[2.33]	[1.33]	[1.00]	[1.12]
Present Analytical	-0.5272	224.3143	-225.3686	-0.49640	55.0787	-56.0714	-0.4863	1.7285	-2.701
% error	[0.17]	[9.82]	[9.78]	[1.41]	[3.82]	[3.78]	[1.71]	[1.50]	[1.58]
Shiyekar and Kant (2011)	-0.50746	247.543	-248.558	-0.49326	56.7572	-57.7437	-0.48872	1.73795	-2.7154
% error	[3.90]	[0.48]	[0.50]	[2.03]	[0.89]	[0.91]	[1.22]	[0.96]	[1.06]
Ray and Mallik (2004)	-0.4915	235.46	-236.4	-0.5022	57.267	-58.276	-0.4941	1.7483	-2.7364
% error	[6.93]	[5.34]	[5.37]	[0.25]	[0]	[0]	[0.14]	[0.37]	[0.29]
Rouzegar and Abad (2015)	-0.53358	226.5447	-227.6118	-0.50494	55.8653	-56.87520	-0.49573	1.75183	-2.74541
% error	[-1.03]	[8.93]	[8.89]	[-0.28]	[2.45]	[2.404]	[-0.18]	[0.175]	[-0.03]
Mallik and Ray (2004)	-0.5281	248.76	-249.82	-0.5035	57.269	-58.276	-0.4948	1.7549	-2.7445

$\bar{\sigma}_{22}\left(\frac{l}{2},\frac{b}{2},\frac{h}{6}\right)$									
Present FEM	-0.2576	41.2429	-41.7581	-0.1869	10.0809	-10.4546	-0.1603	0.2474	-0.5681
% error	[0.19]	[3.03]	[2.99]	[1.68]	[3.61]	[3.55]	[2.43]	[4.69]	[3.41]
Present Analytical	-0.2574	42.3848	-42.8996	-0.186	10.0887	-10.4607	-0.1593	0.2458	-0.5645
% error	[-0.11]	[0.34]	[0.34]	[2.15]	[3.54]	[3.49]	[3.04]	[5.31]	[4.02]
Shiyekar and Kant (2011)	-0.23729	39.4075	-39.8821	-0.18114	9.95995	-10.3222	-0.16003	0.2478	-0.56786
% error	[7.70]	[7.34]	[7.35]	[4.71]	[4.77]	[4.77]	[2.59]	[4.54]	[3.45]
Ray and Mallik (2004)	-0.23480	34.175	-34.645	-0.1849	9.888	-10.258	-0.1641	0.2571	-0.5807
% error	[8.67]	[19.64]	[19.51]	[2.73]	[5.45]	[5.36]	[0.12]	[0.96]	[1.27]
Mallik and Ray (2004)	-0.2571	42.532	-43.046	-0.1901	10.459	-10.84	-0.1643	0.2596	-0.5882

Table 3.14. Non dimensional in-plane and transverse shear stresses of smart composite plate (PFRC/0/90/0) with PFRC actuator at the top of the plate subjected to mechanical and electrical loading
(material property: MM4 (substrate), MP2 (piezoelectric layer); non-dimensional parameter: ND1)

References	S = 10			S = 20			S = 100		
	V = 0	V = 100	V = -100	V = 0	V = 100	V = -100	V = 0	V = 100	V = -100
$\bar{\tau}_{12}\left(0,0,\frac{h}{2}\right)$									
Present FEM	0.0260	-7.3963	7.4483	0.0212	-1.7831	1.8256	0.0195	-0.0519	0.0908
% error	[0.38]	[3.89]	[3.86]	[1.39]	[2.13]	[2.10]	[1.01]	[1.51]	[1.51]
Present Analytical	0.0261	-7.2448	7.2969	0.0212	-1.7665	1.8089	0.0194	-0.0517	0.0904
% error	[0]	[5.86]	[5.82]	[1.39]	[3.04]	[2.99]	[1.52]	[1.89]	[1.95]
Shiyekar and Kant (2011)	0.02473	-7.56623	7.61569	0.02084	-1.79126	1.83293	0.01942	-0.05187	0.09071
% error	[5.24]	[1.68]	[1.70]	[3.07]	[1.68]	[1.70]	[1.42]	[1.57]	[1.61]
Ray and Mallik (2004)	0.0241	-7.0066	7.0547	0.0214	-1.814	1.8565	0.0197	-0.0526	0.0915
% error	[7.66]	[8.95]	[8.94]	[0.46]	[0.43]	[0.44]	[0]	[0.19]	[0.75]
Rouzegar and Abad	0.02196	-7.35976	7.34675	0.02008	-1.79866	1.83883	0.01972	-0.05282	0.09268

(2015)									
% error	[15.86]	[4.36]	[5.17]	[6.60]	[1.28]	[1.39]	[-0.10]	[-0.22]	[-0.52]
Mallik and Ray (2004)	0.0261	-7.696	7.748	0.0215	-1.822	1.8648	0.0197	-0.0527	0.0922
$\bar{\tau}_{13}\left(0,\frac{b}{2},0\right)$									
Present Analytical	-0.3411	24.0043	-24.6864	-0.3708	-	-	-0.3817	-0.1255	-0.6379
% error	[1.06]	[-1.67]	[-1.59]	[3.26]	-	-	[0.78]	[-6.86]	[2.15]
Shiyekar and Kant (2011)	-0.35304	23.0262	-23.7322	-0.37465	-	-	-0.38249	-0.12410	-0.64088
% error	[-2.40]	[2.46]	[2.329]	[2.25]	-	-	[0.57]	[-5.67]	[1.70]
Mallik and Ray (2004)	-0.34476	23.609	-24.298	-0.3833	0.68194	-1.4485	-0.3847	-0.11744	-0.65197
$\bar{\tau}_{23}\left(\frac{a}{2},0,0\right)$									
Present Analytical	-0.1221	24.9075	-25.1517	-0.0933	-	-	-0.0825	0.1611	-0.326
% error	[-0.84]	[-3.50]	[-3.47]	[-12.13]	-	-	[-0.85]	[-1.14]	[-0.97]
Shiyekar and Kant (2011)	-0.11596	23.9406	-24.1725	-0.09144	-	-	-0.08232	0.16094	-0.32558
% error	[4.22]	[0.51]	[0.55]	[-9.90]	-	-	[-0.63]	[-1.04]	[-0.84]
Mallik and Ray (2004)	-0.12108	24.065	-24.307	-0.0832	0.88142	-1.0478	-0.0818	0.15927	-0.32284

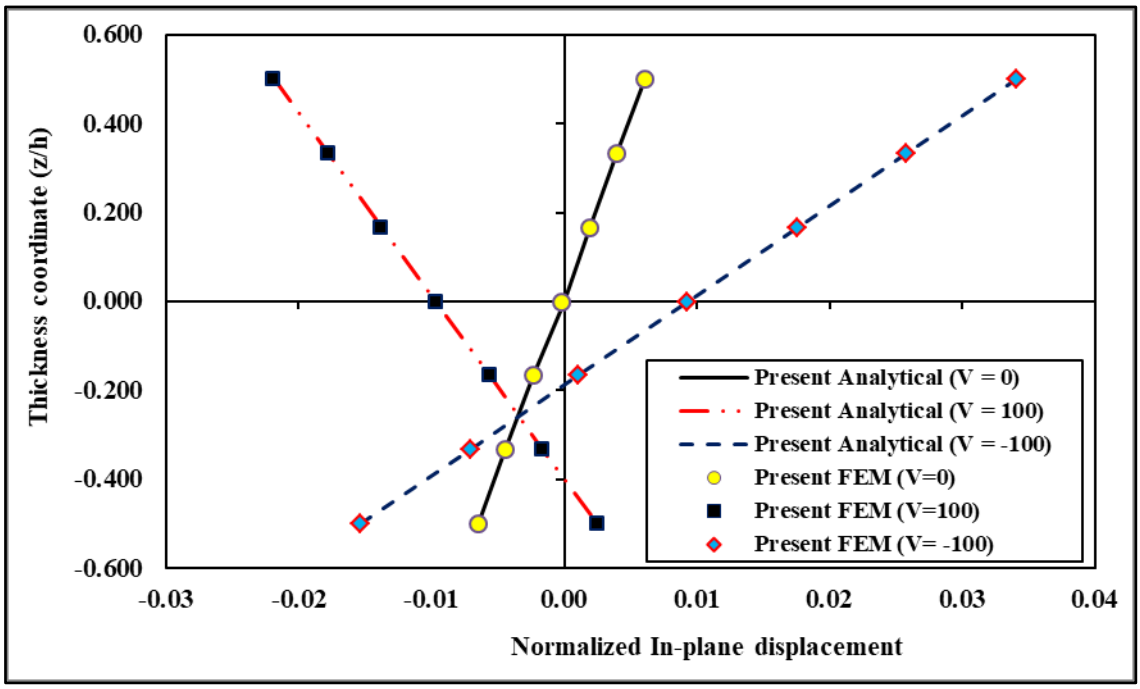

Figure 3.10: Through-thickness variations of in plane displacement ($\bar{U}_1$) for various magnitudes of electromechanical loads (material property: MM4 (substrate), MP2 (piezoelectric layer); non-dimensional parameter: ND1)

Significant differences in the results from the various shear deformation models can be observed in the table. FSDT underestimates the responses of transverse displacement for the thick smart composite plate (S=10). The present analytical and FE results are in close agreement with each other. The FSDT responses of Ray and Mallik (2004) are closer to the present responses when the smart composite plate is thin (S =100).

3.3.4. Static analysis of five-layered smart composite plate with PFRC actuator (PFRC/0/90/90/0) subjected to electromechanical load of sinusoidal variation

In this example, a five-layered traditional laminated composite plate with a PFRC layer placed at the top surface of the plate is considered. The thickness of each ply is 1 *mm* and the thickness of the PFRC layer is 0.25 *mm*. The smart composite plate is subjected to sinusoidal electromechanical load in both x_1 and x_2-direction. The non-dimensional axial

and transverse deflections are tabulated in Table 3.16. The problem is previously solved by Shiyekar and Kant (2011) by employing a HSDT with twelve variables. Mallik and Ray (2004) reported the benchmark elasticity solutions of the problem in the literature. Therefore, the results of the above-mentioned references are also collected in the table for comparison. It is observed in the table that the transverse deflection responses are very accurately predicted using the present model with deviations of 1.61 % and 0.34 % (analytical), and 1.48 % and 1.52 % (FEM) for S = 10 and V = 0 and 100, respectively. Discrepancies of 3.41 % and 2.47 % are noted in the transverse displacement responses of Shiyekar and Kant (2011) for S =10 and V = 0 and 100, respectively. We also observe a decrement in the magnitude of the transverse displacement by 29.61 % with respect to the response obtained for a three-layered smart composite plate considered in the previous example for S=10. This is due to the increase in the stiffness coefficients with the increase in the overall thickness of the smart composite plate. The in-plane displacements are predicted with an error of 7.69 % (analytical) and 4.56 % (FEM) at the top surface of the plate for S =10 and V = 100. The displacements are very sensitive to the polarity of the voltages as the direction of the displacement components changes with the polarity. Next, we present the in-plane normal stresses in Table 3.17. It is observed in the table that the in-plane stress '$\bar{\sigma}_{22}$' is more accurately predicted than '$\bar{\sigma}_{11}$' with the present model. The values of $\bar{\sigma}_{11}$ are predicted with an error of 7.67 % (analytical) and 4.16 % (FEM), and the values of $\bar{\sigma}_{22}$ are predicted with an error of 0.635 % (analytical) and 0.59 % (FEM) at the top and bottom surface of the plate for S = 10 and V = 100. The in-plane shear stress and the transverse shear stresses are collected in Table 3.18. The in-plane shear stress at the top surface of the plate is predicted with an error of 5.36 % for S = 10 and V =100 which is less than 6.09 % noted in the response of Shiyekar and Kant (2011).

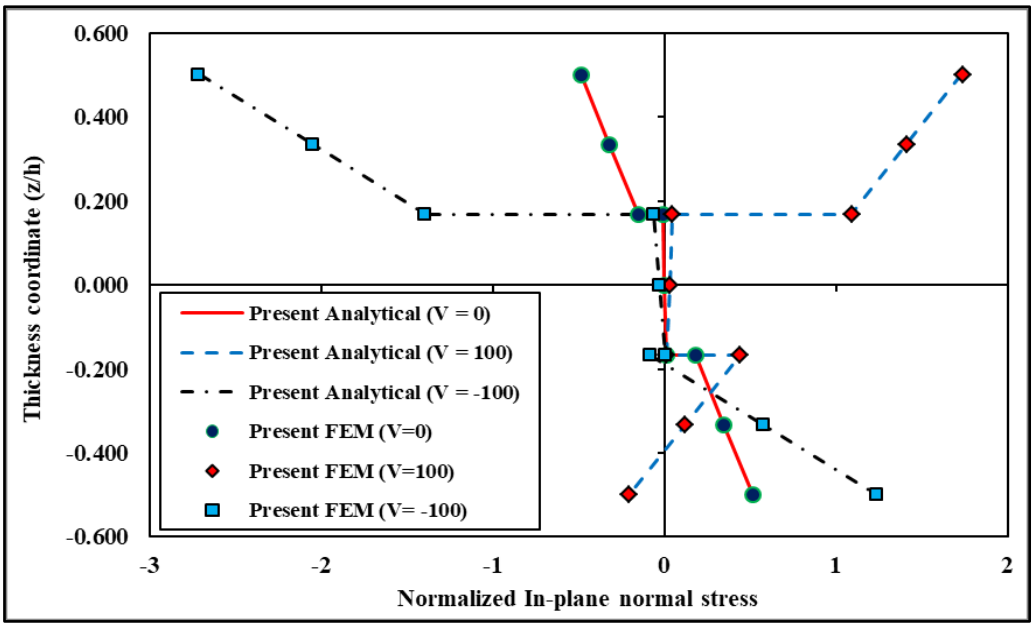

(a)

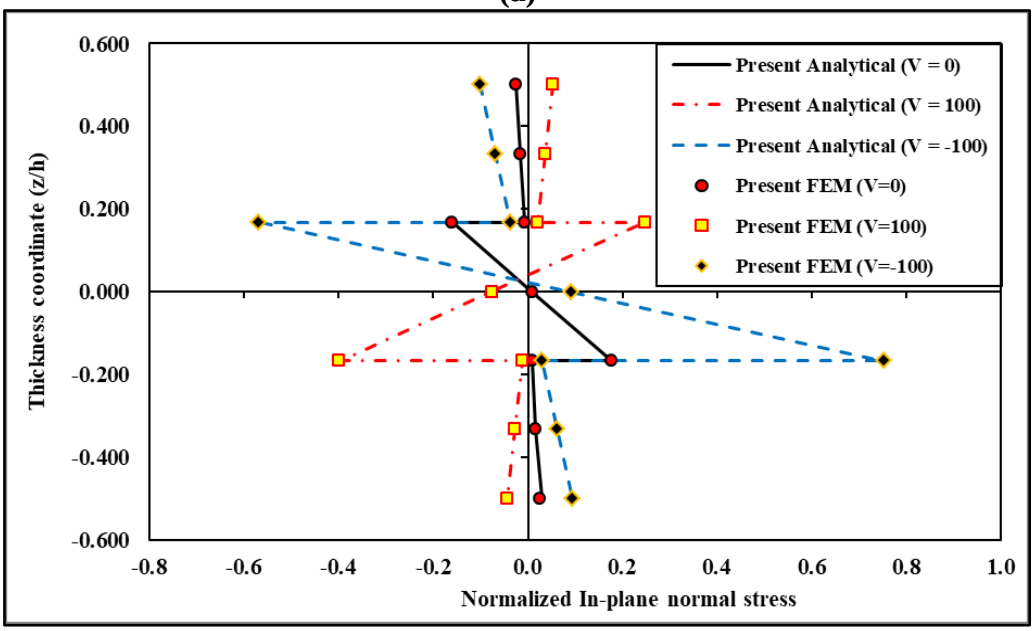

(b)

Figure 3.11 (a). Through-thickness variation of normalized in-plane normal stress $(\bar{\sigma}_{11})$ for various magnitudes of electromechanical loads. (b). Through-thickness variation of normalized in-plane normal stress $(\bar{\sigma}_{22})$ for various magnitudes of electromechanical loads (material property: MM4 (substrate), MP2 (piezoelectric layer); non-dimensional parameter: ND1)

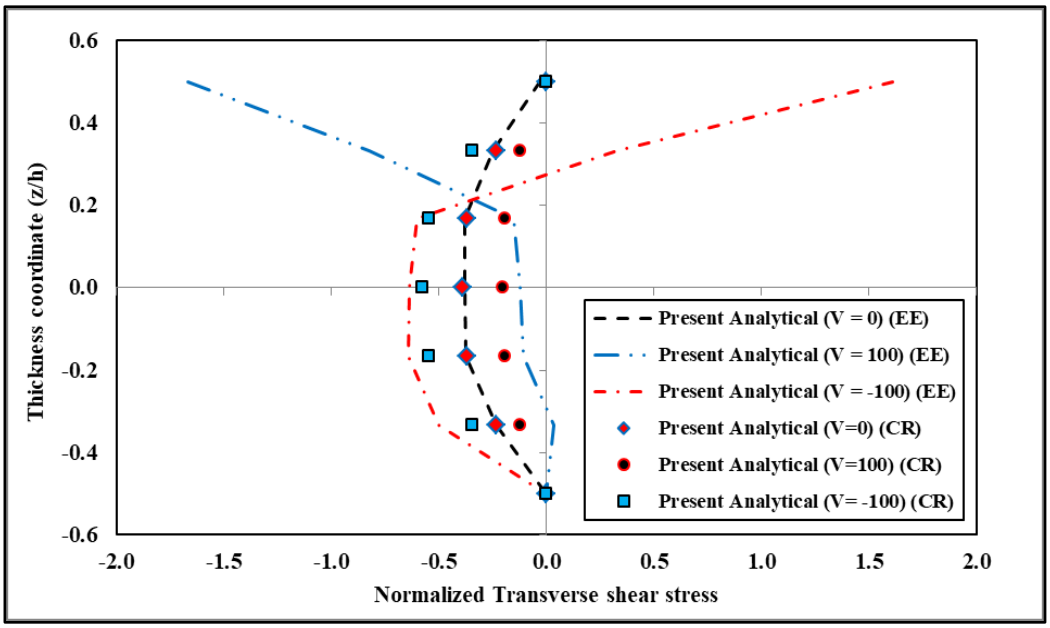

(a)

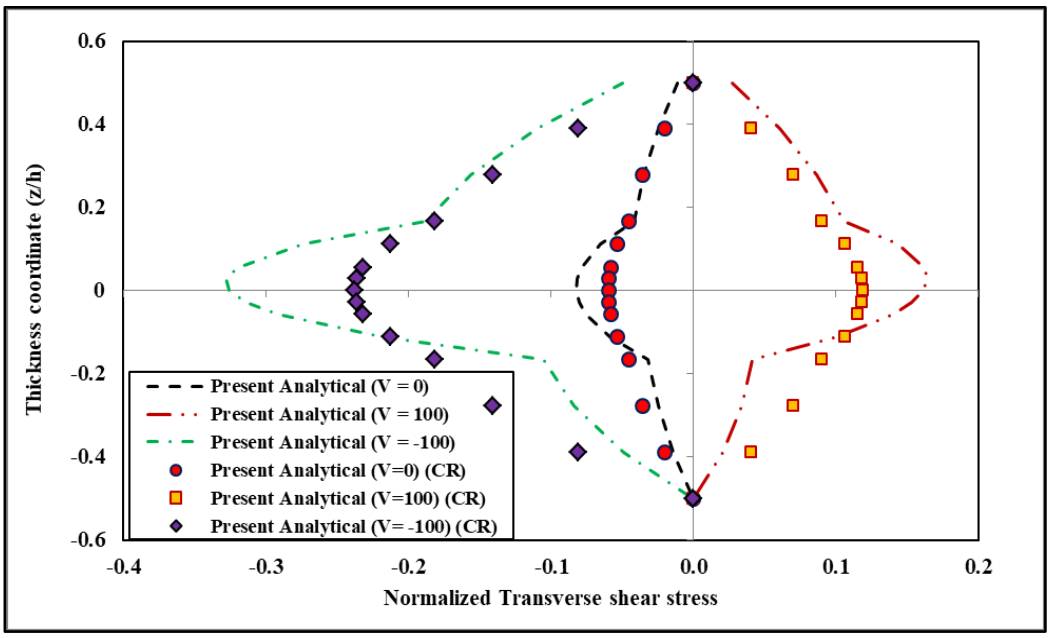

(b)

Figure 3.12 (a). Through-thickness variations of normalized transverse shear stress ($\bar{\tau}_{13}$) for various magnitudes of electromechanical loads. (b). Through-thickness variations of normalized transverse shear stress ($\bar{\tau}_{23}$) for various magnitudes of electromechanical loads (material property: MM4 (substrate), MP2 (piezoelectric layer); non-dimensional parameter: ND1)

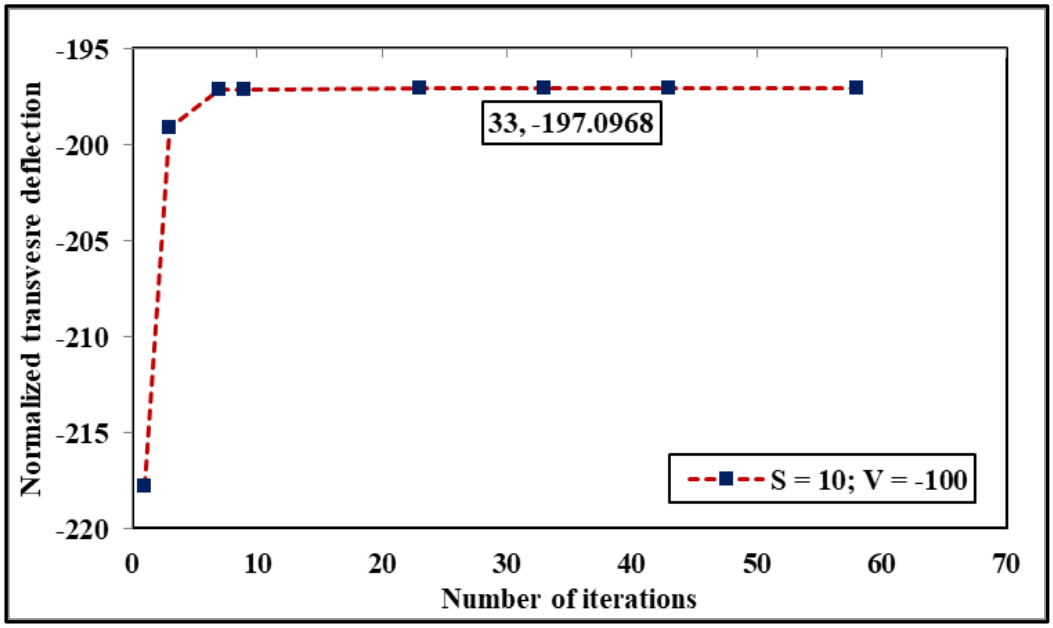

Figure 3.13. Convergence of the present analytical solution
(material property: MM4 (substrate), MP2 (piezoelectric layer); non-dimensional parameter: ND1)

The performance of the present model in predicting the transverse shear stresses using the equilibrium equations is quite appreciable as the deviations noted in the responses of $\bar{\tau}_{13}$ and $\bar{\tau}_{23}$ are 1.17 % and 2.87 % for S =10, respectively. Discrepancies of 8.09 % and 1.51 % can be observed in the results of $\bar{\tau}_{13}$ and $\bar{\tau}_{23}$ reported by Shiyekar and Kant (2011). To show the magnification in the responses due to the PFRC layer, the responses of transverse deflection (U_3) and in plane normal stress $(\bar{\sigma}_{11})$ are shown in Figure 3.14a and 3.14b, respectively for various magnitudes of electromechanical loads. Significant actuation in the responses can be observed in the figures. For V = 200, $\bar{U}_3$ and $\bar{\sigma}_{11}$ have magnifications of 267.6 and 728.82 times the values obtained at V = 0, respectively.

3.3.5. Static Responses of smart composite plates with respect to number of layers and different materials

Next, the static responses of smart composite plates are obtained with the increase in the number of layers. A four-layered (PFRC/0/90/0), five-layered (PFRC/0/90/90/0) and a six-layered (PFRC/0/90/0/90/0) smart composite plate is considered which is subjected to an electrical load of 200 V and mechanical pressure of 40 N/m^2 varying sinusoidally. The thickness of each orthotropic ply is 1mm and the thickness of the PFRC layer is 0.25 mm. The transverse deflection responses are shown in Figure 3.15. As expected, the magnitude of transverse displacement decreases with the increase in the number of layers due to the increase in the stiffness coefficients. The magnitude of $\bar{U}_3$ decreases by 29.53 % for the four-layered plate and 44.156 % for the five-layered plate with respect to the responses of the three-layered plate. The PFRC layer has a higher magnitude of piezoelectric coefficient 'e_{31}' than the conventional piezoelectric materials like the PVDF. As a result, the static responses are expected to significantly actuate due to the PFRC layer. The effect of e_{31} in the static responses of smart composite plates is now investigated with the number of layers. The responses of transverse deflection are shown in Figure 3.16 for various values of e_{31}. It is observed in the figure that the static responses significantly increase with the increase in the magnitude of e_{31}. Next, we investigate the static responses of a four-layered smart composite plate (PFRC/0/90/0) with different materials like Graphite-Epoxy (Gr.-Ep (AS/3501)), Glass-epoxy (Gl.-Ep) and Boron-Epoxy (Br.-Ep). The material properties of the aforementioned composite materials are adopted from Reddy (2004). The non-dimensional results of transverse deflection of the smart composite plates made up of the above-mentioned materials are shown in Figure 3.17. It is observed that the Glass-Epoxy smart composite plate experiences the maximum transverse deflection and the Graphite-Epoxy composite plate experiences the least transverse deflection.

Table 3.15. Non-dimensional transverse deflection of PFRC/0/90/0 plate with uniformly distributed electromechanical load
(material property: MM4 (substrate), MP2 (piezoelectric layer); non-dimensional parameter: ND1)

References	*l*/*h*	V = 100	V = -100
Present FEM	10	193.3033	-195.4674
	20	44.6787	-46.1636
	100	1.1479	-2.3975
Present Analytical	10	194.9346	-197.096
	20	44.7752	-46.2596
	100	1.148	-2.3975
Ray and Mallik (2004)[1]	10	166.07	-167.97
	20	42.851	-44.259
	100	1.1434	-2.3907
Rouzegar and Abbasi (2018)[2]	10	189.43	-191.17
	20	45.161	-46.539
	100	1.1806	-2.4429

[1] FSDT; [2] HSDT with four variables

Now, the static-deflection control of the smart composite plates with PFRC layer is investigated by determining the total amount of electrical load required to discard the mechanical deformation. For this, a four-layered (PFRC/0/90/0) smart composite plate is considered with material properties corresponding to those used by Mallik and Ray (2004). The mechanical pressure applied is sinusoidal in the spatial domain and the corresponding electric voltage is evaluated for which the net deflection is negligible. The static-deflection control of a thick (S=10) and a thin (S=100) plate is shown in Figure 3.18. The figure reflects that the total amount of electric voltage required to nullify the mechanical deflection is higher in thin systems than the thick ones. The reason behind this is, as the plate becomes thin, the stiffness coefficients get reduced due to the increase in the planar dimensions.

Table 3.16. Non dimensional in-plane and transverse displacement of smart composite plate (PFRC/0/90/90/0) with PFRC actuator at the top of the plate subjected to mechanical and electrical loading
(material property: MM4 (substrate), MP2 (piezoelectric layer); non-dimensional parameter: ND1)

References	S=10			S=20			S=100		
	V=0	V=100	V=-100	V=0	V=100	V=-100	V = 0	V = 100	V = -100
$\bar{U}_1\left(0,\frac{b}{2},\frac{h}{2}\right)$									
Present FEM	0.0063	-2.43	2.4427	0.0063	-0.5817	0.5942	0.0062	-0.0170	0.0295
% error	[1.56]	[4.56]	[4.92]	[0.00]	[1.95]	[1.93]	[1.58]	[0.58]	[1.00]
Present Analytical	0.00640	-2.3504	2.3632	0.0063	-0.5766	0.5892	0.0062	-0.0170	0.0295
% error	[0.00]	[7.69]	[8.01]	[0.00]	[2.81]	[2.75]	[1.58]	[0.58]	[1.00]
Shiyekar and Kant (2011)	0.00630	-2.5543	2.5669	0.0063	-0.5917	0.6042	0.0063	-0.0170	0.0295
% error	[1.563]	[-0.31]	[0.08]	[0.00]	[0.27]	[0.28]	[0.00]	[0.58]	[1.00]
Mallik and Ray (2004)	0.00640	-2.5463	2.5691	0.0063	-0.5933	0.6059	0.0063	-0.0171	0.0298
$\bar{U}_3\left(\frac{l}{2},\frac{b}{2}\right)$									
Present FEM	-0.7031	92.4725	-93.8787	-0.4874	21.8507	-22.8255	-0.4115	0.4705	-1.2935
% error	[1.48]	[1.52]	[1.50]	[0.93]	[1.31]	[1.29]	[1.05]	[0.36]	[1.17]
Present Analytical	-0.7022	93.5782	-94.9825	-0.4873	21.905	-22.8800	-0.4115	0.4706	-1.2936
% error	[1.61]	[0.34]	[0.35]	[0.95]	[1.06]	[1.05]	[1.05]	[0.33]	[1.16]
Shiyekar and Kant (2011)	-0.68930	96.2234	-97.6020	-0.4833	22.1061	-23.0727	-0.4119	0.4722	-1.2961
% error	[3.41]	[-2.47]	[-2.39]	[1.76]	[0.15]	[0.22]	[0.962]	[0]	[0.97]
Rouzegar and Abad (2015)	-	95.7006	-96.8654	-	22.3460	-23.2568	-	-	-
% error	-	[-1.916]	[-1.62]	-	[-0.92]	[-0.57]	-	[-1.88]	[-0.11]
Mallik and Ray (2004)	-0.71370	93.9010	-95.3180	-0.4920	22.1410	-23.125	-0.4159	0.4722	-1.3089

Table 3.17. Non dimensional in-plane stresses of smart composite plate (PFRC/0/90/90/0) with PFRC actuator at the top of the plate subjected to mechanical and electrical loading
(material property: MM4 (substrate), MP2 (piezoelectric layer); non-dimensional parameter: ND1)

References	S = 10			S = 20			S = 100		
	V = 0	V = 100	V = -100	V = 0	V = 100	V = -100	V = 0	V = 100	V = -100
$\bar{\sigma}_{11}\left(\frac{l}{2},\frac{b}{2},\frac{h}{2}\right)$									
Present FEM	-0.5085	193.0810	-194.098	-0.5002	46.2411	-47.2414	-0.4985	1.3491	-2.3460
% error	[0.89]	[4.17]	[4.15]	[0.97]	[1.54]	[1.53]	[1.03]	[0.42]	[0.69]
Present Analytical	-0.5112	186.0333	-187.056	-0.499	45.6501	-46.6482	-0.4965	1.3429	-2.3358
% error	[0.37]	[7.67]	[7.63]	[1.20]	[2.80]	[2.76]	[1.42]	[0.88]	[1.12]
Shiyekar and Kant (2011)	-0.5091	205.435	-206.453	-0.5014	47.1483	-48.151	-0.4989	1.3497	-2.3475
% error	[0.78]	[1.95]	[1.94]	[0.73]	[0.38]	[0.36]	[0.95]	[0.38]	[0.63]
Mallik and Ray (2004)	-0.5131	201.5	-202.52	-0.5051	46.966	-47.976	-0.5037	1.3549	-2.3624
$\bar{\sigma}_{22}\left(\frac{l}{2},\frac{b}{2},\frac{h}{4}\right)$									
Present FEM	-0.3826	46.0816	-46.8469	-0.2902	12.0659	-12.6464	-0.2533	0.2519	-0.7586
% error	[0.97]	[0.59]	[0.56]	[0.61]	[1.46]	[1.42]	[0.25]	[0.25]	[0.75]
Present Analytical	-0.3809	46.6523	-47.414	-0.289	12.0588	-12.6369	-0.2523	0.251	-0.7555
% error	[0.52]	[0.635]	[0.63]	[1.02]	[1.52]	[1.49]	[1.59]	[2.71]	[1.99]
Shiyekar and Kant (2011)	-0.3619	44.314	-45.0378	-0.2844	11.9512	-12.52	-0.253	0.2525	-0.7584
% error	[4.48]	[4.40]	[4.40]	[2.60]	[2.39]	[2.40]	[1.32]	[2.13]	[1.62]
Mallik and Ray (2004)	-0.3789	46.358	-47.115	-0.292	12.245	-12.829	-0.2564	0.258	-0.7709

Table 3.18. Non dimensional in-plane and transverse shear stresses of smart composite plate (PFRC/0/90/90/0) with PFRC actuator at the top of the plate subjected to mechanical and electrical loading
(material property: MM4 (substrate), MP2 (piezoelectric layer); non-dimensional parameter: ND1)

References	S = 10			S =20			S=100		
	V = 0	V = 100	V = -100	V = 0	V = 100	V = -100	V = 0	V = 100	V = -100
$\bar{\tau}_{12}\left(0,0,\frac{h}{2}\right)$									
Present FEM	0.0254	-5.7443	5.7951	0.0215	-1.4144	1.4573	0.0199	-0.0374	0.0773
% error	[1.16]	[3.35]	[3.33]	[0.92]	[1.49]	[1.47]	[0.99]	[0.79]	[0.89]
Present Analytical	0.0254	-5.6252	5.6761	0.02140	-1.4021	1.4449	0.0199	-0.0373	0.0770
% error	[1.16]	[5.36]	[5.32]	[1.38]	[2.34]	[2.31]	[0.99]	[1.06]	[1.28]
Shiyekar and Kant (2011)	0.0249	-5.9510	6.0009	0.0213	-1.4311	1.4737	0.0199	-0.0374	0.0772
% error	[3.11]	[0.11]	[0.09]	[1.84]	[0.32]	[0.36]	[0.99]	[0.79]	[1.02]
Mallik and Ray (2004)	0.0257	-5.9440	5.9953	0.02170	-1.4358	1.4791	0.0201	-0.0377	0.0780
$\bar{\tau}_{13}\left(0,\frac{b}{2},0\right)$									
Present Analytical	-0.2929	7.4566	-8.0425	-0.3213	1.4811	-2.1237	-0.3324	-0.2626	-0.4023
% error	[0.88]	[1.17]	[1.15]	[0.58]	[6.08]	[4.48]	[0.53]	[1.23]	[1.63]
Shiyekar and Kant (2011)	-0.2983	6.9344	-7.5311	-0.3232	1.4682	-2.1145	-0.3329	-0.2620	-0.4038
% error	[0.94]	[8.09]	[7.43]	[0.00]	[6.90]	[4.89]	[0.38]	[-1.00]	[1.27]
Mallik and Ray (2004)	-0.2955	7.5453	-8.1363	-0.3232	1.5771	-2.2234	-0.3342	-0.2594	-0.4090
$\bar{\tau}_{23}\left(\frac{a}{2},0,0\right)$									
Present	-0.1946	27.3324	-27.7217	-0.1528	7.0590	-7.3646	-0.1358	0.1578	-0.4294
% error	[1.35]	[2.87]	[2.70]	[0.26]	[0.83]	[0.81]	[0.00]	[0.38]	[0.11]
Shiyekar and Kant (2011)	-0.1878	26.1666	-26.5422	-0.1507	6.9740	-7.2754	-0.1358	0.1580	-0.4296
% error	[2.18]	[1.51]	[1.66]	[1.11]	[0.37]	[0.40]	[0]	[0.50]	[0.16]
Mallik and Ray (2004)	-0.1920	26.568	-26.992	-0.1524	7.0003	-7.3051	-0.1358	0.1572	-0.4289

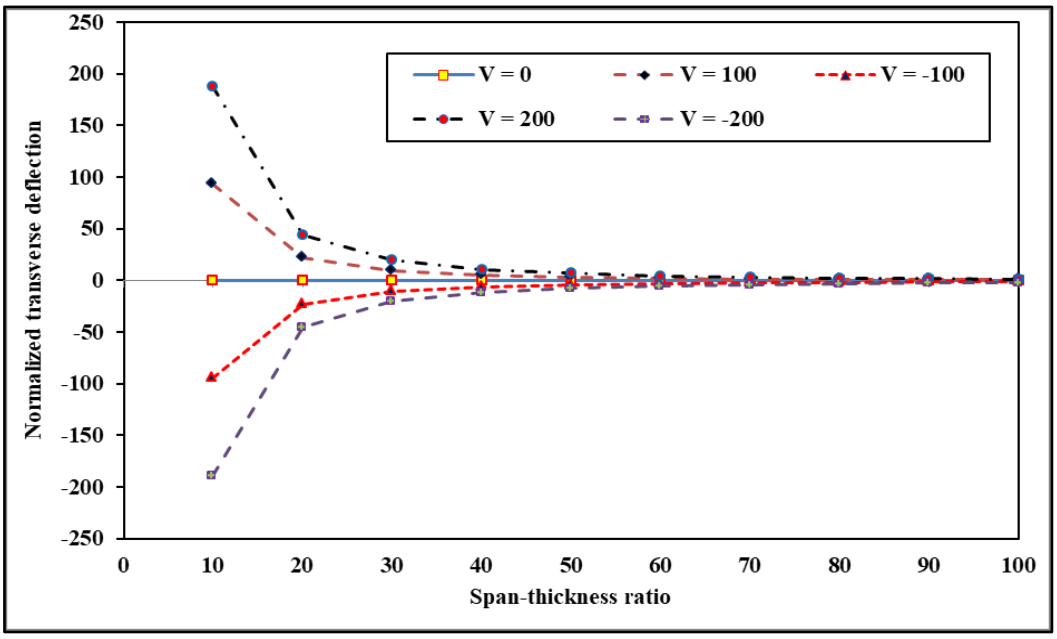

(a)

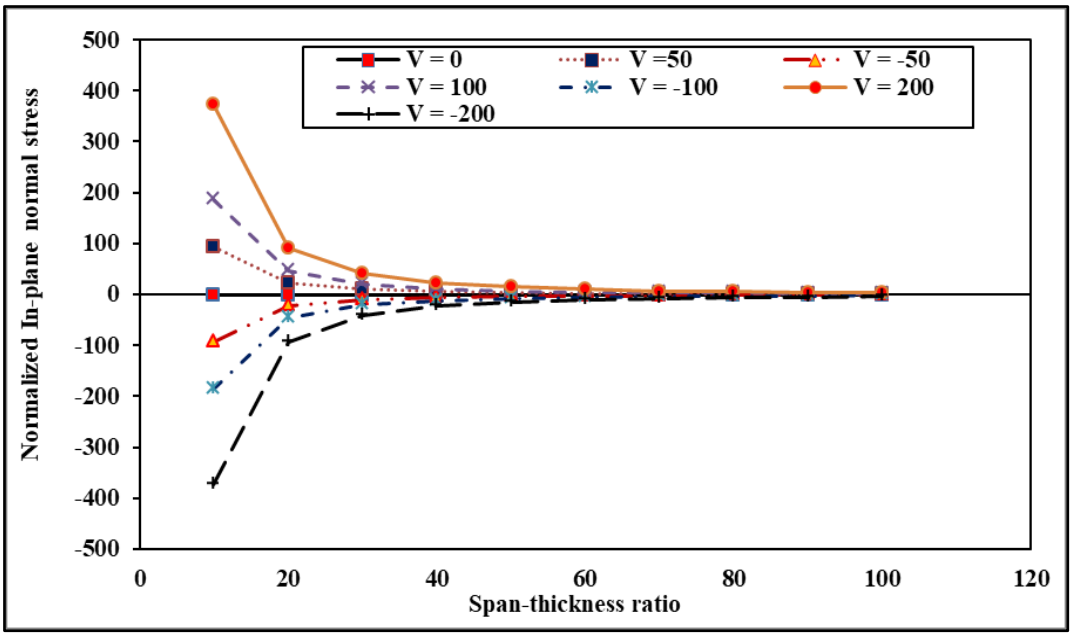

(b)

Figure 3.14 (a). Actuation in the normalized transverse displacement $(\bar{U}_3)$ of five-layered (PFRC/0/90/90/0) smart composite plate for various magnitudes of electromechanical loads. (b). Actuation in the normalized in-plane normal stress $(\bar{\sigma}_{11})$ of the smart composite plate for various magnitudes of electromechanical loads (material property: MM4 (substrate), MP2 (piezoelectric layer); non-dimensional parameter: ND1)

Thus the flexural rigidity gets reduced and higher mechanical deflection and stresses are experienced. To nullify these mechanical responses, a greater magnitude of electrical load is required to counteract the mechanical responses in the thin smart composite plates.

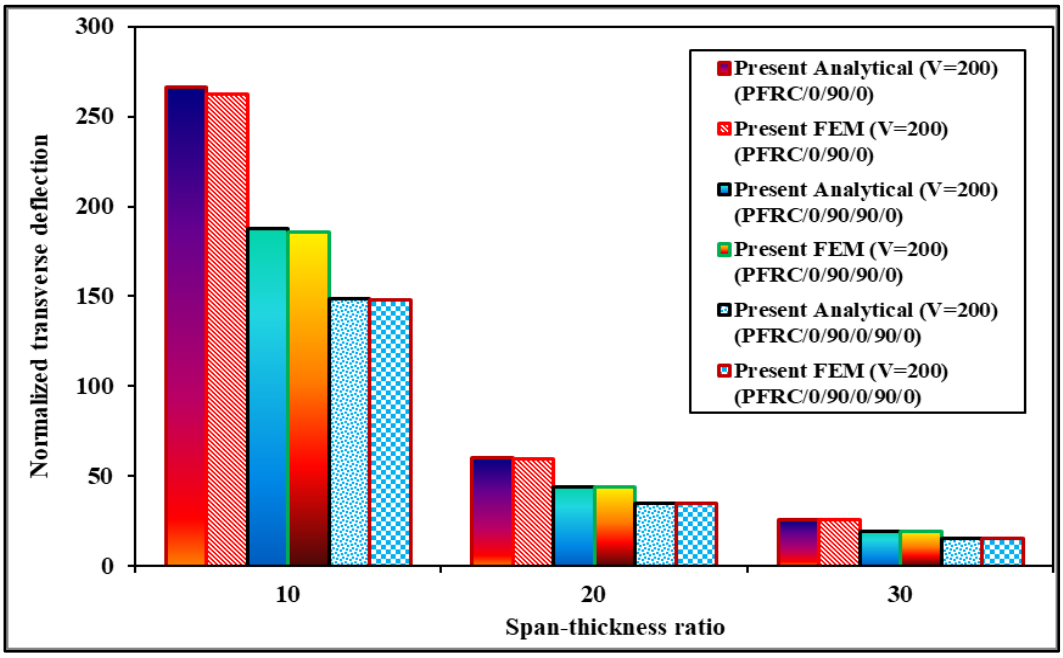

Figure 3.15. Static responses of smart composite plate with respect to number of layers subjected to electromechanical load (material property: MM4 (substrate), MP2 (piezoelectric layer); non-dimensional parameter: ND1)

3.4. Dynamic analysis of traditional laminated composites and sandwich plates

After deriving the static responses of traditional laminated composite plates and smart composite plates with various piezoelectric materials, we now wish to investigate the free vibration responses. The free vibration analysis helps in determining the natural frequencies of the various structural components made up of advanced composite materials. Proper estimation of the natural frequency is very crucial to avoid resonance. Also, the dynamic loadings induce mechanical vibrations in structures that can cause structural damage and it is highly essential to carry out an efficient vibration characteristic research so that an

efficient design can be made. Therefore, in this section, the free vibration analysis, as well as the forced-vibration analysis under various time-dependent mechanical excitations, is presented for laminated composite plates. Attention is also given to the various forms of blast loads to understand the behavior of composites under the action of extreme loading conditions.

3.4.1. Free Vibration analysis of traditional laminated composite plates

The discussion starts with a four-layered (0/90/90/0) traditional laminated composite plate which is diaphragm supported at all the edges. The free vibration responses in terms of the fundamental frequencies of the plate structure are presented in Table 3.19 for various span-thickness ratios (S). The FE results corresponding to various mesh sizes like 4x4, 8x8, 10x10 and 12x12 are provided in the table for S = 5. An excellent convergence of the FE results can be observed in the table. For other span-thickness ratios, the FE results corresponding to the mesh size 10x10 are provided as the results in the higher mesh sizes are exactly similar to the chosen mesh size. For comparison, we have also collected the exact elasticity solutions of the problem derived by Noor (1973) and numerical solutions obtained by employing ZZ-based HSDT and ESL-based HSDT by Chalak *et al*. (2013) and Phan and Reddy (1985), respectively. The present responses are in excellent agreement with the elasticity solutions reported by Noor (1973). The fundamental frequencies increase with the increase in the modular ratio due to the increment in the stiffness coefficients. As a further example, the fundamental frequencies and the higher-order modes of vibration of another four-layered laminated composite plate with different material properties are shown in Table 3.20. The present responses appear to be very efficient in estimating the lowest natural frequency with a maximum discrepancy of 0.01 %. Even the higher-order frequencies presented in the table are also accurately predicted.

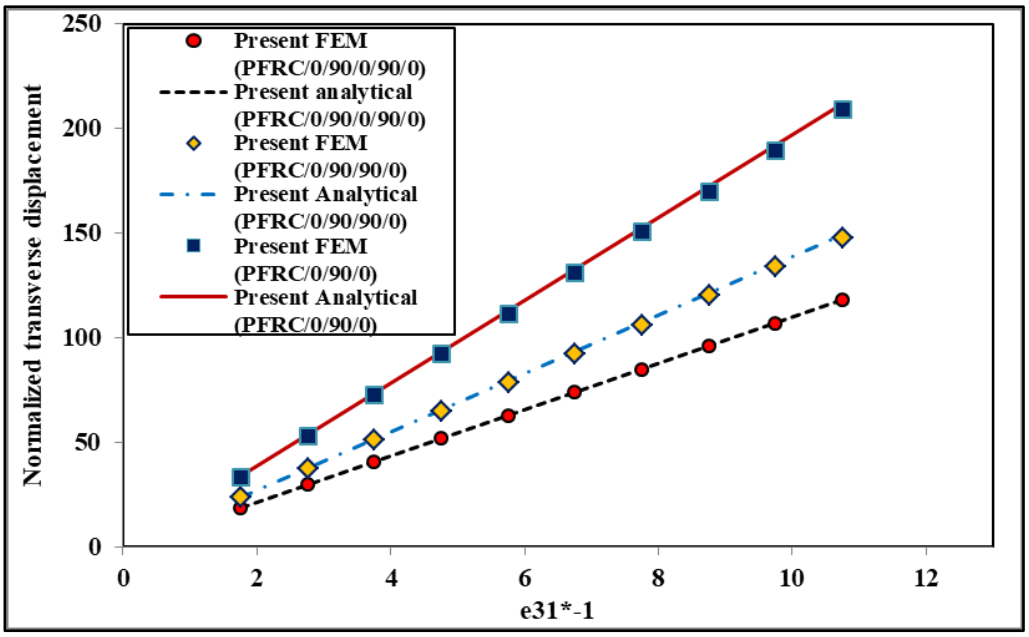

Figure 3.16. Static responses of smart composite plates (*S*=10) with respect to the piezoelectric coefficient 'e_{31}'(material property: MM4 (substrate), MP2 (piezoelectric layer); non-dimensional parameter: ND1)

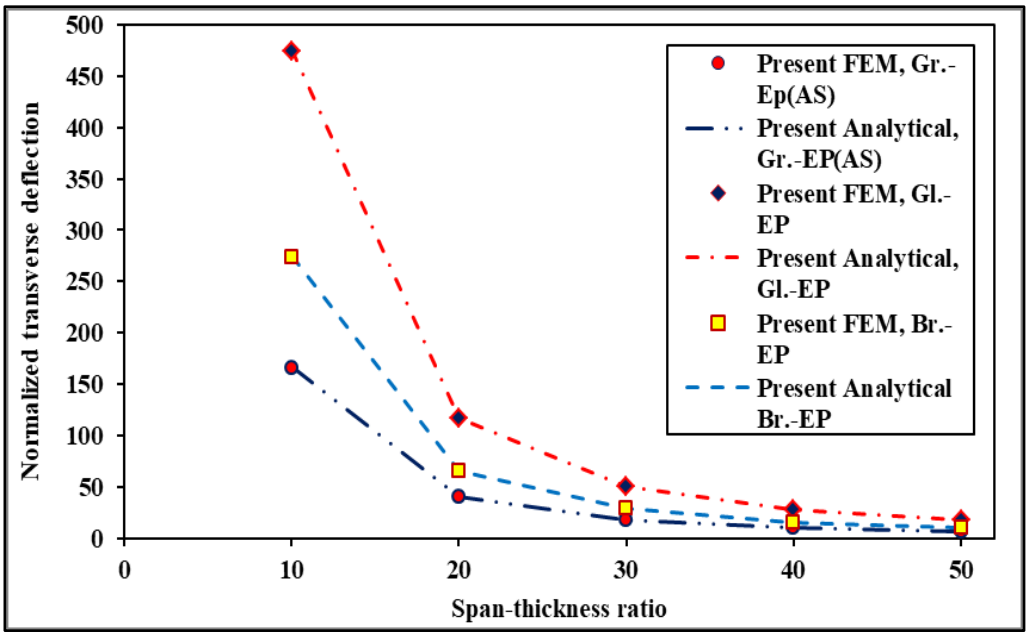

Figure 3.17: Static responses of smart composite plate (PFRC/0/90/0) with different types of composite materials (material property: MM4 (substrate), MP2 (piezoelectric layer); non-dimensional parameter: ND1)

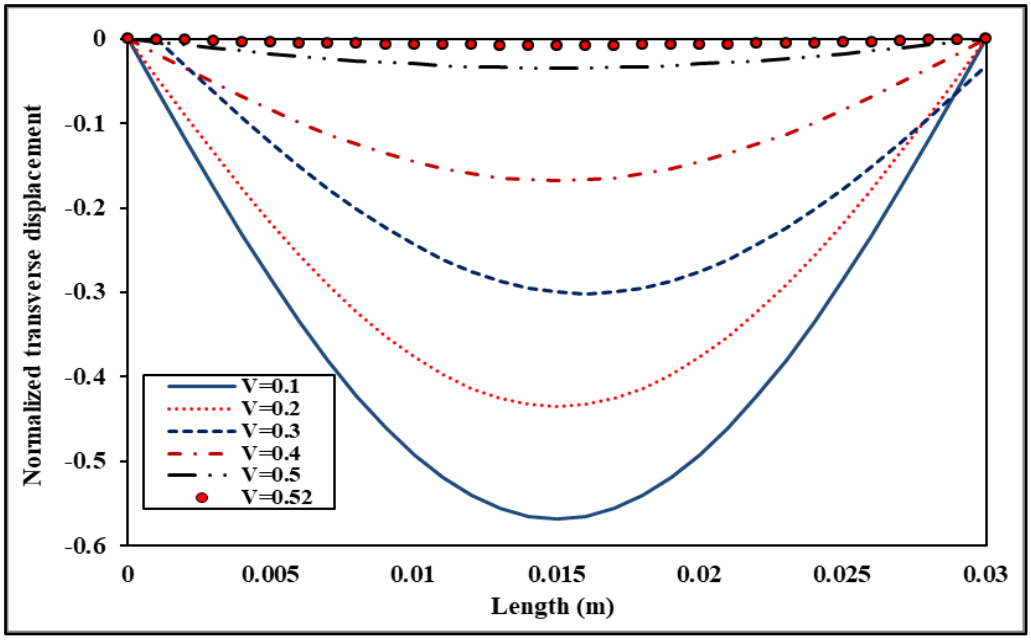

(a)

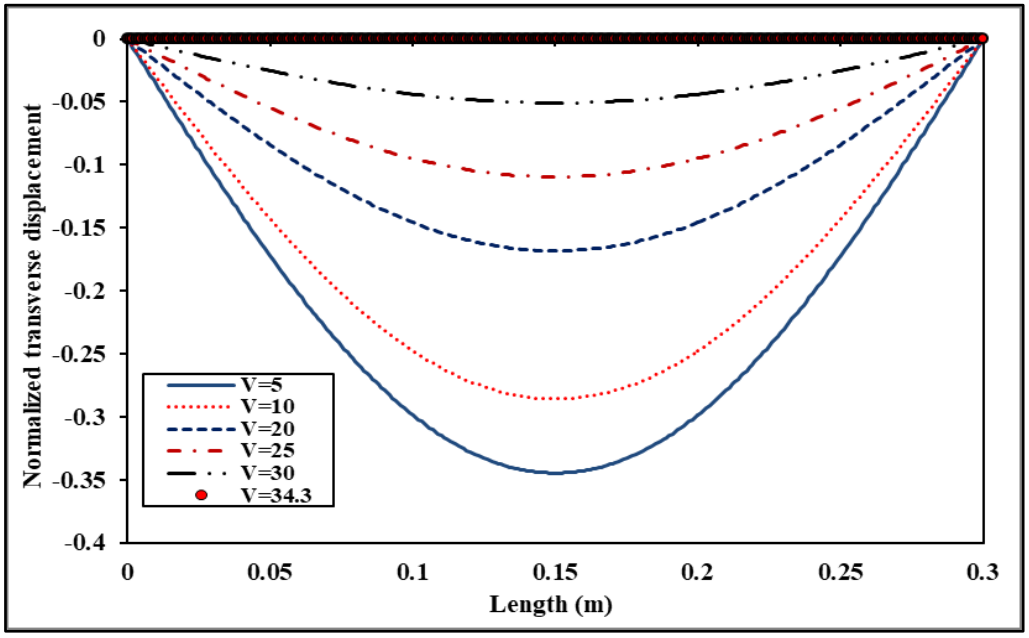

(b)

Figure 3.18 (a). Static-deflection control for a thick (*S*=10) smart composite plate (PFRC/0/90/0). (b). Static-deflection control for a thin (*S*=100) smart composite plate (PFRC/0/90/0) (material properties: MM4 (substrate), MP2 (piezoelectric layer); non-dimensional parameter: ND1)

Next, a parametric investigation on a three-layer laminated (0/90/0) composite plate is carried out by deriving the non-dimensional fundamental frequencies for different span-thickness ratio, aspect-ratio, and modular ratio, and the results are graphically presented in Figure 3.19. It is observed in Figure 3.19a that the natural frequencies are decreasing with the increase in the span-thickness ratio due to the reduction in the stiffness of the plate. In Figure 3.19b, the natural frequencies are observed to increase with the increase in the aspect ratio (l/b). It should be noted that the aspect ratio is increased by keeping length (l) to be constant and decreasing the width (b) of the plate. As a result, the stiffness coefficients increase which is responsible for the reduction in the fundamental frequencies. The first nine modes of vibration and the mode-shapes of the same plate are shown in Figure 3.20. The effect on the fundamental frequencies due to the increase in the number of layers of the laminated plate is now investigated by considering three (0/90/0), four (0/90/90/0) and five-layered (0/90/0/90/0) laminated composite plates. The fundamental natural frequencies of these plates are compared in Figure 3.21a for various span-thickness ratios. Next, the free-vibration responses of a three-layered laminated composite plate are obtained for different materials like Boron-Epoxy composites, Glass-Fiber composites, and Graphite-Epoxy composites (T300/934), and the responses are graphically shown in Figure 3.21b. The material properties of these materials have been obtained from Reddy (2004).

3.4.2. Free Vibration analysis of a three-layered (0/C/0) soft-core sandwich plate

In this example, the fundamental natural frequencies of a three-layered sandwich plate are obtained for different span-thickness ratios. The material properties of the core are presented as the transformed reduced stiffness coefficients written in a matrix presented as follows:

$$[Q]_{core} = \begin{bmatrix} 0.999781 & 0.231192 & 0 & 0 & 0 \\ 0.231192 & 0.524886 & 0 & 0 & 0 \\ 0 & 0 & 0.262931 & 0 & 0 \\ 0 & 0 & 0 & 0.26681 & 0 \\ 0 & 0 & 0 & 0 & 0.159914 \end{bmatrix}$$

The material properties of the face-sheets $([Q]_{face-sheets})$ are obtained by multiplying the material properties of the core with an integer 'R'. The natural frequencies of the sandwich plate for various values of R and span-thickness ratio (*S*) are presented in Table 3.21. The FEM results are corresponding to a mesh size of 10x10 unless specified. The natural frequencies are observed to increase with the increase in the values of R. The increase in the magnitude of R increases the stiffness of the sandwich plate which increases the magnitude of natural frequencies. The effect on the fundamental frequencies is further investigated for various core thicknesses, and the results are shown graphically in Figure 3.22. The natural frequencies tend to increase with a decrease in the thickness of the core (t_c). The increase in the thickness of the core reduces the stiffness of the sandwich plates as the material properties of the core are weaker than those of the face sheets. Therefore the natural frequencies of the sandwich plate decrease with the increase in the thickness of the core.

3.4.3. Free Vibration Analysis of five-layered symmetric (0/90/C/90/0) sandwich plate

A five-layered soft-core sandwich plate is considered here for deriving the free-vibration responses. The thickness of the core layer is considered to be 0.8h while the thicknesses of the face sheets are 0.05h each. The non-dimensional fundamental frequencies of the sandwich plate are tabulated in Table 3.22 and compared with some standard results reported in the literature by Chakrabarti and Sheikh (2004b), Kulkarni and Kapuria, (2008) and Grover *et al*., (2013c). The present responses have deviations of 0.03% (analytical) and 0.02 % (FEM) for a very thick plate of span-thickness ratio, *S* = 6.67.

Table 3.19. Non dimensional fundamental frequencies of a symmetric laminated composite plate (0/90/90/0) with variation in the modular ratio (material property: MM6; non-dimensional parameter: ND2)

l/*h*	References	E_{11}/E_{22}				
		3	10	20	30	40
5	Noor (1973)[1]	6.618	8.21	9.56	10.272	10.752
	Present (FEM) (4x4)	6.5629	8.2764	9.5276	10.267	10.7746
	Present (FEM) (8x8)	6.5593	8.2728	9.5243	10.264	10.7718
	Present (FEM) (10x10)	6.5592	8.2726	9.5241	10.2638	10.7717
	Present (FEM) (12x12)	6.5591	8.2726	9.5241	10.2638	10.7717
	Present (Analytical)	6.5595	8.2791	9.5452	10.3025	10.8295
	Chalak *et al.* (2013)	-	8.3456	9.5703	10.2976	10.7984
	Phan and Reddy (1985)	6.5597	8.2718	9.5263	10.272	10.787
10	Present FEM	7.2431	9.841	12.217	13.863	15.1043
	Present Analytical	7.243	9.843	12.225	13.876	15.125
20	Present FEM	7.458	10.426	13.437	15.747	17.646
	Present Analytical	7.459	10.427	13.439	15.751	17.652
50	Present FEM	7.523	10.613	13.862	16.457	18.672
	Present Analytical	7.523	10.613	13.862	16.457	18.673

[1] Elasticity solution

The results in the table reported by Kulkarni and Kapuria (2008) and Grover *et al*. (2013c) have higher discrepancies as the mathematical models used are ESL-based that do not accommodate the sudden jump in the material properties of the layered structures. In soft-core-sandwich plates, the difference in the material properties of the core and the face sheets are significantly high, and the continuity conditions of the tractions are essential to be maintained at the interfaces for obtaining efficient responses. Further, the variation in the natural frequencies of the same sandwich plate is shown in Figure 3.23 for different densities of the core. It is observed in the figure that by increasing the density of the core, the normalized natural frequency increases, a behavior that correlates with the normalizing factor used for normalizing the results of natural frequencies.

3.4.4. Free Vibration Analysis of five-layered anti-symmetric sandwich (0/90/C/0/90) plate

In this example, the free vibration responses of anti-symmetric sandwich plates with diaphragm supported boundary conditions. The free-vibration responses of a five-layered anti-symmetric sandwich plate for various span-thickness ratios are presented in Table 3.23. The results are compared with the exact solutions of Rao *et al*. (2004) and results reported in the literature by Kant and Swaminathan (2001), Zhen *et al*. (2010), Chalak *et al*. (2013), and Grover *et al*. (2013c) using various kinematic models. The present results agree closely with the exact solutions of Rao *et al*. (2004) for both thick and thin sandwich plates with a marginal error of 0.15 % (analytical) and 0.14 % (FEM) for t_c/t_f = 10. The normalized natural frequencies are observed to increase with the increase in the t_c/t_f ratio. In the next example, the same sandwich plate is analyzed further to derive the natural frequencies for various span-thickness ratios. In Table 3.24 the values of the natural frequencies are collected. The natural frequencies are found to be in excellent agreement with the exact results of Rao *et al*. (2004) with a maximum discrepancy of 0.5 % (analytical) and 0.33 % (FEM) for a very thick plate (S=2). The natural frequencies are observed to increase with the increase in the span-thickness ratio. The higher-order modes of vibration of the same sandwich plate are presented in Table 3.25 for S =10 and 100. The results are also compared with the results obtained with a LW mixed model by Rao *et al*. (2004), analytical and FEM results of Zhen *et al*. (2010) using a local-global model, FEM results of Chalak *et al*. (2013) using a polynomial ZZ model and the analytical results of Kant and Swaminathan (2001) using an ESL based HSDT and FSDT model.

Table 3.20. Non dimensional fundamental modes of vibration of a symmetric laminated composite plate (0/90/90/0) with variation in the span-thickness ratio

(material property: MM5; non-dimensional parameter: ND2)

a/h	Modes	3D[1a]	Present (Analytical)	% error	Present (FEM)	% error	ZZT FE[2]	% error	ZIGT FE[1b]	% error	TOT FE[1c]	% error
10	1	11.298	11.2971	0.01	11.2962	0.01	11.4094	0.99	11.2857	0.11	11.4121	1.01
	2	21.253	21.416	0.77	21.4167	0.77	21.7406	2.29	21.3772	0.58	21.3602	0.5
	3	28.336	28.3509	0.05	28.3252	0.03	28.4337	0.34	28.3239	0.04	28.9828	2.28
	4	34.244	34.3095	0.19	34.2900	0.13	34.581	0.98	34.1788	0.19	34.7299	1.42
20	1	12.721	12.7198	0.01	12.7197	0.01	12.8586	1.08	12.7066	0.11	12.7576	0.29
	2	23.98	24.0304	0.21	24.0325	0.21	24.4625	2.01	23.9855	0.02	23.9939	0.06
	3	38.695	38.6866	0.02	38.6863	0.02	38.8872	0.5	38.6446	0.13	39.1669	1.22
	4	45.094	45.1883	0.21	45.1896	0.21	45.6529	1.24	45.3214	0.5	45.1583	0.14

[1a, 1b, 1c]Kulkarni and Kapuria (2008); [2]Khandelwal *et al*. (2013b)

3D: ABAQUS results; ZZT FE: ZigZag Theory Finite Element; ZIGT FE: Third-Order ZigZag Theory Finite Element

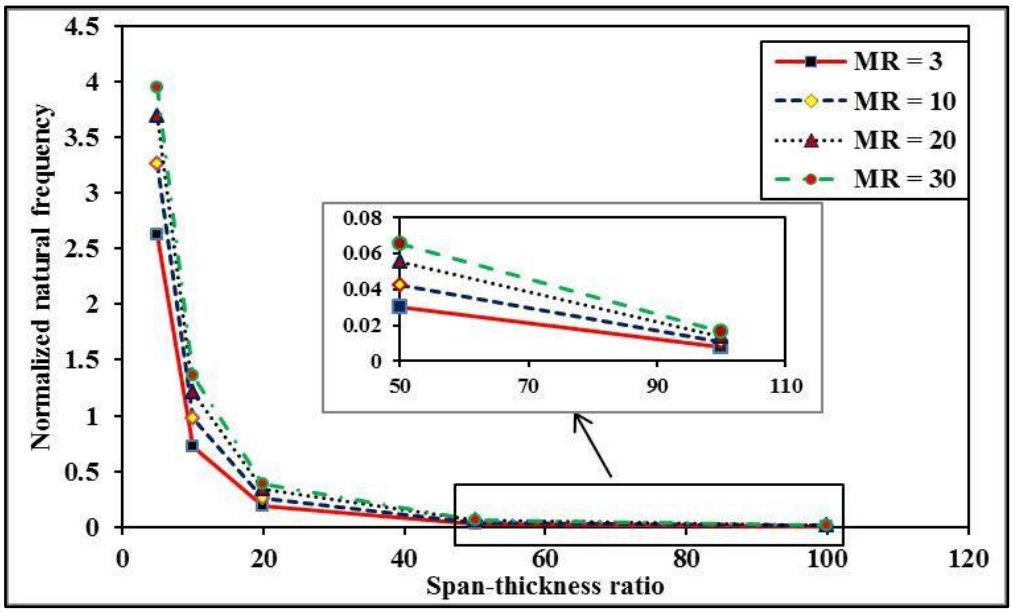

(a)

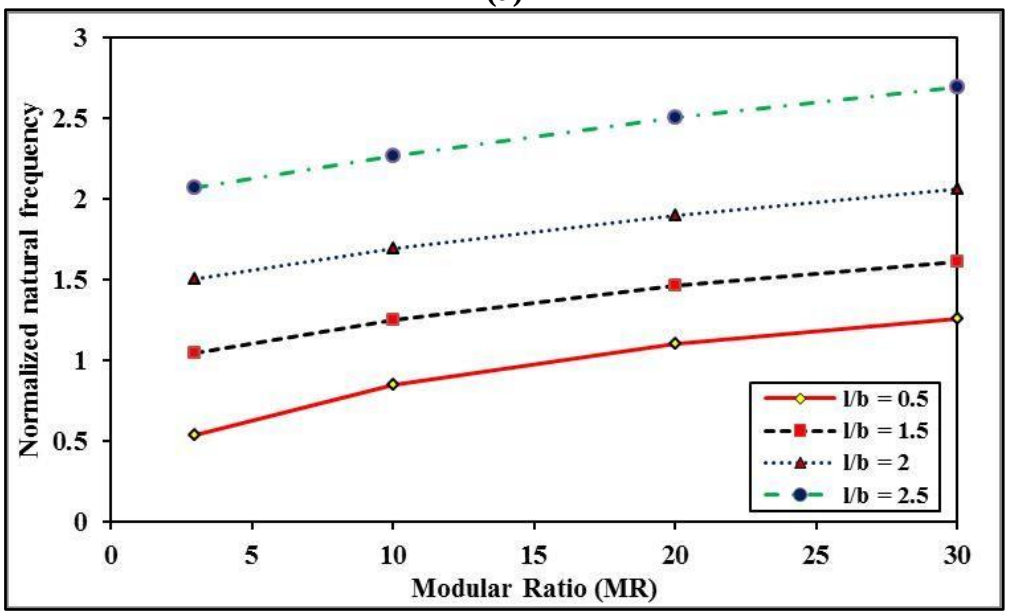

(b)

Figure 3.19(a). Variation of the normalized natural frequency of a 0/90/0 laminated plate with modular ratio (MR) and span-thickness ratio (*l*/*h*). (b). Variation of the normalized natural frequency of a 0/90/0 laminated plate with modular ratio (MR) and aspect ratio (l/b) (material property: MM6; non-dimensional parameter: ND3)

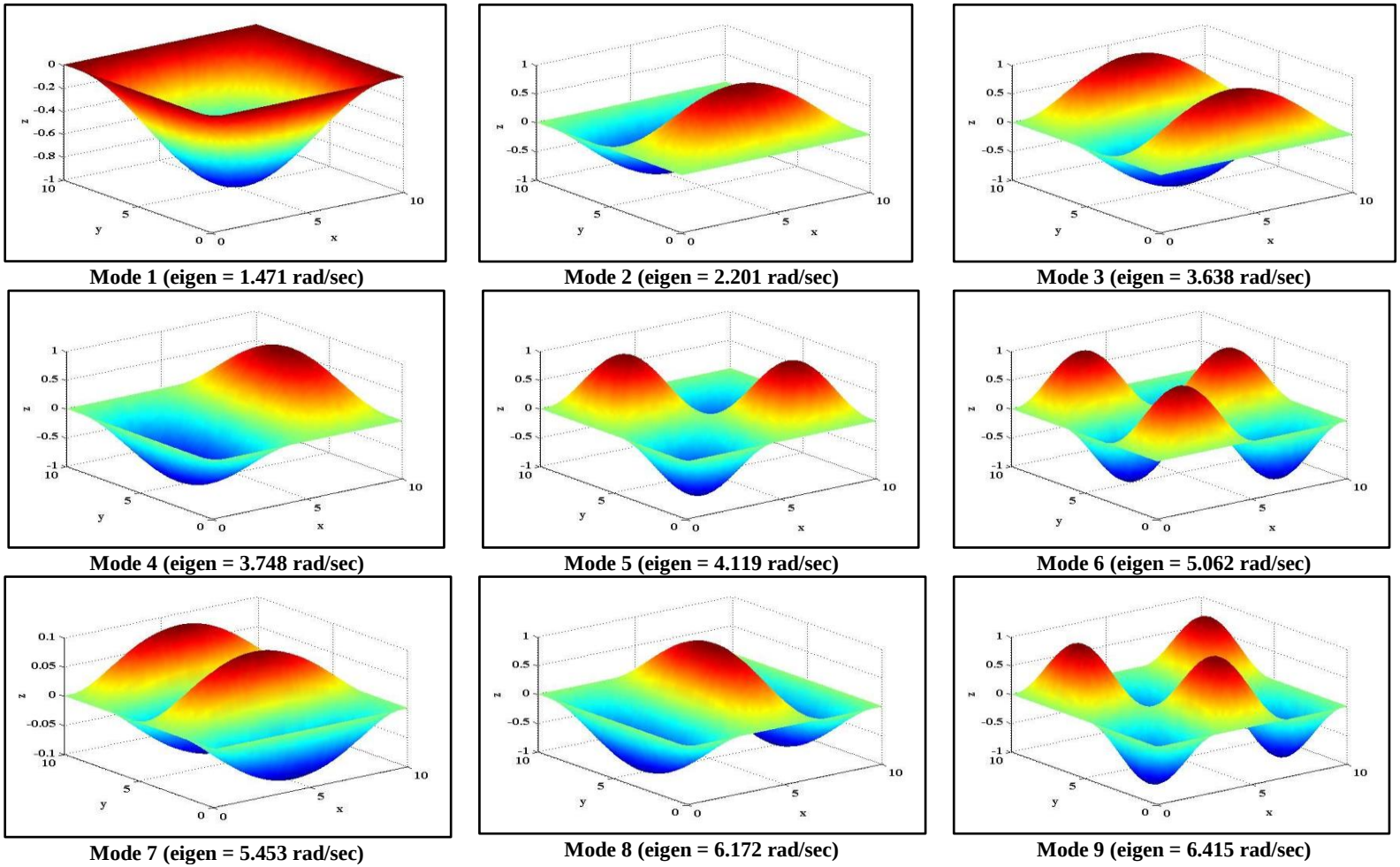

Figure 3.20. Higher order modes of vibration of a 0/90/0 laminated plate with span-thickness ratio, S = 10 and modular ratio, E_{11}/E_{22} = 40 (material property: MM6; non-dimensional parameter: ND3)

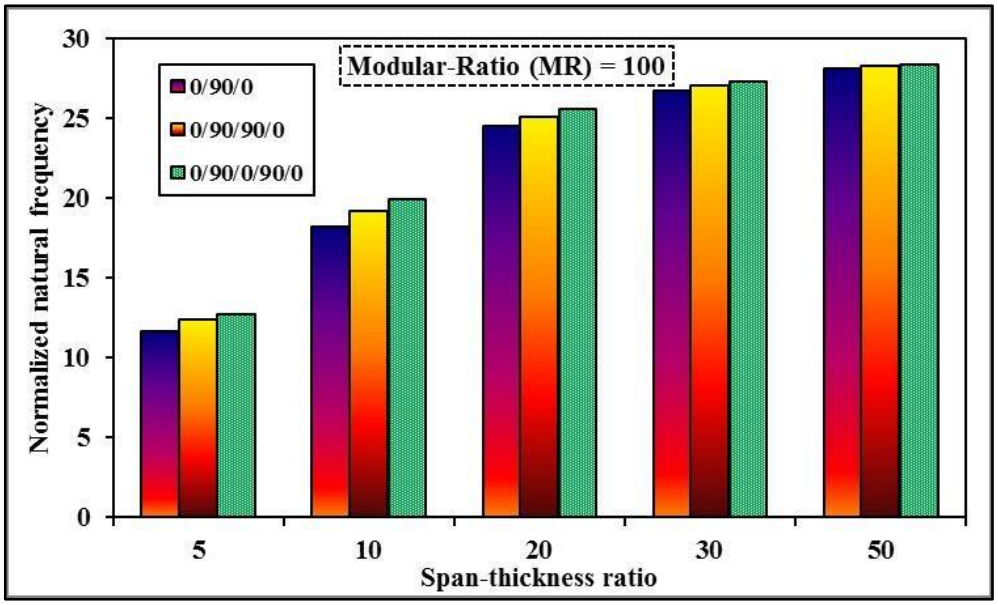

(a)

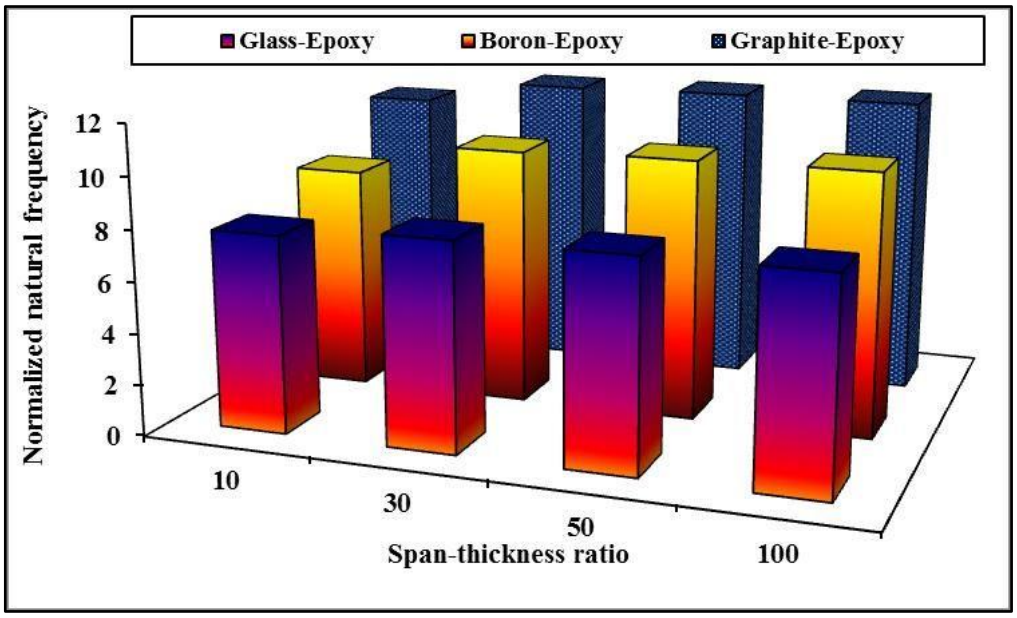

(b)

Figure 3.21(a). Variation of the normalized natural frequency with the number of layers of a laminated composite plate (material property: MM6; non-dimensional parameter: ND2). (b). Normalized natural frequencies of various laminated composite plates

Table 3.21. Non-dimensional fundamental frequencies of a sandwich plate (0/C/0) $\left([\boldsymbol{Q}]_{(face-sheets)} = \mathbf{R}[\boldsymbol{Q}]_{(core)}\right)$ **(non-dimensional parameter: ND4)**

a/h	References	R				
		1	5	10	20	50
4	Present FEM	24.7035	35.0571	40.1280	44.5077	48.8744
	Present Analytical	24.704	35.058	40.129	44.509	48.878
10	Present FEM	4.7405	7.7131	9.8079	12.2228	15.3538
	Present Analytical	4.74	7.713	9.808	12.223	15.354
100	Present FEM	0.0496	0.0852	0.1151	0.1586	0.2458
	Present Analytical	0.0496	0.0852	0.1151	0.1586	0.2458

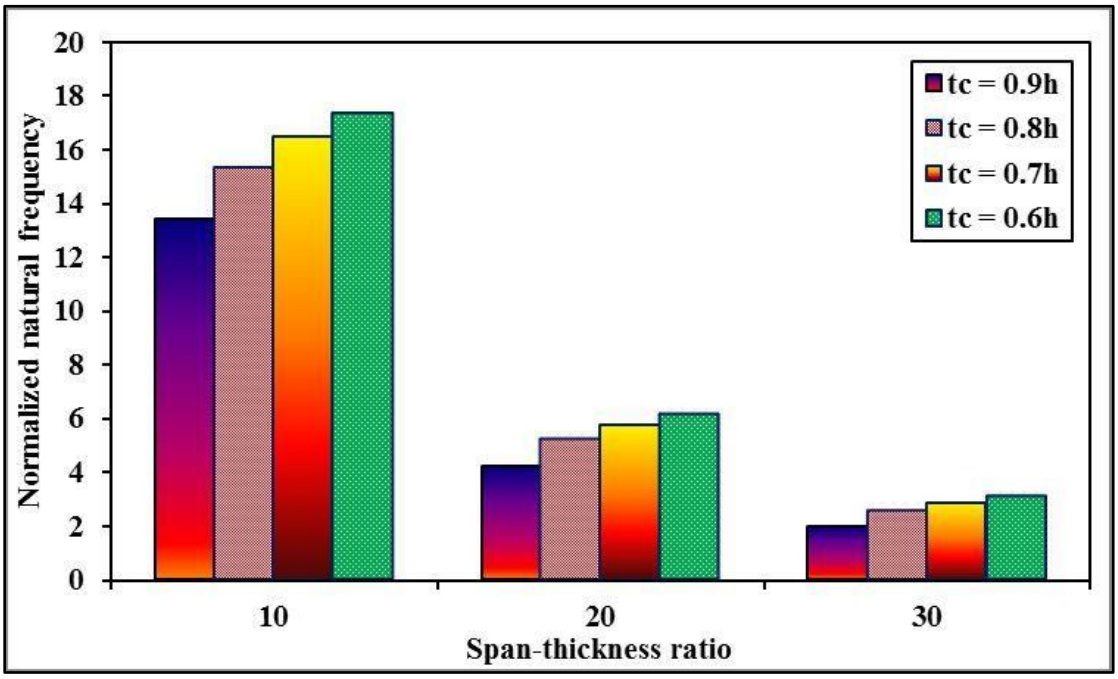

Figure 3.22. Variation of the fundamental natural frequencies of a 0/C/0 sandwich plate with thickness of the core (t_c) and span-thickness ratio (non-dimensional parameter: ND4)

Table 3.22. Non dimensional fundamental frequencies of a 0/90/C/90/0 sandwich plate with variation in the span-thickness ratio (material properties: MM7 (face-sheets), MM8 (core); Non-dimensional parameter: ND5)

Reference	a/h=6.67	a/h=10	a/h=20
Kulkarni and Kapuria (2008)[1a]	10.5235	9.8281	7.6882
Present FEM	10.5190	9.8247	7.6864
% error	(0.04)	(0.03)	(0.02)
Present Analytical	10.5202	9.8257	7.6869
% error	(0.03)	(0.02)	(0.02)
Grover *et al*. (2013c)	12.1389	11.1572	8.3258
Kulkarni and Kapuria (2008)[1b]	10.5255	9.83	7.689
Chakrabarti and Sheikh (2004b)	10.57	10.053	7.93
Kulkarni and Kapuria(2008)[1c]	13.315	12.088	8.721

[1a, 1b, 1c] 3D (ABAQUS), ZIGT (Analytical), TOT FE

ZIGT: Third-Order ZigZag Theory; TOT FE: Third-Order Shear Deformation Theory

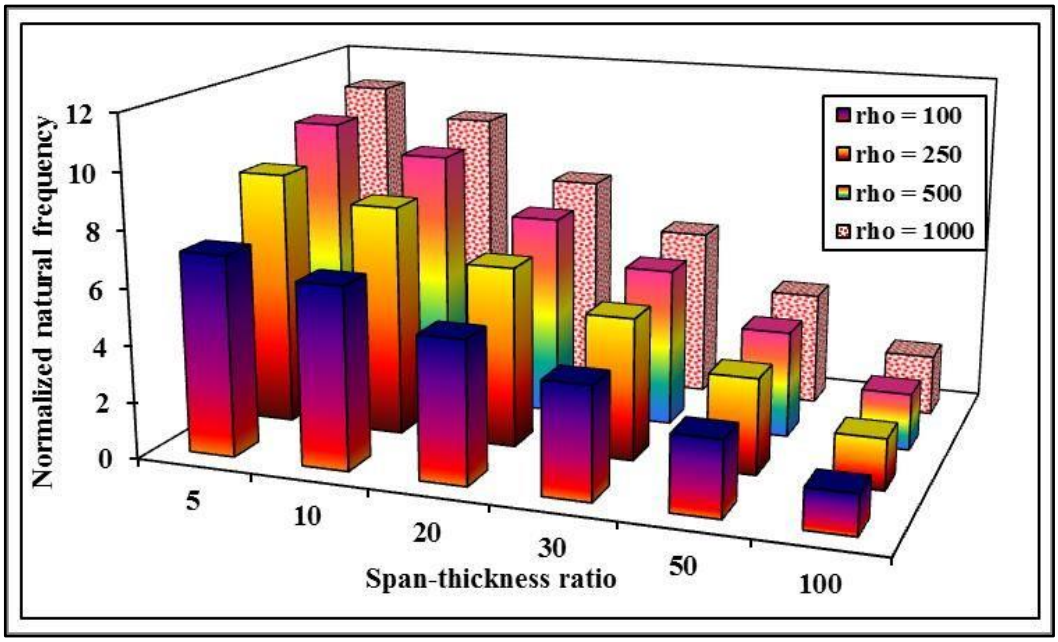

Figure 3.23. Variation in the fundamental frequencies of a 0/90/C/90/0 sandwich plate with span-thickness ratio and core density (rho)
(material properties: MM7 (face-sheets), MM8 (core); Non-dimensional parameter: ND5)

The present results are in good agreement with the results of Rao *et al*. (2004), Zhen *et al*. (2010), and Chalak *et al*. (2013). The results of FSDT and HSDT are grossly overestimating the natural frequencies in comparison with the present results for both thick and thin sandwich plates. This can be attributed to the significant difference in the material properties of the face sheets and the core material. As a result, the ESL-based FSDT and HSDT models overestimate the stiffness of the sandwich plates. As a further example, the natural frequencies of the same sandwich plate are presented for various aspect ratios and compared with the exact results of Rao *et al*. (2004) and results obtained with other shear deformation models by Zhen *et al*. (2010) and Kant and Swaminathan (2001) in Table 3.26. The present results are found to be in excellent agreement with the exact solutions (Rao *et al*., 2004) and also found to be more efficient than the responses of the Zhen *et al*. (2010) and Kant and Swaminathan (2001) in the table.

3.4.5. Transient analysis of traditional laminated composite plates

In this section, we present the transient responses of traditional laminated composite plate structures under the action of various forms of time-dependent mechanical excitations. The key feature of the analysis is the dynamic loadings and the corresponding time-domain responses. The various types of time-dependent loads considered for evaluating the time-dependent responses are presented earlier in Figure 3.3. We start with a three-layered (0/90/0) and a five-layered (0/90/0/90/0) laminated composite plate under the action of a suddenly applied sinusoidal mechanical load. The material properties and the geometrical details of the plates are obtained from Reddy (1982). The results of the maximum time-dependent transverse deflection are presented in Table 3.27 along with the results of Reddy (1982) and Kant *et al*. (1992) who have employed the FSDT and a HSDT with nine variables, respectively.

Table 3.23. Non dimensional fundamental frequencies of an anti-symmetric sandwich plate (0/90/C/0/90) with variation in the thickness of the core to the face sheets (t_c/t_f) (material properties: MM9 (face-sheets), MM10 (core); Non-dimensional parameter: ND6)

t_c/t_f	4	10	20	30	40	50
Rao *et al*. (2004)[1]	1.9084	1.848	2.1307	2.3321	2.469	2.5658
Present FEM	1.9098	1.8506	2.1336	2.3349	2.4715	2.5681
% error	(0.07)	(0.14)	(0.13)	(0.12)	(0.10)	(0.08)
Present Analytical	1.9111	1.8507	2.1336	2.3349	2.4715	2.5681
% error	(0.14)	(0.15)	(0.14)	(0.12)	(0.10)	(0.09)
Chalak *et al*. (2013)	1.9176	1.842	2.1271	2.3301	2.4679	2.5659
Zhen *et al*. (2010)[2a]	2.0962	1.9712	2.288	2.5153	2.6687	2.7765
Zhen *et al*. (2010)[2b]	1.9405	1.9418	2.2831	2.5146	2.6694	2.7777
Kant and Swaminathan (2001)	8.969	4.8519	3.1407	2.8466	2.8255	2.8614
Grover *et al*. (2013c)	5.6969	3.2598	2.9706	3.0615	3.1406	3.1923

[1] Exact; [2a, 2b] Finite Element, Analytical

In addition to the present responses obtained using TZZT, we have also independently obtained the responses using FSDT. Excellent convergence of the FE results can be observed in the table. The FEM responses are observed to converge at a mesh size of 8x8. The responses of TZZT are in good agreement with the FSDT responses, results of Reddy (1982) and Kant *et al*. (1992). It is to be noted that the material properties considered for the individual ply in this example have an equal magnitude of the transverse shear modulus (G_{13} and G_{23}). Therefore, the discontinuity of the transverse shear stresses is automatically removed from the interface of the laminated plate. Hence, the results obtained from ZZ-based TZZT and ESL-based FSDT and HSDT do not have much difference as observed in the table. To verify the significance of enforcing the continuity conditions of transverse shear stresses, the same laminated composite plate is considered with different properties of transverse shear modulus obtained from Pagano (1970) in which G_{13} and G_{23} are not equal. The results corresponding to both equal and unequal shear modulus are presented in Figures 3.24a and 3.24b, respectively. A significant difference in the amplitude and the frequency of vibration can be observed in the results of TZZT and FSDT in Figure 3.24b. This is

attributed to the inter-laminar continuity effect which is considered in TZZT and not in the ESL-based FSDT.

3.4.5.1 Transient analysis of laminated composite plates subjected to sinusoidal loading.

A three-layered (0/90/0) laminated composite plate of thickness (h) = 0.1524 m, length (l) = width (b) = 5h with diaphragm support at all the edges is considered in this example. The material properties of the orthotropic layers are considered from Khdeir and Reddy (1989). The laminated plate is subjected to a sinusoidal time-dependent mechanical load for 0.006 sec and then removed from the plate. The spatial variation of the load is also considered to be sinusoidal in both x_1 and x_2-axes. The displacement-time responses of the laminated plate for 0.008 sec are shown in Figure 3.25 using both TZZT (analytical and FEM) and FSDT (analytical). It is observed in the figure that FSDT underestimates the maximum transverse deflection of the laminated plate. In FSDT the transverse shear stresses are layerwise constant in each layer of the plate, and as a result, the stiffness of the laminated plate is grossly overestimated which results in the underestimation of the transverse displacement. We now consider another example in which the same sinusoidal load acts with frequencies of 500 rad/sec and 1000 rad/sec on the same laminated plate for the entire duration of the plate vibration, and the corresponding responses are shown in Figure 3.26. As expected, the plate is vibrating with different frequencies like the loading history and the entire vibration is under the forced-vibration regime under the action of the sinusoidal load. The natural frequency of the laminated plate is calculated from the free-vibration analysis, and it is noted to be 4373.3 rad/sec. The same plate is now subjected to the sinusoidal load with higher frequencies close to the natural frequency of the plate.

Table 3.24. Non dimensional fundamental frequencies of an anti-symmetric laminated sandwich plate (0/90/C/0/90) with variation in the span thickness ratio (material properties: MM9 (face-sheets), MM10 (core); Non-dimensional parameter: ND6)

a/h	Exact[1]	Present Analytical	% error	Present FEM	% error	ZZ FE[2]	% error	HSDT[3a] FE	% error	HSDT[3b] Analytical	% error	HSDT[4]	% error
2	0.7141	0.7177	0.50	0.7150	0.12	0.7086	0.77	0.7368	3.18	0.7251	1.54	1.1734	64.32
4	0.9363	0.9399	0.38	0.9394	0.33	0.9447	0.90	0.9904	5.78	0.9699	3.59	2.0913	123.36
10	1.848	1.8507	0.15	1.8506	0.14	1.842	0.32	1.9712	6.67	1.9418	5.08	4.8519	162.55
20	3.4791	3.4807	0.05	3.4807	0.04	3.4568	0.64	3.6836	5.88	3.6601	5.20	8.5838	146.72
30	5.0371	5.0385	0.03	5.0385	0.02	5.0032	0.67	5.3034	5.29	5.2875	4.97	11.0788	119.94
40	6.4634	6.4646	0.02	6.4646	0.01	6.4212	0.65	6.7727	4.79	6.7624	4.63	12.6555	95.80
50	7.7355	7.7368	0.02	7.7368	0.01	7.6882	0.61	8.0698	4.32	8.0634	4.24	13.6577	76.56
60	8.8492	8.8507	0.02	8.8508	0.01	8.7995	0.56	9.1929	3.88	9.1894	3.84	14.3133	61.75
70	9.8118	9.8136	0.02	9.8137	0.01	9.7618	0.51	10.153	3.48	10.1515	3.46	14.7583	50.41
80	10.6368	10.6389	0.02	10.639	0.02	10.588	0.46	10.9672	3.11	10.9672	3.11	15.0702	41.68
90	11.3408	11.343	0.02	11.3431	0.02	11.294	0.41	11.6552	2.77	11.6561	2.78	15.2946	34.86
100	11.94	11.9425	0.02	11.9426	0.02	11.896	0.37	12.2358	2.48	12.2374	2.49	15.4647	29.52

[1] Rao *et al.* (2004); [2] Chalak *et al.* (2013); [3a, 3b] Zhen *et al.* (2010); [4] Kant and Swaminathan (2001)

ZZ FE: ZigZag Theory Finite Element; HSDT FE: Higher Order Shear Deformation Theory Finite Element

Table 3.25. Non dimensional higher-order modes of vibration of a five-layered simply supported anti-symmetric laminated sandwich plate (0/90/C/0/90) with variation in the span-thickness ratio (material properties: MM9 (face-sheets), MM10 (core); Non-dimensional parameter: ND6)

a/h	Modes	LW[1]	Present Analytical	Present FEM	ZZT[2]	HSDT[3a] FE	HSDT[3b] Analytical	HSDT[4a]	FSDT[4b]
10	1	1.848	1.8507	1.8506	1.842	1.9712	1.9418	4.8519	13.8694
	2	3.2196	3.2283	3.2282	3.2089	3.4024	3.3625	7.9965	30.6432
	3	4.2894	4.3049	4.3047	4.3354	4.5556	4.4677	10.255	41.5577
	4	5.2236	5.2419	5.2437	5.2839	5.5906	5.4086	11.6809	50.9389
	5	6.0942	6.119	6.1223	6.1836	6.5647	6.306	13.3889	58.3636
	6	7.6762	7.71	7.72	7.927	8.5328	7.9154	16.0039	71.3722
100	1	11.9401	11.9425	11.9426	11.896	12.2358	12.2374	15.4646	16.2175
	2	23.4017	23.4045	23.407	23.4467	24.3246	24.3213	38.9232	44.7072
	3	30.9432	30.9471	30.957	30.7691	32.4813	32.2539	54.633	64.5044
	4	36.1434	36.1476	36.171	36.2601	37.9669	37.83	72.5925	94.9097
	5	41.4475	41.4532	41.516	41.405	44.5687	43.3894	83.2699	108.9049
	6	49.7622	49.7704	49.101	49.5575	52.0489	52.1795	105.1807	143.7969

[1]Rao and Desai (2004); [2] Chalak *et al*. (2013); [3a, 3b] Zhen *et al*. (2010); [4a, 4b] Kant and Swaminathan (2001)

LW: Layer Wise; ZZT: ZigZag Theory; HSDT FE: Higher-Order Shear Deformation Theory Finite Element; FSDT: First Order Shear Deformation Theory

Table 3.26. Non dimensional fundamental frequencies of an anti-symmetric laminated sandwich plate (0/90/C/0/90) with variation in the aspect ratio
(material properties: MM9 (face-sheets), MM10 (core); Non-dimensional parameter: ND6)

a/b	Rao *et al.* (2004)	Present Analytical	Present FEM	Zhen *et al*. (2010)	Zhen *et al*. (2010)	Kant and Swaminathan (2001)[*]	Kant and Swaminathan (2001)[#]
0.5	5.7326	5.7383	5.7382	6.1069	6.028	15.0128	39.484
1.5	1.09	1.0927	1.0927	1.1644	1.143	2.813	9.491
2	0.8048	0.8071	0.8070	0.8584	0.8406	2.4469	10.1655
2.5	0.6627	0.6648	0.6646	0.7045	0.6891	1.566	6.5059
3	0.5804	0.5824	0.5821	0.6145	0.6009	1.2976	5.6588
5	0.4494	0.4513	0.4502	0.4676	0.4585	0.8102	3.6941

[*] HSDT; [#] FSDT

Table 3.27. Convergence and validation of the transient deflection of symmetric laminated composite plates (material property: MM12)

		$\bar{U}_3 = 10^3 U_3$	
E_{11}/E_{22}	Reference	0/90/0	0/90/0/90/0
25	Present FSDT (Analytical)	0.3389	0.2921
	Present TZZT (Analytical)	0.3341	0.2910
	Present TZZT (FEM) (4x4)	0.3350	0.2934
	Present TZZT (FEM) (6x6)	0.3352	0.2940
	Present TZZT (FEM) (8x8)	0.3351	0.2940
	Present TZZT (FEM) (10x10)	0.3351	0.2940
	Reddy (1982)[1]	0.3386	0.2924
	Kant *et al*. (1992)[2]	0.3309	0.2902
40	Present FSDT (Analytical)	0.2986	0.247
	Present TZZT(Analytical)	0.2928	0.2464
	Present TZZT (FEM) (4x4)	0.2941	0.2499
	Present TZZT (FEM) (6x6)	0.2941	0.2504
	Present TZZT (FEM) (8x8)	0.2942	0.2504
	Present TZZT (FEM) (10x10)	0.2942	0.2504
	Reddy (1982)[1]	0.2985	0.2463
	Kant *et al*. (1992)[2]	0.2993	0.2473

[1] FSDT; [2] HSDT with nine-variables

The displacement-time responses are shown in Figure 3.27. It is observed in the figure that as the frequency of the applied sinusoidal load increases and approaches the natural frequency of the plate, the plate starts to vibrate with very high amplitudes. This phenomenon is known as the beating phenomenon. Next, the sinusoidal load is applied on the laminated composite plate with a frequency equal to the natural frequency of the plate (4373.3 rad/sec). The vibration of the plate under the resonance condition is presented in Figure 3.28.

3.4.5.2. Transient analysis of laminated composite plates subjected to pulse loading

Here, the dynamic responses of the laminated plate are presented for time-dependent pulse loading. The mechanical load is in the form of a pulse in the time domain and doubly sinusoidal in the spatial domain. The load is allowed to act for a duration of 0.006 sec, and the vibration of the plate is presented for 0.008 sec in Figure 3.29.

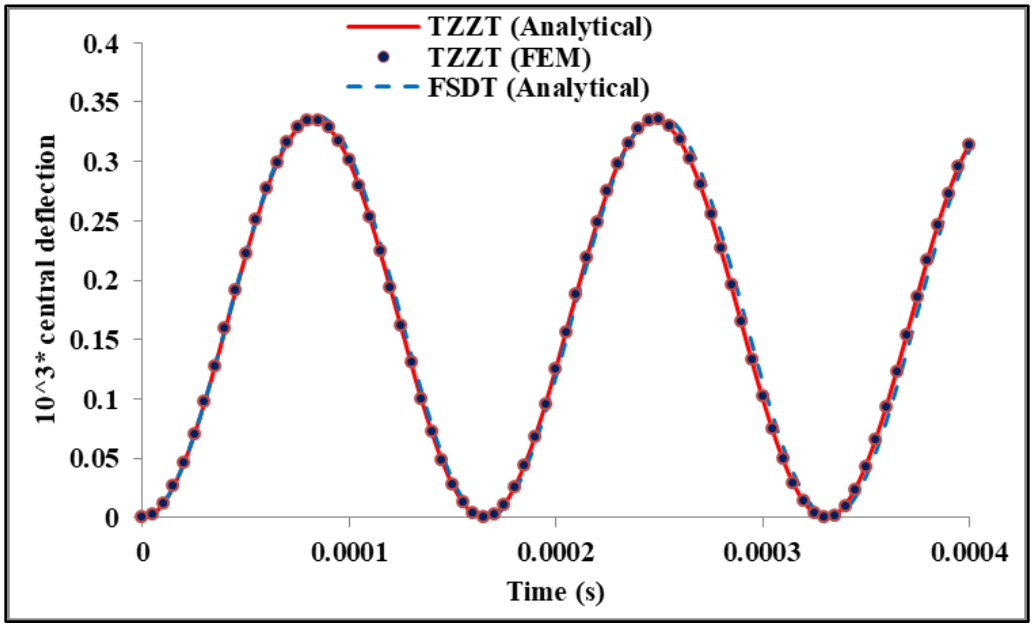

(a)

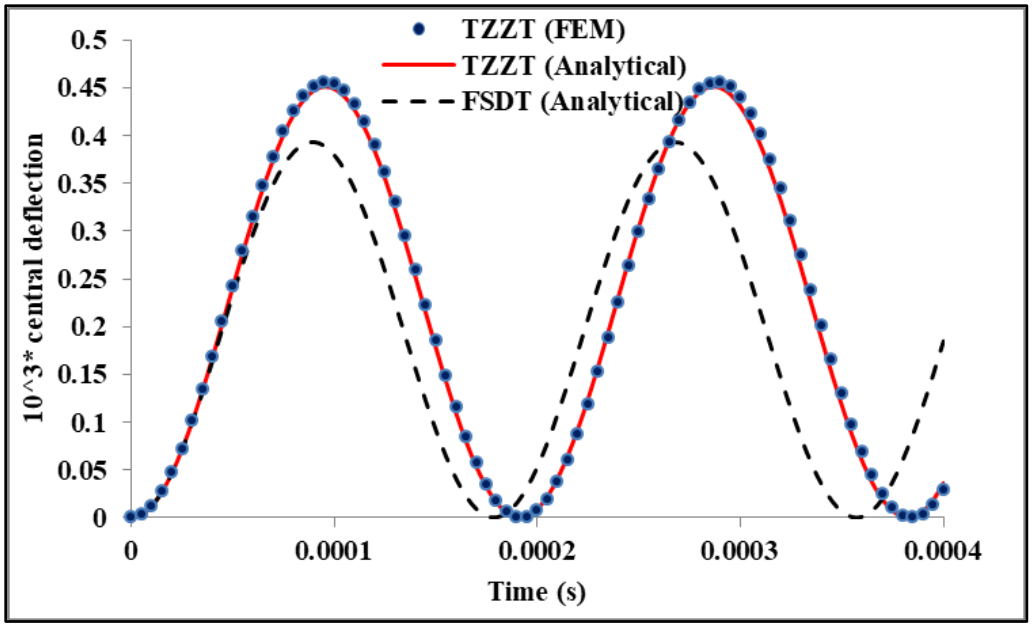

(b)

Figure 3.24 (a) Forced-Vibration response of laminated composite plate with equal transverse shear modulus (Material property: MM12) (b) Forced-Vibration response of laminated composite plate unequal transverse shear modulus (material property: MM13)

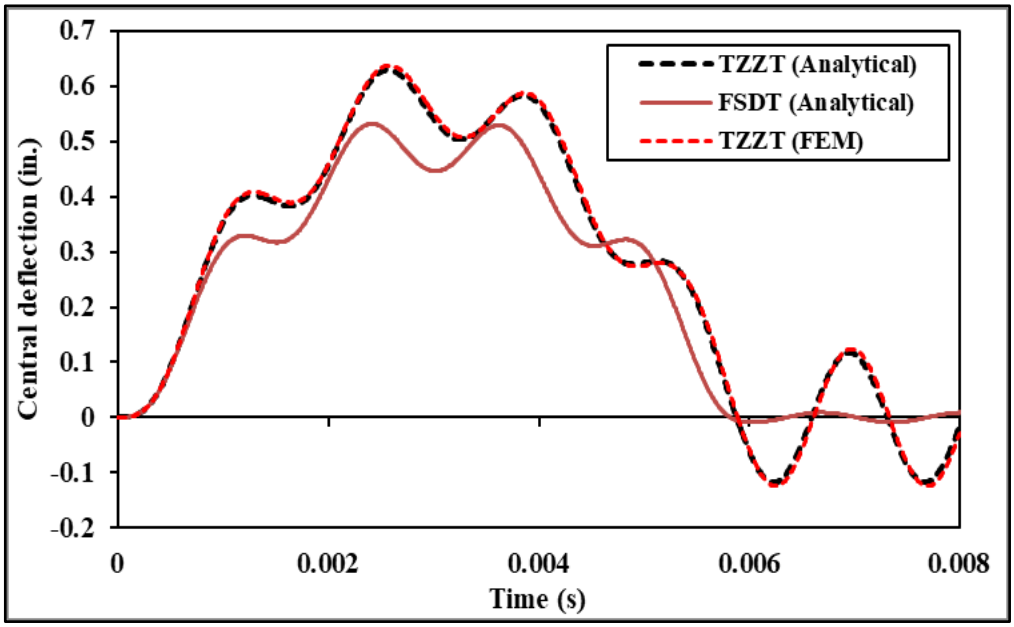

Figure 3.25. Effect of the shear deformation on the forced-vibration responses of the laminated composite plate (material property: MM11) (1 in. = 0.0254 m)

The displacement-time response totally correlates with the loading history as the amplitude of the response is constant like that of the magnitude of the pulse load up to 0.006 sec. The laminated plate enters the free vibration regime after 0.006 sec. The amplitude of the vibration in the free vibration regime is comparatively smaller in the responses of TZZT than the amplitude in the forced vibration regime (t < 0.006 sec).

3.4.5.3. Transient analysis of laminated composite plates subjected to triangular loading

The laminated composite plate is now subjected to a mechanical load that has a triangular variation in the time domain. The dynamic responses of the plate obtained using TZZT and FSDT are shown in Figure 3.30. As expected, the displacement-time response in the figure has decreasing amplitude like that of the triangular load up to 0.006 sec in the forced-vibration regime, and thereafter the plate vibrates with constant amplitude in the free vibration regime. The percentage difference in the amplitude of the transverse deflection of the plate between TZZT and FSDT is 12.48 %.

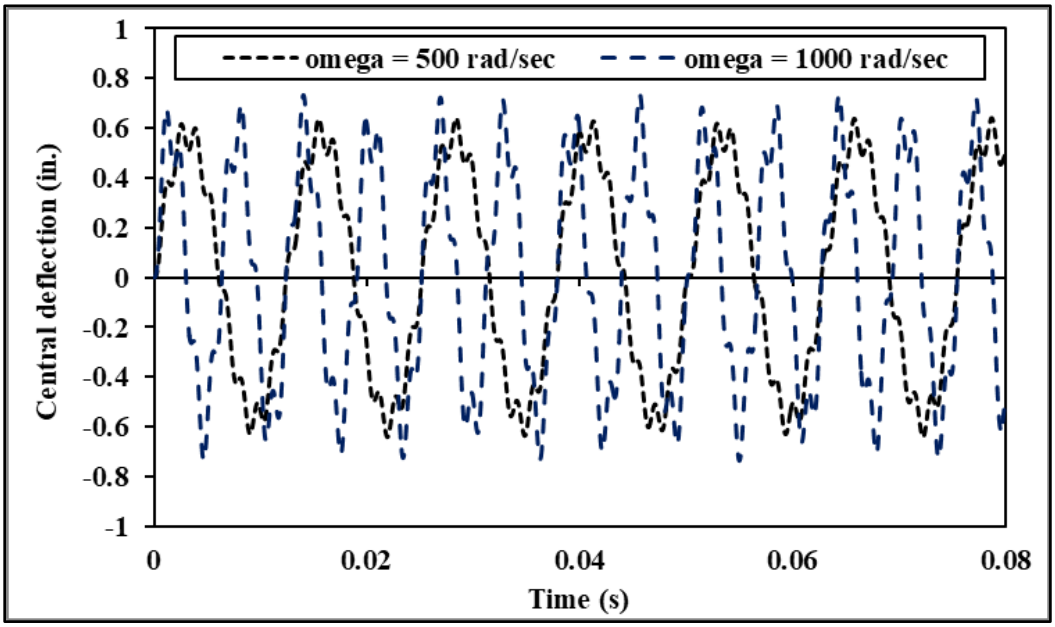

Figure 3.26. Dynamic response of the laminated composite plate subjected to sinusoidal load of different frequencies less than the natural frequency of the plate **(omega- frequency of the sinusoidal excitation) (material property: MM11) (1 in. = 0.0254 m)**

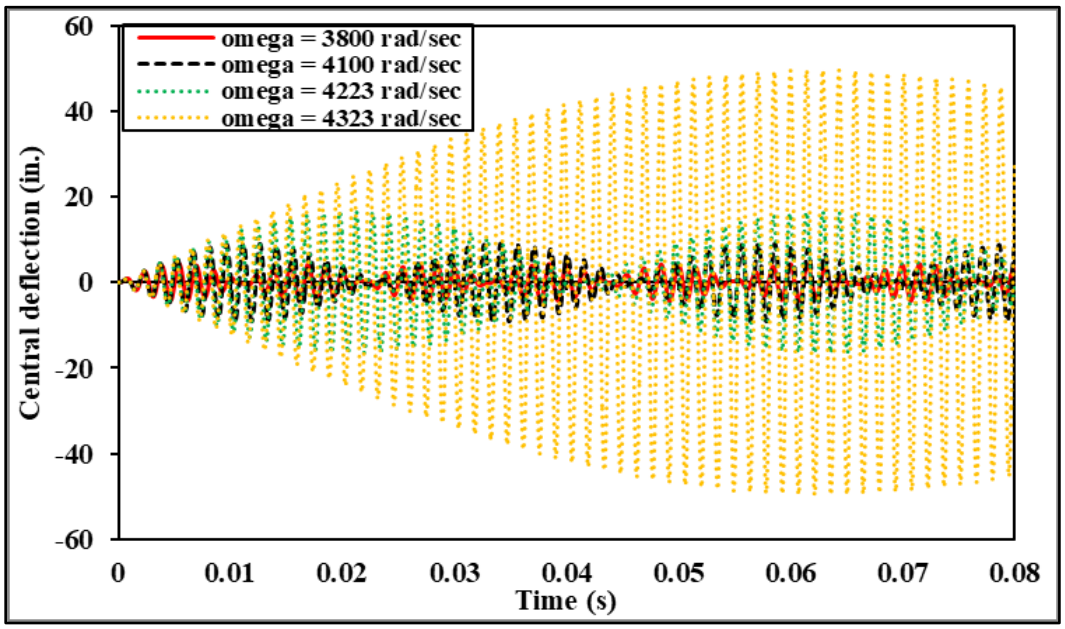

Figure 3.27. Occurrence of the beating phenomenon when the frequencies of the harmonic excitation approach the natural frequency of the plate **(material property: MM11) (1 in. = 0.0254 m)**

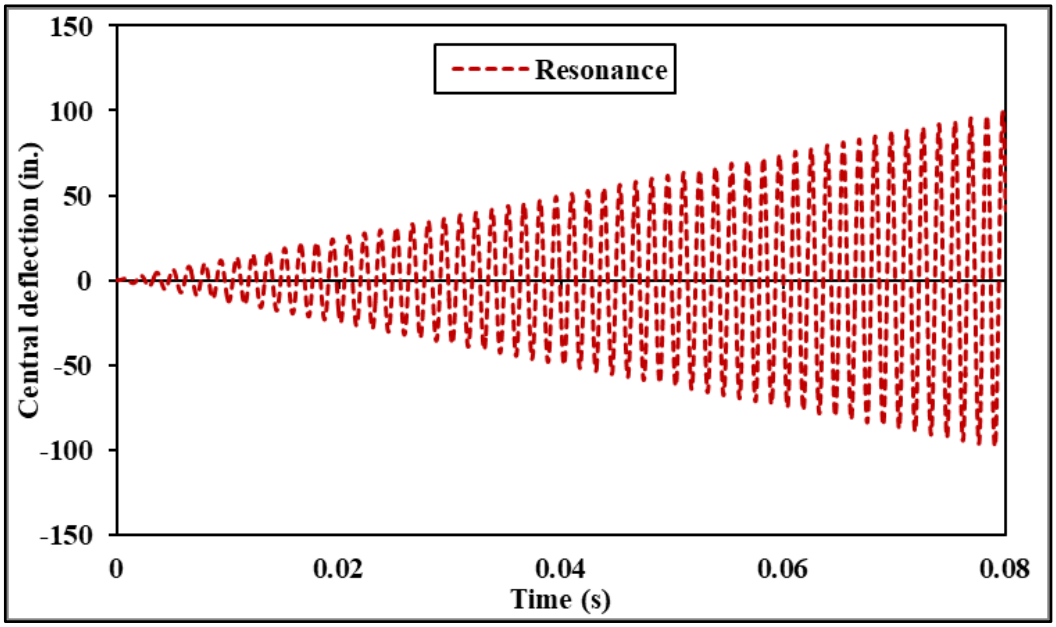

Figure 3.28. Dynamic response of the laminated plate under resonance condition.
(material property: MM11) (1 in. = 0.0254 m)

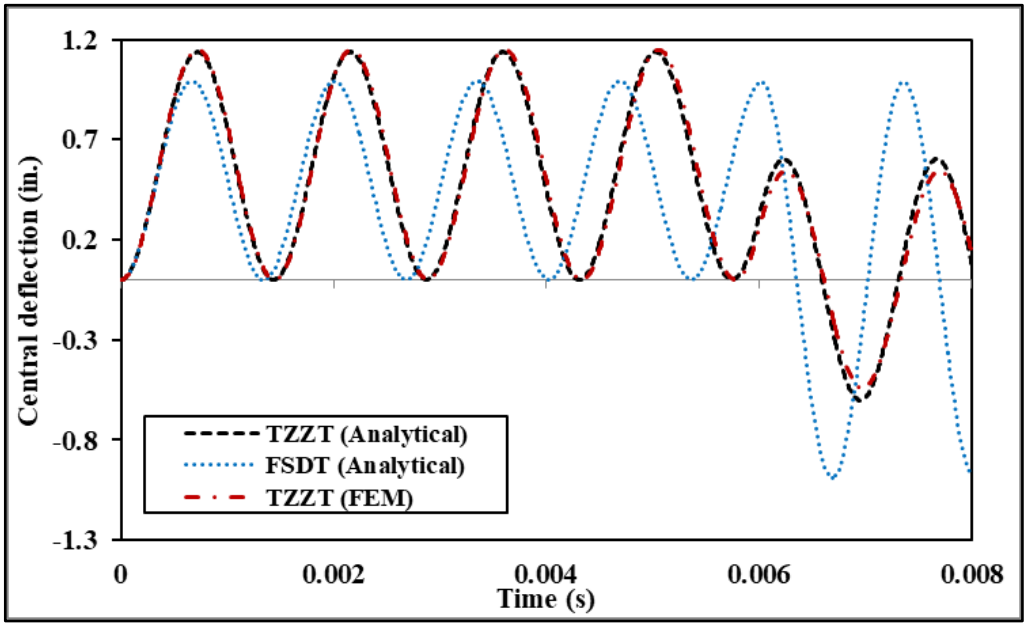

Figure 3.29. Dynamic responses of the laminated plate under pulse excitation for 0.006 sec (material property: MM11) (1 in. = 0.0254 m)

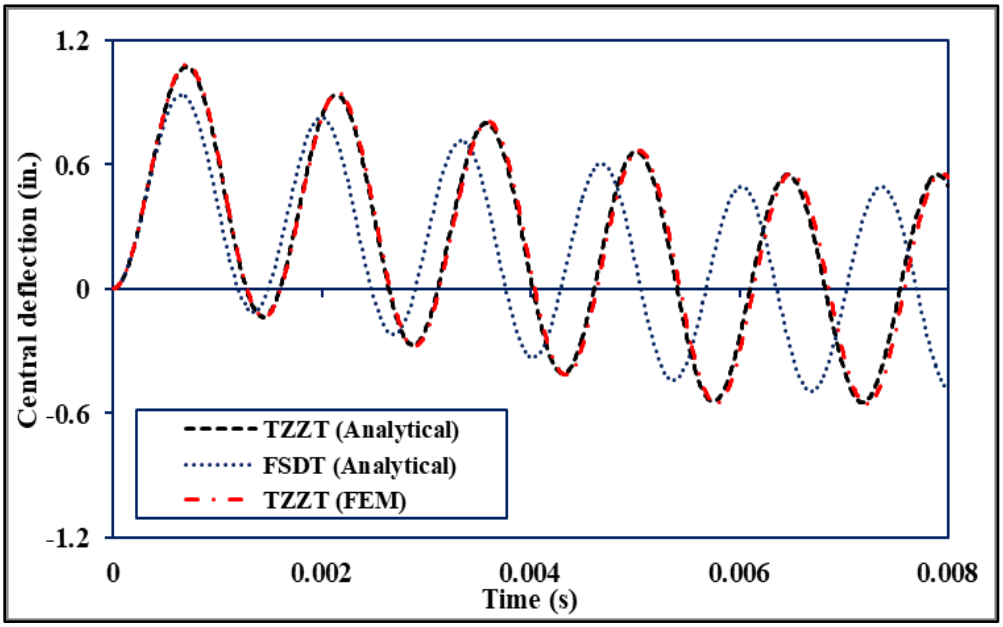

Figure 3.30 Dynamic responses of the laminated plate under triangular excitation for 0.006 sec (material property: MM11) (1 in. = 0.0254 m)

3.4.5.4. Transient analysis of laminated composite plates subjected to exponential loading

The time-dependent load is now in the form of an exponential blast which is mathematically expressed in the time-domain as $q\ (t) = q_{mn}\ e^{-\gamma t}$. γ is known as the decay parameter. The variations of the exponential blast loading for various decay parameters are shown in Figure 3.31a. The dynamic responses of the three-layered laminated plate are presented in Figure 3.31b for various decay parameters. It is observed in the figure that as the decay parameter is increasing, the quicker are the amplitudes of the vibration decaying and attaining the steady-state condition. It is also observed that after 0.007 sec, the amplitudes of the vibration are nearly the same.

3.4.5.5. Transient analysis of laminated composite plates subjected to ramp loading

The laminated composite plate is now subjected to a ramp variation of the mechanical load in the time-domain and the corresponding time-dependent responses are shown in Figure 3.32a.

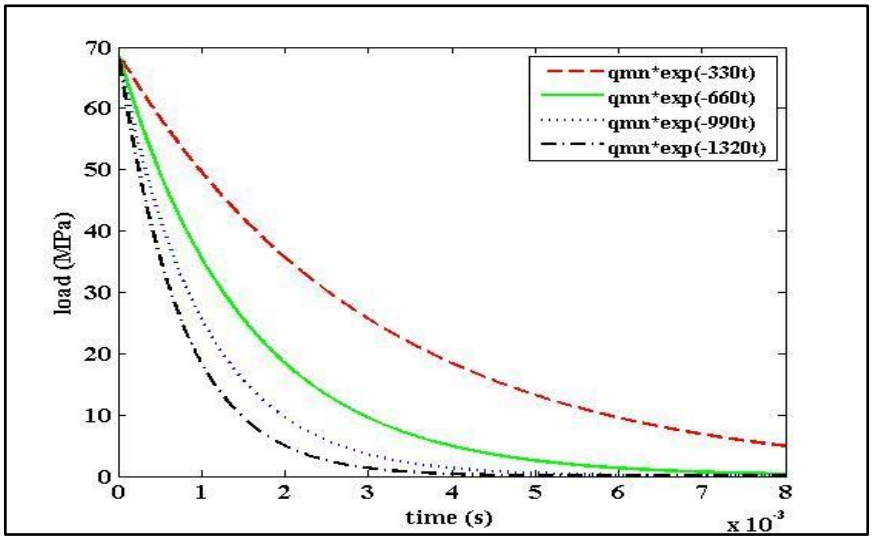

(a)

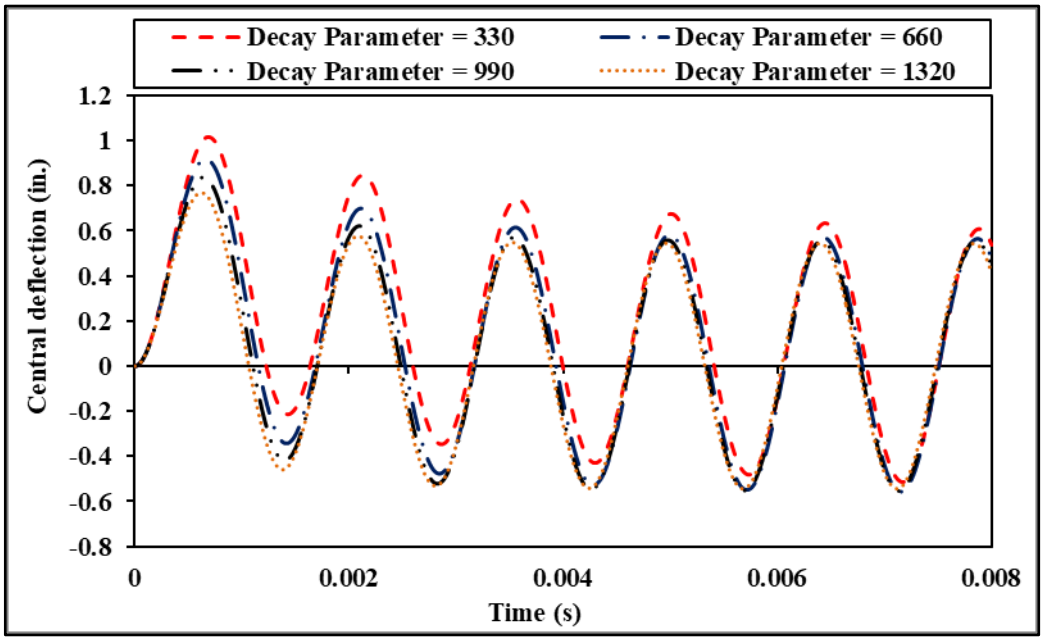

(b)

Figure 3.31 (a). Variations of the exponential blast load with various decay parameters. (b). Dynamic responses of the laminated plate under various exponential blast loads (material property: MM11) (1 in. = 0.0254 m)

The variation of the responses has an increasing trend like that of the ramp loading in the time domain. Next, the ramp loading is allowed to act for 0.006 sec, and then the load is removed from the plate so that the free-vibration responses can also be checked. The displacement-time responses for the aforementioned load are presented in Figure 3.32b. It is observed in the figure that the displacement-time responses have an increasing trend up to 0.006 sec, and thereafter the plate enters into the free vibration response with constant amplitude. The laminated plate is further subjected to ramp-constant mechanical load in the time domain. The time-dependent load has a ramp variation up to 0.006 sec, and thereafter the load behaves like a constant pulse. The dynamic responses of the laminated composite plate subjected to ramp-constant load are presented in Figure 3.32c. The displacement-time responses are similar to the responses shown in Figures 3.32a and 3.32b up to 0.006 sec, and when the load becomes constant in time after 0.006 sec, the plate oscillates around the static condition.

3.4.5.6. Transient analysis of laminated composite plates subjected to staircase loading

In this example, the mechanical load is assumed to vary in the form of a staircase in the time domain. The load varies in the form of various pulses of different amplitudes acting after specific intervals of time. The time-dependent responses for this loading condition are presented in Figure 3.33. The behavior of the responses totally correlates with the load variation as observed in the figure. Also, the responses up to 0.01 sec are exactly similar to the responses obtained earlier in the case of pulse loading. The plate vibrates with constant amplitude within an interval of 0.01 sec and a rise in the amplitude can be observed after every 0.01 sec.

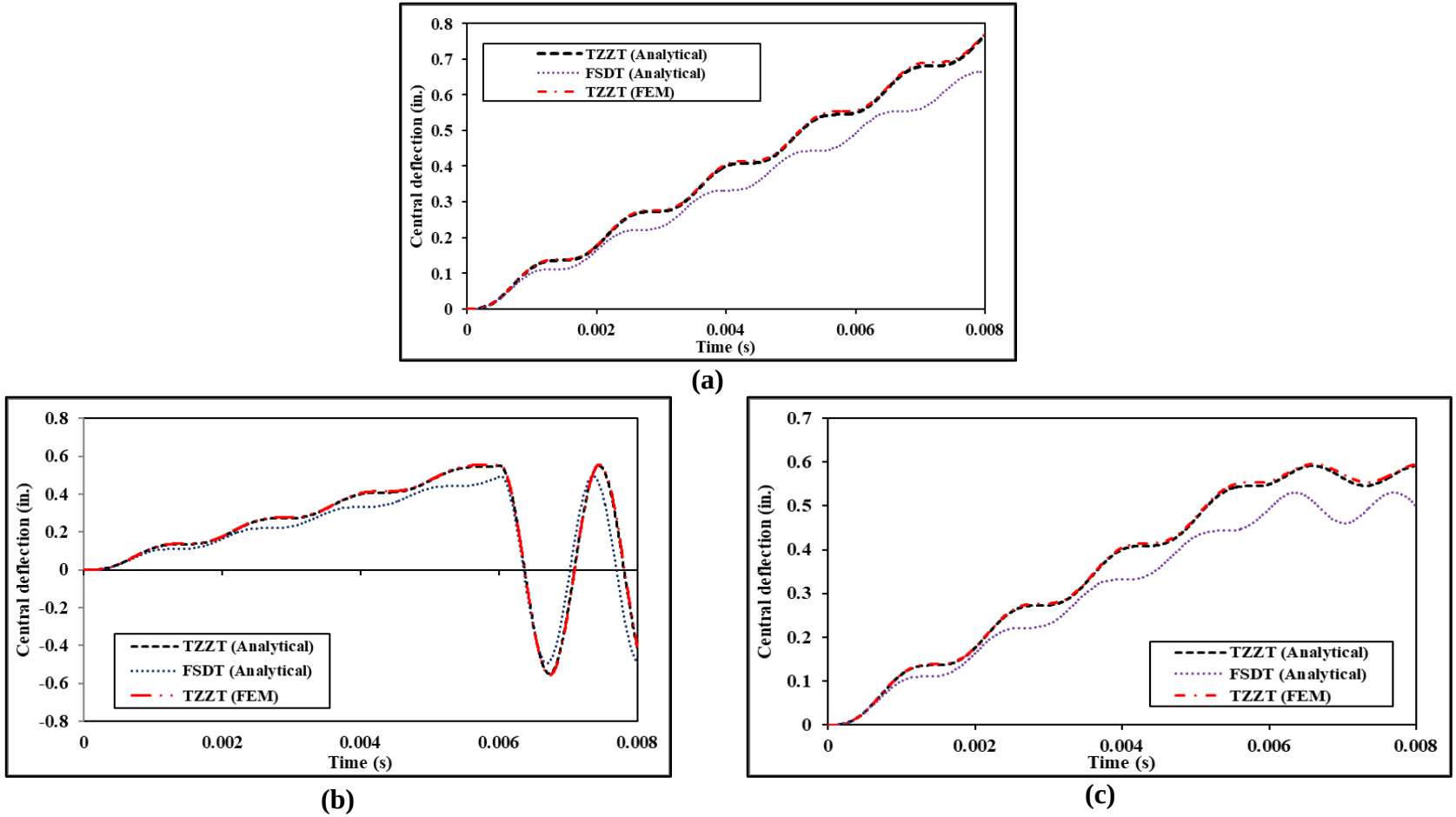

Figure 3.32 (a) Dynamic response of the laminated plate under ramp loading (b) Dynamic response of the laminated plate under ramp loading acting for 0.006 sec. (c) Dynamic response of laminated plate under ramp-constant load (material property: MM11) (1 in. = 0.0254 m)

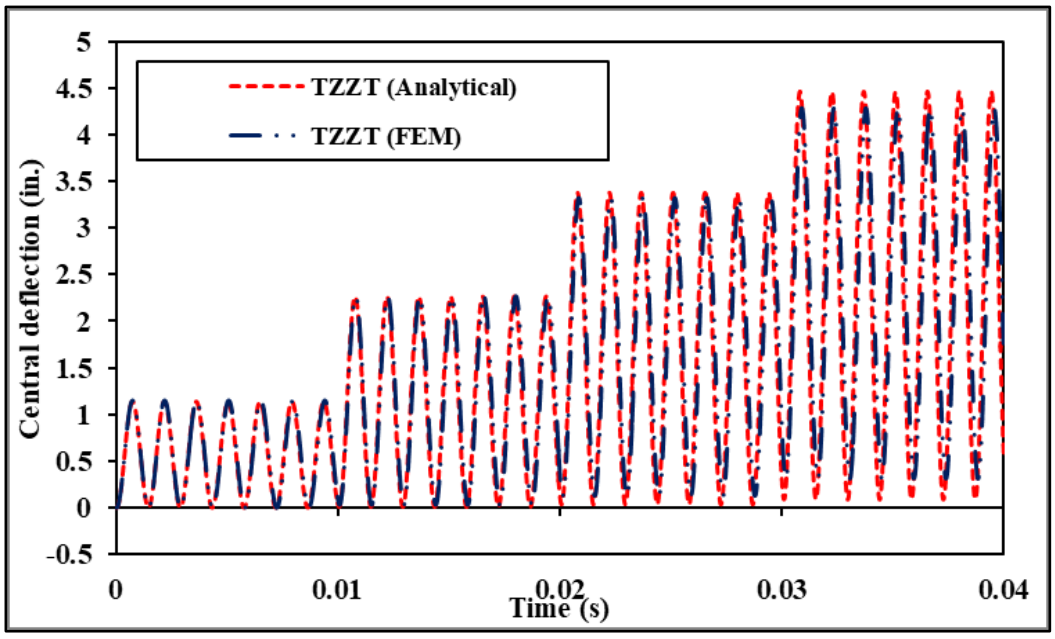

Figure 3.33. Dynamic responses of the laminated plate under staircase load variation (material property: MM11) (1 in. = 0.0254 m)

3.4.5.7. Transient analysis of laminated composite plates under blast-loading

In this section, the dynamic responses of the laminated composite plates are investigated for various types of blast loadings. Multilayered plates made up of advanced composites are widely used in supersonic/subsonic flight vehicles, and such structures are very often subjected to severe dynamic excitations like nuclear explosions and sonic boom pulses. Therefore, understanding the dynamic behavior of multilayered laminated composite plates subjected to various forms of blast loadings is very important for an efficient design.

3.4.5.7.1. Air-blast loading

Air-blast loading is a type of blast loading which is encountered due to accidental gas explosions. Mathematically, the loading is expressed as $q\ (t) = q_{mn}\ (1\text{-}t/t_p)e^{-\alpha t/t_p}$ (Kazanci, 2016) in the time domain. α is defined as the waveform parameter and t_p is the

time up to which the magnitude of the load is positive. Interestingly, the air-blast loading has positive pulses when $t < t_p$ and negative pulses when $t > t_p$. The effect on the dynamic responses of a three-layered laminated plate subjected to the air-blast loading (α = 0.35, t_p = 0.0018s) is first investigated for different aspect ratios (l/b). The displacement-time responses are shown in Figure 3.34. It is observed in the figure that the amplitude of the displacement-time response is decreasing and the frequency of the response is increasing with the increase in the aspect ratio. Next, the effect on the dynamic responses of the same laminated plate is further investigated for various values of the positive phase duration of the load (t_p). The variations of the air-blast load in the time-domain for various values of t_p are shown in Figure 3.35a and the corresponding dynamic responses of the laminated plate are shown in Figure 3.35b. The displacement-time responses in Figure 3.35b are following the load variation in the time-domain, *i.e*, the portion of the response under the positive part of the load is smaller in comparison to the negative part when the magnitude of t_p is the smallest, *i.e*, 0.001s and the response under the positive part of the load are higher than the negative part when the magnitude of t_p is the highest, *i.e*, 0.015s. The positive phase duration of the pulse (t_p) dictates the time for which the loadings are positive, therefore, for a very small value of t_p, the positive part of the load will be lesser than the negative part and vice versa.

3.4.5.7.2. Triangular-blast loading

Here, the dynamic responses of the laminated composite plate are obtained for triangular blast loading. The mathematical expression of the triangular blast load in the time domain is written as

$$q(t) = \begin{Bmatrix} q_{mn}\left(1 - \frac{t}{t_p}\right) \\ 0 \end{Bmatrix} \begin{matrix} 0 < t < t_p \\ t < 0, t > rt_p \end{matrix}$$

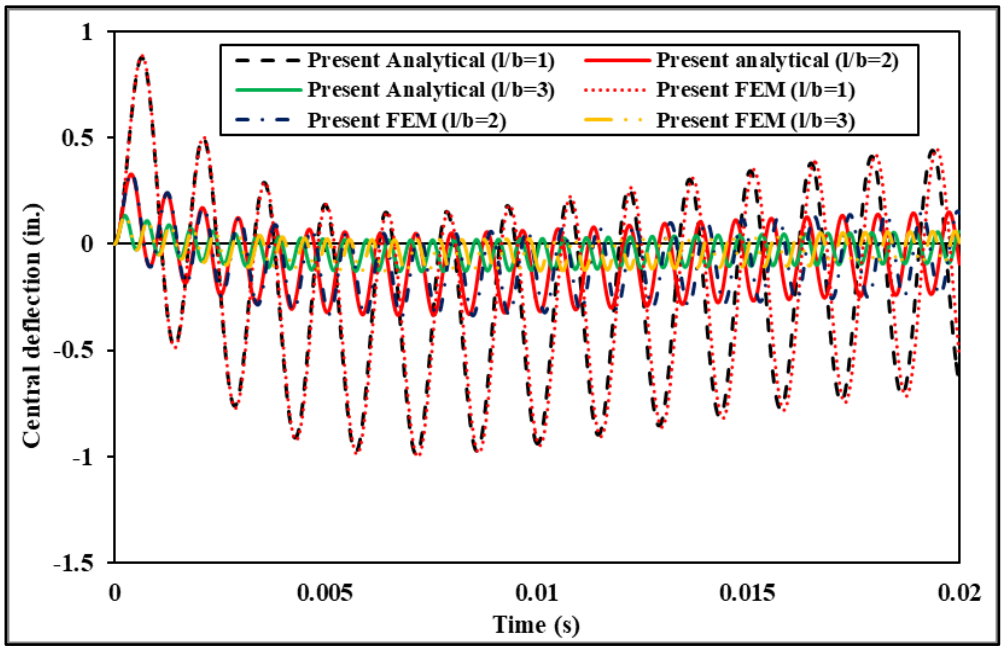

Figure 3.34 Variation of the dynamic response of the laminated plate with aspect ratios (l/b) subjected to air-blast loading (material property: MM11) (1 in. = 0.0254 m)

where *r* is the shock pulse length factor that changes the shape of the pulse in the time domain. The variations of the triangular blast loading in the time domain for various values of shock pulse length factor (*r*) are shown in Figure 3.36a. It is observed in the figure that, for *r* = 2, the triangular load changes to an N-shaped symmetrical load (sonic boom), and for *r* = 3, the symmetric N-shaped load converts to an unsymmetrical N-shaped load. The dynamic responses of the laminated composite plate corresponding to all the aforementioned variations of the triangular load for *r* = 1, 2, and 3 are presented in Figure 3.36b. It is observed in the figure that when the triangular blast load acts for a longer duration (*r* = 3), then the amplitude of the free-vibration response is the highest. The amplitude of the free vibration response for *r* = 2 is the lowest as the amplitude of the response at the time instant when the plate enters into the free vibration regime is the

lowest. Therefore, the triangular blast loading has more adverse effects when the load acts for a longer duration.

3.4.5.7.3. Pulse-blast loading

In this example, the pulse blast loading is considered to act on the laminated plate. The pulse blast loading is mathematically expressed as

$$q(t) = \begin{Bmatrix} q_{mn} \\ 0 \end{Bmatrix}; \begin{matrix} 0 < t < rt_p \\ t < 0, t > rt_p \end{matrix}$$

The time variations of the pulse load for various values of shock length factor (r) are presented in Figure 3.37a and the corresponding dynamic responses of the laminated plate are shown in Figure 3.37b. It is observed in the figure that when r = 2, *i.e*, after the strong blast, the amplitude of the vibration is very high. This is because when the strong blast ends and the free-vibration regime starts at $t = 2t_p$, the amplitude of vibration under the strong blast loading is at the maximum. Therefore the plate vibrates with high amplitude in the free-vibration regime.

3.4.5.7.4. Sinusoidal-blast loading

The sinusoidal blast load is mathematically expressed as

$$q(t) = \begin{Bmatrix} q_{mn}\sin(\pi t/rt_p) \\ 0 \end{Bmatrix}; \begin{matrix} 0 < t < rt_p \\ t < 0, t > rt_p \end{matrix}$$

The variations of the sinusoidal load in the time domain and the corresponding dynamic responses of the laminated plate are shown in Figure 3.38a and Figure 3.38b, respectively. It is observed in Figure 3.38b that the effect of the sinusoidal blast load is severe when the load acts for a short duration ($t = t_p$) as the laminated plate experiences a large amplitude of free vibration response. However, for $t = 2t_p$ and $3t_p$, the amplitude of the vibration after the strong blast is significantly less than that for $t = t_p$.

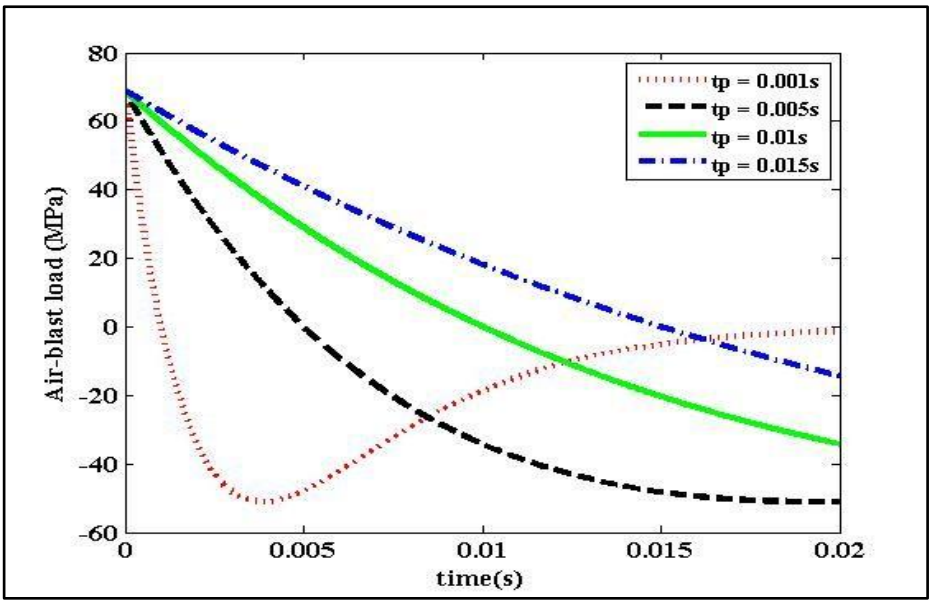

(a)

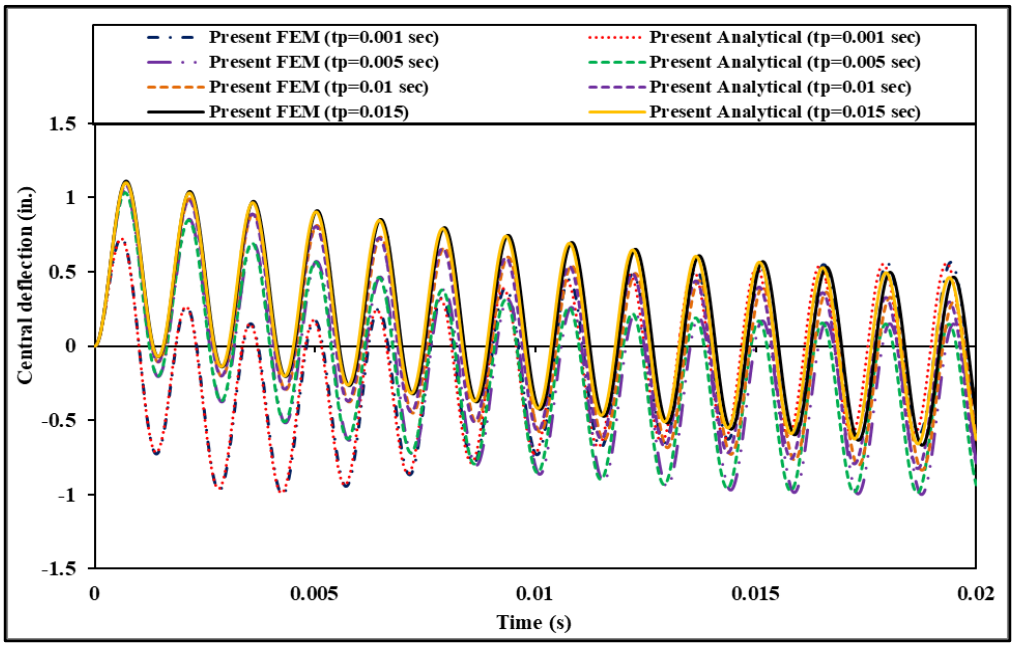

(b)

Figure 3.35 (a). Variation of the air-blast loading with various values of the positive phase duration of pulse (t_p). (b). Dynamic response of the laminated plate with various values of the positive phase duration of pulse in the air-blast load (material property: MM11) (1 in. = 0.0254 m)

3.4.5.8. Effect on the forced-vibration response of laminated composite plates due to material and geometrical features of the laminated plate.

A three-layered diaphragm supported laminated composite plate is considered here for evaluating the transient responses for various modular ratios (E_{22}/E_{11}). The material properties are obtained from Khdeir and Reddy (1989). The responses are normalized using the normalizing factor $\overline{w} = 100E_{22}h^3w/l^4q_{mn}$. The thickness of the plate is considered to be 0.1524 *m*, and the length (*l*) and width (*b*) of the plate are assumed to be five times the thickness (*h*) of the laminated plate. The mechanical load acting on the plate is sinusoidal in the time domain for 0.005 sec and doubly sinusoidal in the spatial domain with a magnitude of 68.4976 MPa. The dynamic responses of the laminated plate for various modular ratios are presented in Figure 3.39a. The amplitude of the dynamic responses is increasing with a decrease in the modular ratio. The decrease in the modular ratio decreases the stiffness of the laminated plate, and thus the amplitude of the vibration increases.

As a further example, the same laminated composite plate is considered for evaluating the dynamic responses for various span-thickness ratios. The thickness of the plate and the modular ratio are now considered to be 0.0508 m and 40, respectively. The time-dependent load is assumed to constant pulse loading acting for the entire duration of the plate vibration. The dynamic responses of the laminated plate are shown in Figure 3.39b. It is observed that the amplitude and frequency of the vibration are increasing and decreasing, respectively with the increase in the span-thickness ratio. The stiffness laminated plate decrease with the increase in the span-thickness ratio which results in the increase and decrease of the amplitude and frequency of the vibration, respectively.

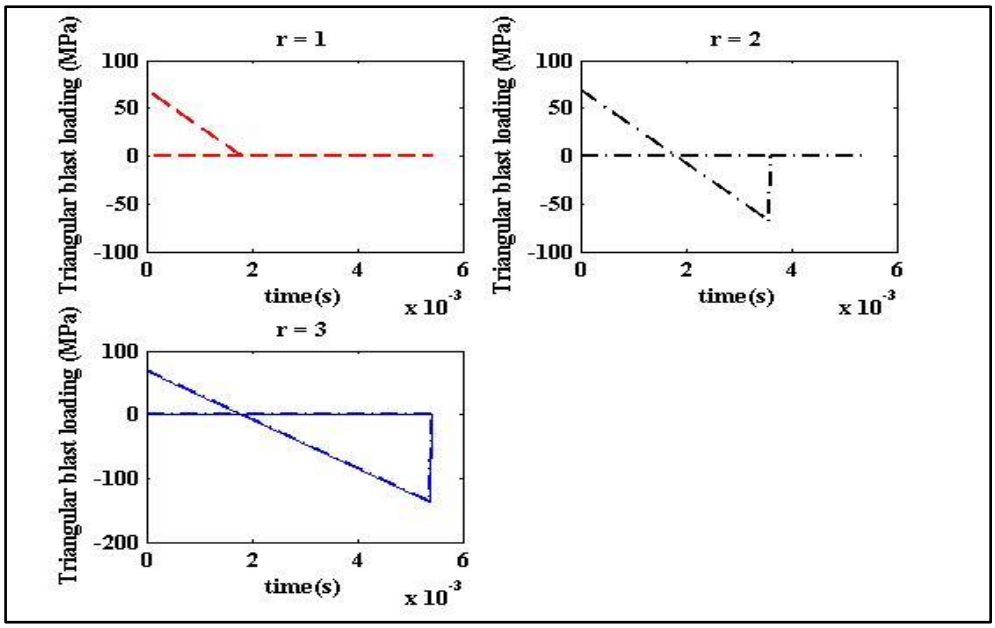

(a)

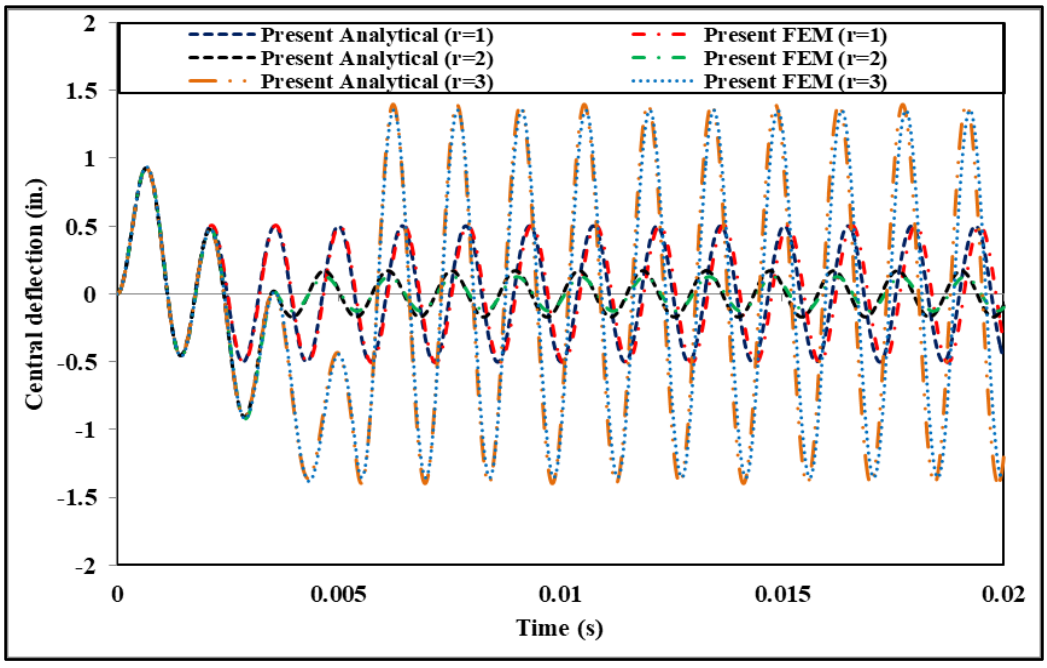

(b)

Figure 3.36 (a). Effect of the shock pulse length factor (*r*) on the variation of the triangular blast load. (b). Effect of the shock pulse length factor on the dynamic response of the laminated plate subjected to triangular blast load (material property: MM11) (1 in. = 0.0254 m)

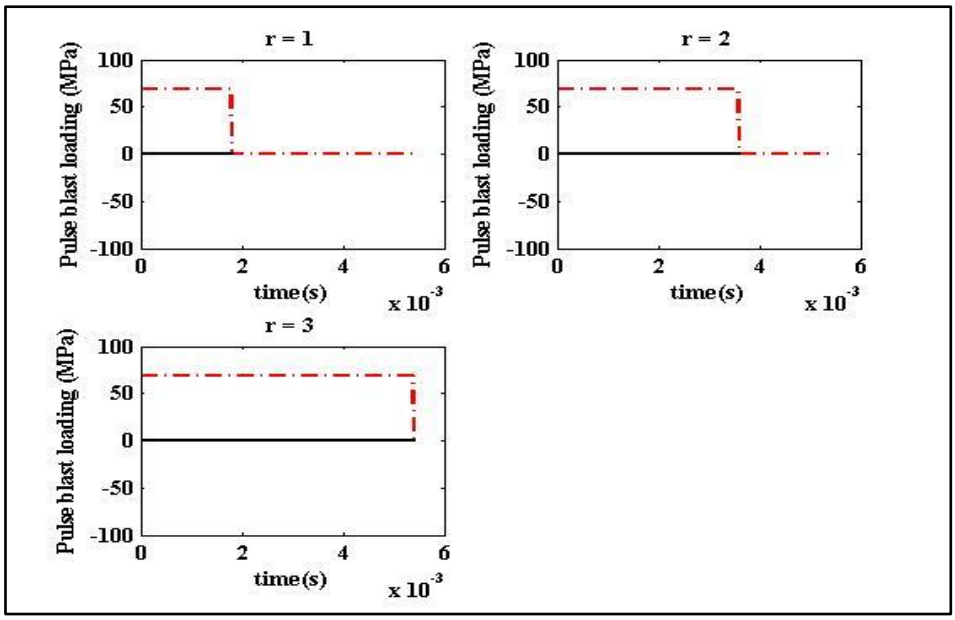

(a)

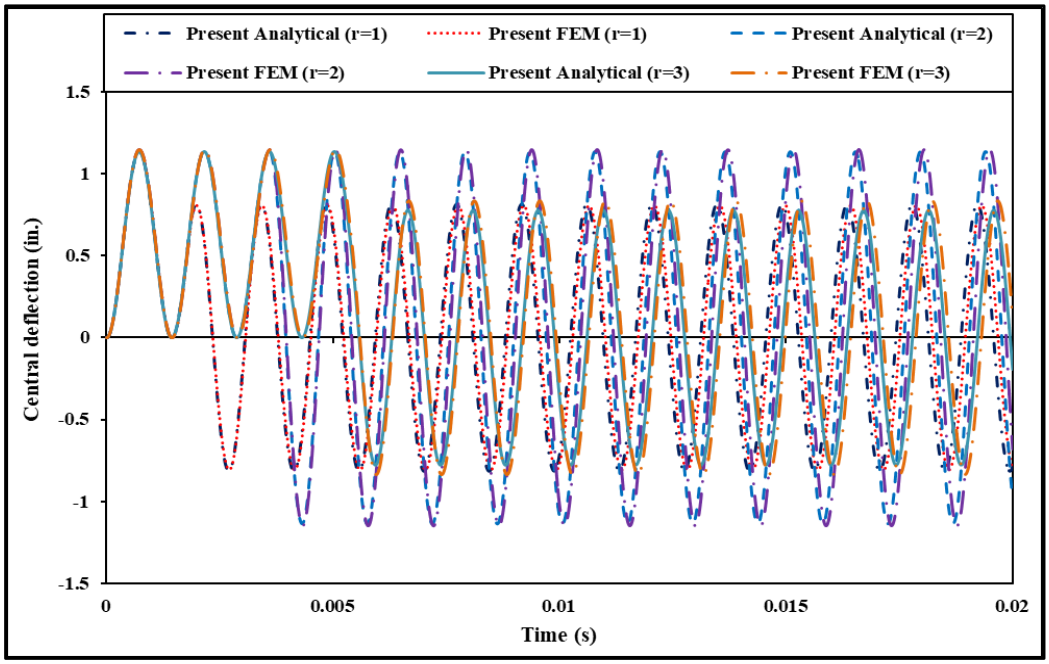

(b)

Figure 3.37 (a). Effect of the shock pulse length factor (r) on the variation of the pulse blast load (b). Dynamic response of the laminated composite plate subjected to pulse blast load (material property: MM11) (1 in. = 0.0254 m)

3.5. Dynamic analysis of smart laminated composites plates

The forced-vibration responses of the smart laminated composite plates under the action of time-dependent loads are presented in this section. The electrical and the mechanical loads are assumed to be in the form shown in Figure. 3.4 in the time domain and in the spatial domain, the loads are assumed to be bi-sinusoidal and uniformly distributed. Various piezoelectric materials like the PVDF and PFRC are used as distributed actuators and sensors integrated with the laminated composite plates. The section starts with the validation of the present responses with standard solutions available in the literature followed by some new results which may serve as benchmark results for future works. The control capacity of the PFRC patches is also shown in the examples by determining the amount of electrical load required to completely remove the mechanical vibrations from the system.

3.5.1. Dynamic response of smart composite plate (PVDF/0/90/0/PVDF) subjected to mechanical excitations only

In this example, the influence of the piezoelectric layer without electrical loads on the dynamic responses of the smart composite plate is examined. The PVDF actuator and sensor are selected as the piezoelectric material. The thickness of the material is considered to be very small, *i.e*, 10 μm and the thickness of the laminated composite is 5 cm with a span-thickness ratio of 4. The material properties of the laminated plate and the piezoelectric layer are available in Jing and Liao (1990) and Ray *et al*. (1998), respectively. A suddenly applied sinusoidal mechanical excitation is assumed to act onto the plate. Figure 3.40 shows the displacement-time responses of the plate computed with TZZT (analytical and FEM) and FSDT (analytical). The displacement-time plot reflects that FSDT underestimates the amplitude of the transverse deflection.

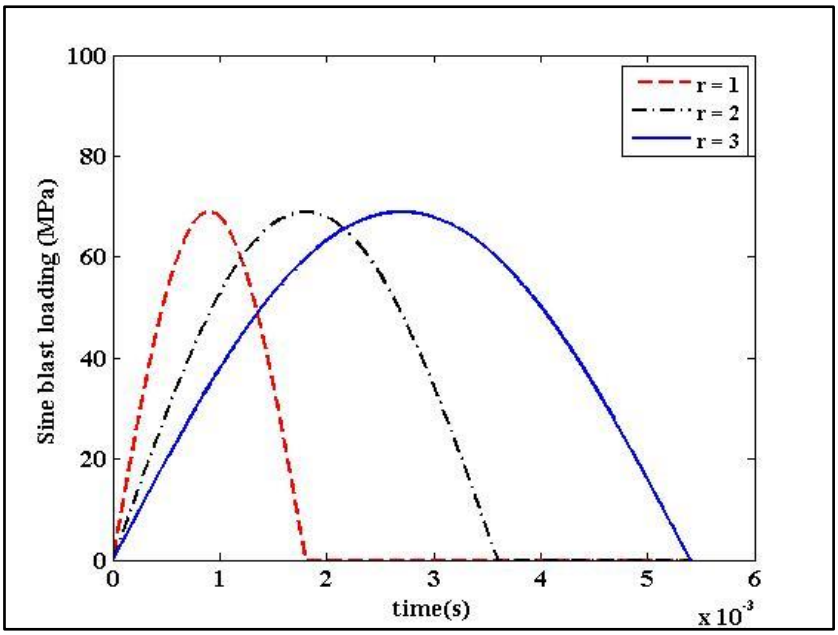

(a)

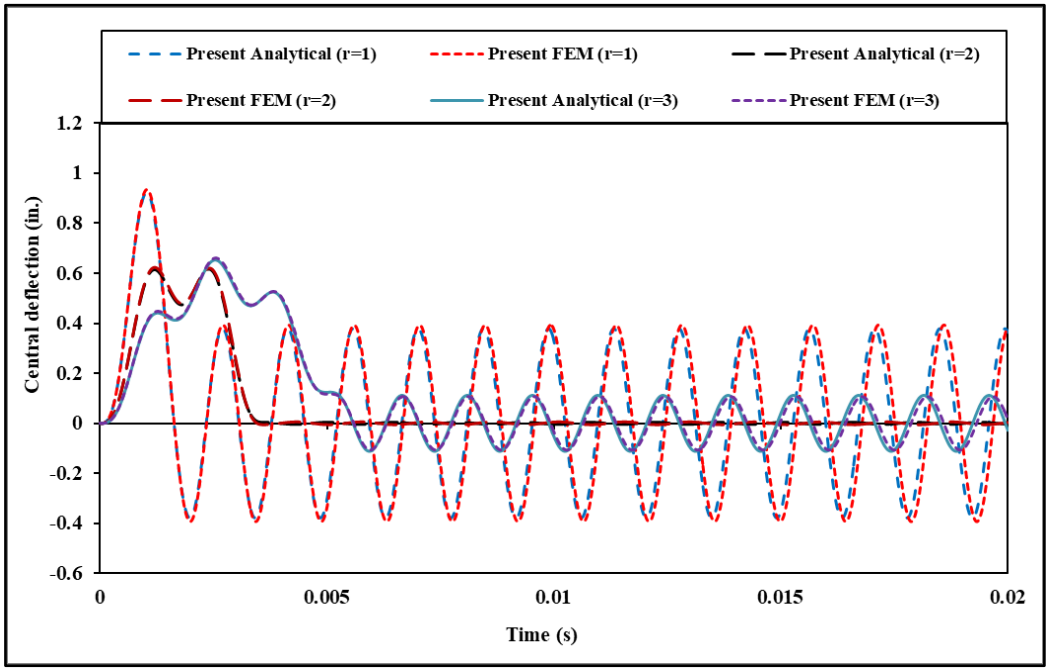

(b)

Figure 3.38 (a) Variation of the sinusoidal blast load with various values of the shock pulse length factor (r). (b) Dynamic response of the laminated composite plate subjected to sinusoidal blast load (material property: MM11) (1 in. = 0.0254 m)

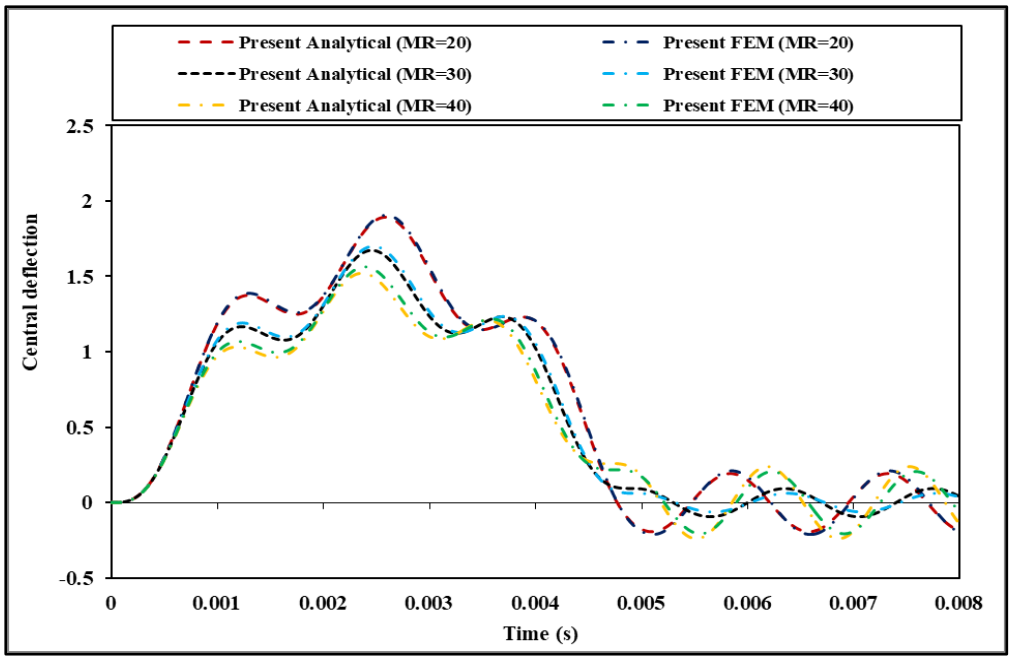

(a)

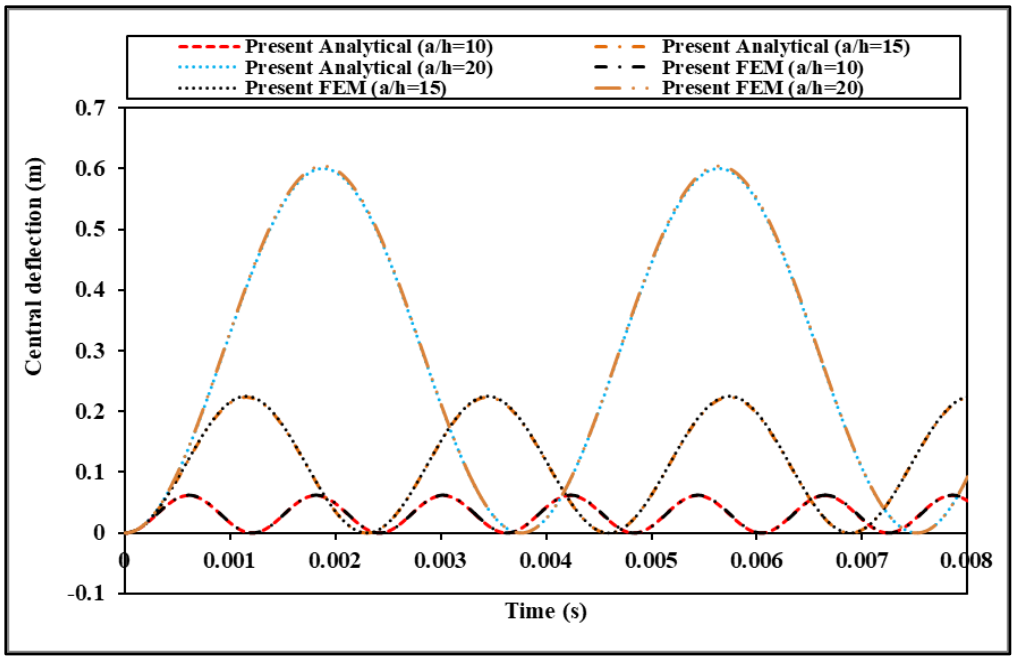

(b)

Figure 3.39 (a). Effect of the modular-ratio (MR) on the dynamic response of the laminated composite plate (*S*=5) (b). Effect of the span-thickness ratio (*S* = a/h) on the dynamic response of the laminated composite plate (material property: MM11) (1 in. = 0.0254 m)

It is also observed that the dynamic responses of the plate without PVDF layers (0/90/0) are similar to the responses of the smart composite plate (PVDF/0/90/0/PVDF) due to the small thickness of the PVDF layers. Therefore, it can also be concluded that when the thickness of the PVDF layers is very small, then the dynamic responses of the smart plate do not differ significantly from that of the traditional laminated composite plates.

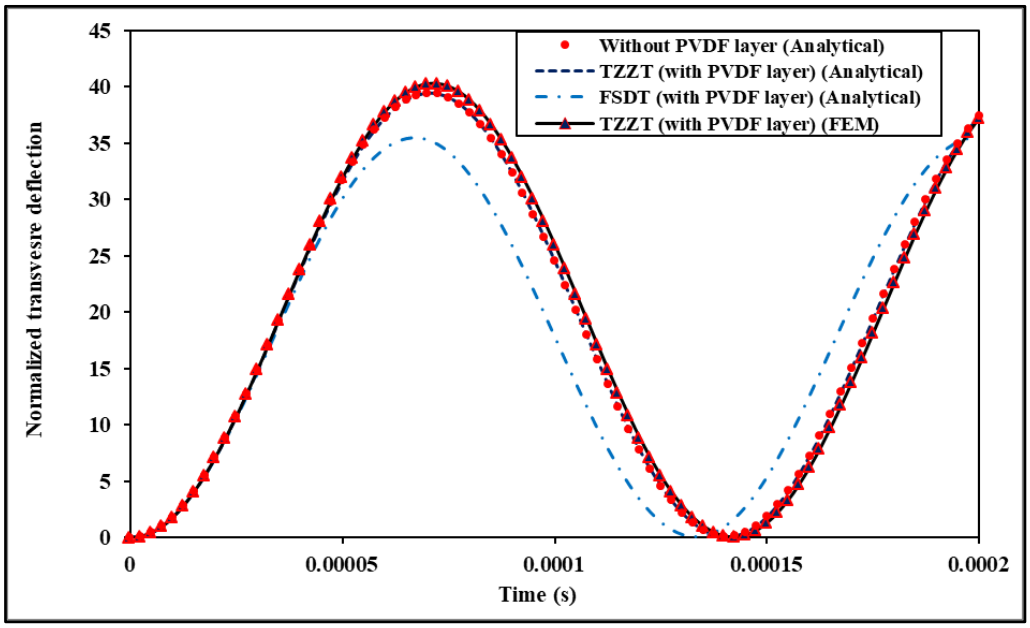

Figure 3.40. Dynamic responses of PVDF/0/90/0/PVDF plate with very small thickness of the PVDF layers under suddenly applied sinusoidal mechanical excitation (material properties: MM12 (substrate), MP1 (piezoelectric layer); non-dimensional parameter: ND7)

3.5.2. Dynamic response of smart composite (PVDF/0/90/0/PVDF) plate subjected to electrical load only.

In this example, the influence of the piezoelectric coefficients on the dynamic responses of the smart plate is examined. Therefore, the electrical loads are only allowed to

act on the system. The electrical loads shall activate the electrical force vector by the piezoelectric coefficients. It is earlier perceived in the previous example that the thickness of the PVDF layers plays a significant role in the dynamic responses of smart structures. Hence, the PVDF layers are assumed to be thicker than that of the previous example, *i.e*, 0.1 *mm*. The material properties of the laminated plate and the PVDF layers are available in Ray *et al*. (1998). The dynamic responses of TZZT (analytical and FEM) in the form of normalized transverse displacement are presented in Table 3.28 and compared with the elasticity solutions presented by Ray *et al*. (1998), finite element results of ESL based-HSDT reported by Samanta *et al*. (1996), FE results of ZZ based-HSDT reported by Topdar *et al*. (2006), FE results of FSDT obtained by Swain *et al*. (2020), and independently obtained analytical results with FSDT. It is observed that the present results are in excellent agreement with the elasticity solutions (Ray *et al*. 1998) for both thick and thin plates. The maximum error for a thick plate (S =10) is observed to be 0.48 % (analytical) and 0.08 % (FEM) from TZZT, 17.45 % from FSDT (analytical), 2.11 % from ZZ based HSDT (Topdar *et al*., 2006), 8% from ESL based HSDT (Samanta *et al*., 1996), and 17.33 % from FE results of FSDT (Swain *et al*., 2020). Figure 3.41 shows the dynamic responses of the smart plate with electrical loads only (V = 100) and with electro-mechanical load ($q_{mn} = 100N/m^2$ and V = 100). It is observed that the amplitude of the dynamic responses of the smart plate subjected to electromechanical load is significantly lower than that of the electrical loads acting only. The deflection due to mechanical excitation is reduced by counteracting electrical excitation.

Table 3.28 Validation of the Forced vibration response of smart composite plate (PVDF/0/90/0/PVDF) (material properties: MM14 (substrate), MP1 (piezoelectric layer); non-dimensional parameter: ND7)

	$\bar{U}_3$				
a/*H*	6	10	20	30	50
Ray *et al*. (1998)	-2.945	-6.2	-20.44	-43.97	-119.6
Present (TZZT) Analytical	-2.99	-6.23	-20.30	-43.69	-119.77
% error	1.52	0.48	0.68	0.63	0.14
Present (TZZT) FEM	-2.9592	-6.2050	-20.2884	-43.6749	-119.6502
% error	0.48	0.08	0.74	0.67	0.04
Present (FSDT) (Analytical)	-2.222	-5.118	-18.216	-40.083	-111.172
% error	24.55	17.45	10.88	8.84	7.04
Topdar *et al* (2006)[1]	-2.915	-6.069	-19.91	-43.16	-122.15
% error	1.01	2.11	2.59	1.84	2.13
Samanta *et al*. (1996)[2]	-2.752	-5.704	-18.65	-39.91	-107.2
% error	6.55	8.00	8.75	9.23	10.36
Swain *et al*. (2020)[3]	-	-5.125	-18.173	-39.815	-109.013
% error	-	17.33	11.09	9.45	8.85

[1] Polynomial ZZ theory (FEM); [2] HSDT with eleven variables (FEM); [3] FSDT (FEM)

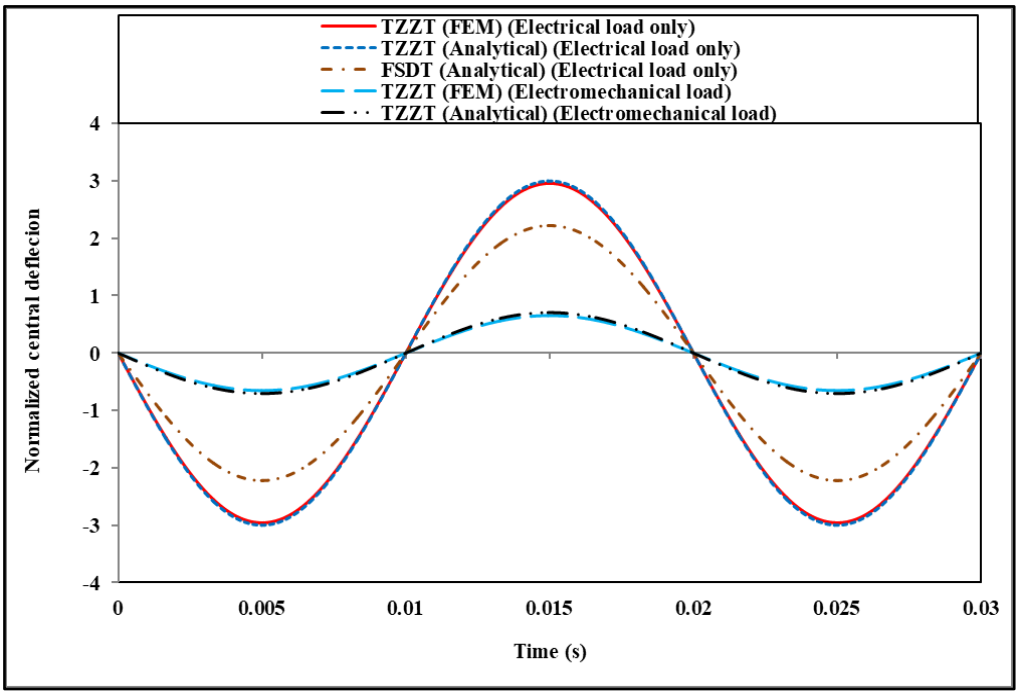

Figure 3.41. Dynamic responses of PVDF/0/90/0/PVDF plate under harmonic electrical and electromechanical excitations (material properties: MM12 (substrate), MP1 (piezoelectric layer); non-dimensional parameter: ND7)

3.5.3. Dynamic analysis of smart composite plate (PFRC/0/90/0) with PFRC actuator at the top.

The dynamic analysis of a smart composite plate with PFRC layer is not carried out in detail in the literature. Hence, in this section, the transient dynamic responses of the laminated composite plate integrated with a PFRC actuator at the top are presented using TZZT. Time-dependent loads like triangular, sinusoidal, pulse, ramp, ramp-constant and staircase are considered. The material and geometrical properties of the laminated composite plate and the PFRC patch and the normalizing factors are available in the reference Shiyekar and Kant (2011). The examples considered here will give a clear view of the dynamic controlling capacity of the PFRC layers.

3.5.3.1. Dynamic response subjected to triangular variation of electromechanical load

A simply supported laminated composite plate with a PFRC layer at the top is considered here subjected to a triangular variation of a time-dependent electro-mechanical load of magnitude -40 *Pa* and 100 *V* acting for duration of 0.03 sec. The variation of the dynamic response with the span-thickness ratio is presented in Figure 3.42(a). It is observed in the figure that the magnitude and frequency of the vibration are decreasing with the increase in span-thickness ratio (*S*) from 50 to 100. The length of the plate increases with the increase in the span-thickness ratio which results in a reduction of the stiffness and mass coefficients as they are inversely proportional to the length of the plate. Therefore, the frequency of the vibration decreases. The behavior of transverse displacement correlates with the definition of the normalizing formula which is also inversely proportional to the length. The dynamic response of the same plate with $S = 50$ is now obtained for different magnitudes of electrical excitations in Figure 3.42(b). It is observed in the figure that the magnitude and direction of the transverse vibration vary with the magnitudes of electrical

loads while the frequency of the vibration remains the same. The reason behind this is the coefficients of the electric force vector change with the magnitude of the electrical loads while the mass and stiffness coefficients remain the same. Next, the variation of the dynamic response with aspect ratios for S =70 is shown in Figure 3.43(a). The amplitude and frequency of the vibration are decreasing and increasing respectively with the increase in the aspect ratio as the increase in aspect ratio (a/b) results in a decrease in the width of the plate which results in the increment of the stiffness and mass coefficients. Next, it is shown in Figure 3.43(b) that the mechanical vibrations are nearly eradicated by counteracting electrical load of 17 V. As expected, the frequency of the vibration does not change as stiffness and mass coefficients remain unaltered.

3.5.3.2. Dynamic response subjected to step variation of electromechanical load

The dynamic response of the same plate with S = 70 subjected to pulse electro-mechanical load acting for 0.03 sec is shown in Figure 3.44(a). The vibration in the forced vibration regime for V = -100 ends at a time instant when the amplitude of vibration is maximum resulting in higher amplitude for -100 V in comparison to 100 V. The frequency remains the same as expected. The mechanically induced vibrations are nearly removed from the same plate by an electrical load of 17 V as shown in Figure 3.44(b). Next, the dynamic response of the same plate is presented in Figures 3.45(a) and 3.45(b) subjected to pulse electro-mechanical load acting for the entire duration for S = 100. The smart plate is vibrating with dynamic amplitude twice that of the static deflection in Figure 3.45(a). The vibration correlates with the loading history as observed in both figures. Finally, the influence of the thickness of the PFRC layer on the magnitude and frequency of the plate vibration is presented in Figure 3.46.

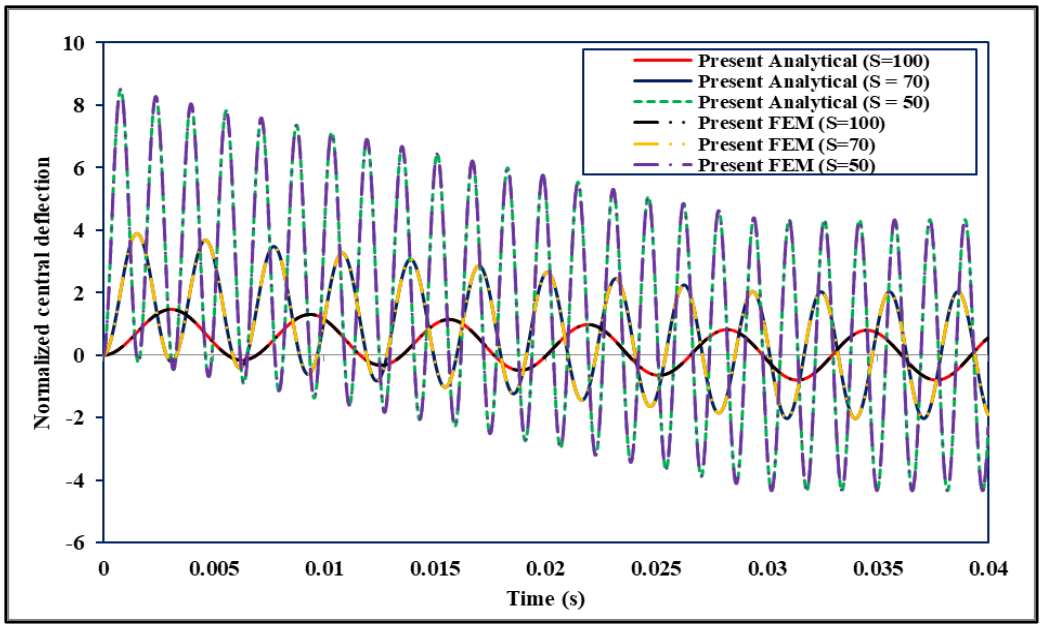

(a)

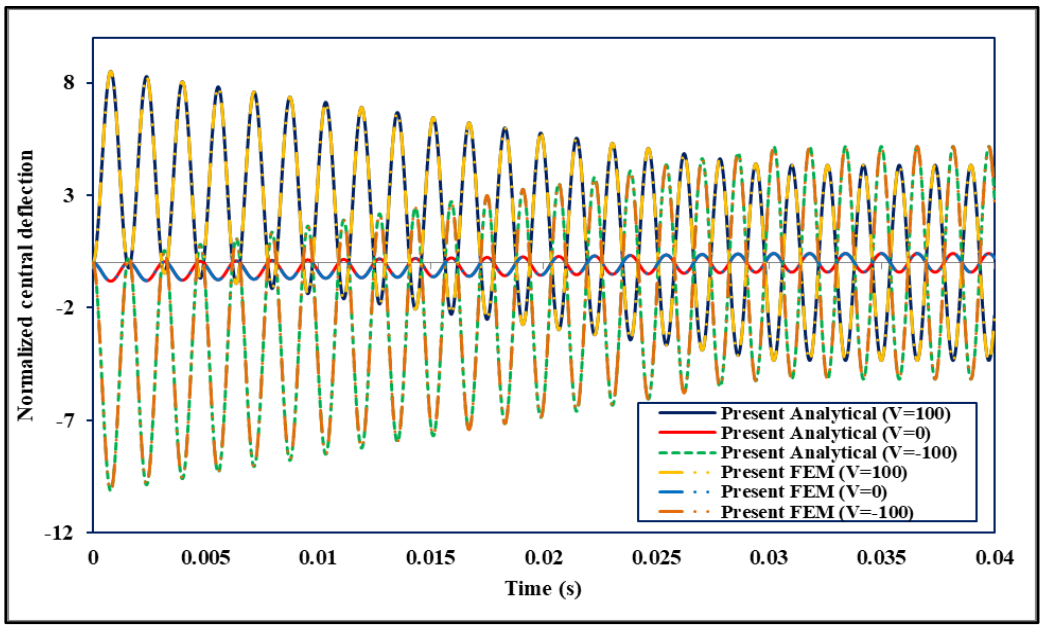

(b)

Figure 3.42(a) Dynamic response of smart plate (PFRC/0/90/0) under triangular load with different span-thickness ratios (b) Dynamic response under different magnitudes of electrical loading (material properties: MM4 (substrate), MP2 (piezoelectric layer); non-dimensional parameter: ND1)

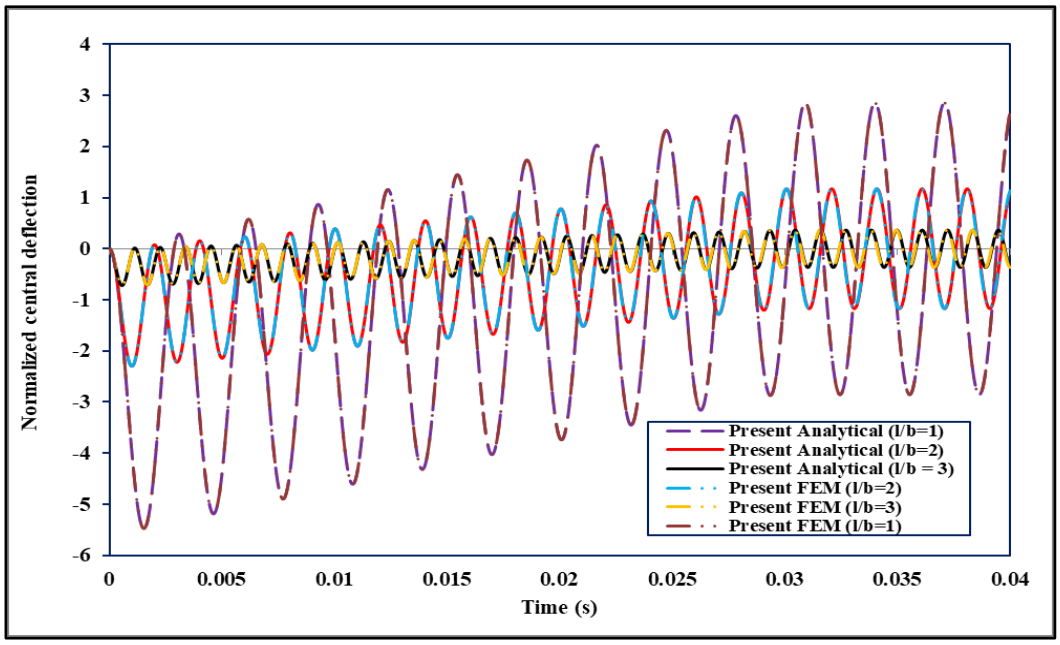

(a)

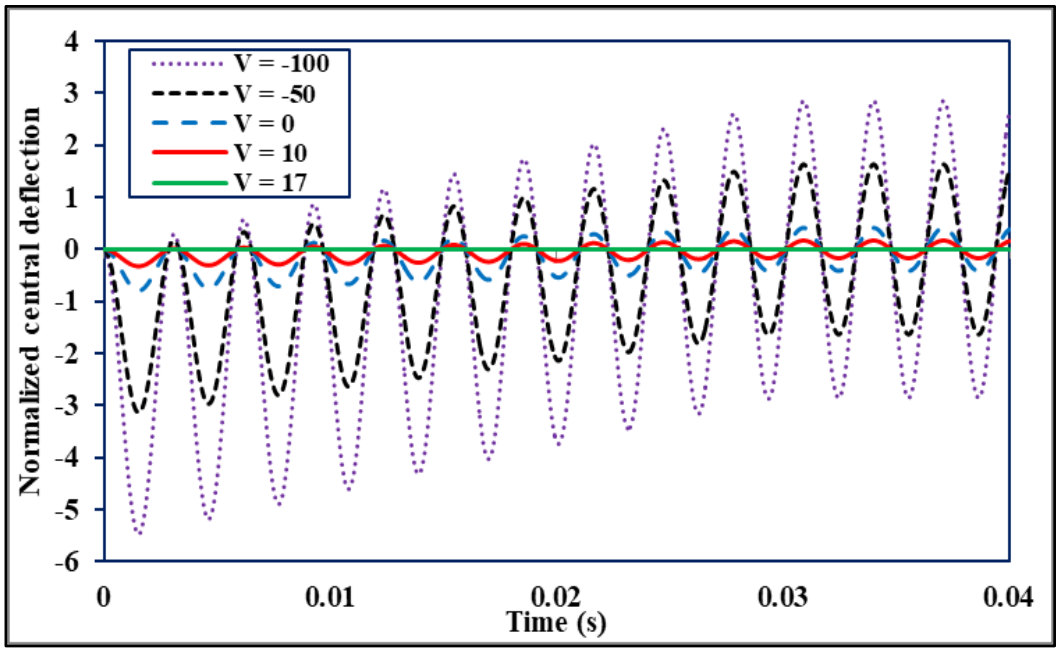

(b)

Figure 3.43(a) Dynamic response of smart plate (PFRC/0/90/0) under triangular load with aspect-ratio (b) Suppression of the dynamic response by triangular electrical loads (material properties: MM4 (substrate), MP2 (piezoelectric layer); non-dimensional parameter: ND1)

The frequency is decreasing with the increase in the thickness of the PFRC layer as the mass and stiffness coefficients are influenced by the material properties of the piezoelectric layer. The frequency decreases as the net increase in the mass coefficients are greater than that of the stiffness coefficients due to the higher density of the PFRC layer in comparison to the laminated layers. The amplitude decreases as the stiffness coefficients increase with the increase in the thickness of the PFRC layer.

3.5.3.3. Dynamic response subjected to sinusoidal variation of electromechanical load

The dynamic response of the same smart plate subjected to a sinusoidal electro-mechanical load acting for 0.03 sec with S = 70 is presented in Figure 3.47(a). The forced vibration responses are following the variation of the electro-mechanical load in the time frame. The amplitude of the free vibration response is comparatively smaller in this situation in comparison to the previous cases as the amplitude of vibration in the forced vibration regime is smaller at the time instant when the plate enters into the free vibration regime. As expected, the mechanical disturbances are eradicated at an electrical load of 17 V because the electrical coefficients in the electric force vector are dependent on the piezoelectric coefficients of the PFRC layer, the magnitude of electrical loads and not on the variation of the electrical loads in the time frame as observed in Figure 3.47 (b). To verify this, another example of a smart composite plate is considered with span thickness ratio S = 50 and 100 subjected to the same magnitude of mechanical loads. It is observed in Figure 3.48 (a) that, electrical loads of magnitude 8.8 V and 34 V are required to nearly eradicate the mechanical disturbances respectively. This leads to another important conclusion that the dynamic controlling capacity of the PFRC patch is greater in the case of a plate with a lower span-thickness ratio as a smaller magnitude of the electrical load is required to nearly eradicate the mechanical vibration.

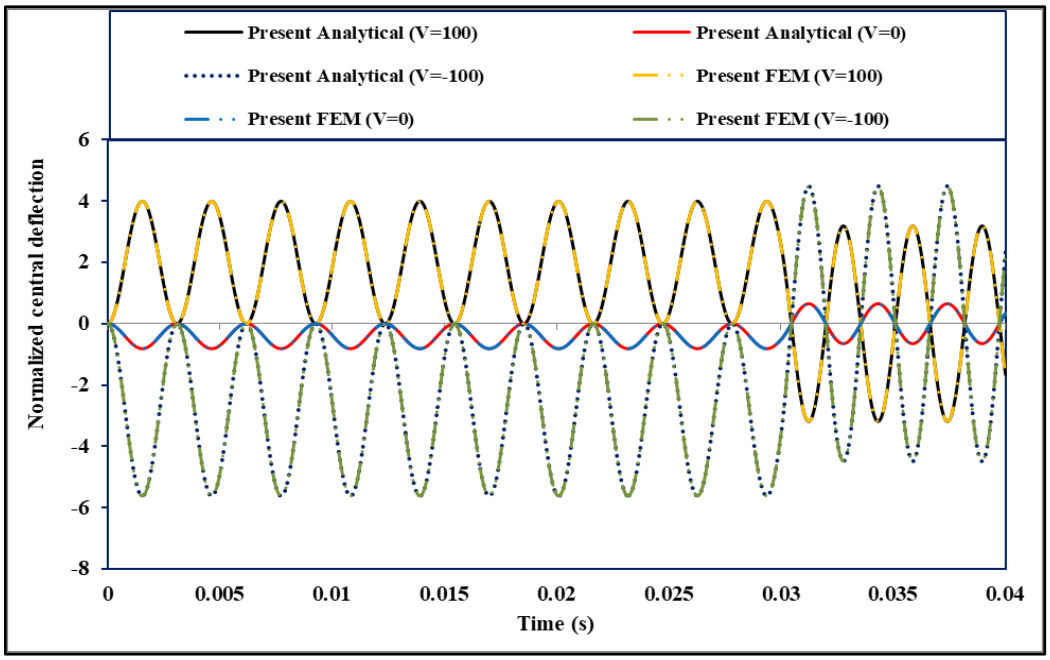

(a)

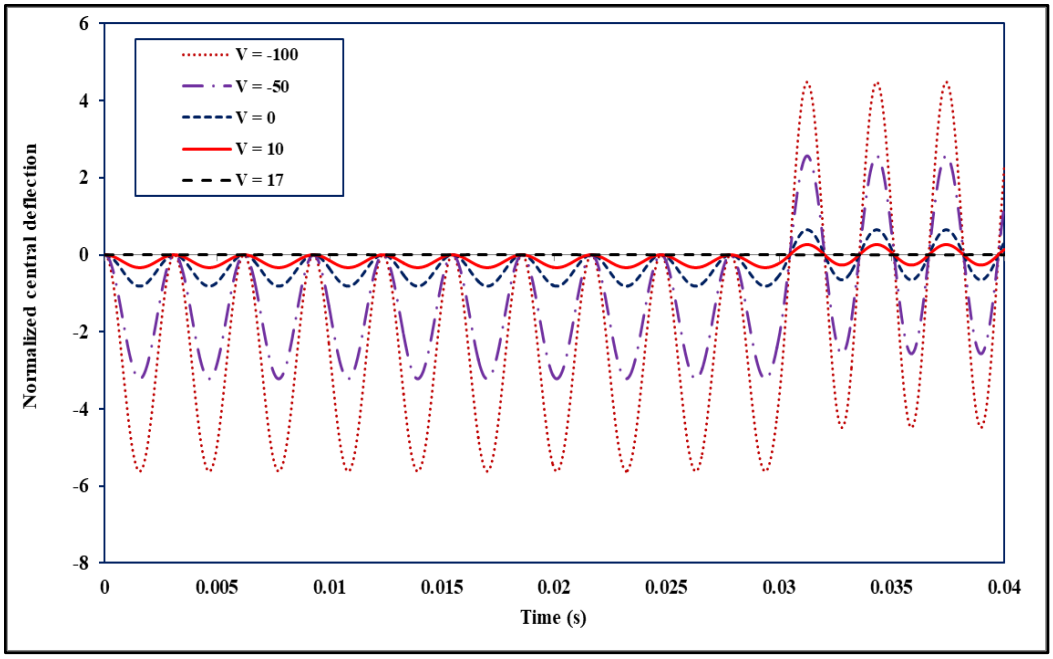

(b)

Figure 3.44(a) Dynamic response of smart plate (PFRC/0/90/0) under pulse loading acting for 0.03 second (b) Suppression of the dynamic response by pulse electrical loads (material properties: MM4 (substrate), MP2 (piezoelectric layer); non-dimensional parameter: ND1)

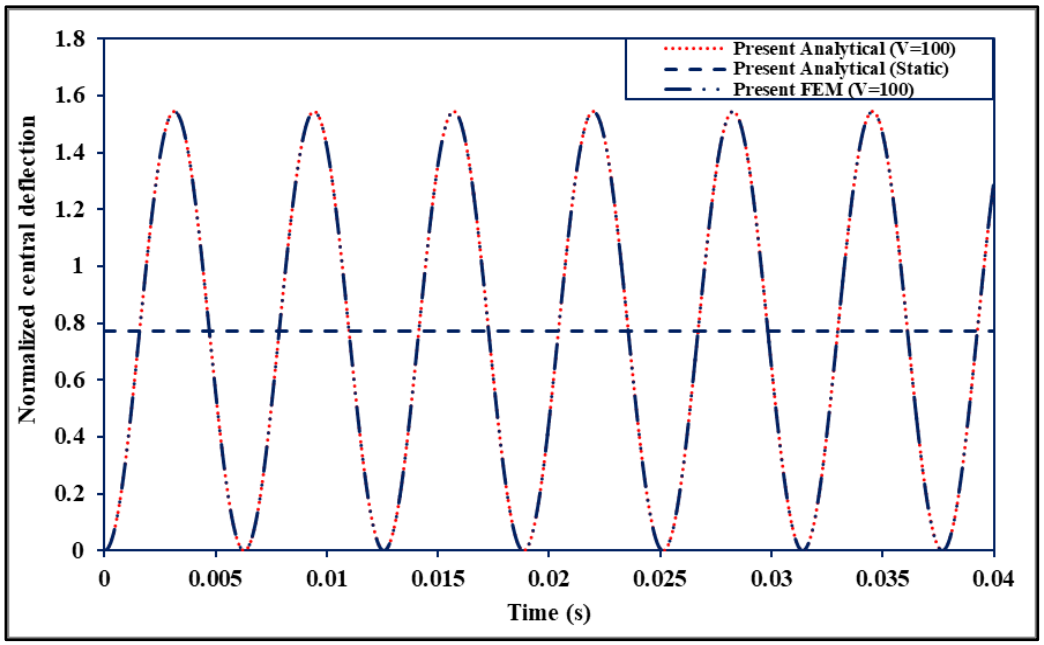

(a)

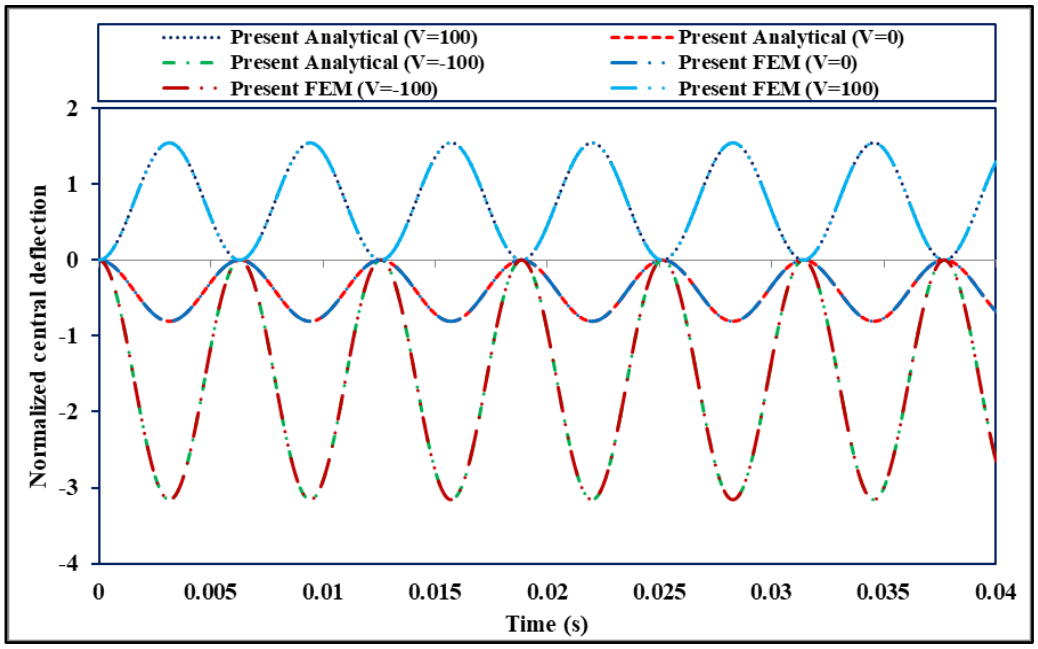

(b)

Figure 3.45(a) Dynamic response of smart plate (PFRC/0/90/0) under pulse loading acting for the entire duration of the plate vibration (b) Dynamic response under different magnitudes of pulse load (material properties: MM4 (substrate), MP2 (piezoelectric layer); non-dimensional parameter: ND1)

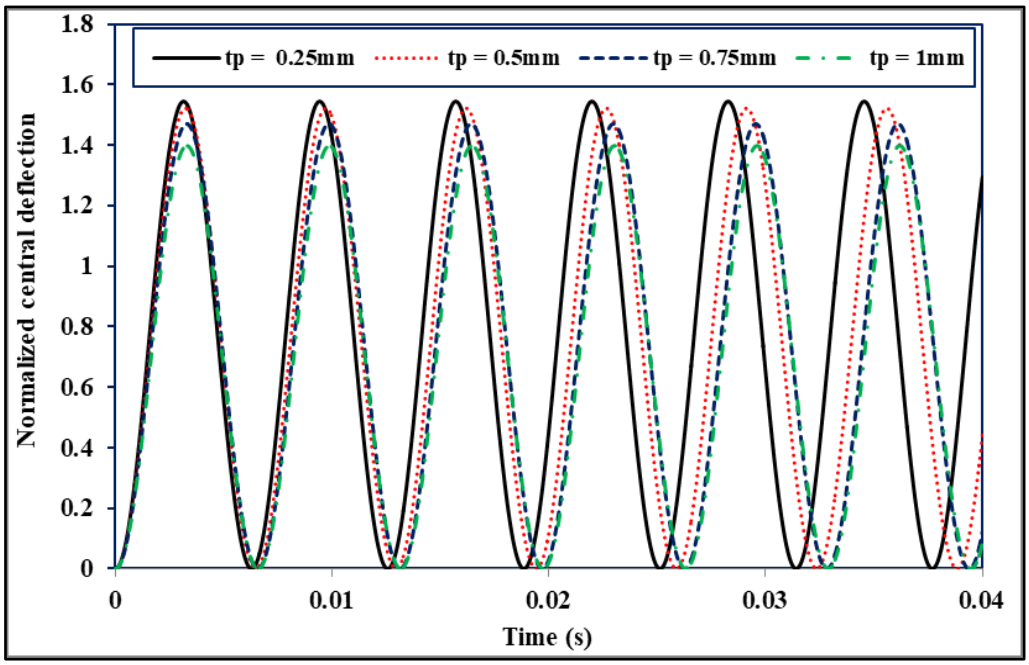

Figure 3.46 Dynamic responses of PFRC/0/90/0 plate with various thickness of the PFRC layer (material properties: MM4 (substrate), MP2 (piezoelectric layer); non-dimensional parameter: ND1)

As the span-thickness ratio decreases, *i.e*, the laminated plate becomes thick, the deformation or stresses generated due to mechanical loads decrease due to higher flexural rigidity. Therefore, the total electrical load required to nullify the mechanical deformations also becomes smaller for thick plates. Next, the sinusoidal electromechanical load is assumed to act in the form '$q\ (t) = q_{mn}\sin(\omega t)$ and $V\ (t) = V\sin(\omega t)$', where 'ω' is the frequency of the applied electromechanical load. The frequency is assumed to be 2032.6 rad/sec which is equal to the natural frequency of the smart plate (S = 70). The dynamic responses subjected to the sinusoidal excitations are presented in Figure 3.48 (b). As expected, the plate vibrates under the resonance condition. On application of electrical loads, the amplitude of the responses decreases, however, the plate still vibrates under the resonance condition.

3.5.3.4. Dynamic response subjected to ramp variation of electromechanical load

Here, the dynamic response of the smart plate is obtained for time-dependent ramp electro-mechanical loading for S = 100 in Figure 3.49(a). The magnitude of the response is increasing with time which totally correlates with that of the loading history and is totally under the forced vibration regime. Then the response of the same plate is obtained for ramp loading acting for 0.01 sec in Figure 3.50(a) to which it is observed that the free vibration amplitude is higher for -100 V in comparison to 100 V and the frequency remains the same. Next, the response of the same plate subjected to ramp-constant electro-mechanical load is presented in Figure 3.51(a). The plate vibrates initially with increasing amplitude like that of the ramp loading and then vibrates with constant amplitude after the load is removed. The mechanical disturbances are removed from the system by counteracting electrical loads for S = 70 at an electrical load of 17 V for all the three cases considered here as shown in Figures 3.49(b), 3.50(b) and 3.51(b), respectively.

3.5.3.5. Dynamic response subjected to staircase variation of electromechanical load

Here, the dynamic response is obtained for time-dependent electro-mechanical load varying in like pulses of different magnitudes at different time intervals, *i.e*, staircase variation for S =100 in Figure 3.52. The vibration totally correlates with that of the loading history and the response up to 0.02 sec is exactly similar to the responses obtained earlier during the case of pulse loading. The amplitude of vibration at a particular time instant depends on the initial conditions and also on the magnitude of the load acting at that time instant.

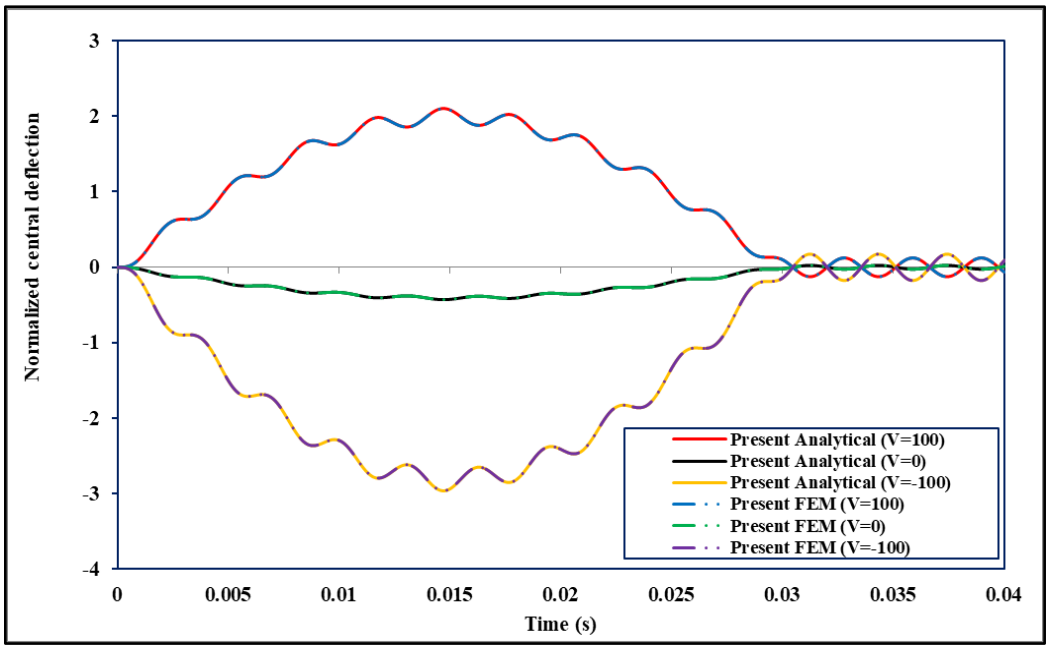

(a)

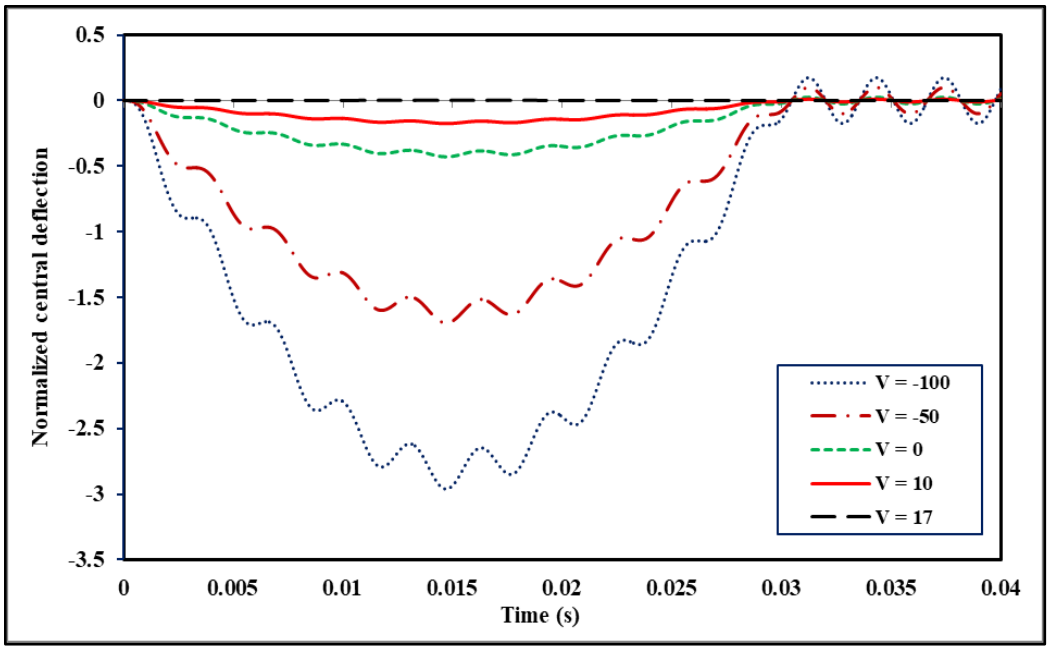

(b)

Figure 3.47(a) Dynamic response of smart plate (PFRC/0/90/0) under sinusoidal load (b) Suppression of the dynamic response by sinusoidal electrical loads (material properties: MM4 (substrate), MP2 (piezoelectric layer); non-dimensional parameter: ND1)

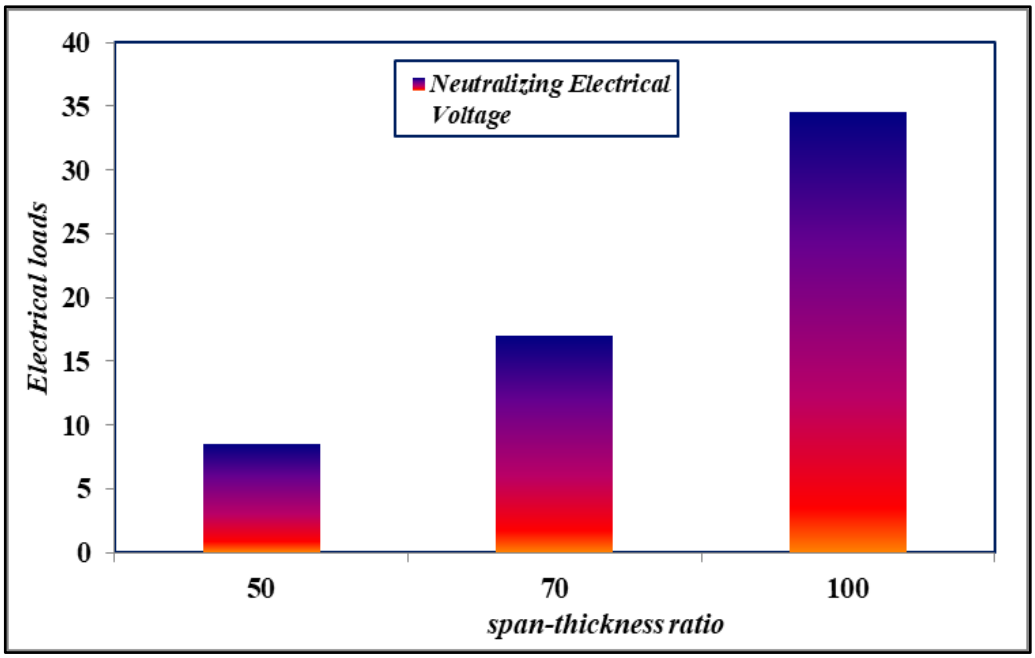

(a)

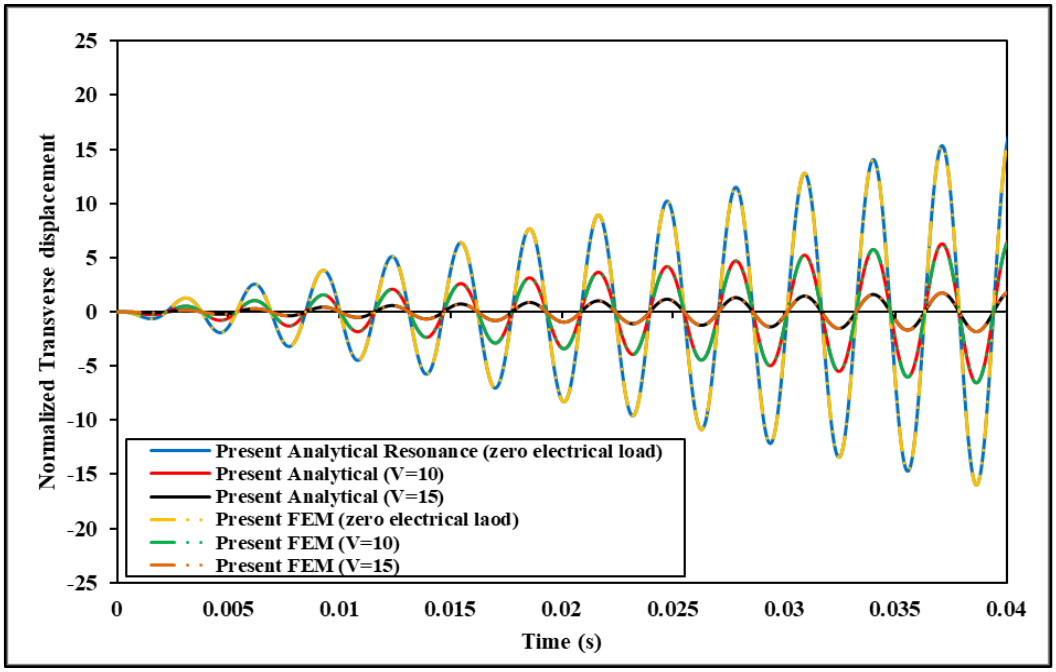

(b)

Figure 3.48(a) Effect of span-thickness ratio on the magnitude of electric loads. (b) Dynamic response of smart plate (PFRC/0/90/0) under resonance condition (material properties: MM4 (substrate), MP2 (piezoelectric layer); non-dimensional parameter: ND1)

3.5.4. Vibration Suppression of laminated composite plates using piezoelectric materials coupled with a control system.

In the previous section, we witnessed that the piezoelectric materials attenuate the mechanical vibration due to the applied mechanical excitations with counteracting electrical voltages. However, the magnitude of the electrical voltage fed to the actuator for reducing the overall mechanical responses was decided based on the vibration response of the system. Thus, it is essential to first examine the vibration response of the system and then decide the magnitude of the electrical load required to suppress the response. Such a process requires high human intervention. To have minimal human intervention, we require an automation technology so that the voltages generated by the piezoelectric sensors on experiencing the mechanical strains can be directly fed to the actuator. Such automation is achieved when we couple the piezoelectric materials with the laminated composite plates using a control system. In this section, the suppressed vibration responses of the smart composites are investigated using a negative feedback controller (Samanta *et al*. 1996; Wang *et al*. 2000 and Moita *et al*., 2005). The negative feedback controller is based on the velocity measurements of the smart system and as the name suggests, the sensor output voltage is fed back to the actuator layer through an amplifier with a change in the polarity. Thus, the control system generates an energy dissipation mechanism which results in vibration damping. First, a problem of a five-layered (PVDF/0/90/0/PVDF) smart composite plate is solved which is subjected to a mechanical load having a uniform variation in the spatial domain. In the time domain, the mechanical load is assumed to have a sinusoidal variation, *i.e,* $q\ (t) = q_{mn} \sin(2\pi f t)$, where '$f$' is the frequency of the load in Hz. The value of f is considered to be 10 Hz.

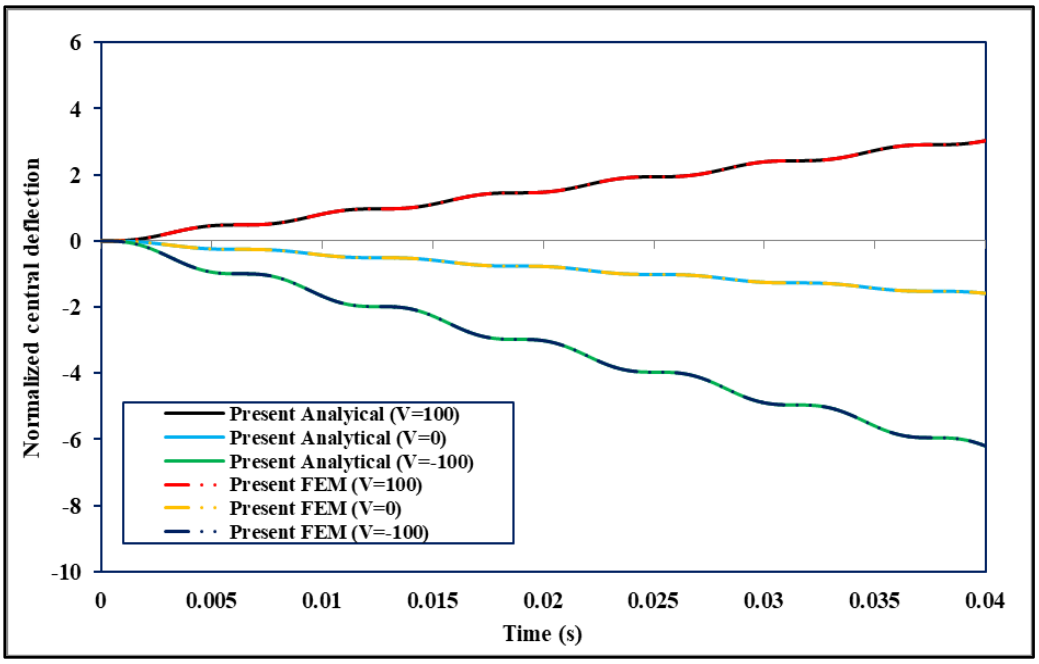

(a)

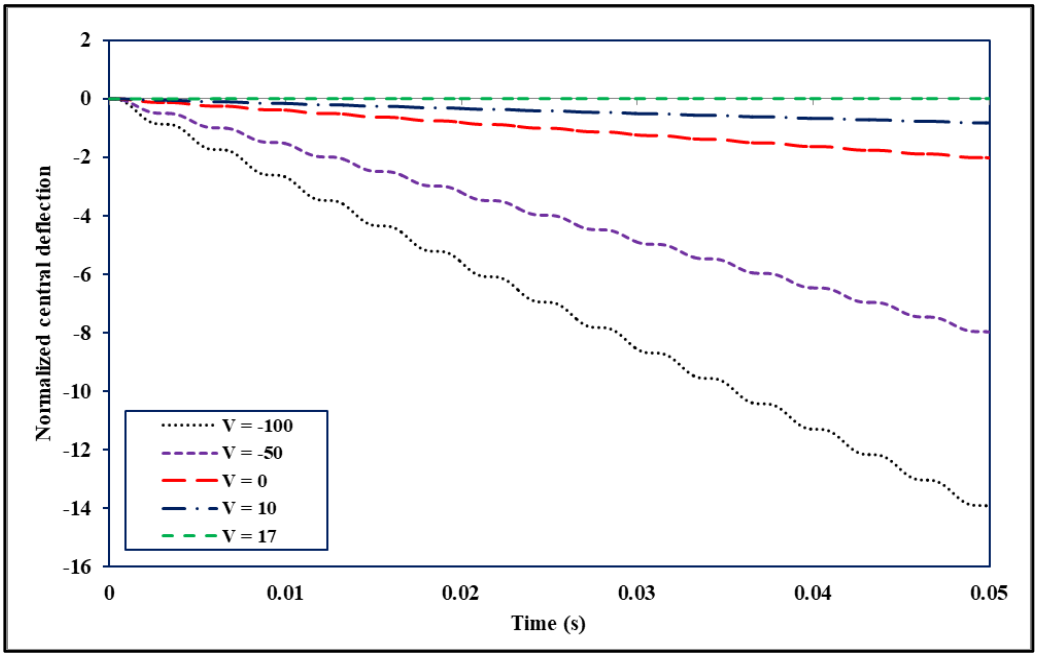

(b)

Figure 3.49(a) Dynamic response of smart plate (PFRC/0/90/0) under ramp loading (b) Suppression the dynamic response under the ramp loading (material properties: MM4 (substrate), MP2 (piezoelectric layer); non-dimensional parameter: ND1)

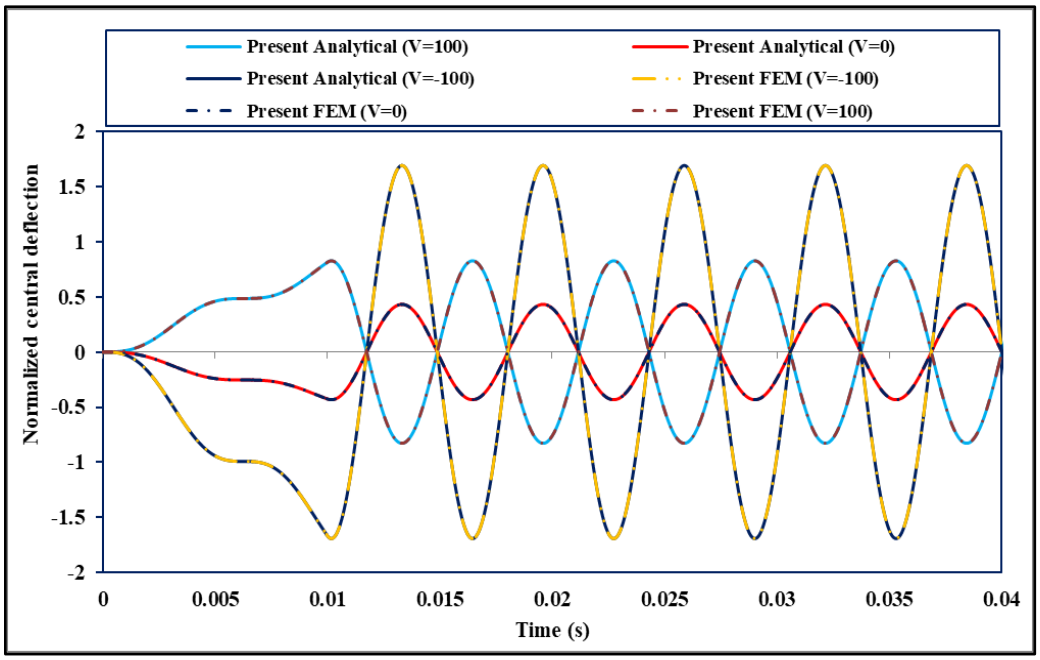

(a)

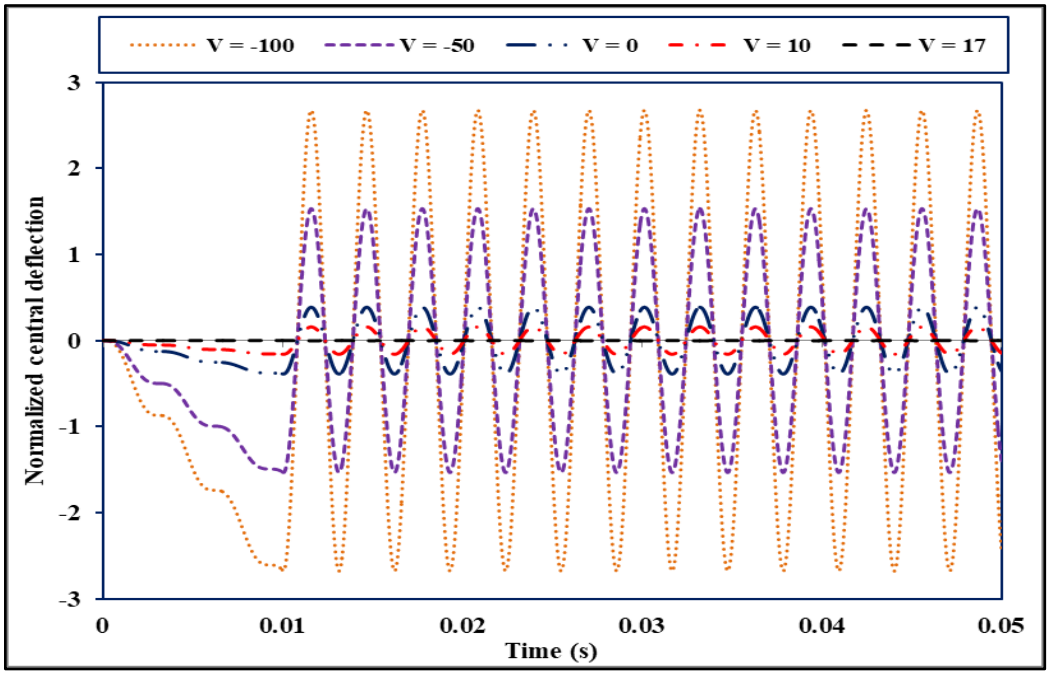

(b)

Figure 3.50(a) Dynamic response of smart plate (PFRC/0/90/0) under ramp loading acting for 0.01 second (b) Suppression of the dynamic response by electrical loads
(material properties: MM4 (substrate), MP2 (piezoelectric layer); non-dimensional parameter: ND1)

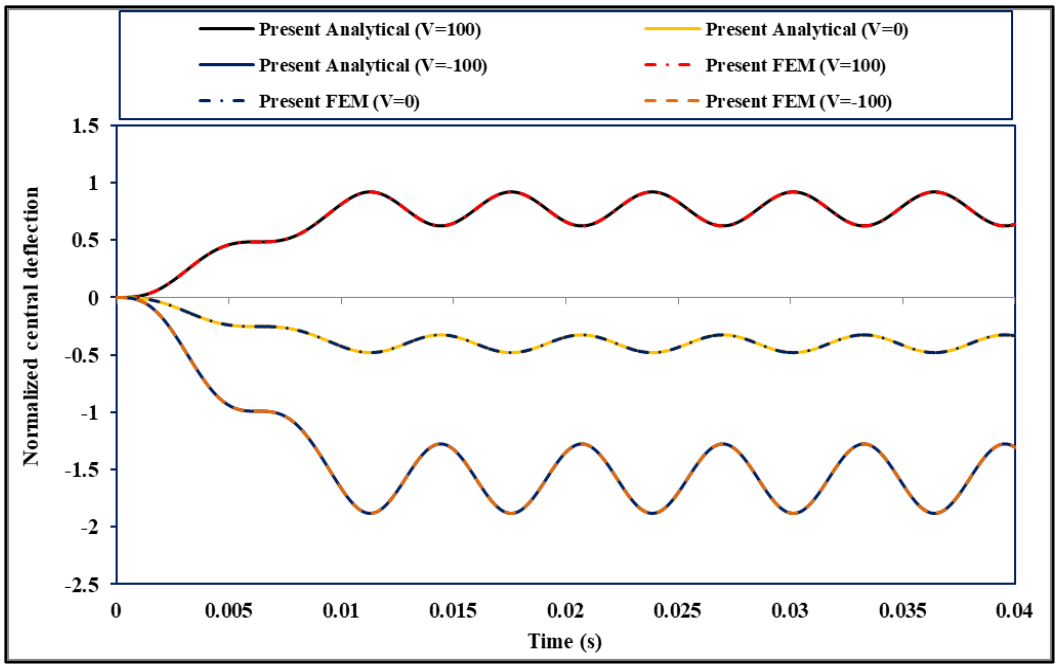

(a)

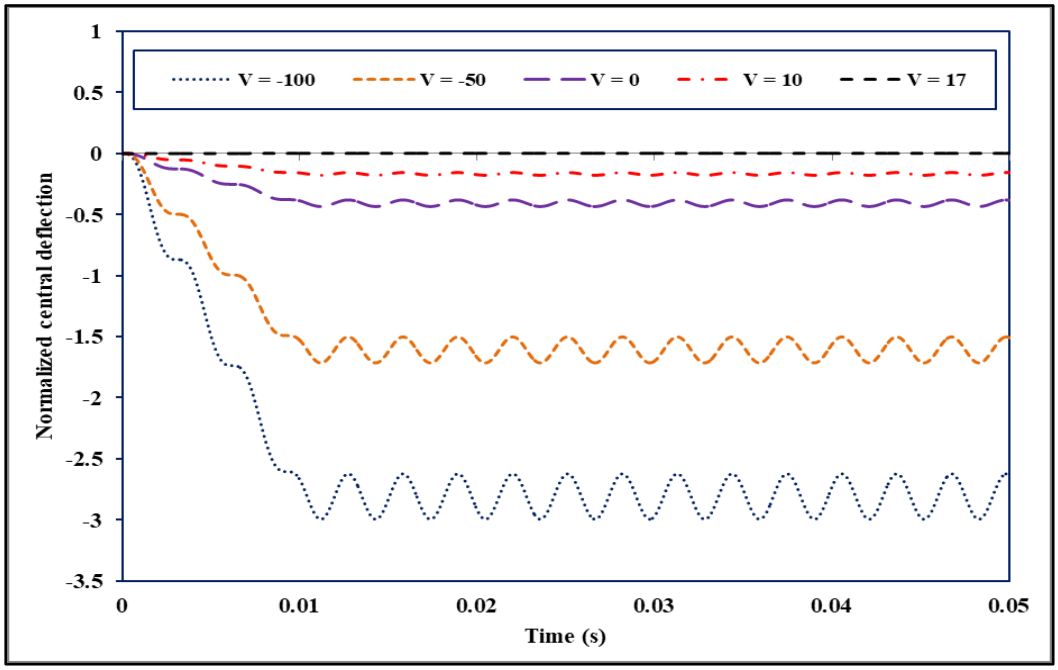

(b)

Figure 3.51(a) Dynamic response of smart plate (PFRC/0/90/0) under ramp-constant electro-mechanical loading (b) Suppression of the dynamic response by electrical loads (material properties: MM4 (substrate), MP2 (piezoelectric layer); non-dimensional parameter: ND1)

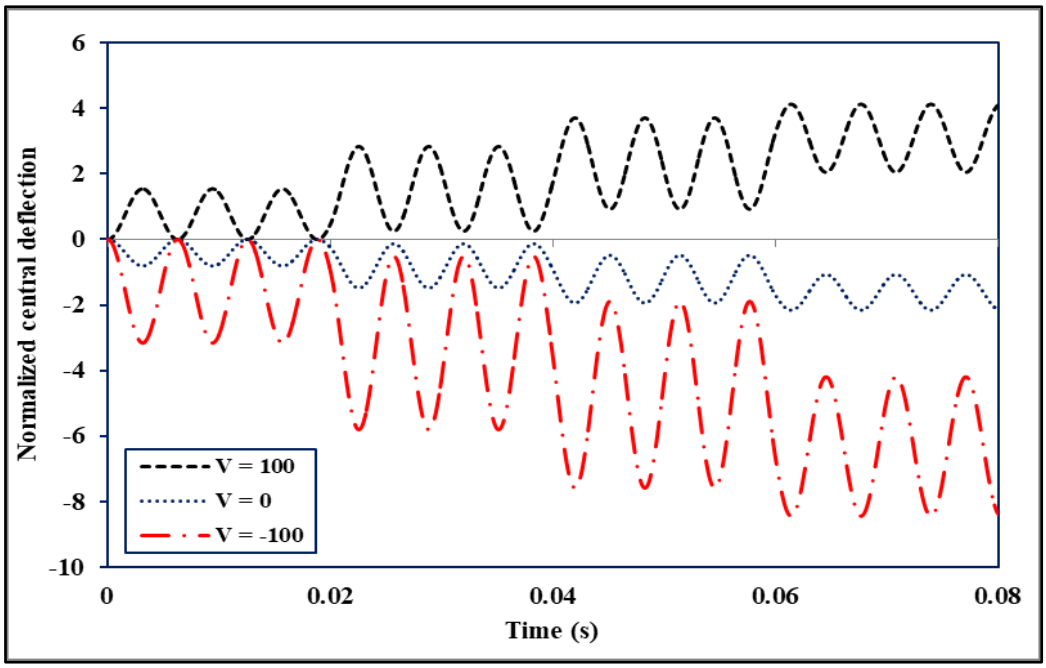

Figure 3.52 Dynamic response of smart plate (PFRC/0/90/0) under staircase loading
(material properties: MM4 (substrate), MP2 (piezoelectric layer); non-dimensional parameter: ND1)

The mechanical and geometrical properties of the orthotropic lamina and the piezoelectric layer are obtained from Moita *et al*. (2005). Moita *et al*. (2005) have earlier presented the responses in the literature by employing the CPT and Reddy's HSDT. The forced-vibration responses of transverse displacement are shown in Figure 3.53. The uncontrolled responses, *i.e*, responses obtained without using any controller are derived using both analytical and FE formulations. However, the controlled responses are derived using the FE formulation. The present responses (both uncontrolled and controlled) are in close agreement with the solutions obtained by Moita *et al*. (2005). It can be perceived from the figure that the amplitude of the uncontrolled vibration response is significantly reduced when coupled with the negative feedback controller.

Next, another problem of a smart composite plate (PVDF/0/90/0/PVDF) is considered which is initially subjected to a static mechanical load of uniform variation in the spatial

domain. The load is then removed from the plate setting it into free vibration. The free vibration responses of the plate are shown in Figure 3.54 for several values of the control gain (G_iG_c). The value adopted for the constant gain 'G_c' of the charge amplifier is considered to be $1.6x10^5$ (Wang *et al*., 2000) whereas the values of the gain 'G_i' are considered to be 50, 100, 150, 200. In addition to the damping generated with the help of the controller, we also introduce the structural damping. For the structural damping we use the Rayleigh damping in which the values of α and β Rayleigh coefficients of proportionality are adopted from Wang *et al*. (2000). The present responses share a similar pattern with the responses of Wang *et al*. (2000) which are obtained using the FSDT. The present uncontrolled damped responses obtained using analytical and FE formulations are observed to be in excellent agreement in the figure. It can be observed in the figure that there is some decay in the uncontrolled responses also due to the presence of the energy dissipation mechanism generated by the structural damping. Also, the amplitude of the controlled free vibration responses is observed to decay faster with the increase in the control gain 'G_i'. Now, we investigate the dynamic responses of the same plate which is now under the action of several forms of time-dependent mechanical excitations like pulse, sinusoidal and triangular variations in the time-domain and uniformly distributed variation in the spatial domain. The Rayleigh damping coefficients considered in the structural damping matrix are similar to that of the previous example. The forced vibration responses corresponding to the above-mentioned load variations are presented in Figures 3.55-57, respectively. In all the cases, the plate is under the action of the load for 0.0015 sec and then the load is removed from the plate. Therefore, the plate is under the forced-vibration regime from 0 to 0.0015 sec and is under the free vibration regime from 0.0015 sec to 0.003 sec. The amplitude of the vibration is observed to decay faster with the increase in

the control gain 'G_i' which is evident from the figures. Also, the present analytical and FE responses of the uncontrolled vibration responses with structural damping are in excellent agreement. The amplitude of the free vibration responses under the action of the sinusoidal excitation in Figure 3.57 is much smaller in amplitude than the amplitude of the forced vibration response. This is because the plate enters into the free vibration regime at t = 0.0015 sec with a smaller amplitude of forced vibration response, thereby experiencing a smaller amplitude of vibration in the free vibration regime. In Figure 3.57, it is observed that the forced vibration responses up to 0.0015 sec under the action of the triangular loading have higher decay than the forced vibration responses under the action of the pulse loading. The triangular load profile has a decreasing variation in time with a maximum value at t = 0 sec and minimum at t = 0.0015 sec. Therefore, the vibration responses under the action of the triangular load have a much higher decay.

3.6. Static analysis of laminated composites and sandwich plates on elastic foundation

Plates resting on an elastic foundation are quite essential in structural engineering and also in other disciplines of engineering. Applications like raft foundations, swimming pools, and storage tanks, etc. require the analysis of plates resting on elastic foundations. Therefore, in this section, the structural responses of plates are investigated by considering the effects of the foundation. The foundation is modeled by using Pasternak's foundation model. We first take a four-layered laminated composite plate with diaphragm support at all the edges. The mechanical pressure is assumed to be sinusoidal in the spatial domain. The normalized transverse displacements at the centre of the plate ($\bar{U}_3$) for various span-thickness ratios are presented in Table 3.29. The present results are compared with the CPT and refined first-order shear deformation theory (RFSDT) results of Setoodeh and Azizi (2015).

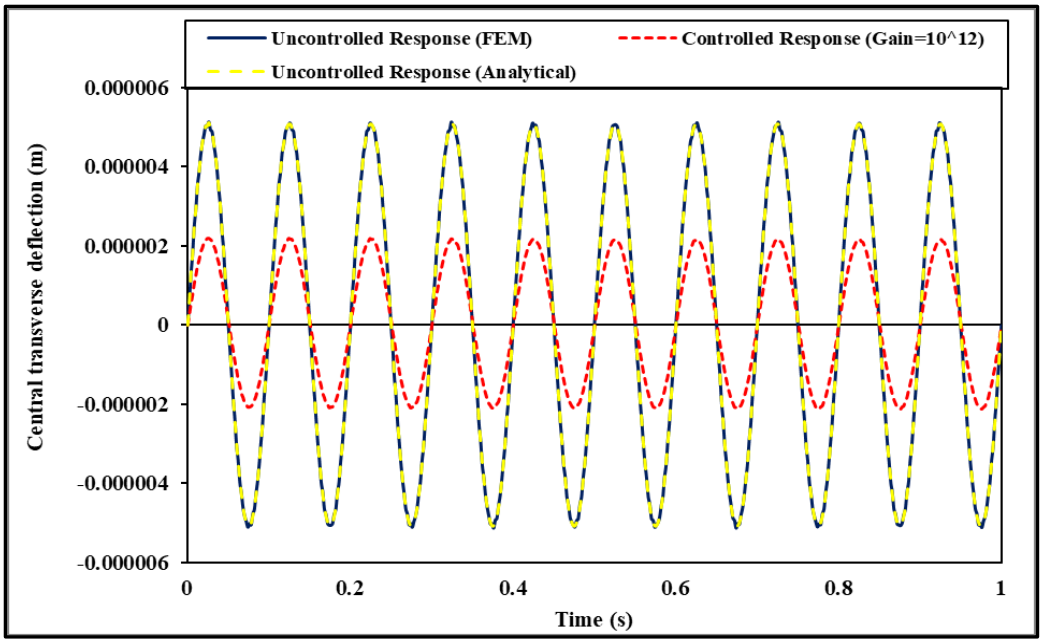

Figure 3.53. Uncontrolled and Controlled Forced-Vibration responses of smart composite plate (PVDF/090/0/PVDF) subjected to sinusoidal excitation in the time-domain and uniformly distributed in the spatial-domain
(material properties: MM15 (substrate), MP1 (piezoelectric layer))

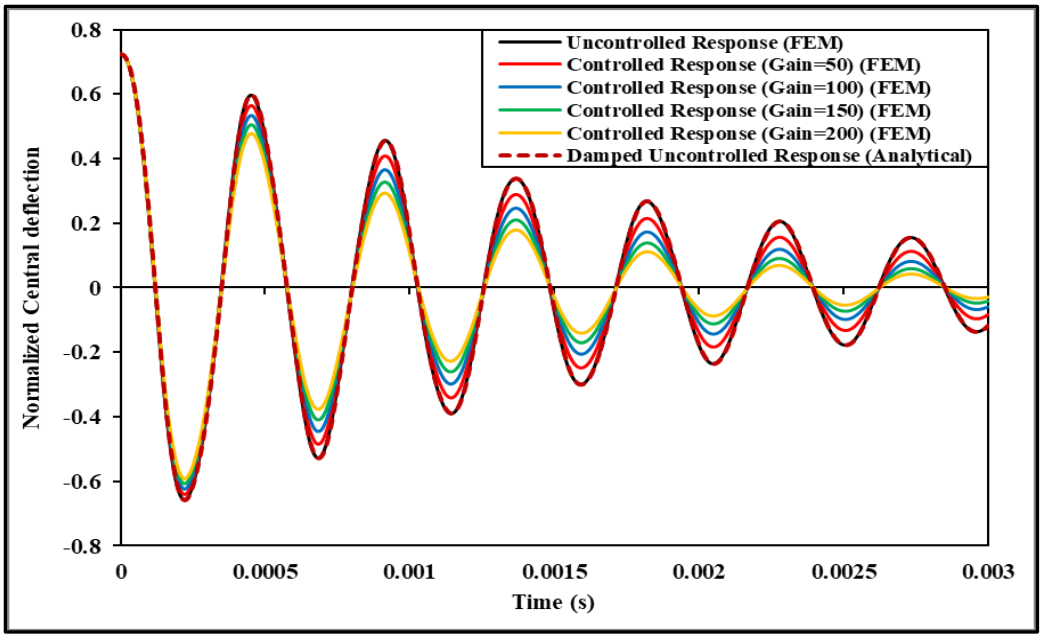

Figure 3.54. Free vibration responses of smart composite plate (PVDF/0/90/0/PVDF) coupled with a negative feedback controller.
(material properties: MM14 (substrate), MP1 (piezoelectric layer); non-dimensional parameter: ND1)

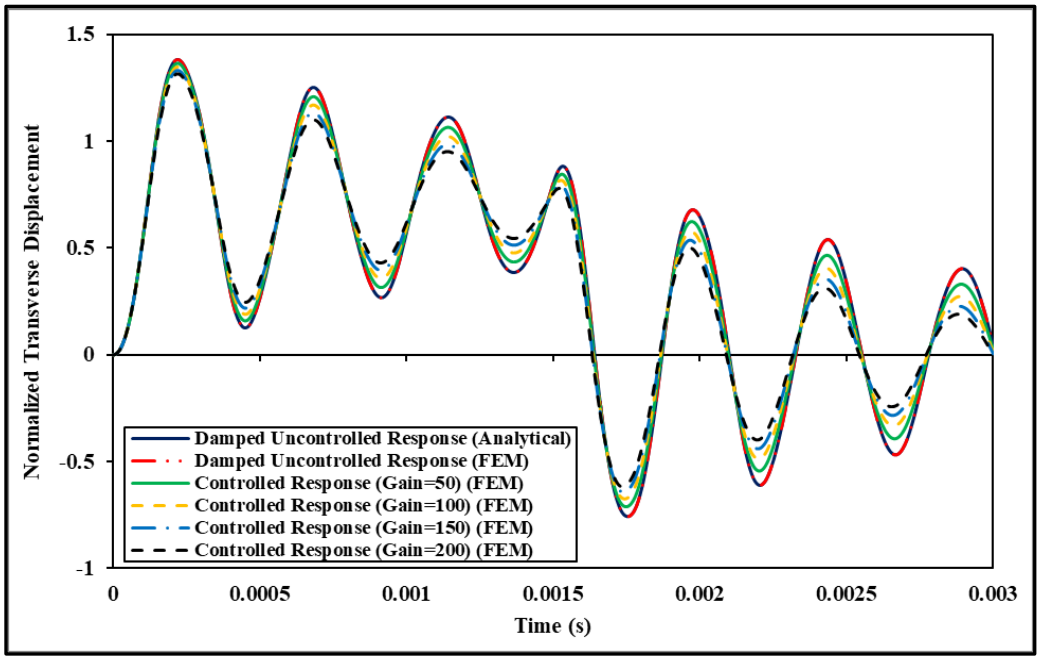

Figure 3.55 Uncontrolled and Controlled dynamic responses of the smart composite plate subjected to pulse variation of the mechanical load acting for 0.0015 sec.
(material properties: MM14 (substrate), MP1 (piezoelectric layer); non-dimensional parameter: ND1)

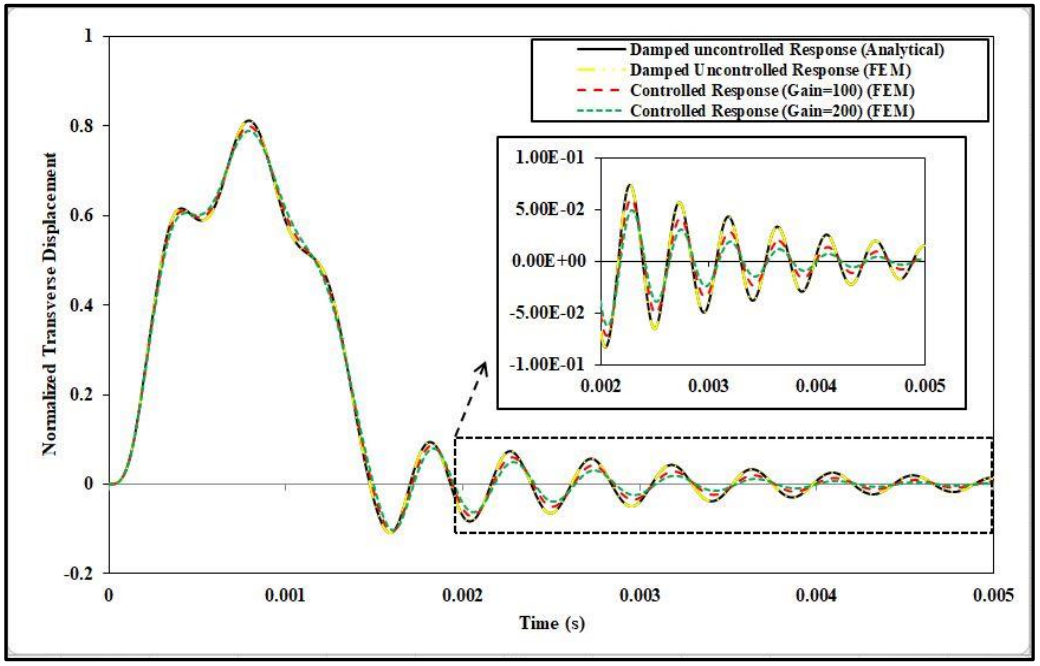

Figure 3.56 Uncontrolled and Controlled dynamic responses of the smart composite plate subjected to sinusoidal variation of the mechanical load acting for 0.0015 sec.
(material properties: MM14 (substrate), MP1 (piezoelectric layer); non-dimensional parameter: ND1)

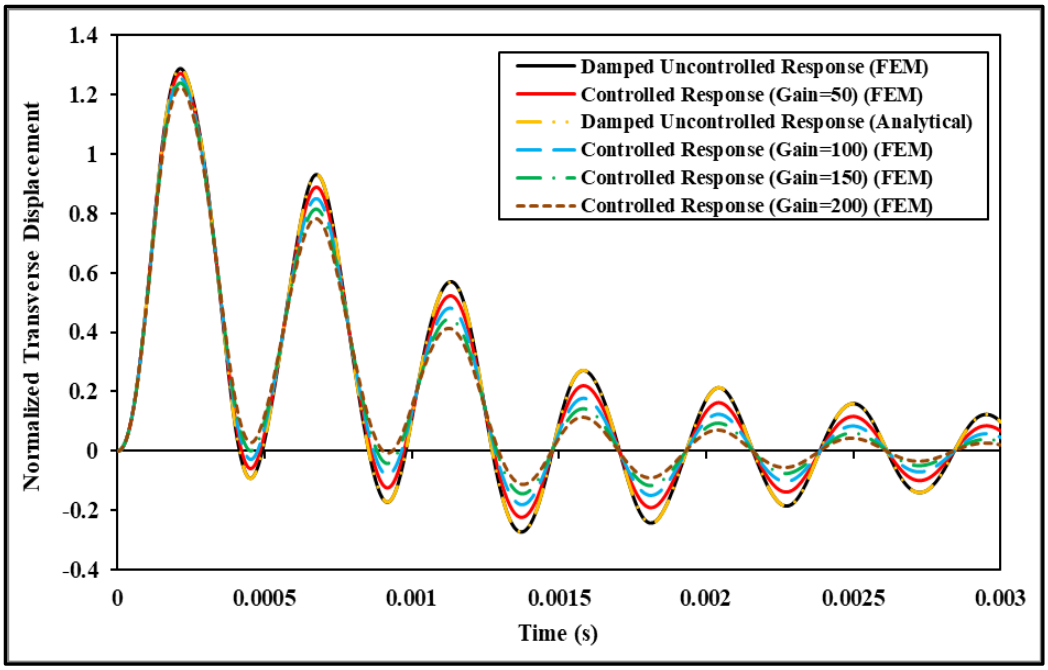

Figure 3.57 Uncontrolled and Controlled dynamic responses of the smart composite plate subjected to triangular variation of the mechanical load acting for 0.0015 sec.
(material properties: MM14 (substrate), MP1 (piezoelectric layer); non-dimensional parameter: ND1)

The FE results of transverse deflection have converged at a mesh size of 8x8 in the table. It is further observed in the table that the net deflection decreases by 42.39 % when only Winker stiffness ($\overline{K}_w$=100, $\overline{K}_s$=0) is considered, and 68.64 % when both the Winkler and shear stiffness of the foundation ($\overline{K}_w$=100, $\overline{K}_s$=10) are considered. The CPT and RFSDT results of Setoodeh and Azizi (2015) underestimate the transverse displacement for a thick plate. As the plate becomes thin, it is found that the present results and the results of Setoodeh and Azizi (2015) have small differences. Figure 3.58 and 3.59 shows the variation of the in-plane stress ($\bar{\sigma}_{11}$) and in-plane stress ($\bar{\sigma}_{22}$) along the global x_1 and x_2-direction, respectively. The FE results of stresses have converged at a mesh size of 20x20, therefore, the values of the stresses in the figures are corresponding to this mesh size. It is observed in the figures that the present analytical and FE results are found to be in excellent agreement. The in-plane stresses are observed to be maximum at the centre of the plate and

zero at both ends. The decrement in the magnitude of the stresses due to the foundation stiffness can be observed in the figures. The variation of the in-plane shear stress ($\bar{\tau}_{12}$) is presented in Figure 3.60. The FE results of $\bar{\tau}_{12}$ are corresponding to a mesh size of 20x20. The in-plane shear stress is observed to be maximum at the ends and minimum at the center of the plate. Figure 3.61 shows the variation of the transverse displacement ($\bar{U}_3$) of the plate with the Winkler and shear stiffness of the foundation.

Table 3.29. Convergence and validation of transverse deflection of laminated composite plate (0/90/90/0) resting on elastic foundation subjected to SSL (material property: MM1; non-dimensional parameter: ND1, ND8)

l/*h*	References	Foundation Stiffness		
		$\bar{K}_w$=0, $\bar{K}_s$=0	$\bar{K}_w$=100, $\bar{K}_s$=0	$\bar{K}_w$=100, $\bar{K}_s$=10
10	Present Analytical	0.7360	0.4240	0.2308
	Present FEM (4x4)	0.7352	0.4226	0.2295
	Present FEM (6x6)	0.7362	0.4238	0.2306
	Present FEM (8x8)	0.7363	0.4240	0.2308
	Present FEM (10x10)	0.7363	0.4241	0.2308
	Setoodeh and Azizi (2015)[1]	0.4312	0.2687	0.1541
	Setoodeh and Azizi (2015)[2]	0.6049	0.3769	0.2161
20	Present Analytical	0.5129	0.3390	0.2031
	Present FEM (4x4)	0.5131	0.3390	0.2029
	Present FEM (6x6)	0.5130	0.3391	0.2031
	Present FEM (8x8)	0.5130	0.3391	0.2031
	Present FEM (10x10)	0.5130	0.3391	0.2031
	Setoodeh and Azizi (2015)[1]	0.4312	0.2924	0.1788
	Setoodeh and Azizi (2015)[2]	0.4747	0.3219	0.1968
100	Present Analytical	0.4346	0.3029	0.1896
	Present FEM (4x4)	0.4341	0.3030	0.1897
	Present FEM (6x6)	0.4346	0.3030	0.1896
	Present FEM (8x8)	0.4346	0.3030	0.1896
	Present FEM (10x10)	0.4346	0.3030	0.1896
	Setoodeh and Azizi (2015)[1]	0.4312	0.3009	0.1885
	Setoodeh and Azizi (2015)[2]	0.4330	0.3021	0.1893

[1] CPT; [2] RFSDT

Further, a three-layered laminated composite is considered which is subjected to a mechanical load of uniform variation in the spatial domain. The analytical and FE results of the normalized displacement are tabulated in Table 3.30. An excellent correlation of the analytical and FE results can be observed in the table. The magnitude of the deflection is found to be larger than the previous case of a four-layered plate subjected to SSL due to the uniform variation of the mechanical load. Next, a three-layered soft-core sandwich plate resting on an elastic foundation is considered for investigating the static responses. The material properties of the face sheets and the core are according to example 3.4.2. The results of normalized deflection ($\bar{U}_3$), and in-plane stress ($\bar{\sigma}_{11}$) are tabulated in Table 3.31 for various values of *R*. The FE results of transverse deflection have converged at a mesh size of 8x8, however, the values of the stresses have converged at a mesh size of 20x20. Therefore, the values of the deflection and stresses in the table are corresponding to a mesh size of 20x20. It is observed that there is a decrement in the magnitude of both deflection and stress due to the stiffness of the foundation. From the results of $\bar{\sigma}_{11}$, it is calculated that the magnitude of the stresses decreases by 68.17 % due to the Winkler stiffness and 86.12 % when both Winkler and shear stiffness are considered for *R*=5. However, when the difference in the material properties of the face-sheets and the core is comparatively higher (*R* =100), the decrement in the magnitude of normal stress is calculated to be 29.39 % and 52.56 % due to Winkler and the combined Winkler-shear stiffness of the foundation, respectively.

3.7. Free vibration analysis of laminated composite plates on elastic foundation

In this section, the effects of the foundation stiffness on the natural frequencies of the laminated composite plates are investigated. A three-layered laminated composite (0/90/0) plate with diaphragm support at all the edges is considered as an example.

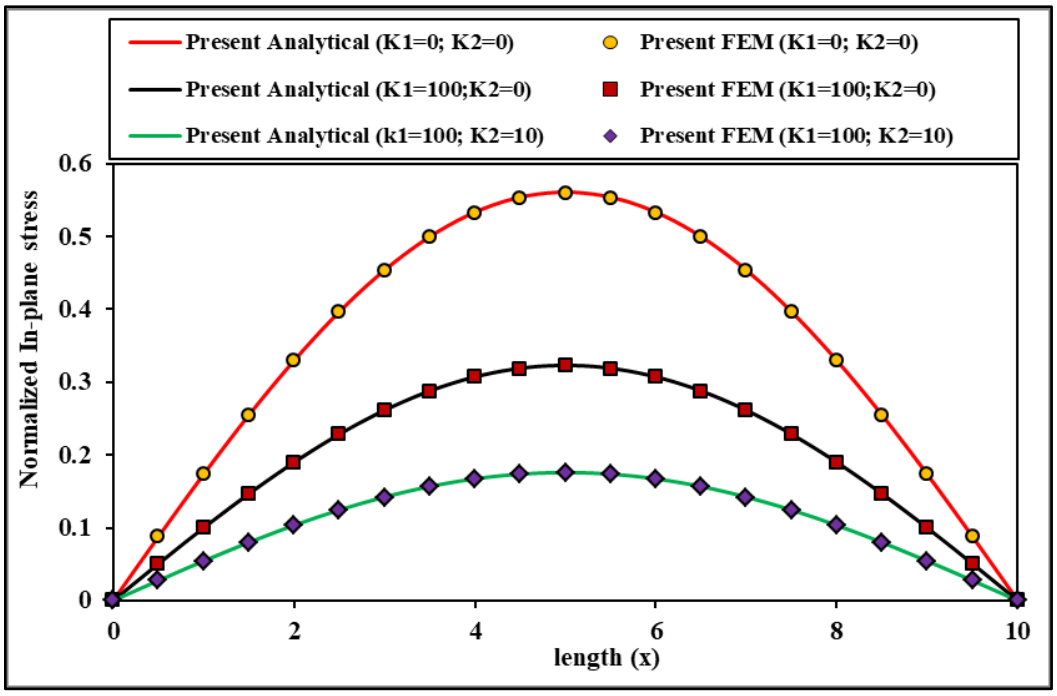

Figure 3.58 Variation of the in-plane stress $(\bar{\sigma}_{11})$ along the length of the plate
(material property: MM1; non-dimensional parameter:ND1, ND8)

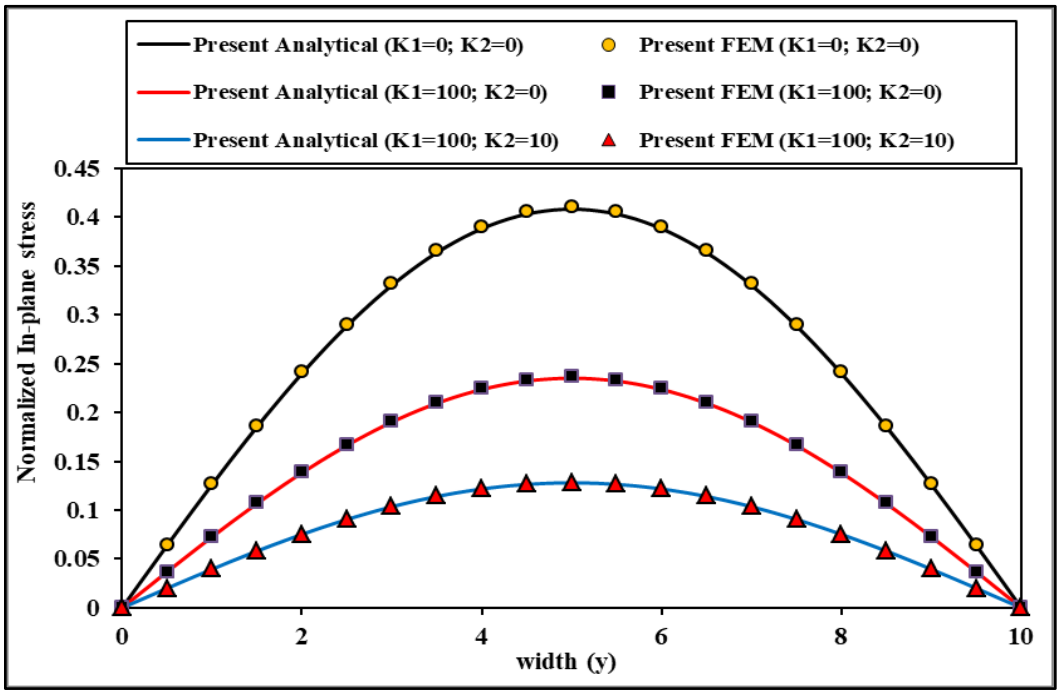

Figure 3.59 Variation of the in-plane stress $(\bar{\sigma}_{22})$ along the width of the plate
(material property: MM1; non-dimensional parameter:ND1, ND8)

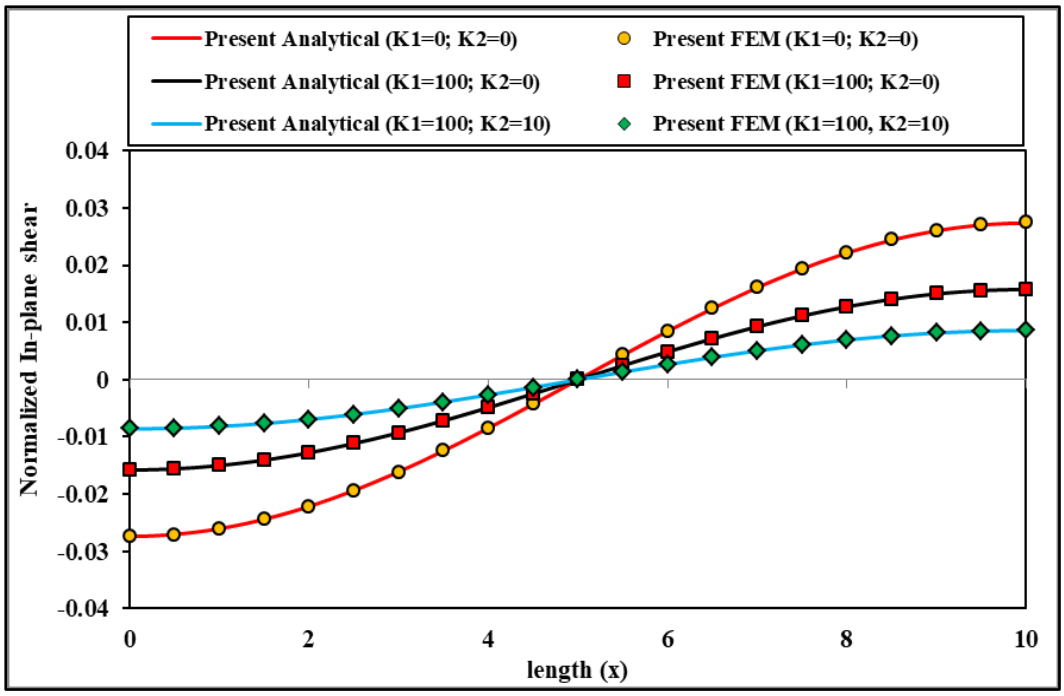

Figure 3.60 Variation of the in-plane stress $(\bar{\tau}_{12})$ along the length of the plate
(material property: MM1; non-dimensional parameter:ND1, ND8)

Table 3.30. Transverse deflection of laminated composite plate (0/90/0) resting on elastic foundation subjected to UDL (material property: MM1; non-dimensional parameter: ND1, ND8)

l/*h*	References	Transverse displacement $(\bar{U}_3)$		
		$\bar{K}_w$=0, $\bar{K}_s$=0	$\bar{K}_w$=100, $\bar{K}_s$=0	$\bar{K}_w$=100, $\bar{K}_s$=10
10	Present Analytical	1.1587	0.6383	0.3434
	Present FEM	1.1586	0.6377	0.3431
20	Present Analytical	0.7963	0.5135	0.3055
	Present FEM	0.7962	0.5134	0.3055
50	Present Analytical	0.6873	0.4670	0.2896
	Present FEM	0.6872	0.4669	0.2895
100	Present Analytical	0.6714	0.4598	0.2870
	Present FEM	0.6714	0.4598	0.2870

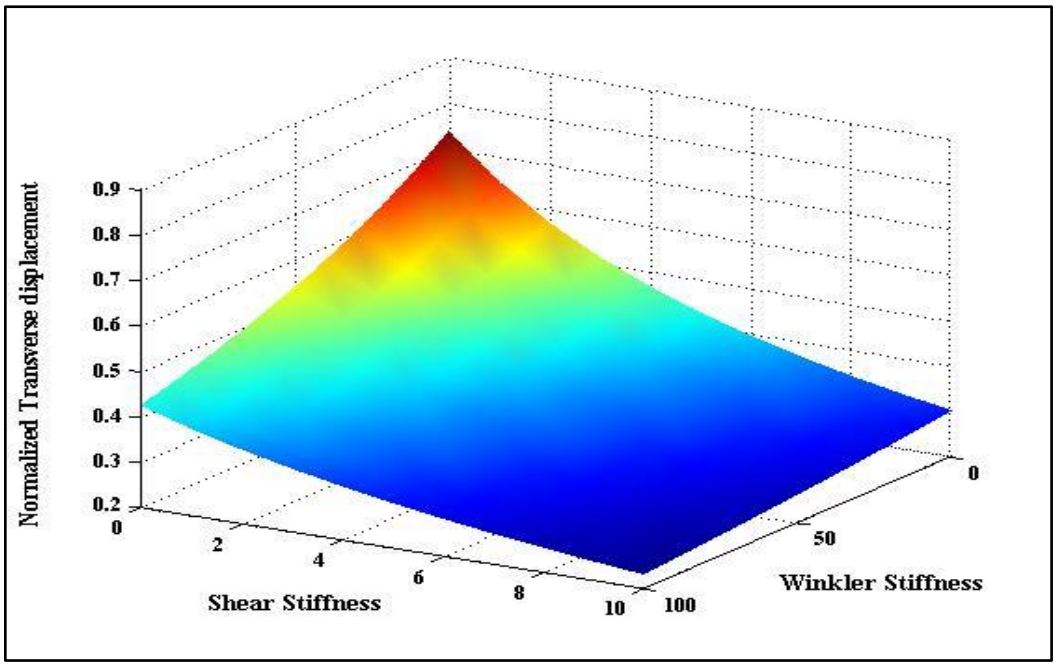

Figure 3.61 Variation of transverse displacement $(\bar{U}_3)$ of a laminated composite plate with Winkler stiffness and shear stiffness of the foundation (material property: MM1; non-dimensional parameter:ND1, ND8)

Table 3.31 Static response of soft-core sandwich plate subjected to uniform pressure resting on elastic foundation (non-dimensional parameter: ND8, ND9)

Foundation Stiffness	References	R=5	R=10	R=15	R=100
		Transverse displacement $(\bar{U}_3)$			
$\bar{K}_w$=0, $\bar{K}_s$=0	Present Analytical	259.2695	159.5937	121.9010	49.7942
	Present FEM	259.2693	159.5935	121.9009	49.7940
$\bar{K}_w$=100, $\bar{K}_s$=0	Present Analytical	92.2301	75.4919	65.7236	36.5169
	Present FEM	92.2298	75.4917	65.7233	36.5164
$\bar{K}_w$=100, $\bar{K}_s$=10	Present Analytical	40.9604	37.3236	34.7758	24.4251
	Present FEM	40.9603	37.3234	34.7756	24.4248
		In-plane stress $(\bar{\sigma}_{11})$			
$\bar{K}_w$=0, $\bar{K}_s$=0	Present Analytical	60.3308	65.2830	66.7210	67.9918
	Present FEM (20x20)	60.5143	65.4819	66.9234	68.1553
$\bar{K}_w$=100, $\bar{K}_s$=0	Present Analytical	19.2010	28.9315	34.2479	48.0060
	Present FEM	19.2824	28.9923	34.3276	48.1031
$\bar{K}_w$=100, $\bar{K}_s$=10	Present Analytical	8.3707	14.0780	17.9097	32.2518
	Present FEM	8.4855	14.1090	17.9532	32.3240

The results of the normalized natural frequencies of the plate are tabulated in Table 3.32 for various span-thickness ratios and modulus ratio (*MR*) = 40. The FE results have converged at a mesh size of 10x10, therefore, the magnitude of the natural frequencies in the table is corresponding to this mesh size. Also, in all the examples under this section, the natural frequencies obtained using FE is corresponding to the mesh size 10x10. The results of Hui-Shen *et al*. (2003) and Akavci (2007) are also collected in the table for comparison. The present analytical and FE results are found to be in good agreement with the results of the references. Figure 3.62 shows the variation of the natural frequency of the plate with various magnitudes of *MR* and Winkler stiffness ($\overline{K}_w = \overline{K}_1$). The magnitude of the natural frequency tends to increase with the increase in the magnitude of the *MR* and Winkler stiffness. The increase in the magnitude of these parameters increases the overall stiffness of the laminated composite plates, and as a result, we can observe an increment in the magnitude of the natural frequencies. Figure 3.63 displays the variation of the natural frequencies with various magnitudes of *MR* and shear stiffness ($\overline{K}_s = \overline{K}_2$) of the foundation. The increase in the shear stiffness also increases the magnitude of the natural frequency as the overall stiffness of the laminated composite plate gets increased due to the presence of the foundation. The increase in the magnitude of the frequencies is comparatively higher in this case. Figure 3.64 shows the variation of the normalized natural frequencies of the same plate with *MR* and span-thickness ratio by considering the combined Winkler stiffness ($\overline{K}_w = 100$) and shear stiffness ($\overline{K}_s = 10$) of the foundation.

3.8. Forced-vibration analysis of laminated composite plates on elastic foundation

In this section, the effects of elastic foundation on the forced-vibration responses of laminated composite plates are investigated. A three-layered laminated composite plate is

considered which is simply supported at all the edges. The plate structure is first loaded with a pulse load acting for 0.006 sec and then removed from the plate. The corresponding displacement-time response under the forced (t = 0 to 0.006 sec) and free vibration regime (t> 0.006 sec) is shown in Figure 3.65 for three different conditions, without considering the foundation stiffness, considering only the Winkler stiffness and considering both Winkler and shear stiffness of the foundation. The FE results of transverse deflection have converged at a mesh size of 8x8, therefore, the results obtained in the forced vibration analysis are corresponding to this mesh size unless specified. It is observed in the figure that the amplitude of the vibration decreases while the frequency increases due to the elastic foundation stiffness. A sharp decrement in the amplitude of the vibration is observed in the figure when both the Winkler and shear stiffness of the foundation is considered.

Table 3.32 Natural frequencies of a three-layered (0/90/0) laminated composite plate resting on elastic foundation (material property: MM16; non-dimensional parameter: ND2, ND8)

		l/*h*			
Foundation Stiffness	References	10	20	50	100
$\overline{K}_w$=0, $\overline{K}_s$=0	Present Analytical	14.7073	17.4824	18.6405	18.8276
	Present FEM	14.7032	17.4822	18.6412	18.8285
	Hui-Shen *et al*. (2003)	14.702	17.483	18.689	-
	Akavci (2007)	14.700	17.481	18.640	-
$\overline{K}_w$=100, $\overline{K}_s$=0	Present Analytical	17.7569	20.1318	21.1519	21.3181
	Present FEM	17.7535	20.1317	21.1526	21.3189
	Hui-Shen *et al*. (2003)	17.753	20.132	21.152	-
	Akavci (2007)	17.751	20.131	21.152	-
$\overline{K}_w$=100, $\overline{K}_s$=10	Present Analytical	22.5992	24.5357	25.3903	25.5308
	Present FEM	22.5967	24.5357	25.391	25.5316
	Hui-Shen *et al*. (2003)	22.596	24.536	25.39	-
	Akavci (2007)	22.595	24.535	25.39	-

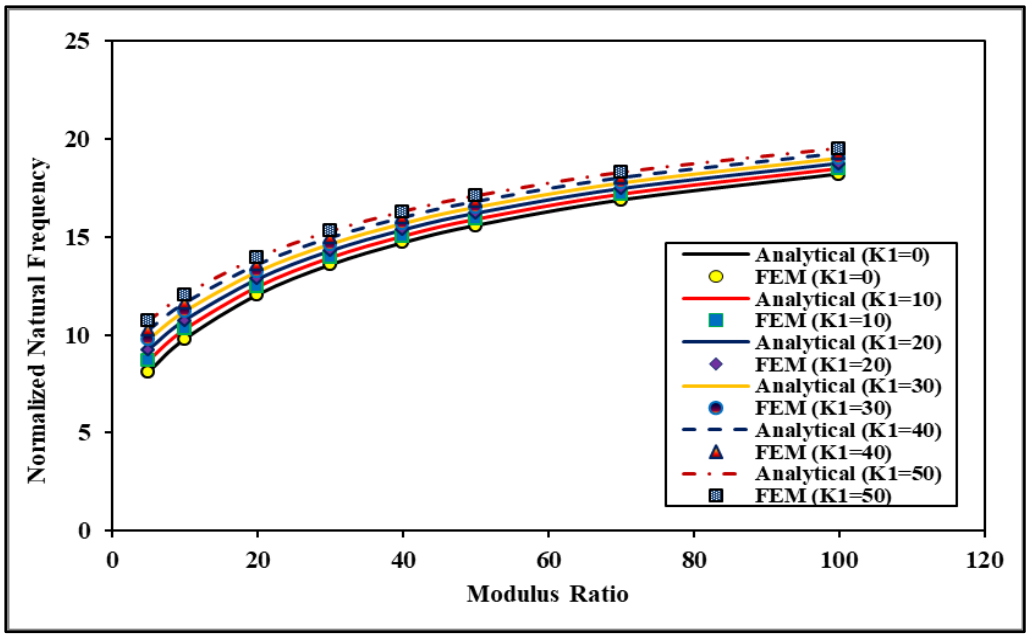

Figure 3.62 Variation of the normalized natural frequency of a laminated composite plate on elastic foundation with modulus ratio (MR) and Winkler stiffness ($\bar{K}_w = \bar{K}_1$)
(material property: MM16; non-dimensional parameter: ND2, ND8)

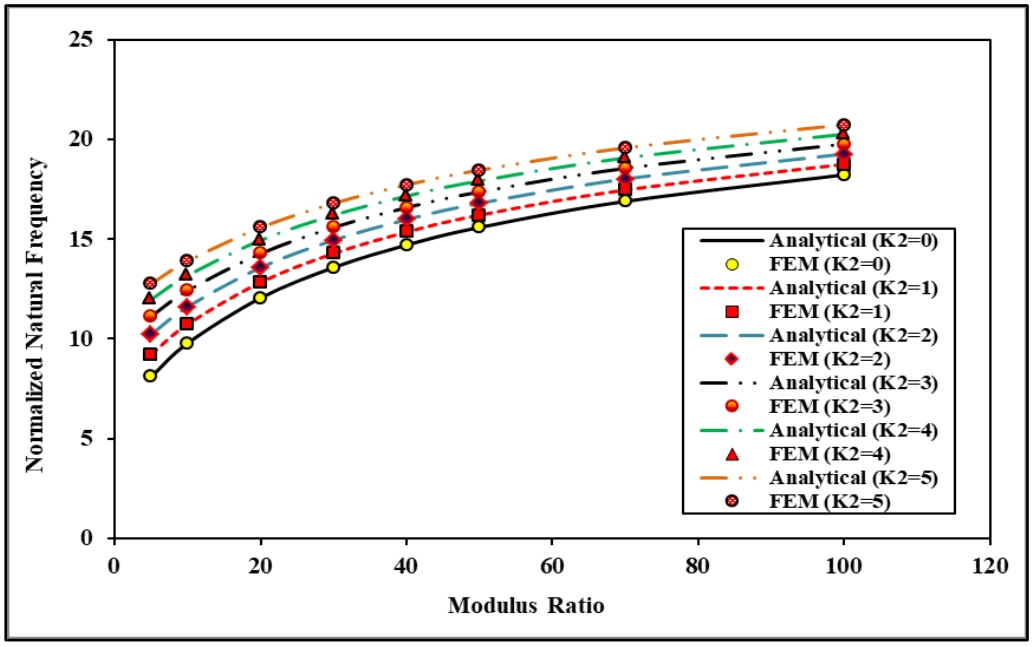

Figure 3.63 Variation of the normalized natural frequency of a laminated composite plate on elastic foundation with modulus ratio (MR) and shear stiffness ($\bar{K}_s = \bar{K}_2$)
(material property: MM16; non-dimensional parameter: ND2, ND8)

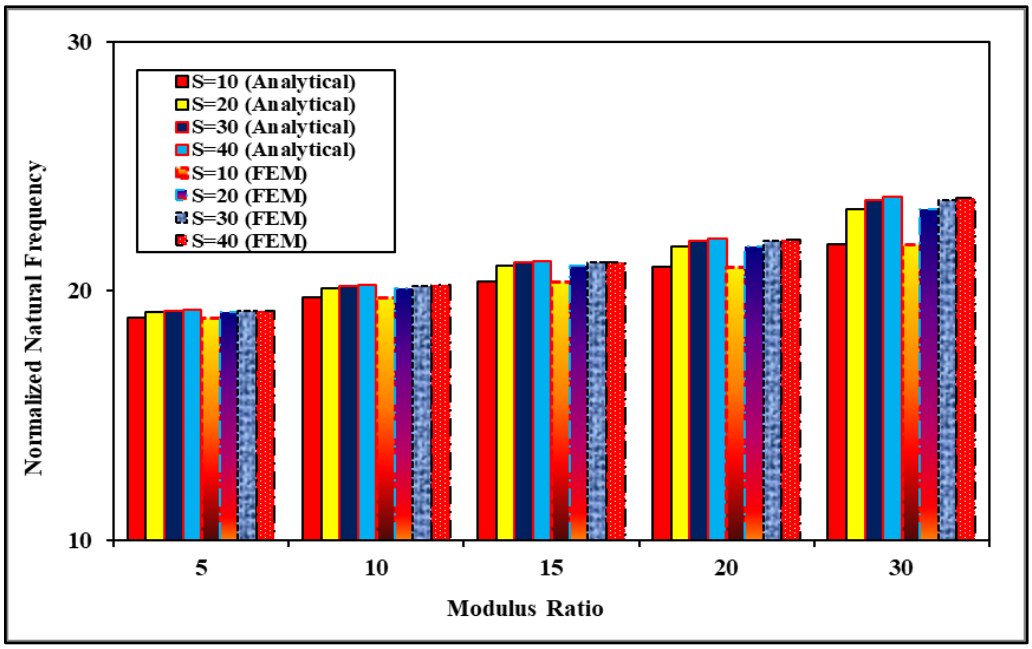

Figure 3.64 Variation of the normalized natural frequency of a laminated composite plate on elastic foundation with modulus ratio (MR) and span-thickness ratio ($\bar{K}_w = 100$; $\bar{K}_s = 10$) (material property: MM16; non-dimensional parameter: ND2, ND8)

Next, a time-dependent triangular load acts on the plate for 0.006 sec and the corresponding responses are shown in Figure 3.66. The amplitude of the responses is decreasing with time which is in accordance to the loading history. An excellent correlation of the analytical and FE responses can be observed in the figure. Next, a sinusoidal excitation is allowed to act on the plate for 0.006 sec and then removed. The variation of the sinusoidal excitation with time and the response under the applied load is shown in Figure 3.67. The displacement-time responses in the figure are in excellent correlation with the variation of the load in the time-domain. The amplitude under the forced-vibration is higher in comparison to the amplitude under the free-vibration regime.

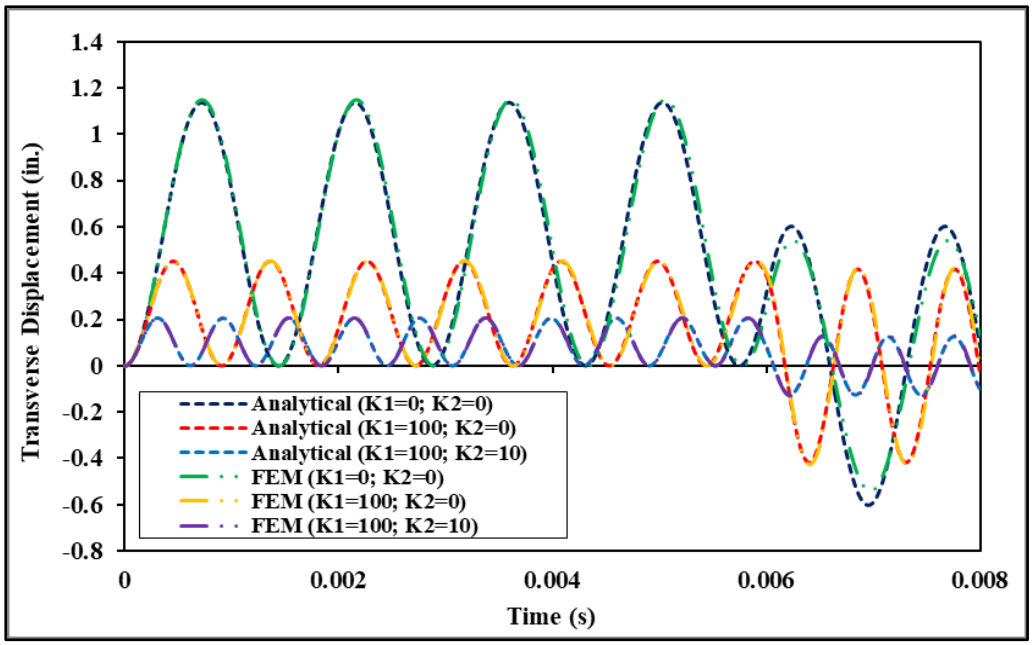

Figure 3.65 Forced and free vibration response of a laminated composite plate resting on elastic foundation under pulse loading acting for 0.006 second **(material property: MM11; non-dimensional parameter: ND8) (1 in. = 0.0254 m)**

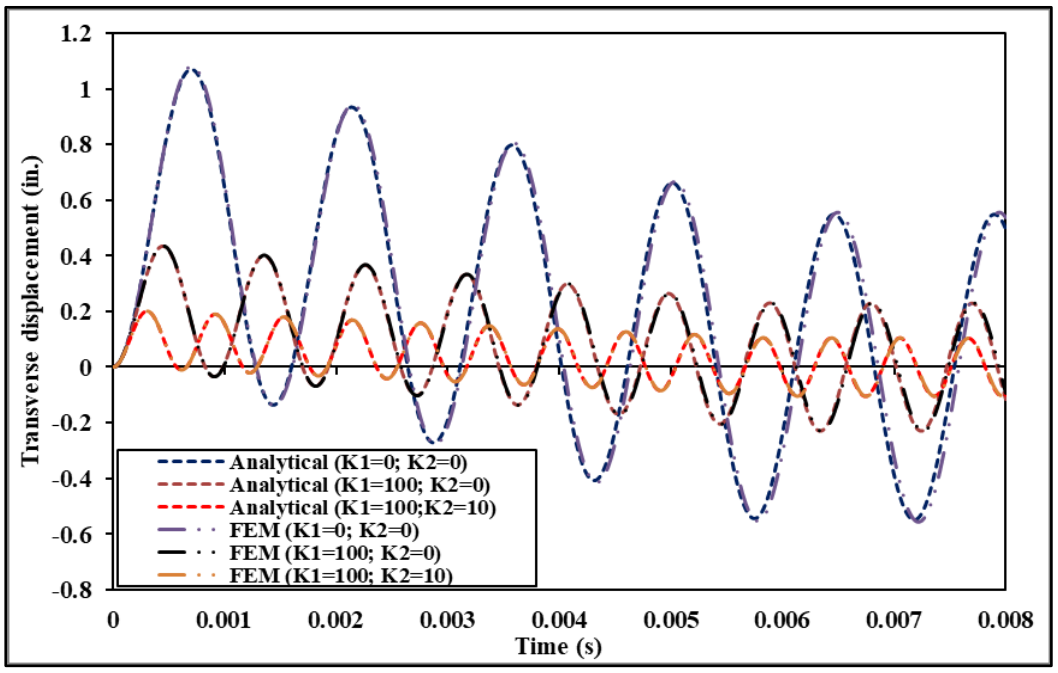

Figure 3.66 Forced and free vibration response of a laminated composite plate resting on elastic foundation under triangular loading acting for 0.006 second
(material property: MM11; non-dimensional parameter: ND8) (1 in. = 0.0254 m)

Next, we apply a sinusoidal excitation at a frequency equal to the natural frequency of the laminated composite plate. The variation of the sinusoidal excitation with time is shown in Figure 3.68 (a). Figure 3.68 (b) shows the forced-vibration response under the sinusoidal excitation without considering the foundation stiffness. As expected, the plate vibrates under the resonance condition. Figure 3.68 (c) shows the forced-vibration regime under the same sinusoidal excitation by considering the Winkler and shear stiffness of the foundation. Interestingly, the plate is not observed to vibrate under the resonance condition anymore as the stiffness of the foundation has changed the natural frequency of the laminated composite plate. Next, the influence of the Winkler and shear stiffness individually on the forced vibration responses of laminated composite plates is shown in Figures 3.69-3.73 under various time-dependent loads like pulse, ramp, ramp-constant and exponential blast load. It is observed in the figures that the shear stiffness of the foundation increases the frequency of vibration of the plate more than the Winkler stiffness and also decreases the amplitude of transverse displacement more than the Winkler stiffness. Figure 3.74 shows the 3 D graphical representation of the displacement-time response of the laminated plate on an elastic foundation ($\overline{K}_w = 100; \overline{K}_s = 10$) subjected to exponential blast load with various decay constants. It is observed in the figure that as the magnitude of the decay constant increases, the faster the plate enters the steady-state condition.

3.9. Static analysis of smart laminated composite plates on elastic foundation

In this section, the static responses of smart composite plates resting on an elastic foundation are investigated by considering two different piezoelectric materials namely, PVDF and the PFRC. First, a five-layered simply supported smart composite plate with PVDF actuator and PVDF sensor placed at the top and bottom surface of a 0/90/0 laminated composite plate is considered for the analysis.

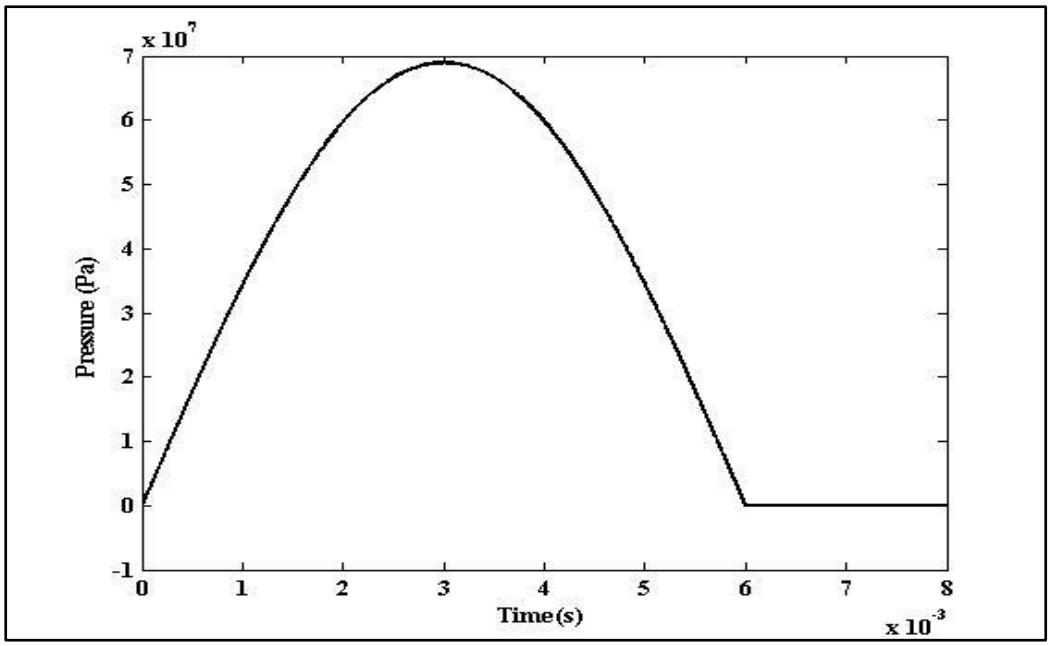

(a)

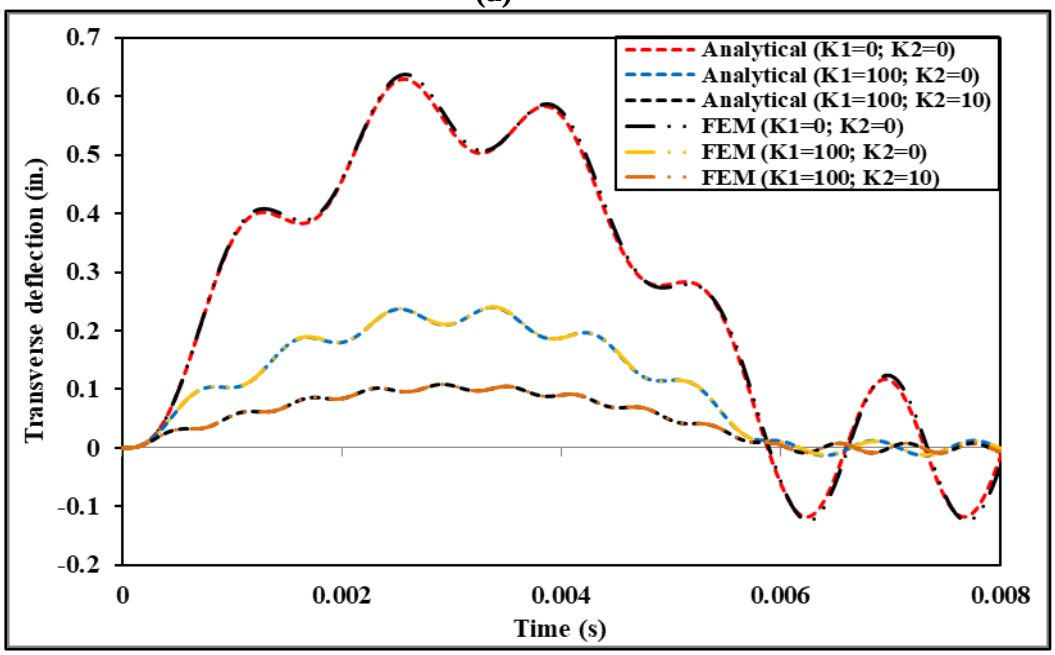

(b)

Figure 3.67 (a) Variation of the sinusoidal excitation with time. (b) Forced and free vibration response of a laminated composite plate resting on elastic foundation under sinusoidal loading acting for 0.006 second (material property: MM11; non-dimensional parameter: ND8) (1 in. = 0.0254 m)

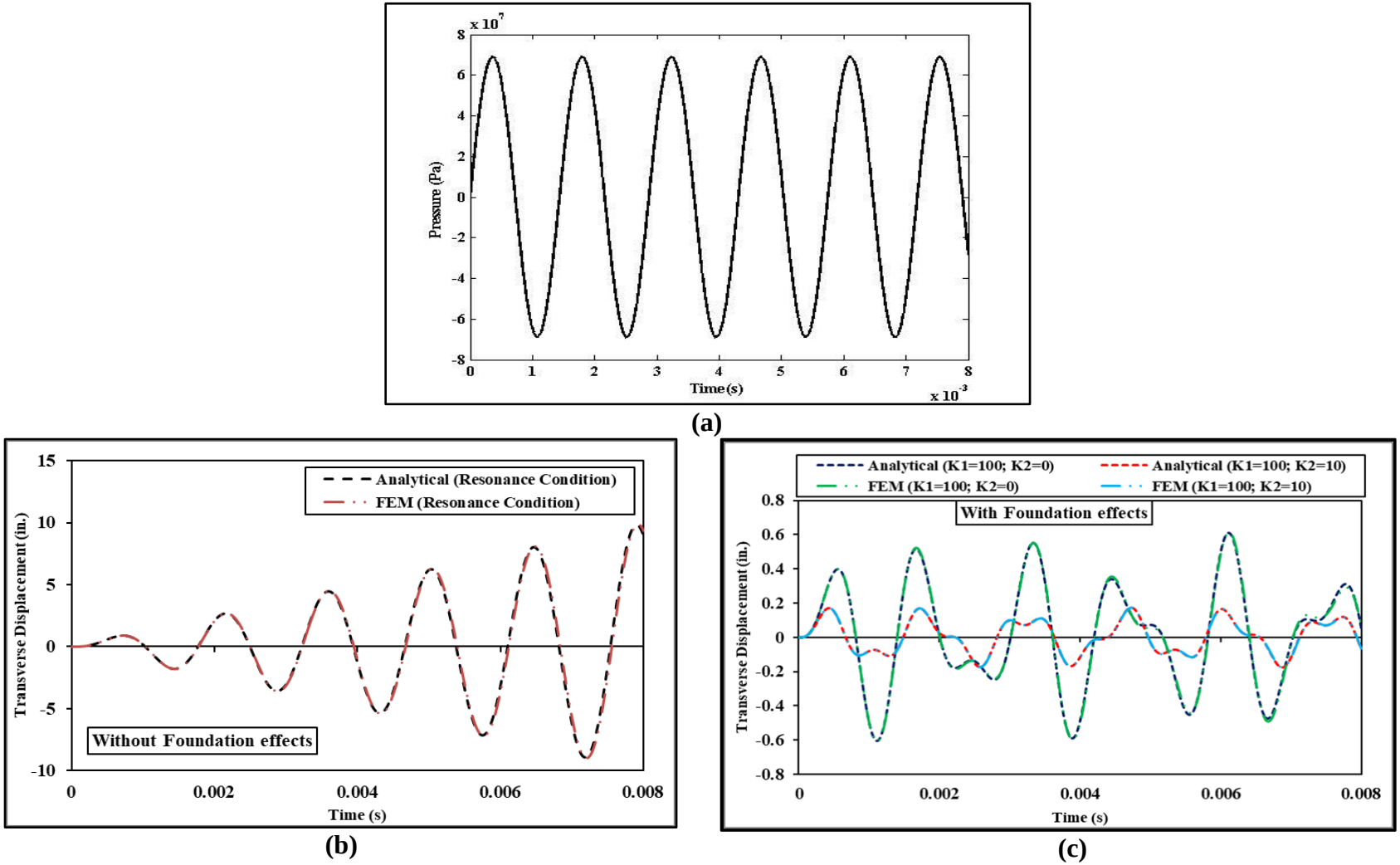

Figure 3.68 (a) Sinusoidal excitation at a frequency equal to the natural frequency of the plate. (b). Vibration response under the sinusoidal excitation without considering the foundation stiffness (c) Vibration response of the plate under the sinusoidal excitation by considering the foundation stiffness (material property: MM11; non-dimensional parameter: ND8) (1 in. = 0.0254 m)

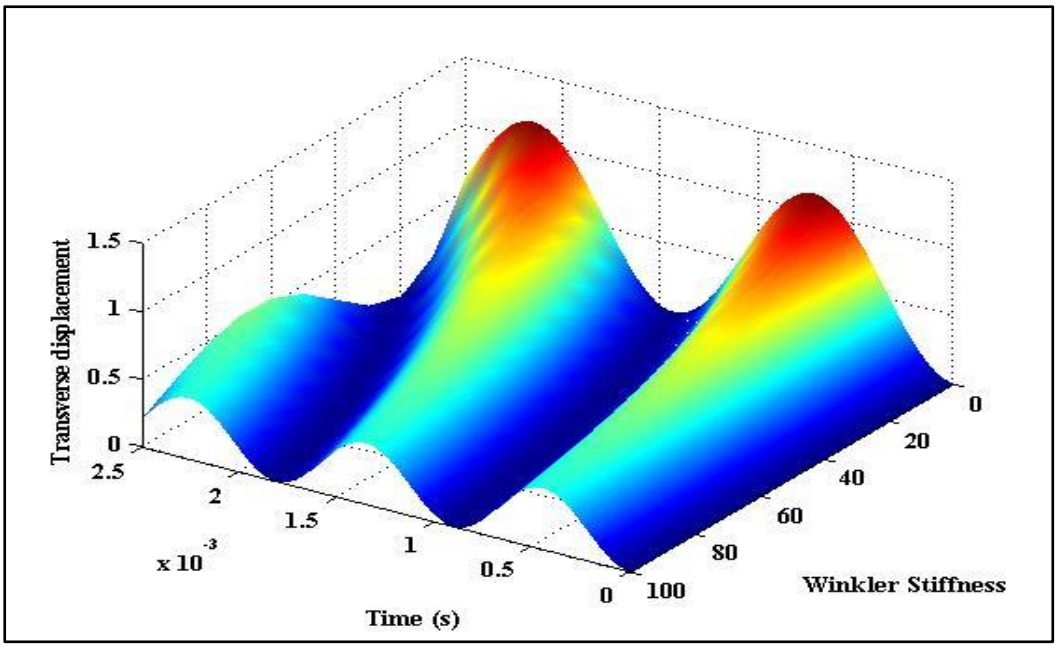

(a)

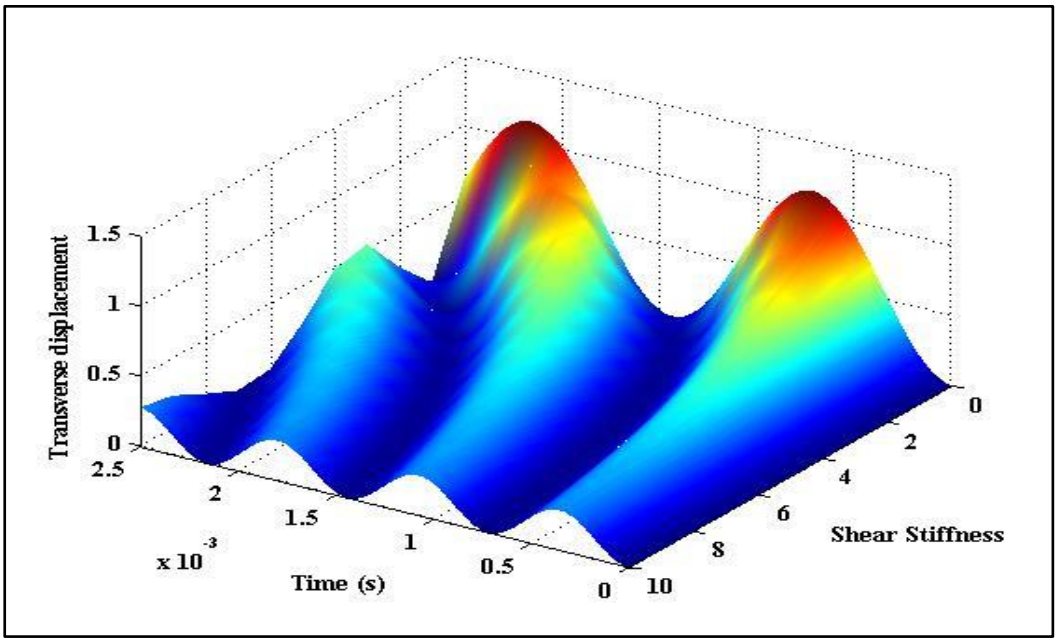

(b)

Figure 3.69 (a). 3D graphical representation of forced-vibration response of laminated composite plate on elastic foundation by considering Winkler stiffness under pulse loading. (b). 3D graphical representation of forced-vibration response of laminated composite plate on elastic foundation by considering shear stiffness under pulse loading (material property: MM11; non-dimensional parameter: ND8)

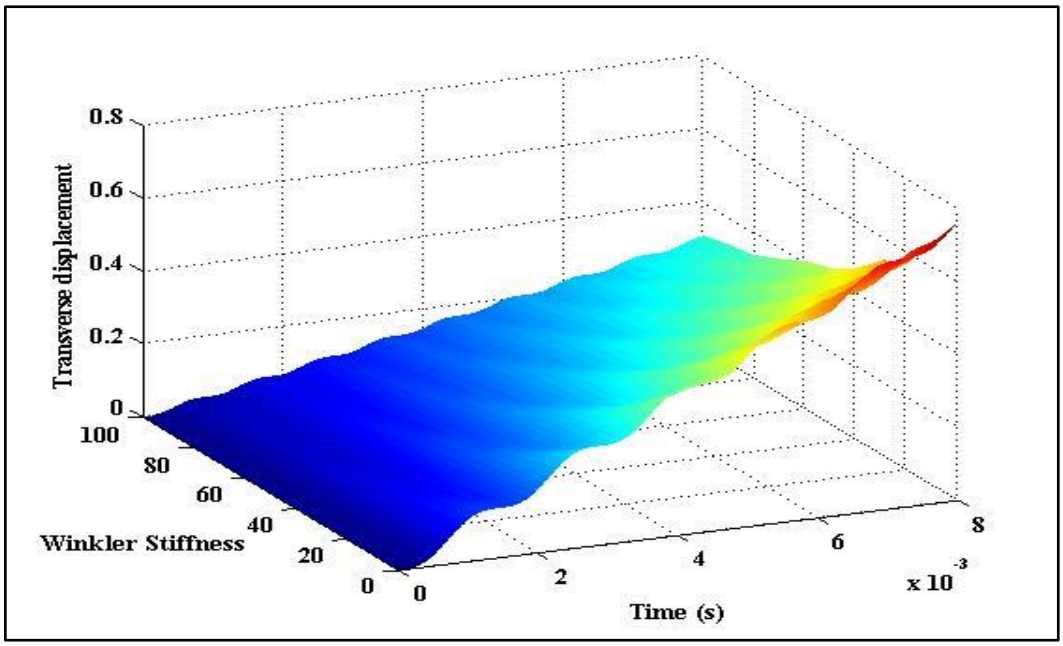

(a)

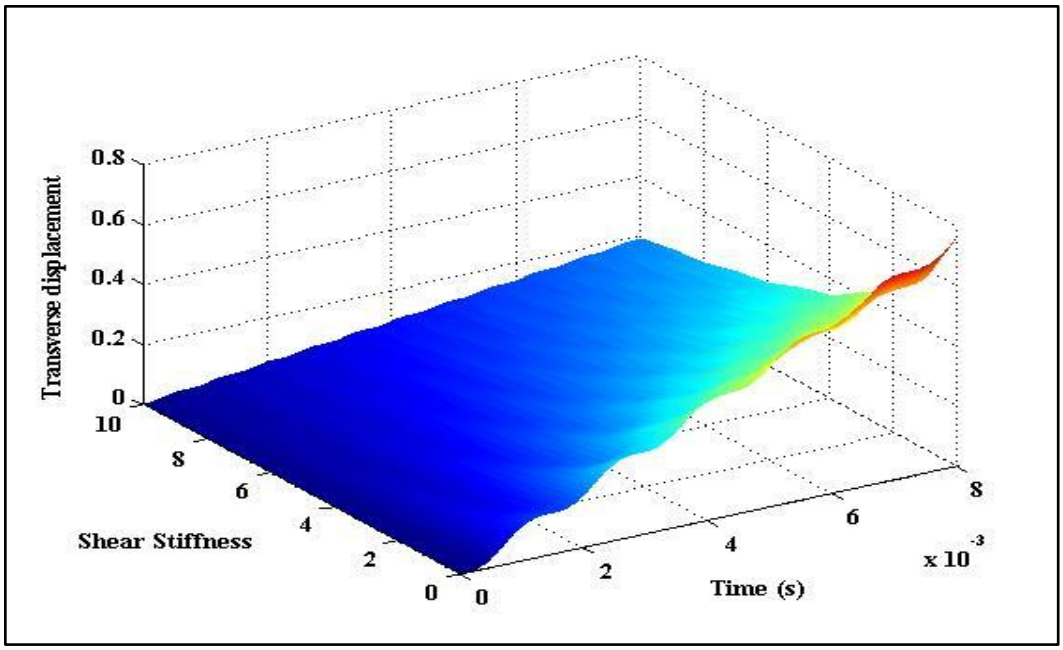

(b)

Figure 3.70 (a). 3D graphical representation of forced-vibration response of laminated composite plate on elastic foundation by considering Winkler stiffness under ramp loading. (b). 3D graphical representation of forced-vibration response of laminated composite plate on elastic foundation by considering shear stiffness under ramp loading (material property: MM11; non-dimensional parameter: ND8)

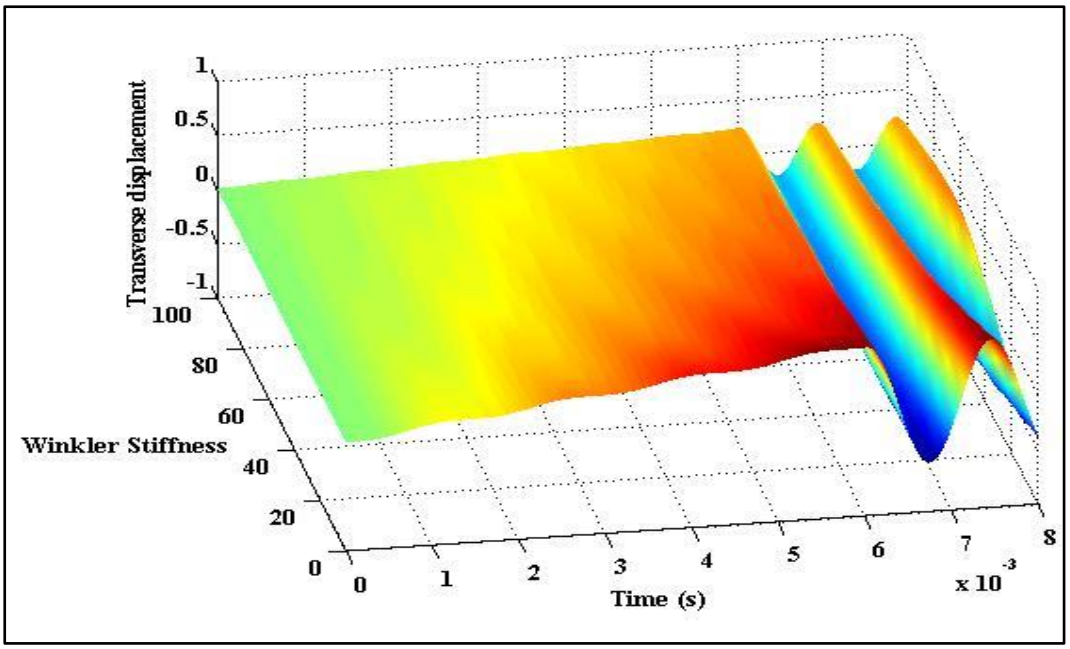

(a)

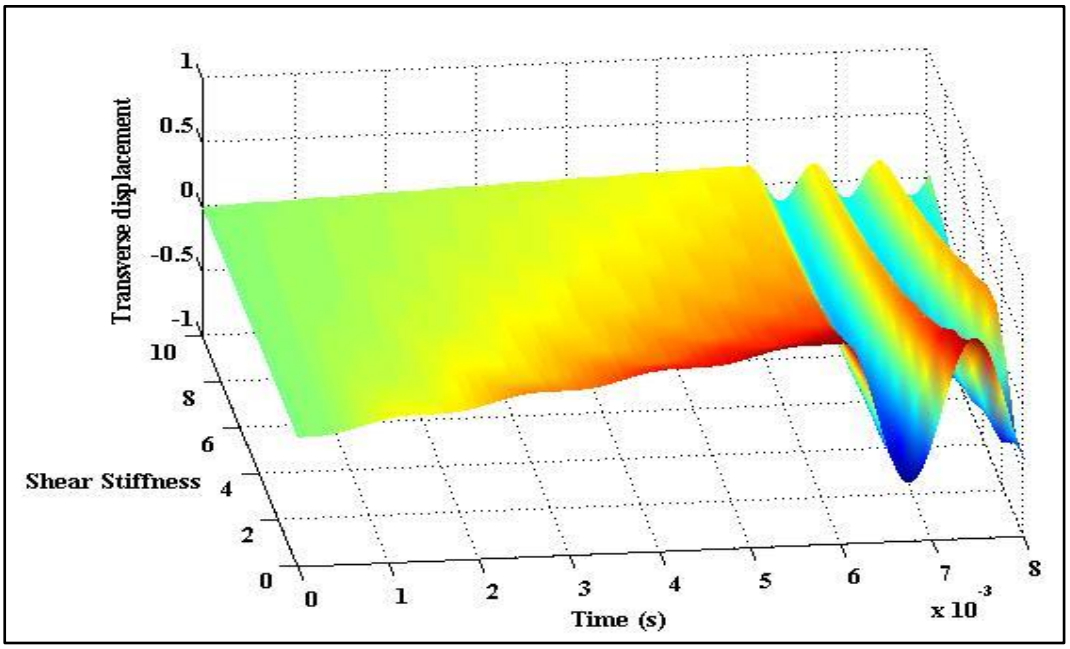

(b)

Figure 3.71 (a). 3D graphical representation of forced-vibration response of laminated composite plate on elastic foundation by considering Winkler stiffness under ramp loading acting for 0.006 sec. (b). 3D graphical representation of forced-vibration response of laminated composite plate on elastic foundation by considering shear stiffness under ramp loading acting for 0.006 sec (material property: MM11; non-dimensional parameter: ND8)

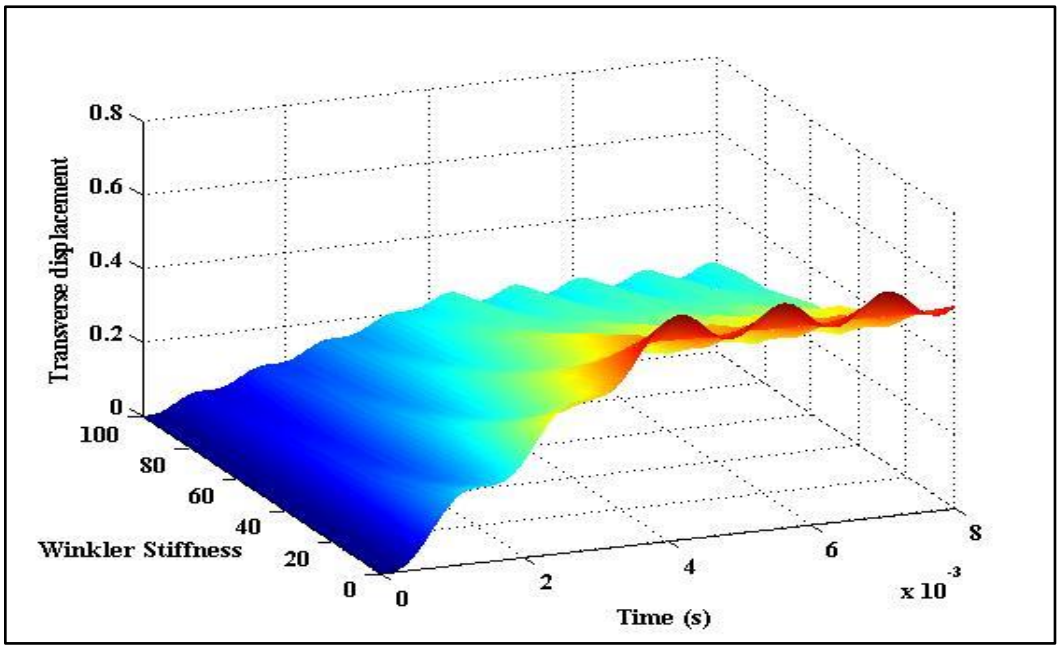

(a)

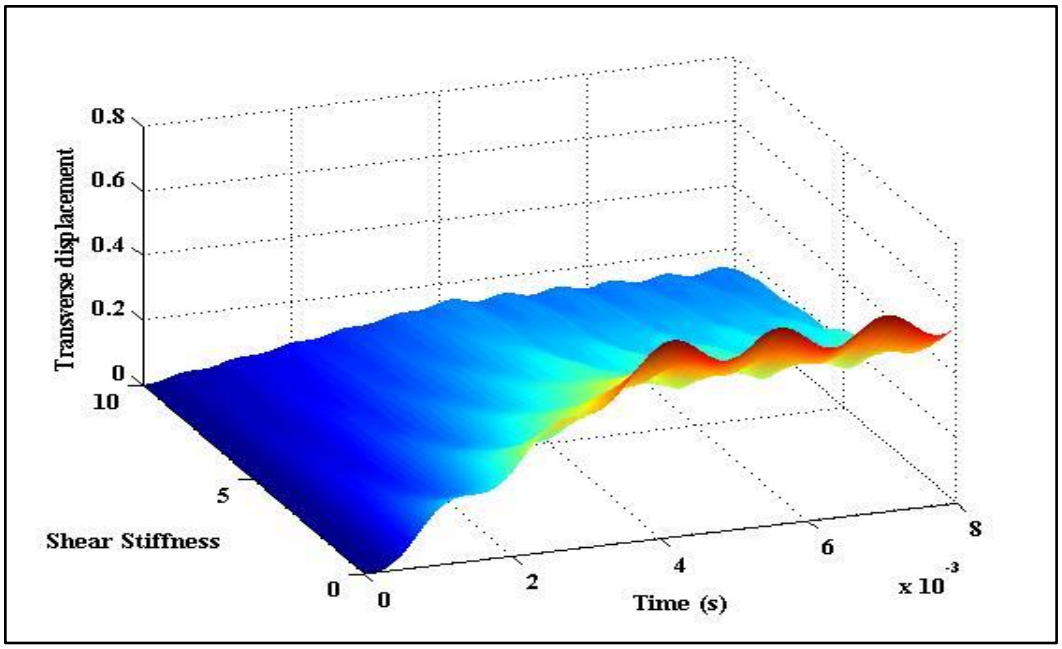

(b)

Figure 3.72 (a) 3D graphical representation of forced-vibration response of laminated composite plate on elastic foundation by considering Winkler stiffness under ramp-constant load. (b) 3D graphical representation of forced-vibration response of laminated composite plate on elastic foundation by considering shear stiffness under ramp-constant load (material property: MM11; non-dimensional parameter: ND8)

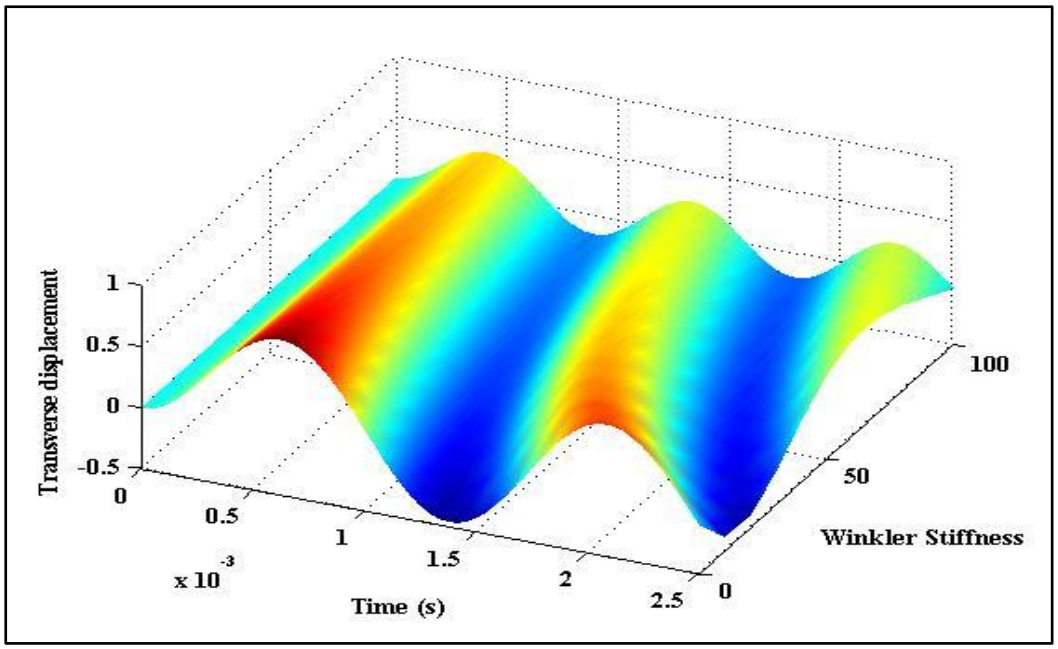

(a)

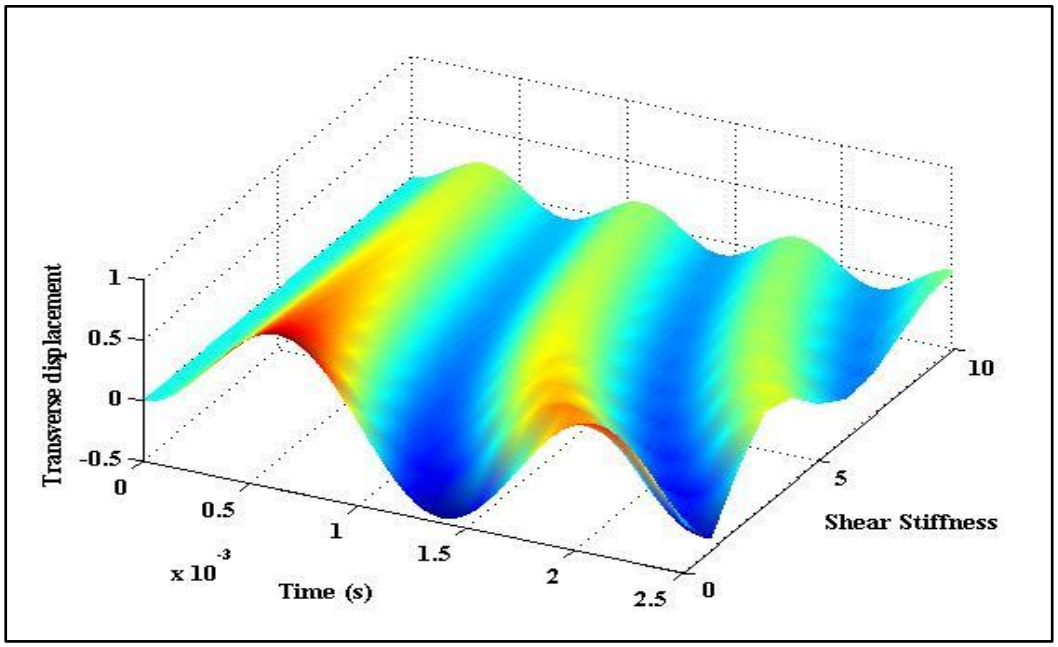

(b)

Figure 3.73 (a). 3D graphical representation of forced-vibration response of laminated composite plate on elastic foundation by considering Winkler stiffness under exponential blast load. (b). 3D graphical representation of forced-vibration response of laminated composite plate on elastic foundation by considering shear stiffness under exponential blast load (material property: MM11; non-dimensional parameter: ND8)

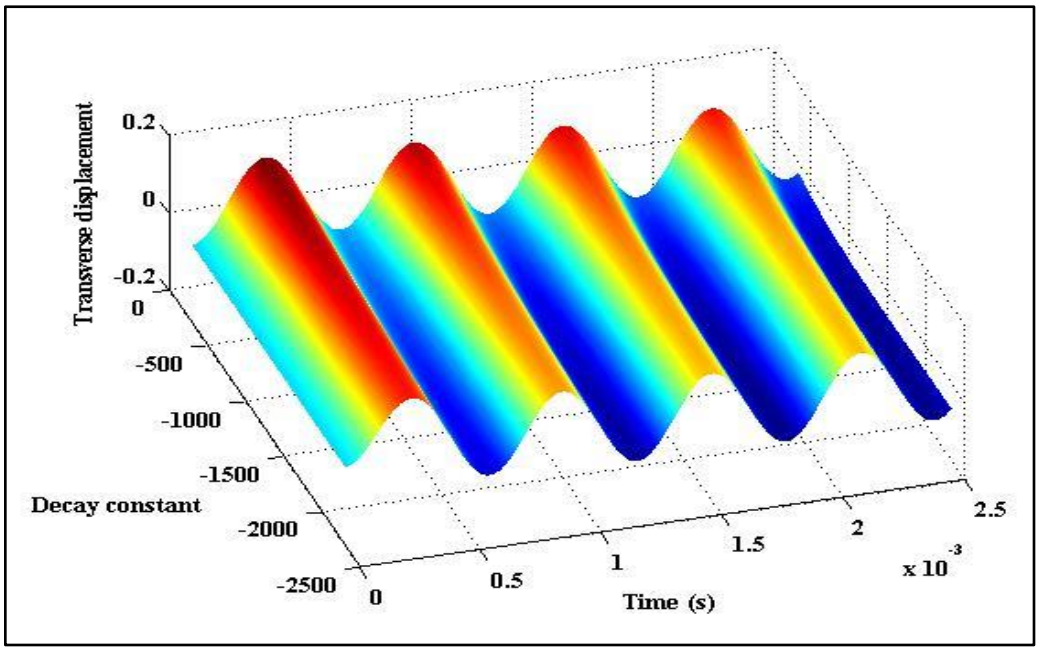

Figure 3.74 3D graphical representation of forced-vibration response of laminated composite plate on elastic foundation subjected to exponential-blast load with various decay constants (material property: MM11; non-dimensional parameter: ND8)

A sinusoidal electromechanical load is assumed to act on the top surface of the smart plate structure. The thickness of each orthotropic layer is considered to be 3 *mm* and the thickness of the PVDF layer is 40 μm (Ray *et al.*, 1993). Analytical and FE results of normalized transverse displacement $(\bar{U}_3)$ and in-plane normal stress $(\bar{\sigma}_{11})$ are presented in Table 3.33 and Figure 3.75, respectively. The magnitude of the transverse displacement in the table is observed to decrease with the inclusion of the foundation. The decrease in the magnitude of $\bar{U}_3$ is calculated to be 43.46 % under the action of electromechanical loads and consideration of Winkler stiffness only for a thick smart composite plate (S=10). The magnitude further decreases by 69.57 % when both Winkler and shear stiffness of the foundations are considered. Similarly, the magnitude of $\bar{\sigma}_{11}$ is also observed to decrease significantly due to the foundation stiffness as observed in Figure 3.75. Next, we consider a PFRC actuator placed on a 0/90/0 composite plate and the results of the normalized

transverse deflection are tabulated in Table 3.34 for various magnitudes of static electromechanical loads. The thickness of each orthotropic layer is 1 *mm* while the thickness of the PFRC layer is 250 μm (Mallik and Ray, 2004). In this case, we observe that the magnitude of $\bar{U}_3$ has decreased by 41.25 % when the Winkler stiffness of the foundation is considered only and 67.62 % when both Winker and shear stiffness of the soil is considered.

3.10. Dynamic analysis of smart laminated composite plates on elastic foundation

In this section, the forced-vibration responses of smart composite plates resting on an elastic foundation and integrated with PVDF and PFRC piezoelectric materials are presented. A three-layered laminated composite plate (0/90/0) integrated with a PVDF actuator and a sensor at the top and bottom surface of the plate subjected to sinusoidal electrical excitations only. The thickness of each orthotropic ply is considered to be 2 *mm* and the thickness of the PVDF layer is 0.1 *mm*. The magnitude and frequency of the electrical excitation are 100 volts and 50 Hz, respectively. Analytical and FE results of maximum transient deflection of the smart composite plate resting on an elastic foundation are presented in Table 3.35 for various span-thickness ratios. An excellent correlation of the analytical and FE results can be observed in the table for all the span-thickness ratios. The amplitude of the transient displacement-time response decreases by 56.88 % and 79.69 % for a thick smart composite plate (*S*=6) due to the Winkler stiffness only and combined Winkler and shear stiffness of the foundation, respectively. Figure 3.76 shows the displacement-time response of the same smart composite plate with a span-thickness ratio of 50 for various cases namely, without consideration of foundation stiffness ($\bar{K}_w = \bar{K}_1 = 0$; $\bar{K}_s = \bar{K}_2 = 0$), considering only Winkler stiffness ($\bar{K}_w = \bar{K}_1 = 100$; $\bar{K}_s = \bar{K}_2 = 0$) and considering combined Winkler and shear stiffness ($\bar{K}_w = \bar{K}_1 = 100$; $\bar{K}_s = \bar{K}_2 = 10$) of the

foundation. Figure 3.77 shows the forced-vibration response of a four-layered (PFRC/0/90/0) smart composite plate with simply-supported boundary conditions at all the edges. The thickness of each orthotropic ply is 1 *mm* and the thickness of the PFRC layer is 0.25 *mm*. The time-dependent electromechanical excitation is constant in the time-domain and sinusoidal in the spatial domain. The magnitude of the electrical and mechanical pressure is 100 volts and 40 N/m^2, respectively. It is observed in the figure that there is a significant decrease and increase in the amplitude and frequency of vibration of the smart composite plate, respectively under the applied electromechanical excitation. The analytical and the FE responses are also observed to be in excellent correlation with each other in the figure. Figures 3.78-3.80 shows the 3 D variation of the displacement-time response of the smart composite plate for various magnitudes of electrical excitation (-100 volts to 100 volts) by neglecting the foundation stiffness ($\overline{K}_w = \overline{K}_1 = 0$; $\overline{K}_s = \overline{K}_2 = 0$), considering only Winkler stiffness ($\overline{K}_w = \overline{K}_1 = 100$; $\overline{K}_s = \overline{K}_2 = 0$) and considering the combined Winkler and shear stiffness ($\overline{K}_w = \overline{K}_1 = 100$; $\overline{K}_s = \overline{K}_2 = 10$) of the foundation. It is observed that the direction of the transverse displacement gets altered when the polarity of the electrical excitations changes from negative to positive and vice versa. Next, a sinusoidal mechanical excitation of magnitude 40 N/m^2 and frequency equal to the natural frequency of the smart composite plate is applied to the plate. At first, the foundation stiffness is not considered and it is observed in Figure 3.81 that the plate vibrates under the resonance condition. Then, along with the mechanical excitation, electrical excitation of magnitude 17 volts and frequency equal to the natural frequency of the smart laminated composite plate is applied to the plate. The amplitude of the vibration decreases, however, the plate still vibrates under the resonance condition. Then, the foundation stiffness is considered and the electromechanical load of the same magnitude and frequency is applied on to the plate. It is

observed that the plate vibrates with significantly lower amplitude. The presence of the foundation stiffness changes the frequency of the vibration and as a result, the plate does not vibrate under the resonance condition.

3.11. Closure

Detailed investigations on traditional composites and smart composite plate structures are presented in this chapter. New examples of laminated composites and smart composite plate structures supported with and without elastic medium have been solved which would be beneficial for future research work. The performance of the present TZZT model is verified against several existing plate models and the elasticity solutions available in the literature. The comparison of the present responses with the established results indicates the accuracy and efficiency of the present analytical and FE formulations. It is found that the present responses are in close agreement with the elasticity solutions and are found to yield efficient static and dynamic responses of both traditional laminates and smart composite plate structures. The secant function used in the model for refining the bending behavior of the plate structures and the satisfaction of the inter-laminar continuity conditions of transverse shear stresses is the two primary features of the present model which are responsible for the better performance of the present model over the existing models.

Table 3.33 Normalized Transverse deflection of smart composite plate (PVDF (actuator)/0/90/0/PVDF (sensor)) resting on elastic foundation subjected to electromechanical load of sinusoidal variation (material property: MM3 (substrate), MP1 (piezoelectric layer); non-dimensional parameter: ND1, ND8)

		Elastic Foundation Stiffness								
		$\bar{K}_w$=0; $\bar{K}_s$=0			$\bar{K}_w$=100; $\bar{K}_s$=0			$\bar{K}_w$=100; $\bar{K}_s$=10		
l/*h*	References	Electric Voltage			Electric Voltage			Electric Voltage		
		V=0	V=100	V=-100	V=0	V=100	V=-100	V=0	V=100	V=-100
10	Present Analytical	0.7691	-2.2252	3.7634	0.4348	-1.2578	2.1273	0.234	-0.6769	1.1448
	Present FEM	0.7698	-2.2126	3.7521	0.4350	-1.2502	2.1201	0.234	-0.6727	1.1407
50	Present Analytical	0.4569	0.3673	0.5465	0.3136	0.2521	0.3751	0.1937	0.1557	0.2317
	Present FEM	0.4569	0.3673	0.5465	0.3136	0.2521	0.3751	0.1937	0.1557	0.2317
100	Present Analytical	0.4464	0.4242	0.4685	0.3086	0.2933	0.3239	0.1918	0.1823	0.2013
	Present FEM	0.4464	0.4242	0.4685	0.3086	0.2933	0.3239	0.1918	0.1823	0.2013

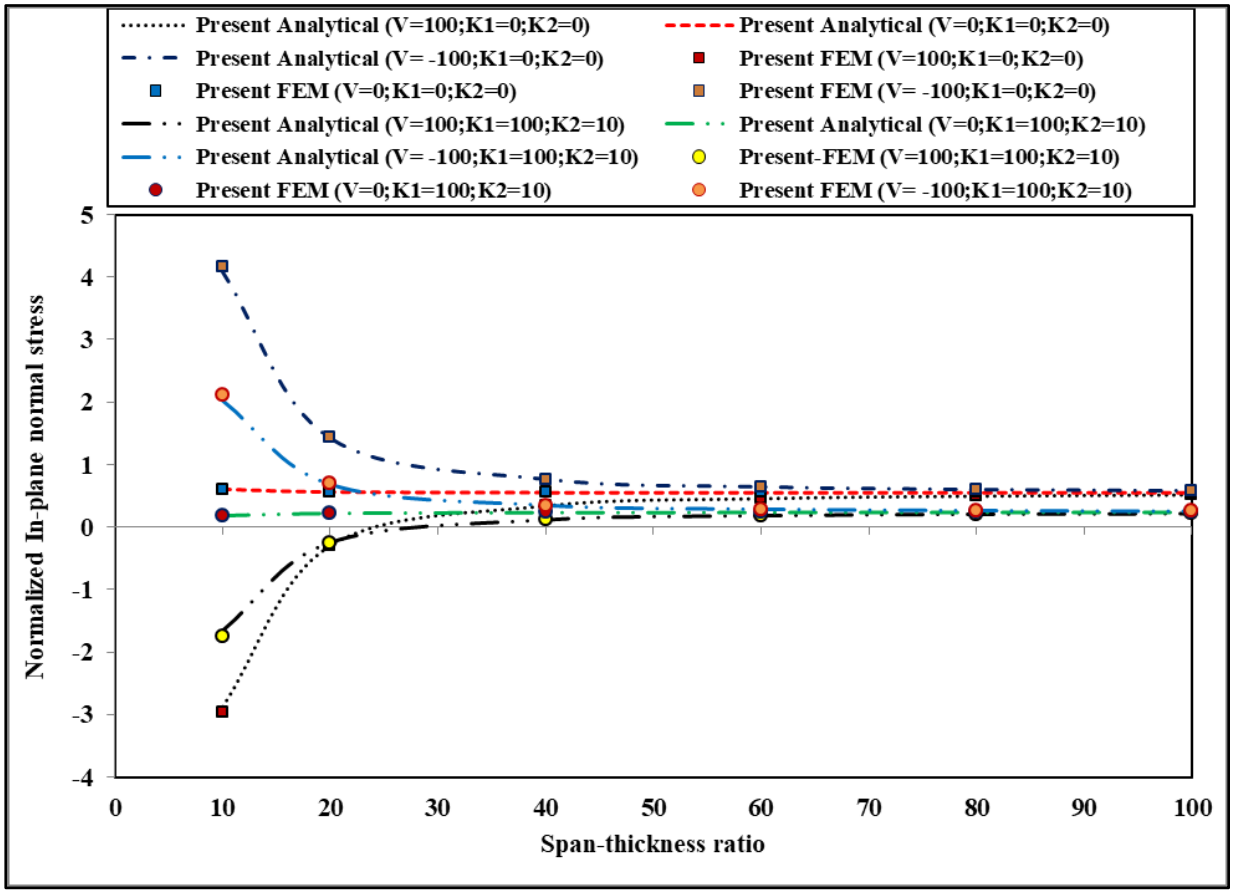

Figure 3.75 Variation of the in-plane normal stress $(\bar{\sigma}_{11})$ at the top surface of a smart composite plate (PVDF/0/90/0/PVDF) resting on elastic foundation subjected to combined electromechanical load **(material property: MM3 (substrate), MP1 (piezoelectric layer); non-dimensional parameter: ND1, ND8)**

Table 3.34 Normalized Transverse deflection of smart composite plate (PFRC (actuator)/0/90/0) resting on elastic foundation subjected to electromechanical load of sinusoidal variation (material property: MM4 (substrate), MP2 (piezoelectric layer); non-dimensional parameter: ND1, ND8)

		Elastic Foundation Stiffness								
		$\bar{K}_w$=0; $\bar{K}_s$=0			$\bar{K}_w$=100; $\bar{K}_s$=0			$\bar{K}_w$=100; $\bar{K}_s$=10		
l/*h*	References	Electric Voltage			Electric Voltage			Electric Voltage		
		V=0	V=100	V=-100	V=0	V=100	V=-100	V=0	V=100	V=-100
10	Present Analytical	-0.7024	132.9469	-134.3517	-0.4126	78.0945	-78.9197	-0.2274	43.0411	-43.4959
	Present FEM	-0.7043	130.9229	-132.3316	-0.4133	76.8171	-77.6436	-0.2276	42.3059	-42.7611
50	Present Analytical	-0.4132	4.3093	-5.1358	-0.2924	3.0493	-3.6341	-0.1854	1.9334	-2.3042
	Present FEM	-0.4133	4.3072	-5.1338	-0.2924	3.0477	-3.6326	-0.1854	1.9324	-2.3032
100	Present Analytical	-0.4034	0.7722	-1.5789	-0.2874	0.5502	-1.1251	-0.1834	0.3510	-0.7178
	Present FEM	-0.4034	0.7720	-1.5788	-0.2874	0.5501	-1.1250	-0.1834	0.3510	-0.7177

Table 3.35 Transient deflection of smart composite plate on elastic foundation subjected to electrical load of sinusoidal variation (material properties: MM14 (substrate), MP1 (piezoelectric layer); non-dimensional parameter: ND7, ND8)

Foundation Stiffness	References	6	10	20	30	50
$\bar{K}_w$=0; $\bar{K}_s$=0	Present FEM	-2.9592	-6.205	-20.2884	-43.6749	-119.65
	Present Analytical	-2.9900	-6.23	-20.3000	-43.69	-119.77
$\bar{K}_w$=100; $\bar{K}_s$=0	Present FEM	-1.2758	-3.4243	-12.9607	-28.7772	-80.0473
	Present Analytical	-1.2968	-3.4400	-12.9737	-28.793	-80.0771
$\bar{K}_w$=100; $\bar{K}_s$=10	Present FEM	-0.6009	-1.8169	-7.5652	-17.1934	-48.3479
	Present Analytical	-0.6115	-1.8256	-7.5729	-17.2029	-48.3654

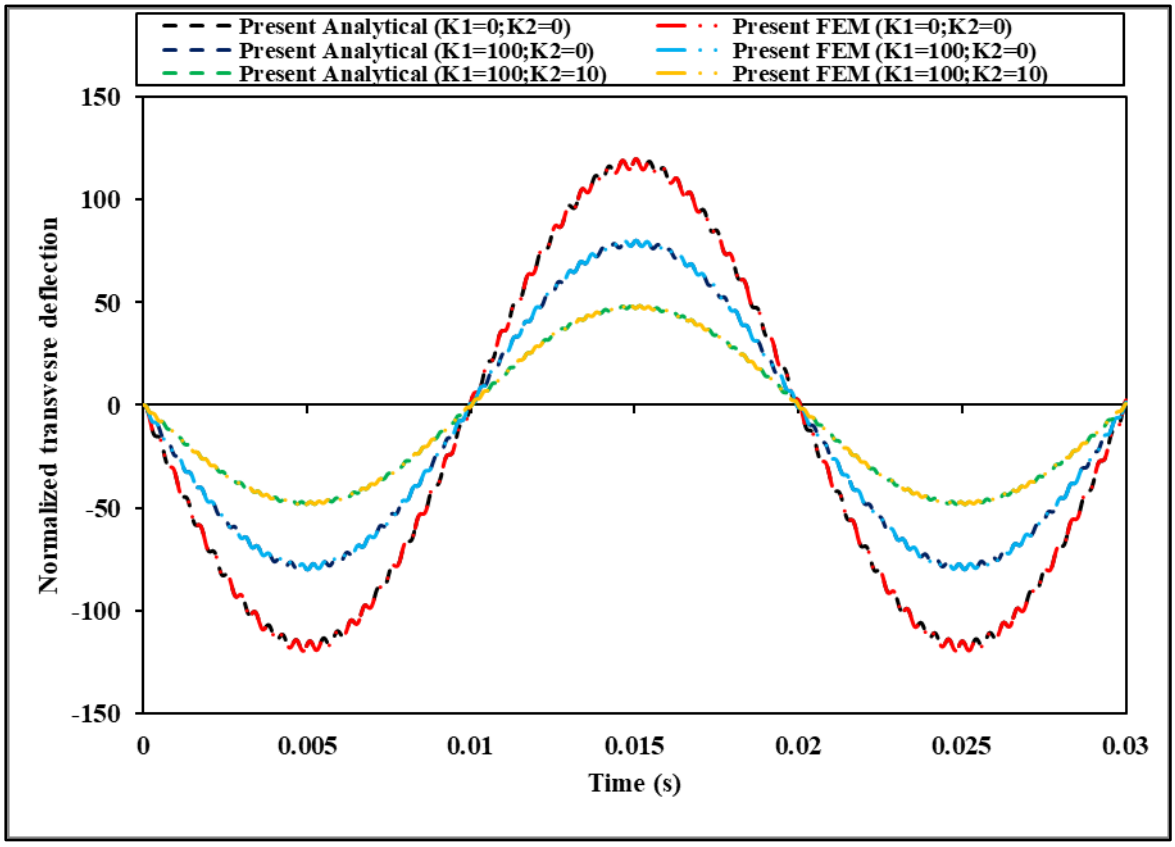

Figure 3.76 Displacement-time response of a smart composite plate (PVDF/0/90/0/PVDF) on elastic foundation subjected to sinusoidal electrical excitation (S=50) (material properties: MM14 (substrate), MP1 (piezoelectric layer); non-dimensional parameter: ND7, ND8)

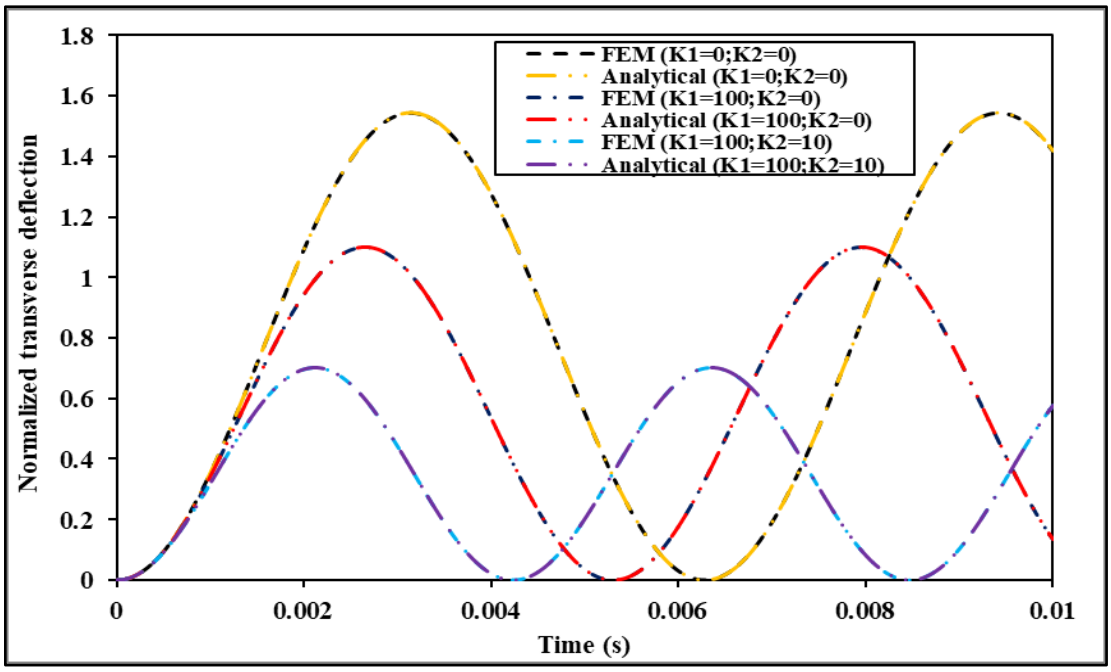

Figure 3.77 Displacement-time response of a smart composite plate (PFRC/0/90/0) on elastic foundation subjected to pulse electromechanical excitation (*S*=100) **(material properties: MM4 (substrate), MP2 (piezoelectric layer); non-dimensional parameter: ND1, ND8)**

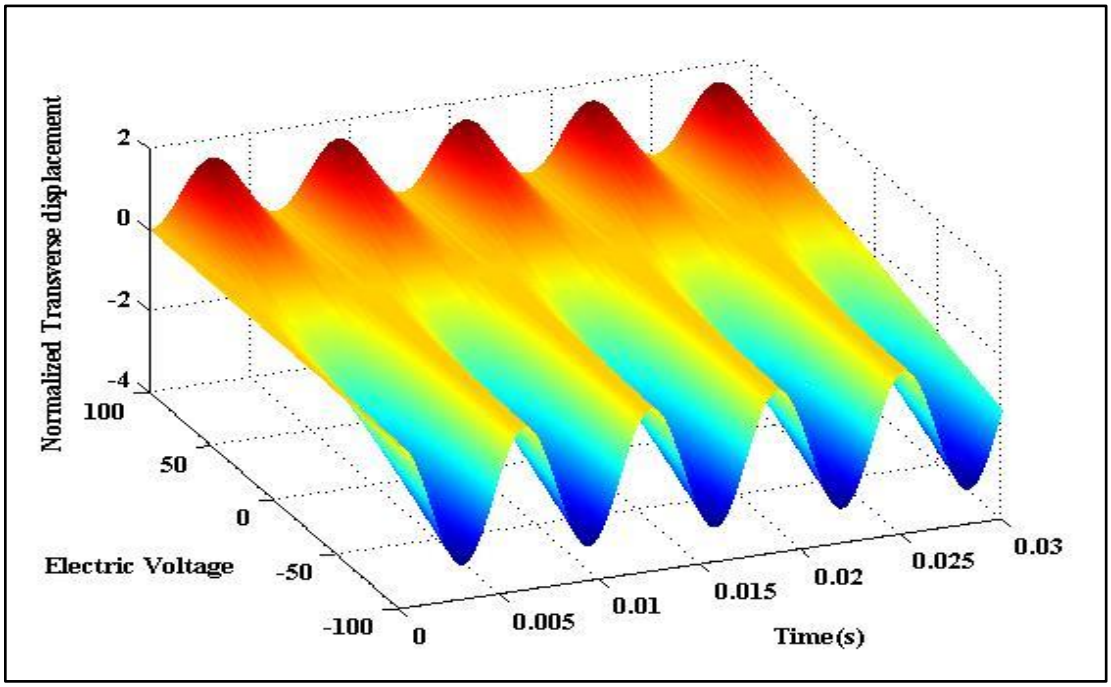

Figure 3.78 3D graphical representation of forced vibration of a smart composite plate (PFRC/0/90/0) without considering foundation stiffness for various magnitudes of pulse electrical excitation (*S*=100) **(material properties: MM4 (substrate), MP2 (piezoelectric layer); non-dimensional parameter: ND1, ND8)**

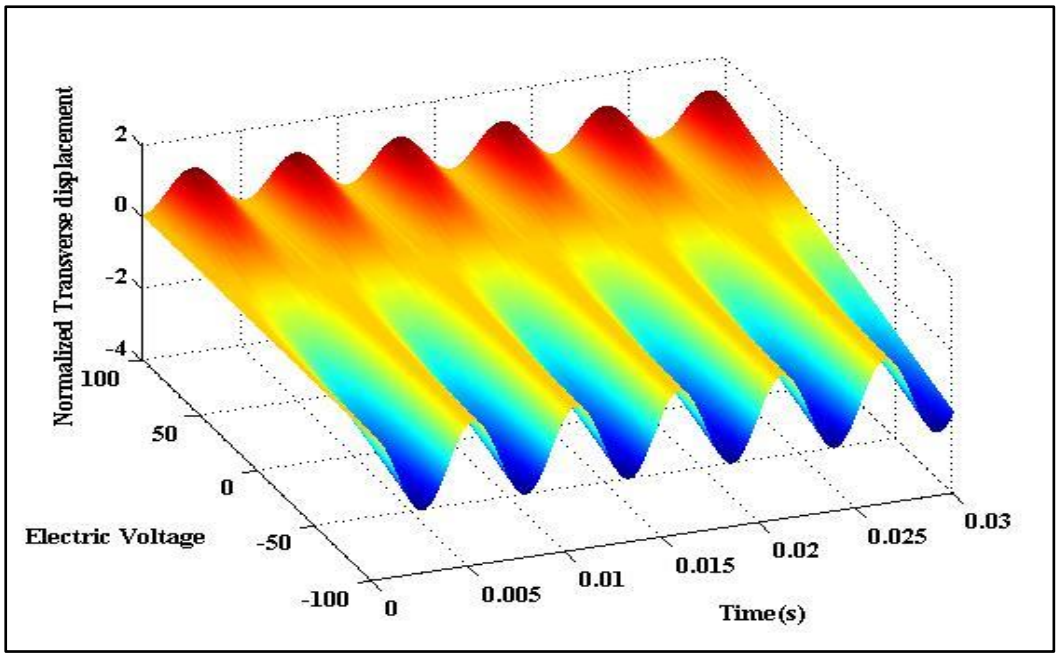

Figure 3.79 3D graphical representation of forced vibration of a smart composite plate (PFRC/0/90/0) by considering Winkler foundation stiffness for various magnitudes of pulse electrical excitation (*S*=100) (material properties: MM4 (substrate), MP2 (piezoelectric layer); non-dimensional parameter: ND1, ND8)

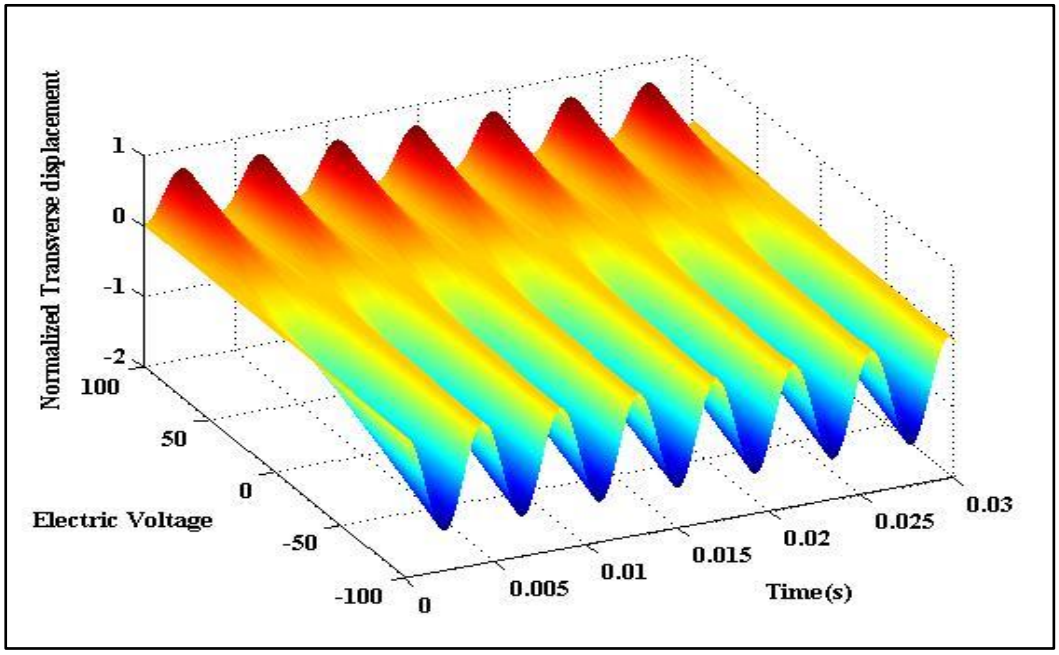

Figure 3.80 3D graphical representation of forced vibration of a smart composite plate (PFRC/0/90/0) by considering both Winkler and shear foundation stiffness for various magnitudes of pulse electrical excitation (*S*=100) (material properties: MM4 (substrate), MP2 (piezoelectric layer); non-dimensional parameter: ND1, ND8)

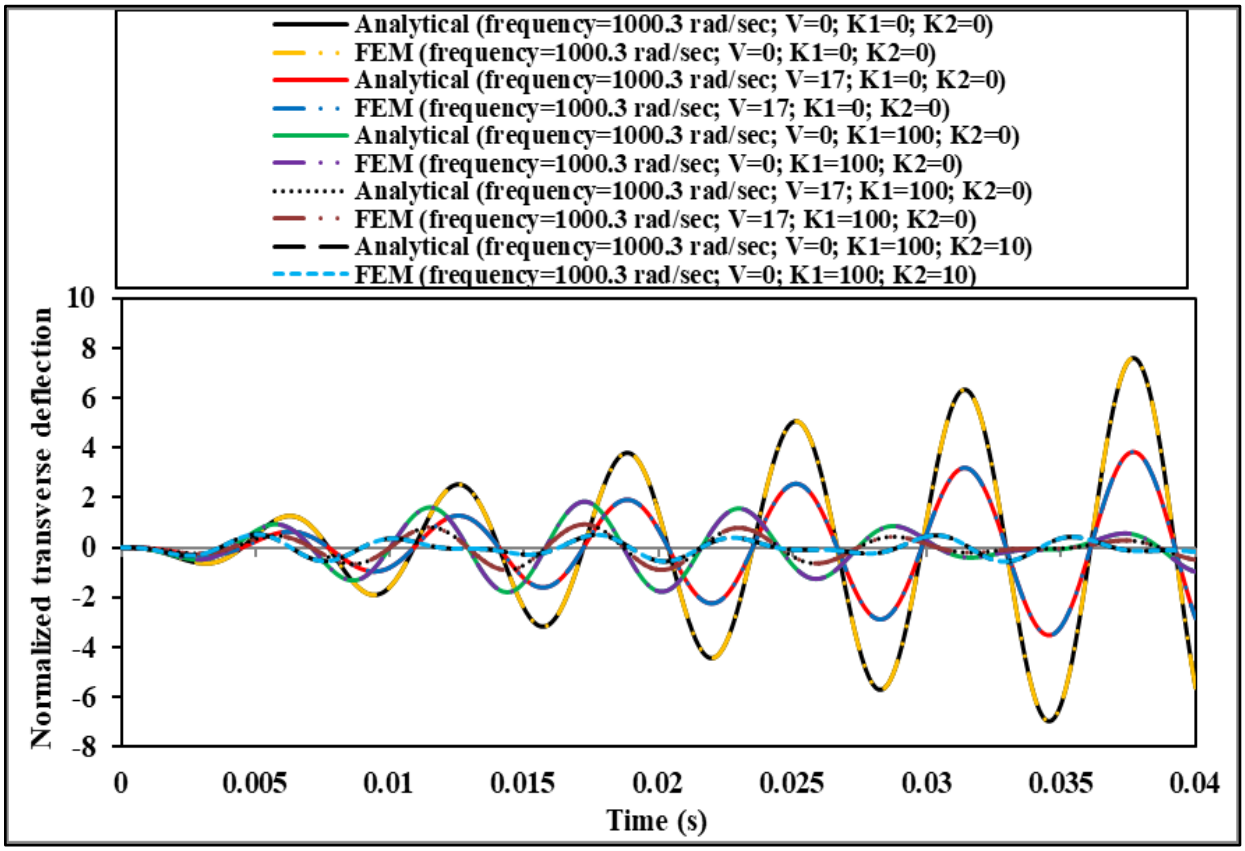

Figure 3.81 Displacement-time response of a smart composite plate (PFRC/0/90/0) on elastic foundation subjected to sinusoidal excitation of frequency equal to natural frequency of the smart composite plate (*S*=100) (material properties: MM4 (substrate), MP2 (piezoelectric layer); non-dimensional parameter: ND1, ND8)